Sox10 Mediates Luminal Lineage Identity and Tumor-Initiating Capacity in HER2/Neu-Driven Mammary Tumorigenesis

Brennan Garland

A thesis submitted to the University of Ottawa in partial fulfilment of the Ph.D. program in Cellular and Molecular Medicine

Department of Cellular and Molecular Medicine
Faculty of Medicine
University of Ottawa
Ottawa, Ontario, Canada

Abstract

The SRY-HMG-Box transcription factor SOX10 plays a critical role in neural crest development. While it has recently been identified as a mediator of the mammary stem/progenitor state, as well as a marker for aggressive basal-like breast cancer, its precise function in epithelial tumorigenesis remains unclear. Here, we identify Sox10 as a key regulator of tumor-initiating activity in HER2/Neu-driven mammary cancers. Genetic ablation of Sox10 in the luminal compartment of mice resulted in delayed but normal mammary gland development. In a murine model of HER2-positive breast cancer, Sox10 deletion conferred a dose-dependent delay in tumor onset, with a complete loss of tumor initiation in Sox10-deficient luminal cells. CRISPR/Cas9-mediated Sox10 inactivation in HER2/Neu-transformed tumor cells led to reduced 3D invasion and diminished self-renewal in mammosphere assays. Established Sox10-deficient cell lines exhibited markedly impaired growth in orthotopic transplant models and failed to colonize lung tissue following tail vein injection, suggesting a loss of tumor-initiating capacity. Transcriptomic profiling revealed that Sox10-deficiency in HER2/Neu-transformed tumor cells leads to erosion of luminal cell identity and acquisition of basal/stem-like markers. Collectively, these findings demonstrate that Sox10 is required for a permissive cell progenitor state for HER2/Neu-driven tumor initiation and is critical to sustain the invasive and self-renewing traits that drive tumor progression and metastasis. The findings provide a novel therapeutic approach in the targeting of Sox10 signalling programs in the mammary epithelium which seemingly give rise to tumor cells of origin in $HER2^{+}$ breast cancers.

Table of Contents

Table of Figures

Table of Tables

List of Abbreviations

αSMA	Alpha smooth muscle actin
ACK	Ammonium-chloride-potassium
ADCC	Antibody-dependent cell-mediated cytotoxicity
AKT	Protein kinase-B
AR	Androgen receptor
ARG	Amphiregulin
ASCO	American Society of Clinical Oncology
BP	Basal progenitor
BPE	Bovine pituitary extract
BSA	Bovine serum albumin
BTC	Beta-cellulin
CAP	College of American Pathologists
CC3	Cleaved caspase-3
CD	Cluster of differentiation
cDNA	Complementary DNA
CK	Cytokeratin
CNS	Central nervous system
CRISPR	Clustered regularly interspaced short palindromic repeats
CSC	Cancer stem cell
DAB	3,3'-diaminobenzidine
DAPI	4',6-diamino-2-phenylindole
DBP	Ductal branch point

DCT	Dopachrome tautomerase
DEG	Differentially expressed gene
DIM	Dimerization domain
DMEM	Dulbecco's modified eagle media
DNA	Deoxyribonucleic acid
DTT	Dithiothreitol
E	Embryonic day
ECD	Extracellular domain
ECM	Extracellular matrix
EGF	Epidermal growth factor
EGR2	Early growth response-2
EGTA	Ethylene glycol-bis(β-aminoethyl ether)-N,N,N',N'-tetraacetic acid
ELF5	E74-like factor 5
EMT	Epithelial-mesenchymal transition
ErbB1	Erb-B2 receptor tyrosine kinase-1
EpCAM	Epithelial cell adhesion molecule
EPG	Epigen
ER^+	Estrogen receptor-positive
ERK	Extracellular signal-regulated kinase
ESR1	Estrogen receptor-1
Ets1	ETS proto-oncogene-1
Etv1	ETS Variant Transcription Factor-1
FACS	Fluorescent activated cell sorting

FBS	Fetal bovine serum
FGF	Fibroblast growth factor
FGFR	Fibroblast growth factor receptor
FFPE	Formalin-fixed paraffin embedded
Foxa1	Forkhead Box A1
FSH	Follicle-stimulating hormone
GFP	Green fluorescent protein
GH	Growth hormone
GRB2	Growth factor receptor-bound protein-2
GSEA	Gene set enrichment analysis
H&E	Haematoxylin and Eosin
HB-EGF	Heparin-binding EGF-like growth factor
HER2	Human epidermal growth factor-2
HER3	Human epidermal growth factor-3
HER4	Human epidermal growth factor-4
HMG	High mobility group
HR	Hormone responsive
HRP	Horseradish peroxidase
IGF	Insulin-like growth factor
IHC	Immunohistochemistry
IRES	Internal ribosomal entry site
ISH	In situ hybridization
JAK	Janus kinase

LacZ	Beta-galactosidase
LH	Luteinising hormone
Lin	Lineage marker
LP	Luminal progenitor
LTR	Long terminal repeat
MAPK	Mitogen-activated protein kinase
MaSC	Mammary stem cell
MBP	Myelin basic protein
MCS	Multiple-species conserved sequence
MMTV	Mouse mammary tumor virus
MIC	PyMT-IRES-Cre
MITF	Microphthalmia-associated transcription factor
mRNA	Messenger RNA
MUC	Mucin
NC	Neural crest
NCG	NOD-Prkdc^{em26Cd52}Il2rg^{em26Cd22}/NjuCrl
NDL	Neu-deletion 2-5
NES	Normalized enrichment score
NFκB	Nuclear factor-kappa B
Ngfr	Nerve growth factor receptor
NIC	Neu-deletion 2-5-IRES-Cre
NMI	N-myc interactor
NRG	Neuregulin

NTC	Non-targeting control
OLIG1	Oligodendrocyte transcription factor-1
ORF	Open reading frame
P	Postnatal day
PAGE	Polyacrylamide gel electrophoresis
PARP	Poly (ADP-ribose) polymerase
PAX3	Paired box gene 3
PBS	Phosphate buffered saline
PCNA	Proliferating cell nuclear antigen
PCR	Polymerase chain reaction
PFA	Paraformaldehyde
PGR	Progesterone receptor
PI3K	Phosphoinositide 3-kinase
PLC-γ	Phospholipase C-gamma
PMSF	Phenylmethylsulfonyl fluoride
Poly-HEMA	Poly-(2-hydroxyethyl methacrylate)
PR^+	Progesterone receptor-positive
PyMT	Polyoma middle-T antigen
PTEN	Phosphatase and tensin homolog
PVDF	Polyvinyldene difluoride
qPCR	Quantitative polymerase chain reaction
RFP	Red fluorescent protein
RFU	Relative fluorescent unit

RIPA	Radioimmunoprecipitation assay
RNA	Ribonucleic acid
RTK	Receptor tyrosine kinase
rtTA	Reverse tetracycline transactivator
Sca-1	Stem cell antigen-1
SDS	Sodium dodecyl sulfate
SEM	Standard error of the mean
sgRNA	Single guide RNA
SHC	Src homology 2 domain-containing
SLK	Ste20-like kinase
SOX	Sex determining region Y-related high mobility group-box
STAT	Signal transducer and activator of transcription
TA	Transactivation domain
TBS-T	Tris-buffered saline with Tween 20
TCGA	The Cancer Genome Atlas
TEB	Terminal end bud
TetO	Tetracycline operator
TGF	Transforming growth factor
TIC	Tumor initiating cell
TLDU	Terminal duct lobular unit
Tfr1	Mouse transferrin receptor-1
TNBC	Triple-negative Breast Cancer
TNFα	Tumor necrosis factor-alpha

UMAP	Uniform manifold approximation and projection
WB	Western blot
X-gal	5-bromo-4-chloro-3-indolyl-β-D-galactopyranoside

Significant Contributions

John Abou-Hamad established Sox10^{fl} allele in the FVB/n background and assisted in flow cytometry analyses.

Samuel V. Delisle performed all bulk RNA sequencing analysis and figure preparation, as well as assisted during orthotopic and tail vein injections.

Riana Zuccarini ran the western blot in Fig. 5.6 F.

Christiano Tanese de Souza performed orthotopic injections in Fig. 5.4.

David P. Cook performed all single cell RNA sequence interrogation.

The Louise Pelletier Histology Core Facility performed the paraffin embedding and sectioning of all tissues.

Genome Quebec performed all bulk RNA sequencing.

StemCore Facility performed all Sanger Sequencing.

Acknowledgements

The idiom ‘it takes a village’ is typically used in the context of raising a child, yet I am a 30-year-old man. Nonetheless, I feel this statement perfectly embodies the ‘village’ of shoulders I have been fortunate to lean on throughout the work presented in this manuscript.

First, I would like to thank my supervisor Dr. Luc Sabourin. Your mentorship and encouragement to always follow my nose have given me the agency to pursue a project that I can truly hang my hat on. Thank you for always reminding me to trust the data, to be comfortable with being wrong, and in instances where we do not have time to do it the right way, *we’ll always have time to do it again.* You’ve often told me that a good scientist is someone who can learn to walk and chew gum at the same time. While I’ve yet to gain a complete mastery of the art, your willingness to teach, paired with your seemingly unlimited scientific curiosity have provided me enough practice to build a moderately compelling case for such abilities. If nothing else, at least I don’t get caught by health and safety anymore.

To Drs. Doug Gray and Josée Coulombe, thank you for your patience and for watering the soil of my academic journey. To Drs. Christina Addison, Yannick Benoit, and Pierre Mattar, thank you for your investment, direction, and commitment throughout the duration of this project. Also, thank you for *your* patience in sitting through some of my more thorough (read: long-winded) committee meetings.

To the SW, Sabourin lab, and Carole, thank you for making these past years so memorable. I wouldn’t have been able to, nor would I have wanted to do any of this without you. I keep the wrench for the CO_2 tank regulators on top of the Auer -20˚C.

To John, and Sam, while I may not have known it at the time, I will cherish the evenings, weekends, and holidays we missed together. Thank you for *never* shying away when challenging

my ideas; I am a better scientist today for it. Also, John & Marlena, please forgive me for planning my wedding on the same day as yours…

To my father Greg, mother Teresa, and sister Ashley; thank you for your endless encouragement and support throughout this degree. My trips back to Lakefield, however increasingly infrequent they became in the later stages of my PhD, gave me much needed time to step away from the lab and appreciate what is truly important.

Finally, to Laura (Sophia and Hugo, included); thank you for always sharing with me my victories, and shouldering my failures. I love you. This thesis is a product of your endless support, and it is as much yours as it is mine. For that, I dedicate this to younger you, who joined me on this journey; to current you, who carried me through it; and to future you, who will be by my side for the next one.

Chapter 1: General Introduction

1.1 Breast cancer heterogeneity

Breast cancer is the most common cancer type among Canadian women and accounted for 26% of all cancer diagnoses in women in 2025 (1). Based on the expression of specific molecular markers (2–4), breast cancers are divided into three major subtypes. These include the Luminal A/B, HER2-positive (Human epidermal growth factor receptor 2), and Triple-negative breast cancers (TNBC). Luminal A and B subtypes are defined by the presence of hormone receptors, but differ in terms of proliferation, HER2 status and prognosis.

Luminal A breast cancers are the most common and are characterized by the expression of estrogen-receptor (ESR1) and/or progesterone-receptor (PGR), lack of HER2 expression and a low proliferative index (Ki-67 < 14%) (4–6). Conversely, luminal B subtypes often exhibit reduced or absent PGR expression, higher incidence of HER2 and increased proliferation (Ki-67 >14%) (4,5,7–10). Compared to luminal A, luminal B tumors can often present as a higher grade, exhibit worse prognosis and recurrence-free survival, and often require adjuvant chemotherapy paired with targeted ER/PR-receptor endocrine therapy (7,8,11–13). Together, the luminal subtypes are the most common, ranging from 65-75% of all breast cancer diagnoses (14–16).

HER2-positive breast cancers account for approximately 20% of all breast cancer cases and are characterized by overexpression of the HER2 receptor and/or amplification of the *ERBB2* gene encoding HER2 on chromosome 17 (2,6,17–19). In a clinical setting, defining HER2-positivity is done through immunohistochemical (IHC) or in situ hybridization (ISH) methods. Current ASCO/CAP guidelines define tumors as HER2-positive if they show complete circumferential membrane staining in more than 10% of tumor cells or exhibit gene amplification

as detected by ISH (18–22). Tumors presenting either of these characteristics are eligible for current HER2-targeted treatments, including trastuzumab and pertuzumab.

Finally, TNBCs account for the remaining 10-20% of breast cancer diagnoses and are defined by lack of ER, PR, and HER2 expression (23–29). TNBCs represent the most aggressive form of breast cancer and are associated with poor clinical outcomes. Due to the absence of unique targetable receptors or other biomarkers, treatment options are very limited and rely on chemotherapy as the standard care (23,24,27,29,30).

1.2 HER2 in breast cancer

1.2.1 EGFR family of receptors

HER2 is a member of the epidermal growth factor receptor (EGFR) family of type I receptor tyrosine kinases (RTK) including HER1 (EGFR), HER2, HER3, and HER4 (31–36). Sharing up to 45% sequence homology, these transmembrane glycoproteins consist of two repeating extracellular ligand binding domains linked through cysteine-rich regions, and an intracellular catalytic domain with tyrosine kinase activity (Fig. 1.1) (37,38). To facilitate receptor activation, ligand-induced homo-, or heterodimerization events are required. There are 13 known ligands to the EGFR family of receptors, which can be categorized into neuregulins (NRG), which primarily activate HER3 and/or HER4, and EGFR-activating ligands (38). There are 7 canonical EGFR ligands: epidermal growth factor (EGF), transforming growth factor α (TGFα), amphiregulin (ARG), epigen (EPG), epiregulin (EPR), β-cellulin (BTC) and heparin-binding EGF-like growth factor (HB-EGF), and neuregulins 1 through 6 (NRG1-6) (36,39–44). Interestingly, HER2 has no known ligands and acts as an “orphan” co-receptor that can only be co-activated through

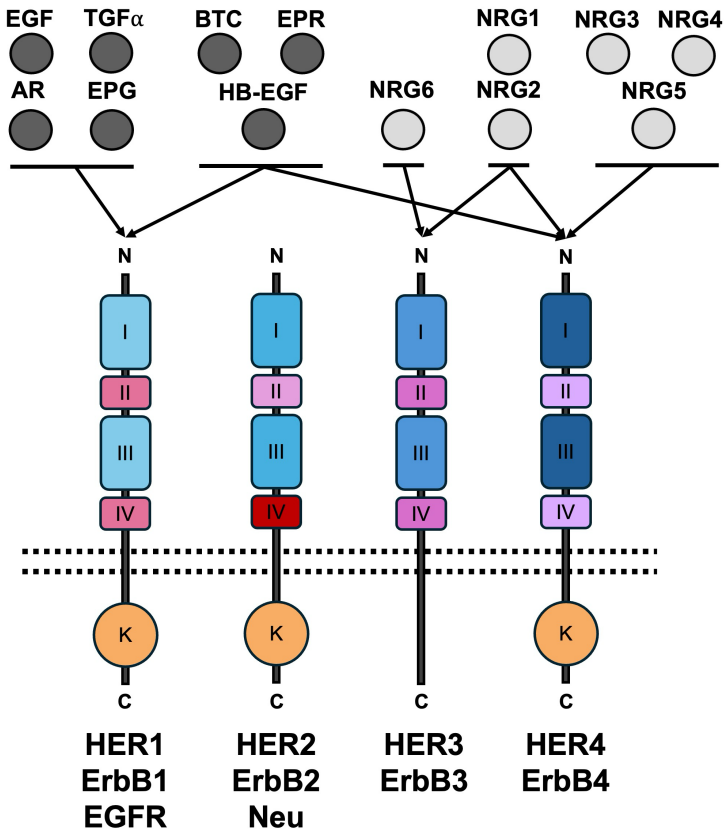

Figure 1.1. Schematic of HER/ErbB family receptors and their respective ligands. HER/ErbB receptors are comprised of paired repeats of distinct extracellular domains (I, II, III, IV) coupled to a cytoplasmic tyrosine kinase domain (K) by a single transmembrane region. Receptor specific extracellular domains I and III (blue), and II and IV (pink/purple) share sequence homology, respectively**.** All respective domains are conserved in HER1 and HER4, while HER3 lacks kinase activity, and HER2 domain IV lacks conserved residues necessary for ligand binding (red). Canonical ligands specific to EGFR (dark grey) are epidermal growth factor (EGF), transforming growth factor α (TGFα), amphiregulin (AR) and epigen (EPG), epiregulin (EPR), β-cellulin (BTC), and heparin-binding EGF-like growth factors (HB-EGF), of which the latter three also bind with HER4. Neuregulins (light grey) 1 and 2 (NRG1/2) target both HER3 and HER4 while NRG6 is specific to HER3. NRG3-5 are specific to HER4.

dimerization with ligand-bound partners (36,39,40,45,46). Unlike other members of the family, HER2 retains an open conformation despite the absence of ligand binding, which is believed to arise from two key residues in its autoinhibitory domain IV contact region which are not conserved (47). Consistent with this permanently 'open' configuration, HER2 has been identified as the preferred dimerization partner among all members in the EGFR family (48). Upon dimerization, a conserved 220 amino-acid region downstream of the catalytic domain is activated through auto-, or trans-phosphorylation events, recruiting activators that ultimately initiate subsequent downstream signalling events (36,38). In normal cells, HER2-based dimers activate MAPK, PI3K-AKT, and JAK/STAT-dependent signalling pathways, mediating cell proliferation, survival and differentiation (32,34,36). While HER2 signalling can activate proliferation and survival pathways, sustained receptor activation in a normal context is insufficient to drive the tumor initiation observed in $HER2^{+}$ breast cancers.

1.2.2 HER2/Neu as an oncogene

HER2 can become oncogenic through multiple cellular mechanisms. Somatic alterations leading to increased HER2 gene copy number are most commonly reported for elevated cellular HER2 expression (49–51). Notably, it has been observed that the HER2 locus harbors local genomic features that predispose it to palindromic amplification events, rendering it particularly susceptible to duplication (52). Indeed, genomic amplification events of the chromosome 17q12-q23 locus harboring the *ERBB2* gene have been well documented (6,53–55). However, it is apparent that HER2 does not only acquire its oncogenic potential through gene amplification. Human breast tumor-derived cell lines have been reported to overexpress HER2 transcripts up to 6-8 fold higher per gene copy compared to normal mammary cell lines, independently of the status of HER2 gene amplification (56,57). Finally, although observed in only 4% of patients, activating

somatic mutations have also been reported in HER2-positive breast cancers (58). The most common HER2 mutations occur in the kinase domain between amino acids 755 and 781, followed by extracellular domain mutations at amino acid 309 or 310 (58). Kinase-domain mutations, including L755S, D769H/Y, and V777L variants, have been shown to increase kinase activity and induce HER2-HER3 heterodimer-dependent activation of the PI3K and MAPK pathways (59). Similarly, mutations in the extracellular-domain, most commonly the S310F mutation, have been shown to promote hyperphosphorylation and stronger dimerization, locking HER2 in an active conformation (60). Such reports demonstrate the dynamic relationship between HER2 amplification, overexpression, and mutation in these cancers lending to aberrant activation of downstream signalling pathways. In some extreme cases, these mechanisms can culminate in cancers exhibiting up to 500-fold increases in the HER2 receptors at the tumor cell surface (61). At sufficiently high expression and activation levels, HER2 has even been shown to bypass its dependence on heterodimerization and recruit PI3K via Y1139 for direct activation (62).

Similar to HER2, the rat ortholog Neu is a highly homologous RTK that lacks known ligands and signals through dimerization events with other ErbB receptors, activating PI3K and MAPK pathways (63,64). The Neu transmembrane receptor harbors distinct tyrosine phosphorylation sites that regulate its RTK-dependent transformation potential. Tyrosine residues Y1144 and Y1227 have been shown to independently activate MAPK signalling through complexing with Grb2 and Shc, respectively (65,66). PI3K-dependent oncogenic signalling through Neu has also been demonstrated through its ability to recruit the p85 subunit of PI3K to its phosphorylated tyrosine residues (67). The ability of Neu to transform cells in culture is conferred through an activating V664E point mutation (NeuNT) within the transmembrane domain resulting in increased dimerization and kinase activity (68–71). Subsequent studies of Neu

overexpression in mouse mammary epithelium revealed that efficient formation of mammary tumors is largely dependent on deletion mutations within the extracellular juxta-membrane region, further driving receptor activation (72–74).

While Neu-induced transformation often requires mutational activation, similar studies using human HER2 have highlighted fundamental differences in their ability to drive transformation events. Indeed, overexpression of wild-type HER2 in mouse fibroblasts, human breast cancer cell lines, and normal mammary epithelial cells has been shown to be sufficient to induce cell transformation and tumorigenic growth (75–80). While these studies show that HER2 harbors tumorigenic potential merely through its overexpression, mutagenesis studies targeting the transmembrane region of HER2 have been shown to further increase its transformation potential (81). However, such activating mutations have not been observed in spontaneous human HER2-driven cancers. Despite their respective requirements for mutational activation, or lack thereof, both the human and rat receptors have been established as potent oncogenes.

1.2.3 Current treatment methods for HER2-positive breast cancer

There are several first-, and second-line treatment options currently used for targeting HER2-positive breast cancers. Monoclonal antibody therapy is currently the most common method for primary anti-HER2 therapies. Trastuzumab (Herceptin®, Genentech) is a monoclonal IgG1 humanized murine antibody which can bind to the extracellular domain IV of HER2 (82,83). First introduced in 1998 as an approved treatment for HER2-positive breast cancer, Trastuzumab-bound HER2 receptors exhibit reduced ligand binding and receptor dimerization, as well as the ability to induce antibody-dependent cell-mediated cytotoxicity (ADCC) by interacting with natural killer immune cells (84,85). Pertuzumab (Perjeta®, Genentech), another monoclonal antibody, targets

the extracellular domain II of HER2 molecule and inhibits its dimerization with HER3 (86). Like Trastuzumab, Pertuzumab can also interact with Fc receptor on immune cells, further amplifying the ADCC phenomenon when administered in conjunction (87). Efficacious cytotoxic regimens have included Trastuzumab and Pertuzumab paired with a combination of a taxane-based (docetaxel, paclitaxel), platinum-based (carboplatin, cisplatin), anthracycline-based (doxorubicin, epirubicin), or anti-metabolite-based (fluorouracil) chemotherapies (88).

Despite the demonstrated clinical efficacy of anti-HER2 targeted therapies, diminished efficacy is frequently observed through both *de novo* and acquired resistance associated with continued treatment (89). Resistance mechanisms are numerous such as loss of tumor suppressor PTEN expression (20-25% of HER2-positive cancers), mutational activation of PI3K signalling (25% of HER2-positive cancers), loss of the extracellular domain (ECD) IV Trastuzumab epitope (30% of HER2-positive cancers), overexpression of HER3 leading to high levels of trastuzumab-resistant HER2-HER3 heterodimers (45% of HER2-positive cancers), and tumor necrosis factor α (TNFα) induced overexpression of mucin 4 (MUC4) leading to masking of the trastuzumab-binding epitope on HER2 (60% of HER2-positive cancers) (90–99). The prevalence of such resistance mechanisms and metastatic spread in current anti-HER2 targeted therapies highlight the need for alternative, or supplemental treatment methods that extend beyond receptor blockade alone. Specifically, identifying upstream transcriptional programs that sustain tumorigenic states may highlight novel targets and/or pathways to improve $HER2^+$ breast cancer treatment.

1.3 Transgenic models of HER2-positive breast cancer

1.3.1 The Mouse Mammary Tumor Virus (MMTV) promoter

The MMTV promoter is a hormone-responsive transcriptional element derived from a milk-transmitted retrovirus identified in the 1930's for its ability to induce mammary tumors in mice (100–102). MMTV viral particles can infect host mammary epithelium cells through binding and internalization with the mouse transferrin receptor 1 (Tfr1) (103). Subsequent hormone-induced morphogenic events lead to virus replication and pro-viral integration, resulting in activation of growth promoting genes and eventually tumorigenesis (104–106). Interestingly, previous studies have since found that the self-renewing stem/progenitor cells of the mammary epithelium are the ultimate targets for viral infection and expression (101). Several hormone-responsive elements in the long terminal repeat (LTR) of the MMTV promoter have been identified as key mediators of its mammary tissue-specific expression (107–111). Although the MMTV promoter is largely exclusive to the mammary epithelium, detectable levels of viral RNA have also been observed in the kidneys, salivary glands, seminal vesicles, and testes (112). Despite this, due to the observed mammary-epithelium-specific activity of the MMTV promoter, many transgenic mouse models currently employ a truncated LTR variant that exhibits efficient mammary-specific transgene expression without pro-viral DNA insertion (113).

1.3.2 MMTV-Cre

Studying the role of specific genes in mammary gland development through global somatic loss-of-function approaches have had limited use as they often result in non-specific physiological defects or embryonic lethality (114). To overcome these limitations, tissue-restricted genetic approaches have been developed to enable the conditional inactivation of target genes within

defined tissues and cellular subsets. The first application of the MMTV-LTR for conditional gene deletion studies was in combination with the Cre-*loxP* recombination system (115). Using Cre recombinase under control of the MMTV-LTR, it became possible to induce spatially restricted gene deletion within mammary epithelium as early as 6 days of age (115,116).

Today, three main MMTV-Cre transgenic strains are widely used: A, D, and F (117). These lines were generated with the same transgenic construct, however, they exhibit different spatial and temporal kinetics of Cre expression. For example, lines A and F exhibit Cre activity as early as one day of age, whereas Cre activity in line D has previously not been observed until approximately 3 weeks of age (116,118). However, lines A and F have also been associated with severe *de novo* developmental defects in alveolar development and differentiation (117,119). Differing levels of mosaicism have also been observed between strains, resulting in varying proportions of cells displaying non-recombined alleles, or Cre 'escapees' (120). Nevertheless, despite mosaicism observed in strain D, complete deletion is observed in older mice, likely due to chronic hormonal activation of the MMTV-LTR with each subsequent estrus cycle (117). Although these strains were generated using the same transgenic construct, it is believed that the observed differences in kinetics are likely a result of different sites of transgene integration and that chromosomal integration of the transgene may also affect the expression of genes critical for mammary gland development (117).

1.3.3 MMTV-NeuNT, NeuNDL, and NIC

The first HER2 breast cancer murine model was generated in 1988 and demonstrated that expression of the activated c-Neu oncogene (NeuNT) harboring the V664E point mutation under control of the MMTV-LTR promoter is sufficient to sustainably form mammary adenocarcinomas

that histologically resemble human HER2-positive tumors by 95 days of age (121,122). Subsequent studies further demonstrated that effective oncogenic activation of wild-type Neu was correlated with mutations in conserved cysteine residues in the extracellular domain promoting dimerization and a constitutively active conformation (123–125). The discovery of such rate-limiting steps in Neu-induced tumorigenesis led to the widespread use of MMTV-Neu deletion 2-5 (NeuNDL) models of breast cancer. These Neu variants harbor a 5 amino acid deletion which prevents cysteine bridge formation and promotes disulfide-stabilized dimers resulting in constitutive activation (125). While this model provides a novel pre-clinical platform to study HER2/Neu-driven mammary tumorigenesis, it is limited in its ability to assess target gene function in malignant transformation. Thus, to achieve concomitant Neu and Cre expression in the same cells, a new transgenic strain was generated. The MMTV-NIC strain harbors a MMTV-driven bicistronic construct containing the active **N**euNDL oncogene followed by a **C**re recombinase under the translational control of an internal ribosomal entry site (**I**RES) (126). In this model, mammary epithelium-specific expression of constitutively active NeuNDL is coupled to Cre expression which significantly limits the possibility for Cre-escape in cells that undergo Neu-mediated transformation (125,126). While minimally-focal primary adenocarcinomas arise in this model by approximately 146 days, these mice exhibit a low propensity for metastatic colonization, specifically in the lungs (126,127). Nevertheless, the MMTV-NIC model has since been used in several pre-clinical applications to identify potential therapeutic targets and characterize their respective roles in HER2/Neu-induced mammary tumorigenesis (127–131).

1.3.4 Polyoma Middle T Antigen and MMTV-rtTA/MIC mice

The polyoma middle-T antigen (PyMT) is a protein derived from the murine Polyoma virus identified for its ability to induce multifocal tumors in the salivary glands of infected mice (132).

It was found that expression of the middle-T protein is sufficient to transform F2408 rat fibroblast cells *in vitro* which subsequently develop into tumors upon transplantation into rats (133). PyMT is a transmembrane protein that acts as a potent oncogene through the Src kinase-dependent activation of three independent intracellular tyrosine residues (134–138). Resultant activation of downstream signalling programs, including the Ras/MAPK, PI3K, and PLC-γ pathways, occurs in a residue-specific mutually-exclusive manner (135–142). Despite the absence of an intrinsic kinase domain, activated PyMT can induce signalling cascades congruent to that of a constitutively active RTK, driving transformation events through increased cell survival and growth pathways (135,143).

The first application of this potent oncogene to model breast cancer was established using the MMTV-LTR to drive mammary epithelium-specific expression of PyMT (144). To bypass potential deleterious effects of early PyMT expression on mammary gland development, a doxycycline-inducible model using the MMTV-LTR to drive expression of a reverse tetracycline transactivator (rtTA) was established (MMTV-rtTA) (145). When crossed with mice harboring a tetracycline-inducible (tetO) oncogene, this system permits complete mammary gland development prior to malignant transformation.

To study target gene function through conditional Cre-mediated recombination, a tetO-driven bicistronic construct containing the Py**M**T oncogene with an **I**RES linked **C**re recombinase was established (tetO-MIC) (146). This configuration, similar to the MMTV-NIC model, precludes the possibility of Cre escape. Upon treatment of MMTV-rtTA:tetO-MIC (rtTA/MIC) bigenic mice with doxycycline, the mice develop multifocal, aggressive tumors that exhibit a high propensity for lung metastases (146). Tumorigenic progression follows through distinct

morphological stages: hyperplastic lesions, adenoma, intraepithelial neoplasia, local carcinomas, and finally dissemination to secondary sites, recapitulating the progressive histological stages observed in human breast cancer (141,147). Interestingly, due to the inducible nature of this model, PyMT is seemingly recognized as a tumor-specific antigen which is targeted by the immune system, rather than a self-antigen (141). Due to this immune-selective pressure, mammary tumors are not fully penetrant, as only around 87% of females develop tumors (146,148).

Although the rate at which tumorigenesis proceeds appears to be dramatically influenced by background strain, stage-dependent transcriptional profiling has revealed that during early hyperplastic stages, PyMT tumors exhibit a luminal-like $ER^+/PR^+/HER2^-$ expression profile (134,135,147,149,150). However, as tumors progress through the neoplastic state, ER/PR expression is lost and tumors acquire HER2-positive expression (134,135,147). Although they exhibit quite significant intertumoral heterogeneity, a vast proportion of late PyMT tumors have transcriptional profiles that are similar to $HER2^+$ breast cancer (151). To this end, whole exome sequencing studies have revealed that latent acquisition of a HER2-positive profile may be, in part, due to palindromic duplication events of chromosome 11 that are common in PyMT tumors (67,141,152). Chromosome 11 is syntenic with human chromosome 17q12-q23 harboring the murine *Erbb2* gene. Indeed, chromosome 11 genes, including *ErbB2, Septin9, Col1a1*, and *Chad* frequently exhibit elevated expression in both PyMT tumors and human HER2-positive breast cancers (53,54,67,151–154).

1.4 Biological landscape of the murine mammary gland

1.4.1 Mammary gland development

Mammary gland development is a highly dynamic, hormone-regulated process that, unlike most non-reproductive organs, occurs predominantly following the neonatal stage (155). Starting at embryonic day 10 to 11 (E10, E11), lens-shaped ectodermal placodes appear along opposing ventral milk lines, subsequently forming bulb-shaped buds increasing in size up to E15 (156). At this stage, sexual dimorphism is determined via sex-specific androgen signalling which induces condensation of the mammary epithelium in males, preventing extensive gland formation (157). In the female, however, these bud structures continue to proliferate into the fat pad precursor, which differentiates into white adipose tissue at birth, where the formation of a hollow lumen and subsequent epidermal invagination at the skin surface results in nipple formation. During these late gestational stages, the canalized bulb undergoes limited branching, generating a rudimentary ductal tree consisting of approximately 15-20 ducts by birth (158).

Following birth, ductal growth proceeds isometrically (1.13 times relative to the rate of gross body surface area growth) for the first 3-week neonatal period (159). During this time, the mammary gland is comprised of a fibroblast-rich stroma of adipose and connective tissue surrounding the rudimentary ductal network partitioned by a laminin-containing basement membrane (160). The rudimentary ductal tree, filling only a small fraction of the mammary fat pad, is characterized by a cytokeratin (CK) $8^+/11^+/18^+/20^+/22^+$ luminal epithelium surrounded by a single alpha smooth muscle actin $(\alpha SMA)^+/CK5^+/14^+$ myoepithelial cell layer (161,162). Despite their limited growth at this stage, neonatal mammary tissues appear to be functionally committed to the epithelial secretory lineage. Previous studies have shown that fetal mammary tissue can

respond to heterotypic salivary stroma by the formation of a salivary-like pattern of branching (163,164). Salivary glands, like mammary glands and other epithelial-based secretory organs, share numerous molecular signalling pathways that result in branching phenotypes to increase surface area (165). Interestingly, in lactating hosts the salivary-like mammary epithelium structures express lactose synthetase and produce milk-like secretions (164). These observations support the existence of a progenitor-rich epithelial compartment that is functionally specified prior to birth, permitting the mammary anlagen to remain malleable to stromal cues during developmental processes.

At around 21 days of age, ductal expansion accelerates rapidly through highly proliferative terminal end buds (TEB) that drive rapid ductal elongation, branching, and fat pad invasion in an allometric manner (3.92 times relative to the rate of gross body surface area growth) (159). TEBs consist of four-to-six layers of proliferating cuboidal epithelium, giving rise to luminal cells in the subtending mature ducts as well as cap-localized myoepithelial cells (166). Their motile behavior is facilitated by a hyaluronic acid-rich end bud basal lamina that lacks extensive collagen networks which serves to reduce adhesions during stromal invasion (166,167). Indeed, the penetration of stromal tissue by the invading end bud appears to be a forceful, physical process, indicated by the mutual distortion of end bud basal lamina and apposed adipocytes (166).

As ductal elongation proceeds, TEBs undergo bifurcation, giving rise to additional primary ducts which are then subject to subsequent lateral secondary-branching (168). Such morphogenic signals are initiated and maintained by various hormones, growth factors and cytokines (169). This hormonal regulation is mediated by two main endocrine groups: pituitary-derived factors (growth hormone; GH, follicle-stimulating hormone; FSH, luteinising hormone; LH) and ovarian-derived

factors (ER and PR), which are directly induced by FSH and LH, respectively (165). In addition to hormonal regulation, appropriate stromal matrix is necessary for sufficient ductal development. When cultured *in vitro*, mammary epithelial cells fail to establish sufficient cell polarity to induce ductal and/or end bud formation, even when cultured in 3D collagen gel. This phenotype, however, can be rescued when transplanted into de-epithelialized mammary glands (170–172). Strikingly, recent organoid studies have demonstrated that with supplementation of physiologically relevant stromal and hormonal factors, a single mammary epithelial cell can develop into a complex organoid that undergoes full branching morphogenesis, as well as estrus and pregnancy cycles, including lactation, *in vitro* (173). These resulting organoids can develop into fully functional mammary glands when transplanted into cleared fat-pad hosts *in vivo*.

Upon completion of puberty by approximately 8-weeks of age, ductal structures reach the periphery of the fat pad mesenchyme where TEBs become restricted to only single layers of each luminal and myoepithelial population (174–176). The final, and most expansive stage of mammary gland morphogenesis is reached during pregnancy and lactation stages following a surge of distinct hormonal cues (165,177). After the weaning of offspring, these hormonal signals drop resulting in subsequent involution of the expanded mammary gland through a controlled cell death cascade, restoring mammary gland morphology to a state resembling that preceding pregnancy (165). With each subsequent estrous cycle, a scaled-down version of this proliferative-apoptotic cascade is initiated, but then quickly aborted (165).

Such complex developmental stages highlight the spatial and temporal coordination required to mediate the highly plastic nature of the postnatal mammary gland. Understanding how the stem/progenitor populations that drive these processes are maintained among the mammary

epithelial hierarchy will help contextualize both normal mammary gland biology and the mechanisms by which developmental programs are dysregulated during malignant transformation.

1.4.2 Mammary epithelial hierarchy

The cellular plasticity required to enable extensive mammary gland morphogenesis during developmental, estrous, and pregnancy cycles has implicated the existence of a stem cell-rich epithelial population. Indeed, the extent of just how plastic these tissues can be was first observed in 1959 when mice with de-epithelialized mammary fat pads were able to regenerate entire ductal trees following the transplantation of normal epithelial tissue (178). To this end, more recent studies have established fully functional mammary glands in similar de-epithelialized hosts through implantation of a single mammary stem cell (MaSC) derived from adult donors (179).

These seminal studies have provided the foundation for a hierarchical model of mammary epithelial organization. In this model, MaSCs represent the cellular unit that harbors the highest degree of stemness and differentiation potential, ultimately giving rise to progressively lineage-restricted progenitor populations (180–182). MaSC enriched subpopulations are comprised of long-term label-retaining cells, consistent with the presence of quiescent and asymmetrically dividing cells commonly observed in stem cell populations (183). These progenitor populations, which include basal (BP), and luminal progenitors (LP; which include hormone-responsive (HR^+) ductal and HR^- alveolar progenitors), subsequently differentiate into myoepithelial, and mature ductal and alveolar cells, respectively. Eventual LP cell fate is decided by mutually repressive master regulators for HR^+ and alveolar lineages, ER and E74-like factor 5 (ELF5), respectively (184).

Experimentally, interrogation of these discrete populations can be achieved using fluorescence activated cell sorting (FACS) in conjunction with lineage-specific surface markers that are conserved across human and murine epithelium (182). For example, staining lineage depleted (Lin^-) human epithelial cells derived from breast tissue with fluorescent antibodies targeting EPCAM and CD49f can fractionate into mature luminal ($EPCAM^+$ $CD49f^-$), LPs ($EPCAM^+$ $CD49f^+$), MaSC-enriched basal/myoepithelial ($EPCAM^-$ $CD49f^+$), and stromal cell ($EPCAM^-$ $CD49f^-$) populations (185). In mice, EpCAM and CD49f similarly segregate luminal and basal compartments, while alternative marker combinations such as CD24/CD29 and CD24/CD49f among others, have also been widely used to enrich for specific subpopulations (Fig. 1.2) (179,182,186). In mice, MaSCs are highly enriched in the cap cells surrounding the TEBs in pubertal mammary glands and can be isolated in the $CD29^{hi}$ $CD24^+$ or $CD49f^{hi}$ $CD24^{hi}$ populations (179,187,188). Conversely, LPs can be isolated from the pan-luminal $EpCAM^+$ $CD49f^+$ subpopulation based on their CD61, CD14, or CD49b and Sca-1 status (186,189,190).

1.4.3 Lineage commitment in normal mammary gland

Despite the prospective isolation of distinct mammary epithelial subsets enriched for stem and progenitor activity in both mice and humans, the precise relationships between these populations have yet to be defined. While BPs and LPs are proposed to arise from MaSCs, the prevailing body of lineage-tracing literature suggests that, under normal physiological conditions, progenitor populations become largely lineage-restricted following differentiation from the MaSC compartment (182,191). In particular, the LPs appear to play a central role in maintaining luminal lineages during adult homeostasis. Lineage-tracing studies also suggest that luminal cells are sustained predominantly by unipotent LP populations (191–193).

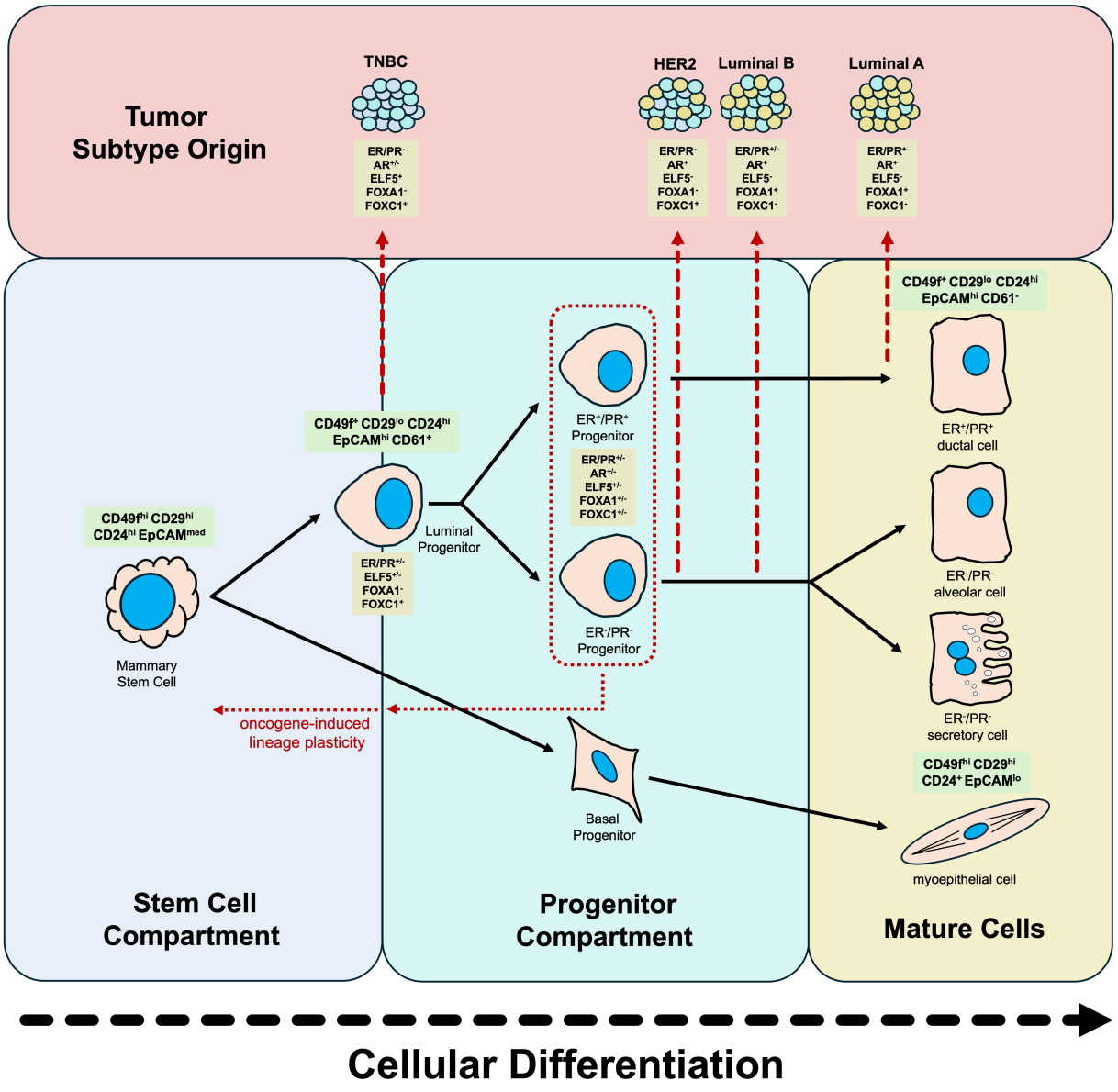

Figure 1.2. Schematic model of epithelial hierarchy in the mammary gland and the respective origin cell population for tumor subtypes. Summary of respective stem, progenitor, and mature cell compartments along the differentiation hierarchy with their associated surface markers for isolation of respective populations. Thick red dotted arrows indicate the hypothesized cells of origin for the major tumor subtypes based on concomitant transcriptional profiles. Thin red dotted arrows indicate the luminal progenitor population that undergoes dedifferentiation under oncogenic insult.

The intrinsic lineage restriction of epithelial cell fate within the mammary gland may be actively regulated by extrinsic signals from neighboring cell populations. Previous lineage tracing experiments have shown that BPs and LPs co-transplanted will only contribute to cells in their respective differentiated lineages in resulting ductal outgrowths (191). However, when BPs are transplanted alone, they are sufficient in generating ductal outgrowths containing cells in both luminal and basal lineages through reactivation of a multipotent state (191,194). This phenomenon has been shown to be mediated, at least in part, by paracrine signalling through luminal cell-expressed tumor necrosis factor (TNF), which restricts reactivation of basal progenitor multipotency under normal conditions (194). Thus, it appears that lineage maintenance within the mammary epithelium is actively maintained through paracrine signalling within the epithelial hierarchy.

1.4.4 Oncogene-induced lineage plasticity

While lineage maintenance is largely preserved under normal physiological conditions, accumulating evidence indicates that cellular fate change and lineage infidelity can be induced by oncogenic insults during malignant transformation. In the case of breast cancer, such dedifferentiation phenomenon have been described in a number of different mouse models (195). For example, *in vivo* lineage-tracing studies have shown that luminal-specific expression of PyMT, Neu, or the PI3K mutant, $PI3KCa^{H1047R}$, results in the emergence of basal-like cells, producing hyperplastic lesions and tumors composed of mixed lineages (196–198). In contrast, oncogene expression exclusively in the basal cells results in partial dedifferentiation into luminal-like cells before giving rise to less aggressive luminal-like tumors (196,197). Importantly, the observed lineage infidelity was demonstrated to occur well in advance of overt tumor formation, suggesting that oncogene-induced reprogramming establishes the cellular heterogeneity that later

characterizes advanced disease. Further studies have also shown that the inactivation of tumor suppressors in the luminal populations results in tumors with mesenchymal features (199,200). Together, these studies support that breast cancer heterogeneity may be a byproduct of lineage promiscuity within the mammary epithelium during malignant transformation. Consequently, such hypotheses would posit that the expression of lineage-specific markers may not be a reliable indicator of the lineage origin of mammary cancers.

1.4.5 Breast cancer cells of origin

Conventionally, expression of cell-specific cytokeratins has been considered to be a byproduct lineage identity, rather than a determinant (184). Thus, rather than solely identifying tumor cell type based on ER/PR/HER2 and cytokeratin expression, pathologists can establish a much more comprehensive cell-of-origin identity by also interrogating lineage specific transcription factors. Indeed, such lineage-determining factors, including GATA3, androgen receptor (AR), forkhead box A1 (FOXA1), ELF5, and forkhead box C1 (FOXC1), have been widely implicated in human breast cancer gene expression clusters (184). The factors GATA3, AR, and FOXA1 commonly associated with the luminal/hormone-responsive lineage frequently associate with the core luminal and HER2-positive breast cancer gene clusters, where higher GATA3 and lower AR expression is observed in the more differentiated luminal cluster (182,184). FOXA1 is an upstream mediator of ER signalling and the subsequent differentiation into the HR^+ lineage (201). Conversely, ELF5 and FOXC1 are key transcription factors in the differentiation of LPs into alveolar lineage and are found at the core of basal-like clusters (202).

To this end, further molecular profiling of human breast cancer subtypes has revealed striking parallels with the normal differentiation hierarchy of the mammary epithelium, supporting

that tumor phenotypes likely reflect the identity of the precursor cells from which they arise (Fig. 1.2) (182,185,203). At the transcriptomic level, MaSC-enriched populations show strong similarities to claudin-low breast cancers, while LP populations exhibit molecular profiles closely aligned with basal-like/TNBC tumors (185,204). In contrast, HER2-positive, luminal A, and luminal B tumors appear to correspond to distinct differentiation states within the luminal lineage, with luminal A tumors, the most differentiated subtype, displaying transcriptional programs most closely resembling mature luminal epithelial cells (182).

In human breast cancer, tumors are conventionally thought to arise from the luminal epithelium-rich terminal duct lobular units (TDLUs) (193,205,206). Accordingly, the most parsimonious explanation for the origin of both luminal and basal-like human breast cancers is from the transformation of LP-rich populations in these structures (184). In contrast to human breast cancers, some models of murine mammary tumors can exhibit myoepithelial differentiation and mixed histologies (184). Historically, such mosaic phenotypes have been interpreted as evidence for transformation within the MaSC compartment (184). However, the previously mentioned lineage-tracing studies on lineage plasticity prior to oncogenic insult support a novel dedifferentiation phenomenon of committed progenitor lineages as a possible mechanism for the lineage heterogeneity observed in murine breast cancers.

Historically, two models have been proposed to justify the biological basis of intertumoral heterogeneity observed across cancers: the genetic mutation model and the cell-of-origin, or cancer stem cell model (193). The genetic mutation model argues that tumor phenotype is dictated by the compounding effect of oncogenic mutations acquired by a cell, whereas the cancer stem cell model proposes that the tumor phenotype reflects intrinsic properties of the transformed cell-of-origin

(193,207). In fact, it seems probable that these two theories can both be true. A longstanding argument favoring stem cells as the cells-of-origin for cancer is that malignant transformation typically requires serial accumulation of genetic mutations, a highly time-intensive process (208). To this end, quiescent, and perhaps asymmetrically dividing cells, such as stem cells, would persist long enough to acquire the mutational burden necessary for transformation. In support of this theory, cancer risk has been shown to correlate with the cumulative number of stem cell divisions required to maintain tissue homeostasis over an organism's lifetime (209). Evidence of such long-lived murine stem/progenitor cell populations, particularly LPs, has recently been demonstrated through lineage-tracing studies, where ER^+ hormone-sensing cells are maintained by quiescent LP populations (191,210,211). Robust LP populations within the luminal lineage have also been shown to be precursory to differentiated alveolar cells and are candidate cells-of-origin in heterogenous tumors following various oncogenic insults (212). Specifically, ELF5 has been shown to regulate these long-lived LP populations (202,213,214). Thus, LPs appear to represent a uniquely vulnerable cell type for oncogenic transformation. Indeed, numerous studies in MMTV-Neu and MMTV-PyMT models have demonstrated that mammary tumors likely originate from LP populations (215–218). Specifically, the cellular fraction harboring the highest degree of tumor-initiating cell (TIC) potential is enriched in the CD61-expressing LP compartment (190,215,217). Other lineage tracing studies have shown that basal-like breast tumors etiologically arise from LPs rather than from basal stem cells, supporting a model of luminal-to-basal reprogramming during tumorigenesis (185,219,220).

While lineage tracing and transcriptomic profiling are informative approaches for identifying prospective cells of origin, oncogene-induced lineage infidelity can complicate the identification of tumor origin. As discussed above, expression of lineage-specific markers does

not reliably indicate the cell-of-origin following malignant transformation. For example, genetic profiling of human basal-like/TNBC tumors closely resemble those of LP populations, and canonical "basal" markers such as CK5 and 17 have been shown to be expressed by luminal epithelial cells within the TDLUs from which most human breast cancers are believed to originate (184,221,222). Thus, functional studies that assess tumor-initiating capacity *in vivo* provide much needed context for efficiently defining tumor-initiating cells-of-origin. An example of such nuance can be observed in a previous study where luminal-specific ablation of p38α, a mediator of the LP population, resulted in repression of luminal programs and induction of basal-like features, all while impairing tumor-initiating capacity (223). Here, the apparent acquisition of basal-like identity does not reliably indicate basal-origin, nor does it equate to enhanced functional stemness as commonly associated with basal-like signatures.

Collectively, these findings support the notion that transcriptional regulators governing progenitors, and thus lineage identity, play a central role in oncogene-induced plasticity within the mammary epithelium. Given the apparent contribution of LPs as cells-of-origin in murine breast cancer, specifically in Neu-, and PyMT-induced tumorigenesis, it is reasonable to posit that targeted disruption of lineage-defining transcriptional programs will affect their responsiveness to malignant transformation and possibly identify novel regulators of HER2/Neu-induced tumorigenesis.

1.5 SOX10 in development, lineage regulation and cancer

1.5.1 SOX family of transcription factors

First identified for their role as testis-determining factors, the sex determining region Y-related high mobility group-box (*SOX*) family of genes are highly conserved transcription factors

implicated in numerous developmental processes (224,225). SOX proteins have established roles in early stem cell-dependent processes including gastrulation, embryogenesis, neural induction, organ formation, and tissue differentiation (226). The SOX group, characterized by a highly homologous sequence specific DNA-binding high mobility group (HMG) domain, consists of twenty different factors categorized into subgroups SOXA through SOXH (227,228). Members of the same subgroup exhibit more than 70% shared amino acid homology and are often implicated in similar biological processes, but share very little sequence identity with members of other groups outside of the conserved HMG domain (226,229). The conserved HMG group recognizes the common consensus motif 5-(A/T)(A/T)CAA(A/T)G-3 and binds to the minor groove of DNA. This results in the bending of regulatory regions facilitating interactions with other factors to form transcriptional complexes (226,228–230). The HMG region is flanked with two nuclear localization signals and one internal nuclear export signal which facilitates nucleocytoplasmic shuttling (231,232). Supporting their importance in development, Sox-like genes have been identified in single celled choanoflagellates, suggesting an origin that precedes multicellularity (226,233).

1.5.2 The SOXE group

One of the most phylogenetically old and well documented groups, SOXE, consists of SOX8, SOX9, and SOX10. SOXE factors are specifically implicated in sex determination (SOX8/9), chondrogenesis (SOX9), melanogenesis (SOX9/10), and neural crest cell development and differentiation (SOX8/9/10) (226,234–238). Their respective expression programs have been shown to exhibit unique, additive, and/or redundant effects on these biological processes (238). The SOXE subgroup is characterized by shared protein interaction (K2), c-terminal transactivation (TA), and dimerization (DIM) domains, the latter of which facilitates homo-, or heterodimerization

with other members of the SOXE family on palindromic Sox motifs (236,238,239). Upon DNA-binding, cooperative action of the transactivating K2 and TA domains leads to transcriptional activation (238).

SOX8 exhibits similar expression patterns to both SOX9 and SOX10 and maintains more prominent roles in adult tissue homeostasis including regulating adipose tissue, Sertoli cells, and central nervous system (CNS) myelination rather than in early cell-fate decisions (240). Due to this apparent functional redundancy, there have been limited studies on SOX8-specific function. Nevertheless, mutational studies on murine Sox8 have established its partial requirement in early developmental processes (241–243). Furthermore, genetic variants and alterations of SOX8 have been linked to multiple sclerosis, familial essential tremor infertility, and worse cancer prognosis (240).

The most functionally diverse member of the SOXE family, SOX9, has been widely studied for its role in sexual determination. Sox9 is sufficient and necessary to drive male determination in pre-Sertoli cells and its inactivation can even induce sex reversal (244–246). Furthermore, Sox9 has been shown to be critical for the chondrogenic process as its deletion in murine limb buds prevents bone and cartilage formation and a loss of expression of chondrogenic factors Sox5 and Sox6 (247,248). Complementary gain-, and loss-of-function studies have also shown that SOX9 is required for the development of embryonic and adult neural stem cells and the multipotent neural crest (NC) cell population in the CNS development (248–250). Due to its apparent function in tissue-specific stem cell maintenance, dysregulation of such states and their subsequent differentiation pathways are logical candidates for malignant transformation. Indeed, SOX9 has been implicated in the formation and growth of tumors in various meso-, endo-, and ectodermal tissues including in prostate, skin, pancreas, CNS, ovary, esophagus, and breast (248).

In murine breast cancer models, it was found that luminal populations exhibited increased Sox9 expression, which has recently been identified as a mediator of luminal-basal plasticity (200,251). Specifically, Sox9 has been shown to cooperate with Slug to drive mammary epithelial plasticity as well as facilitate endocrine treatment resistance through Esr1 silencing (251,252).

1.5.3 Sox10 in development and tissue homeostasis

1.5.3.1 Sox10 in embryonic development

Initially identified in 1993, mouse Sox10 and human SOX10 gene transcripts both encode 466 amino acid peptides that share 92% nucleotide and 98% amino acid sequence homologies, respectively (232,253). Sharing highly overlapping functions with SOX9, the primary function of SOX10 appears to be in the regulation of multipotent progenitor populations where its canonical role has been most extensively characterized in neural crest (NC) lineage maintenance. Sox10 expression is maintained throughout NC cell delamination and migration and mediates subsequent differentiation into numerous cell types including peripheral glial and neuronal cells, pigment, skeletal, and smooth muscle cells, and adult stem cells, among others (254–257). Human patients and mice exhibiting Sox10 dysfunction present with various NC-derived melanocyte, enteric, and peripheral nervous system abnormalities collectively referred to as neurocristopathies (e.g. Waardenburg syndrome and Hirschsprung disease) (254,258–261).

1.5.3.2 Sox10 transcriptional control and downstream signalling

Although the role of Sox10 in developmental processes has been well defined, the current understanding of regulatory pathways that drive Sox10 expression, as well as its downstream target genes, remains elusive (Fig. 1.3). Fourteen multiple-species conserved sequences (MCS)

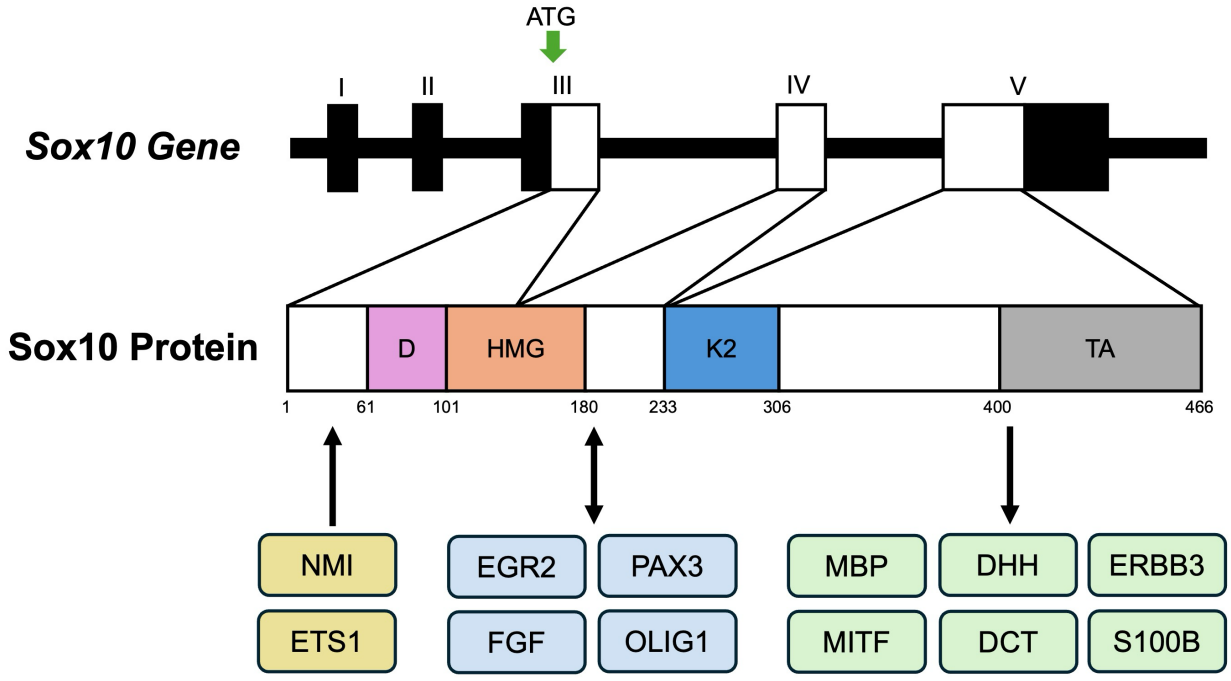

Figure 1.3. Sox10 and its upstream and downstream targets. Schematic representation of the murine Sox10 gene and encoded protein domains. Transcriptional regulators of Sox10 include NMI, ETS1. Sox10 mutual activators include EGR2, PAX3, FGF, and OLIG1. Sox10 target genes include MBP, DHH, ERBB3, MITF, DCT, and S100B. The Dimerization (D), High Mobility Group (HMG) DNA-binding domain, K2 transactivation domain, and C-terminal transactivation (TA) region are shown.

controlling *Sox10* have been identified, two of which (MCS4 and MCS7) exhibit specific expression patterns that overlap with endogenous Sox10 expression in the CNS (262). These elements contain dimeric SoxE binding sites which are required for functional enhancer activity of these sequences, suggesting a SoxE-dependent regulation of *Sox10* itself (262). Although some studies have demonstrated that Sox9 can induce *Sox10*, others have reported mutual repression in certain contexts (263–265). Indeed, we have demonstrated in MMTV-NDL cell lines that Sox10 expression is dependent on phosphorylated Sox9 which was shown to be directly bound to a -7kb enhancer element upstream of the *Sox10* TSS (266). Fibroblast growth factor (FGF) signalling, specifically FGF10 signalling through FGF receptors (FGFR), has been shown to regulate Sox10 expression in NC-based developmental processes as well as in ocular organs and mammary epithelial cells (263,267,268). Supporting this, FGFR inhibition reduces Sox10 expression in LP derived organoids and reduces their functional stem/progenitor cell activity (267). Sox9 ablation reduces FGFR-mediated signalling by downregulating the expression of several FGF-pathway target genes, suggesting a mutual feedback mechanism between FGF and Sox9-dependent modulation of Sox10 expression (263). Furthermore, the ETS proto-oncogene 1 (Ets1), which has diverse roles in cancer biology, has been shown to interact with *Sox10* during melanocyte differentiation through activation of the MCS4 enhancer (269,270).

Other established Sox10 co-factors include N-myc interactor (Nmi), oligodendrocyte transcription factor-1 (OLIG1), paired box gene 3 (PAX3) and microphthalmia-associated transcription factor (MITF) in various NC-based processes (268). Interestingly, SOX10/MITF represents a key axis in NC lineage development and dysregulation of this SOX10-MITF signalling pathway has been implicated in melanomagmenesis (271). Other genes that appear to be directly regulated by Sox10 are myelin basic protein (MBP), dopachrome tautomerase (DCT), desert hedgehog (DHH), S100b,

Early growth response-2 (Egr2), as well as the Egfr family member Erbb3 (268,272,273). Specifically, Sox10 maintains neural crest progenitor competence by sustaining Erbb3/Nrg-1 signalling and preventing Bmp2-mediated loss of neuronal and glial differentiation potential (274,275). Notably, the regulation of Erbb3 by Sox10 suggests an interplay between Sox10-dependent progenitor competence and Egfr family signalling.

1.5.3.3 Sox10 in murine mammary gland homeostasis

Although Sox10 exhibits overlapping expression profiles with Sox9 during certain developmental processes, unlike Sox9, Sox10 expression is retained in select tissues following NC delamination in the developing embryo. As a result, its expression in postnatal tissue homeostasis is largely sustained, a specific example being in the postnatal mammary epithelium (254). Upon induction of branching morphogenesis in ductal rudiments, early epithelial transcriptomic programs are silenced and replaced with later branching programs (276,277). Indeed, Sox10 appears to belong to this latter group as demonstrated by recent studies showing that Sox10 expression is undetectable at embryonic day E13.5, but increases drastically by E16.5 (276). Consistent with this temporal regulation, mammary epithelium-specific Sox10-deficient mice develop mammary rudiments, but fail to undergo extensive branching morphogenesis and fat pad invasion during puberty, further supporting its requirement in normal postnatal processes (278). In contrast to Sox10, Wnt/β-catenin signalling is largely downregulated at the onset of ductal branching in late embryogenesis (276). Thus, in mice expressing stabilized β-catenin, E16.5 embryos exhibit compromised mammary rudiment branching accompanied with lack of Sox10 induction, suggesting that suppressed Wnt/β-catenin is necessary for Sox10 upregulation (276,277).

While Sox10-associated transcriptional programs have been identified, attempts to characterize its precise role in the postnatal mammary epithelium have only recently been undertaken. Sox10 has been found to mark mammary epithelial cell populations exhibiting the highest degree of stem/progenitor activity, including both fetal and adult cells *in vivo* and in organoid systems *in vitro* (267). Within the adult luminal compartment, $Sox10^+$ pan-luminal cells exclusively demarcate the LP population, while the more differentiated HR^+ mature luminal cells are exclusively $Sox10^-$. Importantly, it appears that Sox10 is a functional requirement in these stem/progenitor populations as its deletion results in reduced progenitor activity that can be increased upon its overexpression (267). Further lending to this functional requirement, transplantation of $Sox10^+$ fetal MaSCs are able to reconstitute cleared mammary fat pads, while Sox10-deficient variants fail to do so (267). Subsequent mechanistic studies showed that Sox10 directly binds to the promoter region of the genes that regulate stem/progenitor cell maintenance and epithelial plasticity (279).

Together, these observations support a model in which Sox10 functions to actively maintain progenitor competence during postnatal ductal morphogenic events. Given that mammary stem and progenitor populations are widely implicated as cells-of-origin in breast cancers, it is not unreasonable to position Sox10 as a potential driver of functional competence during malignant transformation.

1.5.4 Sox10 as an oncogenic marker

Currently, the role of Sox10 in cancer biology remains elusive and controversial with different observations reported across several types of cancer (268,280). Supporting its role in melanocyte differentiation, tumors of the skin and soft tissue were the first to establish SOX10 as a marker for cancer (281). Since then, SOX10 has been identified as a biomarker for

basal/myoepithelial based carcinomas, including those of the salivary gland and TNBCs (216,282–288). Specifically, it appears that high expression of SOX10 is found in 30-40% of TNBC cases (287,288). Although its precise biological function in these cancers remains unclear, it appears that SOX10 contributes to the malignancy of TNBC cells *in vitro* by modulating the epithelial-mesenchymal transition (EMT) pathway (286). Others have reported that in murine models of basal-like mammary tumorigenesis, Sox10-expressing tumors exhibit a de-differentiated, mesenchymal-like phenotype (279). Sox10 haploinsufficiency in C3-TAg mice, a model of basal-like breast cancer, significantly prolongs survival, further implicating Sox10 in basal-like breast cancer progression. Recent analyses of human TNBC samples have revealed extensive rewiring of SOX10-associated transcriptional programs commonly associated with LPs which lead to a more dedifferentiated NC-like state (289). The observed rewiring events correlate with epigenetic erosion events leading to promoter hypomethylation, particularly at lineage-defining CpG-island sites. Progressive epigenetic erosion in $SOX10^{+}$ tumor-initiating cells may therefore facilitate NC-like reprogramming events lending to the poor clinical outcomes associated with $Sox10^{+}$ TNBC (289). Supporting this notion, it has been demonstrated that SOX10 is sufficient to reprogram human fibroblasts into induced NC cells when combined with epigenetic modifiers (290). These findings support a model where Sox10 expression in basal-like breast cancers may be the result of increased cellular adaptability from the reactivation of primitive developmental programs under oncogenic insult. As a critical stem/progenitor cell regulator, Sox10 may also act as a gatekeeper of "transformation competence" in LP populations.

While Sox10 appears to be functionally implicated in basal-like breast cancers, the current body of evidence for its role in HER2/Neu-induced tumorigenesis is limited. We have recently demonstrated that approximately 15% of The Cancer Genome Atlas (TCGA)-sourced HER2-

positive breast cancers exhibit high SOX10 expression (266). Consistent with this, others have shown substantial variability in the proportions of $SOX10^{+}$ populations (2%-79%) among HER2-positive tumor samples (291–295). Interestingly, $SOX10^{hi}$ cohorts were associated with a stem-like phenotype and worse prognosis, suggesting that $SOX10^{+}$/HER2-positive tumors represent a more aggressive de-differentiated subtype (291,293,294). Finally, we have shown that the tumorigenic capacity of MMTV-NIC derived tumors and cell lines correlates with Sox10 expression (294).

Importantly, these findings suggest that while Sox10 expression may correlate with increased HER2/Neu-induced tumorigenicity, it is unclear whether its activity itself is required to sustain functional tumor-initiating capacity, or if it merely demarcates a plastic transcriptional state during malignant transformation.

1.6 Rationale, Objectives, and Hypothesis

SOX10 has been implicated as a determinant of NC specification, lineage plasticity, and maintenance of stem/progenitor competence. In the mouse mammary gland, Sox10 influences ductal morphogenesis and epithelial differentiation and marks mammary stem and LP populations. Upon oncogenic insult, SOX10 has been repeatedly associated with aggressive, basal-like breast cancers with poor clinical outcomes. Finally, SOX10 has recently been associated with more aggressive, de-differentiated instances of $HER2^{+}$ breast cancers.

Despite these observations, a few fundamental questions remain: how does Sox10 specifically govern mammary epithelial progenitor populations? And does this regulation confer tumor-initiating capacity, or does it merely reflect a plastic transcriptional state? An attempt to address these questions, particularly in the context of HER2/Neu-driven tumorigenesis, will be put forward in this thesis. Employing a combination of luminal-restricted genetic models and

complementary *in vitro* approaches, we aimed to further elucidate the role of Sox10 in mammary development, tumor initiation, and luminal lineage maintenance. We believe that Sox10 functionally defines the LP compartment which is required for the establishment and maintenance of a tumor-initiating competent state. Thus, our global hypothesis was that luminal-specific ablation of Sox10 would result in developmental defects and hindered HER2/Neu-induced mammary tumorigenesis.

In Chapter 3, we aimed to define Sox10's role specifically in luminal-associated lineage maintenance and mammary gland development. It was revealed that luminal Sox10 is required, at least in part, for efficient mammary gland development, and that loss of luminal Sox10 directly depletes the LP population, indicating a requirement for Sox10 in maintaining progenitor competence during normal epithelial homeostasis.

In Chapter 4, we wanted to address whether tumor initiation and progression from HER2/Neu-induced transformation of the luminal epithelial compartment is Sox10-dependent. We demonstrated that Sox10 is crucial for malignant transformation of the luminal epithelium *in vivo* and that tumor initiation, progression and dissemination to secondary sites is completely abrogated upon Sox10 deletion.

Finally, in Chapter 5, we assessed whether Sox10 regulates functional stemness or plasticity in the luminal epithelial lineage following malignant transformation. It was found that loss of Sox10 results in transcriptional reprogramming leading to erosion of programs sustaining luminal identity and subsequent collapse of tumor-initiating activity.

Chapter 2: Materials and Methods

2.1 Animal care and experiments

2.1.1 Animal husbandry

All animal experimental procedures were pre-approved and conducted in accordance with University of Ottawa Animal Care and Veterinary Service guidelines. Rosa26R-LacZ, MMTV-NDL, MMTV-NIC, MMTV-Cre, MMTV-rtTA and tetO-MIC transgenic mice were generously provided by Dr. William Muller (McGill University) and Lewis Chodosh (MMTV-rtTA; U Penn), while Sox10$^{fl/fl}$ mice were a kind gift from Dr. Michael Wegner (Friedrich-Alexander-Universität, Germany). Other than immune compromised hosts, all mice were maintained in an FVB/n background. Founder NCG mice were purchased from Jackson Laboratories and bred in-house. All pups were weaned at P21, and breeder females were retired after five litters. Any females harboring transgenic alleles leading to spontaneous mammary transformation (MMTV-NIC and MMTV-NDL) were not used as breeders.

2.1.2 Genotyping

Genotyping was performed using DNA extracted from ear notches collected at the time of weaning using the DNeasy Blood & Tissue Kit (Qiagen, Cat. No:69504) as per manufacturer's protocol. PCR was performed using REDTaq DNA Polymerase (VWR, Cat. No:76620-472). DNA amplification was carried out as follows: denaturation at 95˚C for 5 mins, then 35 cycles of denaturation at 95˚C for 30 seconds, annealing at 58-62˚C for 30 seconds, and elongation at 72˚C for 45 seconds, and a final elongation step of 72˚C for 3 minutes. PCR reaction mixtures were ran on a 1% agarose gel containing 1:20,000 RedSafe (FroggaBio, Cat. No:21141) and DNA standard ladder (FroggaBio, Cat. No:DM001-R500-G) until sufficient band separation was achieved. Primer sequences and annealing conditions are listed in Table 2.1.

2.1.3 Tumor models

For survival studies of spontaneous tumor models, MMTV-NIC, and MMTV-NDL females were monitored twice weekly for tumor development starting at 16-weeks of age. Tumor onset was defined by a total tumor burden of 5 mm^3, and progression was tracked until endpoint of 17 mm^3, at which time mice were euthanized and tumors collected. For hyperplasia analysis, NIC females were sacrificed at 16-, and 24-weeks of age.

Onset and endpoint tumor volumes were defined by the University of Ottawa Animal Care and Veterinary Service guidelines. Tumor volume was calculated using the formula $4/3\pi r^3$. For MMTV-rtTA:tetO-MIC studies, experimental and control female mice of at least 8-weeks of age were given irradiated drinking water in dark water bottles containing 3.9 mM doxycycline which were changed once weekly. Treated mice were monitored for mammary tumor formation via abdominal palpation twice weekly following doxycycline induction and euthanized at endpoint.

2.1.4 Orthotopic injections

For orthotopic injection studies, 10^3, 10^4, 10^5, or 10^6 cells were resuspended in a 1:1 PBS:Matrigel mixture and injected as 100µL fractions into the third or fourth mammary gland of 12-, to 16-week-old female NCG mice. Right flanks were used for experimental injections, whereas left flanks were used for PBS:Matrigel only controls. Tumor development was monitored twice weekly by palpation until endpoint was reached. All animals of the same cohort were euthanized once the first mouse reached 17 mm^3.

2.1.5 Intravenous injections

For intravenous tail vein injections, 10^6 cells were resuspended in PBS and injected into the left or right lateral tail vein of 12-, to 16-week-old female NCG mice. Mice were monitored

twice weekly for changes in body weight, respiration rate, and behavioral changes such as hunched posture and lack of grooming until the end of the 28-day study period.

2.2 Histology

2.2.1 Mammary gland whole mounting

Fourth inguinal mammary glands were harvested and dry-mounted on glass slides. Glands were then defatted in 100% acetone for 7 days, stained in hematoxylin overnight, and subsequently destained in 70% EtOH:1% HCl for 48-72 hours. Glands were then dehydrated in 100% ethanol (2 x 30 minutes) followed by xylene overnight. Stained and dehydrated glands were then mounted using Permount™ mounting medium (Fisher, Cat. No:SP15-100) and imaged using a ZEISS™ Axioscan 7 microscope and analyzed with Zen 2.3 software. Absolute numbers of epithelial end bud and ductal branch points were enumerated for each gland using FIJI's manual cell counter function. Fat pad invasion was determined by measuring the distance from the origin of the mammary ductal tree to the furthest epithelial end bud and dividing this length by the distance from origin of mammary ductal rudiment to the most distant fat pad boundary. Respective lengths were determined using FIJI.

2.2.2 X-gal staining

Fourth inguinal mammary glands from euthanized female MMTV-Cre Rosa26R-LacZ transgenic mice were dry-mounted on glass slides. Glands were fixed in 1% formaldehyde:0.5% glutaraldehyde:PBS for 30 minutes and then washed in 0.02% NP40: 0.01% Na-Deoxycholate: 2 mM $MgCl_2$:PBS detergent buffer (3 x 5 minutes). Tissues were incubated overnight in detergent buffer supplemented with 2.45 mM X-gal, 5 mM $K_3Fe(CN)_5$, 5 mM $K_4Fe(CN)_6$, and 1 mM EGTA with gentle agitation overnight and protected from light. Glands were destained with serial PBS

washes until solution ran clear. Glands were then mounted using Permount™ mounting medium (Fisher, Cat. No:SP15-100) and imaged using a ZEISS™ Axioscan 7 microscope and analyzed with Zen 2.3 software.

2.2.3 Tissue processing, embedding and sectioning

Fourth inguinal mammary glands were harvested from euthanized female mice and fixed in 10% buffered formalin for 72 hours. Fixed glands were then washed in PBS (3 × 5 min) and stored in 70% ethanol at 4°C until processing. Paraffin embedding and sectioning (4 μm thickness) were performed by the University of Ottawa Pathology Core facility.

2.2.4 Immunohistochemistry and immunofluorescence

FFPE sections were deparaffinized in xylene (3 x 5 minutes) and serially rehydrated in 100% EtOH (2 x 5 minutes), 95% EtOH (2 x 5 minutes), 80% EtOH (1 x 5 minutes), and 70% EtOH (1 x 5 minutes) before undergoing antigen retrieval in 10 mM sodium citrate buffer (pH 6.0) in a pressure cooker for 10 minutes. Sections were slowly cooled to room temperature and subsequently quenched of endogenous peroxidase activity using 3% hydrogen peroxide (Sigma, Cat. No:H1009) for 15 minutes. Sections were then permeabilized and blocked using 0.1% Tween, 0.05% NP-40, 1% BSA in PBS for 15 minutes and incubated overnight at 4°C with the indicated primary antibodies (Table 2.1) in 5% goat serum (Abcam, Cat. No:ab7481) in PBS.

For immunohistochemistry, sections were then washed in PBS (3 x 5 minutes) and incubated with SignalStain® Boost IHC Detection Reagent (NEB, Cat. No:8125S/8114S) for one hour at room temperature. Sections were washed again and probed with Vector DAB Peroxidase Substrate Kit (MJS BioLynx, Cat. No:VECTSK4100), followed by hematoxylin/eosin counterstaining. Sections were dehydrated using 70% EtOH (1 x 5 minutes), 80% EtOH (1 x 5

minutes), 95% EtOH (2 x 5 minutes), 100% EtOH (2 x 5 minutes), and finally xylene (3 x 5 minutes). Sections were then mounted using Permount™ mounting medium (Fisher, Cat. No:SP15-100) and imaged using a ZEISS™ Axioscan 7 microscope and analyzed with Zen 2.3 software.

For immunofluorescence, sections incubated with primary antibodies were washed in PBS (3 x 5 minutes) and incubated with Alexa Fluor-conjugated secondary antibodies (1:1000, Invitrogen; Table 2.2) and counterstained with DAPI (1:5000, ThermoFisher, Cat. No:D1306). Sections were mounted and imaged using a ZEISS™ Axio Imager 2 microscope with Zen 3.3 software.

2.3 Cell culture

2.3.1 Cell line isolation

Tumor-bearing female MMTV-NDL mice were sacrificed at endpoint. Tumors were removed and mechanically dissociated using a scalpel. The resulting tissue slurry was incubated overnight at 37°C in Gentle Collagenase/Hyaluronidase digestion medium (1:10 in DMEM; StemCell Technologies, Cat. No:7919). Following brief trituration, cells were pelleted (400 × g, 4 min, 4°C) and red blood cells were lysed in ACK buffer (50 mM NH_4Cl, 10 mM $KHCO_3$, 0.1 mM EDTA, pH 7.2-7.4) for 5 min on ice. Cells were pelleted, resuspended in 32.3 µM DNase I (Sigma, Cat. No:10104159001) and passed through a 40 µm strainer to obtain a single-cell suspension. Lineage-negative (Lin^-) cells were isolated using the Mouse Mammary Stem Cell Enrichment Kit (StemCell Technologies, Cat. No:19757), according to the manufacturer's protocol. Cells were resuspended and plated in NDL culture medium (1:1 mix of DMEM (Corning, Cat No: 17-207-CV) and Ham's F-12 (ThermoFisher, Cat. No:11765070) supplemented with 10% FBS (Corning,

Cat. No:35-016-CV), 1.3 nM IGF (ThermoFisher, Cat. No:PHG0071), 0.484 nM EGF (ThermoFisher, Cat. No:PHG0311), 10 µg/mL BPE (ThermoFisher, Cat. No:13028014), 1.38 µM hydrocortisone (ThermoFisher, Cat. No:A16292.03), 1% Pen/Strep (ThermoFisher, Cat. No:15140122), and 1% L-glutamine (ThermoFisher, Cat. No:25030081). Media was replaced daily until a doubling time of 24 hours was reached. Cells were then used for downstream experimental studies.

2.3.2 Routine cell culture

All primary murine cell lines isolated from MMTV-NDL tumors were cultured in NDL medium. Human lines were cultured in DMEM (Corning, Cat No: 17-207-CV) supplemented with 10% FBS (Corning, Cat. No:35-016-CV), 1% Pen/Strep (ThermoFisher, Cat. No:15140122), and 1% L-glutamine (ThermoFisher, Cat. No:25030081). Primary murine cell lines were used within 20 passages of initial isolation. All cell lines were incubated in a humidified incubator set to 37˚C and 5% CO_2. Routine passaging was carried out as follows: spent cell media was aspirated and cells were washed in PBS and then incubated with 0.25% Trypsin, 2.21 mM EDTA in PBS (Fisher, Cat. No:MT25053CI) at 37˚C for 5 minutes or until cell detachment. Trypsin was inactivated by adding FBS containing medium at a 5: 1 media: trypsin ratio. Cell suspension aliquots were diluted 1:1 with trypan blue and counted using a hemacytometer. Live cells were seeded at 2.5 x 10^5 to 1 x 10^6 cells depending on the cell line.

2.3.3 Mycoplasma testing

Cell lines were routinely checked for mycoplasma contamination by taking 2 µL aliquots of depleted media for PCR-based detection. PCR was performed using REDTaq DNA Polymerase (VWR, Cat. No:76620-472) as per manufacturer's protocol using media aliquots as template DNA.

DNA amplification was carried out as follows: denaturation at 95˚C for 5 mins, then 40 cycles of denaturation at 95˚C for 30 seconds, annealing at 58˚C for 30 seconds, and elongation at 72˚C for 45 seconds, and a final elongation step of 72˚C for 3 minutes. PCR reaction mixtures were ran on a 1% agarose gel containing 1:20,000 RedSafe (FroggaBio, Cat. No:21141) and DNA standard ladder (FroggaBio, Cat. No:DM001-R500-G) until sufficient band separation was achieved. Primer sequences are listed in Table 2.1.

2.3.4 CRISPR-Cas9 mediated Sox10 inactivation

For CRISPR-Cas9 mediated Sox10 inactivation, guide RNAs targeting upstream and inside of the Sox10 ORF in exons 2 and 3, respectively, were designed using Benchling (Benchling.com). Annealed oligos (Table 2.1) were cloned into BsmBI-digested pLKO-H2B-mRFP-2A-puro (gift from Dr. Daniel Schramek, University of Toronto). Annealing was performed in a thermocycler: 37°C for 30 min, 95°C for 5 min, then ramped down by 5°C per min to 25°C.

To generate Cas9-expressing lentivirus, 5×10^6 HEK-293T cells were co-transfected with 10 µg pLenti-Cas9-Blast (Addgene, Cat. No: 52962), 8 µg pCMV-dR8.2-dVPR (Addgene, Cat. No:8455), and 2 µg pCMV-VSV-G (Addgene, Cat. No:8454) using Lipofectamine 3000 (ThermoFisher, Cat. No:L3000001) as per manufacturer's protocol. Media was replaced 12 hours post-transfection and viral supernatant collected at 72 hours was then filtered through a 0.4 µm strainer. Target MMTV-NDL cell lines were transduced overnight with viral supernatant in the presence of 10 µg/mL polybrene and replaced with fresh media in the morning. 48 hours post-transduction, cells were selected in 10.9 µM blasticidin for 4 days. For guide expression, selected cells were subsequently transduced with the pLKO-H2B-mRFP-2A-puro plasmid containing Sox10-targeting sgRNA guides and RFP^+ cells were flow sorted using a Sony MA900. Cas9 expression and Sox10 knockout efficiency were confirmed by Western blot.

2.3.5 Sanger sequencing

To assess the nature of indels following CRISPR-Cas9-mediated Sox10 inactivation, genomic DNA was isolated from cell cultures using the DNeasy Blood & Tissue Kit (Qiagen, Cat. No:69504) and primers flanking exons 2 and 3 were used to PCR amplify the targeted region. Amplified products were subsequently cleaned up using the QIAquick PCR Purification Kit (Qiagen, Cat. No:28104) and 1 ng/µL of amplicon were mixed with 2µM of upstream forward primers for sanger sequencing using an Applied Biosystems 3730XL DNA Analyzer . Sanger sequencing was ran by the Ottawa Hospital Research Institute StemCore Laboratory Facility.

2.3.6 Immunocytochemistry

Cell lines were grown on uncoated coverslips until desired confluency was reached. Coverslips were washed with PBS and fixed with 4% paraformaldehyde for 10 min at room temperature. Cells were then permeabilized and blocked using 0.1% Tween, 0.05% NP-40, 1% BSA in PBS for 15 minutes and then incubated overnight at 4°C with the indicated primary antibodies (Table 2.2) in 5% goat serum (Abcam, Cat. No:ab7481) in PBS. Coverslips were washed in PBS (3 × 5 minutes) and then incubated with Alexa Fluor-conjugated secondary antibodies (1:1000, Invitrogen; see Table 2.2) for 1 hour at room temperature. Cells were then counterstained with DAPI (1:5000, ThermoFisher, Cat. No:D1306) for 5 min and washed again. Coverslips were mounted on slides using Dako Fluorescence Mounting Medium (Agilent, Cat. No:S302380) and imaged using a ZEISS™ Axio Imager 2 microscope with Zen 2.3 software.

2.3.7 Proliferation assay

$2.5x10^4$ cells were plated in 6-well plate and grown for 24-, 48-, 72-, and 96-hours. Media was collected and cells were trypsinized, pelleted (400 × g, 4 min, RT) and resuspended in 1.5 mL

of PBS. Absolute cell numbers were counted using trypan blue exclusion Vi-Cell cell counter (Beckman Coulter). Each cell line was seeded in three technical replicates for each time point and repeated as three independent experiments.

2.3.8 Haptotactic Boyden chamber migration assay

Cultures were serum starved overnight the day prior to seeding the assay. The next morning $5x10^4$ cells in 400 µL were seeded in the upper chamber of 10 ug/mL rat tail type I Collagen (VWR, Cat. No:354236) coated 8 µm pore Corning™ Transwell™ inserts (Corning, Cat. No:07-200-150) containing 1% FBS DMEM/F12. Lower chambers were also filled with 400 µL of the same media. 4 hours post-seeding, membranes were washed in PBS (3 x 1 minute) and fixed for 10 minutes in 4% PFA. Residual cells on the top membrane that did not migrate were removed using a cotton tipped applicator. After a second wash, membranes were cut out of the inserts and mounted with Prolong™ Gold Antifade Mountant with DNA Stain DAPI (ThermoFisher, Cat. No:P36931). Absolute cell numbers were counted using a ZEISS™ Axioscan™ 7 microscope and analyzed with Zen™ 2.3 software.

2.3.9 3-Dimensional invasion assay

To form tumor spheres, 96-well v-bottom plates (Fisher, Cat. No:NC0068972) were coated with 5 mg/mL Poly-HEMA (Sigma, Cat. No:P3932-10G) in 95%EtOH by adding 60uL per well and left to evaporate overnight. 5 x 10^3 cells were added to each well and placed on an orbital shaker and incubated at 37˚C for 48-hours. Spheres were lifted off agarose by gently pipetting off 10 µL of media containing the single sphere. Each sphere was then resuspended in 40 µL of 1:1 Matrigel:Collagen type I mixture and plated into the center of a 24-well plate and incubated at 37˚C for 30 minutes until solidified. Suspended sphere droplets were then covered with 2% FBS

DMEM/F12 and cultured for 7 days. Spheroids were imaged every 24-hours using an EVOS™ M5000 (Invitrogen, Cat. No:AMF5000SV).

2.3.10 Mammosphere forming assay

For primary mammospheres, 2×10^3 cells were seeded into ultra-low-attachment 24-well plates (Sigma-Aldrich, Cat. No:CLS3473) in 1:1 DMEM:F12 supplemented with Mammary Epithelial Growth Supplement (ThermoFisher, Cat. No:S0155) and B-27 (ThermoFisher, Cat. No:17504044) and cultured for 7 days. Spheres ≥ 50 μm in diameter were enumerated, pooled, and pelleted at 120 × g for 5 min. Sphere pellets were trypsinized for 10 minutes at 37°C and mechanically dissociated by passing through a 25-gauge needle three times. For secondary mammospheres, single-cell suspensions were counted using a hemacytometer and reseeded using the same conditions as for primary spheres. Cells were seeded at clonal density, cultured for 7 days, and spheres were subsequently enumerated.

2.4 RNA expression

2.4.1 RNA isolation

For fresh tissue, sections were excised from euthanized animals and homogenized in 1 mL of TRIzol (ThermoFisher, Cat. No:15596026) using a handheld tissue homogenizer. For cell lines, culture medium was aspirated and cells were immediately detached in 1 mL TRIzol using a cell scraper. Following incubation at room temperature for 10 minute, 200 μL of chloroform was added to the sample solution and shaken vigorously for 15 seconds and then again incubated at room temperature for 5 minutes. Samples were centrifuged at 12,000 x g for 15 minutes at 4˚C for phase separation. The upper aqueous phase was transferred to a new tube and RNA was precipitated out of solution by adding 500 μL of isopropanol and incubated for 10 minutes at room temperature.

RNA was then pelleted at 12,000 x g for 10 minutes at 4˚C, washed with 70% EtOH, and subsequently centrifuged at 7,500 x g for 5 minutes at room temperature. EtOH was aspirated off and pellets were left to dry for 10 minutes at room temperature and then resuspended in 50 µL of RNase-free water. Samples were then cleaned of DNA using the RNeasy Kit™ (Qiagen, Cat. No:74104) as per manufacturer's protocol. RNA concentrations were determined using a Nanodrop™ Spectrophotometer (Fisher, Cat. No:13-400-518).

2.4.2 First strand cDNA synthesis

For first strand cDNA synthesis, 500 ng of DNase treated RNA, 50 ng of random primers (ThermoFisher, Cat. No:48190011), 250 ng of oligo(dT)$_{12\text{-}18}$ (ThermoFisher, Cat. No:18418012) and 10 nM of dNTP (ThermoFisher, Cat. No:R0181) was brought to a volume of 13 µL in RNase-free water and incubated at 65°C for 5 minutes. To complete reverse transcription, 4 µL of 5X First Strand Buffer, 1 µL of RNaseOUT (ThermoFisher, Cat. No:10777019) , 1 µL of 0.1 M DTT, and 1 µL of SuperScript™ III Reverse Transcriptase (ThermoFisher, Cat. No:18080044) were added to the reaction mixture and incubated at 25°C for 5 minutes, 55°C for 60 minutes and 70°C for 15 minutes. The 20 µL reaction mixtures were then diluted to 200 µL in nuclease-free water.

2.4.3 Quantitative PCR.

For RT-qPCR analysis, a mastermix was set up containing the following: 17.5 µL of 2X iTaq Universal SYBR Green Supermix (BioRad, Cat. No:1725124), 2.1 µL of indicated primers at 10µM, 3.5 µL of cDNA and 11.9 µL of nuclease-free water. 10 µL from each mastermix was added to triplicate wells in a 96-well qPCR plate. RT-qPCR was performed using an Applied Biosystems 7500 Real-Time Fast PCR thermocycler as follows: initial denaturation at 95°C for 10 minutes, followed by 40 cycles of denaturation at 95°C for 15 seconds, and annealing and

extension at 60°C for 60 seconds. Relative mRNA expression was calculated using the ΔΔCT method and normalizing to total levels of ribosomal 18S. The primers used for RT-qPCR can be found in Table 2.1.

2.5 Protein expression

2.5.1 Western blotting

Protein lysates were prepared from either cultured cell lines or freshly resected tumor tissue. Samples were washed in ice-cold PBS, then homogenized and lysed in RIPA buffer supplemented with protease and phosphatase inhibitors (0.05% SDS, 1% Triton X-100, 1% NP-40, 50 mM Tris-HCl pH 7.5, 150 mM NaCl, 2 mM EDTA pH 8.0, 12 mM sodium deoxycholate, 10 mM NaF, 1 mM DTT, 10 mM β-glycerophosphate, 0.6 mM sodium orthovanadate, 1 mM PMSF, 10 μg/mL leupeptin, 10 μg/mL aprotinin, 10 μg/mL pepstatin, and 100 μM benzamide). Samples were lysed on ice for 30 minutes with intermittent vortexing every 5 minutes followed by snap freezing at -80˚C. Cell debris was removed by centrifugation at 14,000 × g for 10 minutes at 4°C, and the resulting supernatant was collected for protein quantification.

Protein concentration was determined using the Bio-Rad Protein Assay Dye Reagent Concentrate (Bio-Rad, Cat. No:5000006). A total of 28 μg of protein was denatured at 100°C for 5 minutes in RIPA buffer containing 4× SDS sample buffer (0.2 M Tris pH 7.4, 0.4 M DTT, 8% SDS, 40% glycerol, 6 mM bromophenol blue). Proteins were resolved by SDS-PAGE on 8% polyacrylamide gels in 1x SDS running buffer (25 mM Tris-HCl, 192 mM glycine and 0.1% SDS) at 50 mA for 45 minutes. Gels were transferred to PVDF membranes in 1X transfer buffer (48 mM Tris-HCl, 39 mM glycine and 20% methanol) at 100V for 90 minutes. Membranes were blocked in 5% BSA in TBS-T (50 mM Tris, pH 7.4, 150 mM NaCl, 0.05% Tween 20) and incubated

overnight at 4°C with primary antibodies (see Table 2.2). After being washed in TBS-T (3 x 5 min), membranes were incubated for 1 hour at room temperature with HRP-conjugated goat anti-host IgG secondary antibody (Bio-Rad, Cat. No:1706515 or 1706516). Following additional washes, protein detection was performed using Clarity Western ECL Substrate (Bio-Rad, Cat. No:1705061). Chemiluminescent signals were visualized using the Bio-Rad ChemiDoc™ Imaging System (Bio-Rad, Cat. No:12003153).

2.5.2 Flow cytometry

Fourth inguinal mammary glands were pooled and digested overnight at 37 °C in Gentle Collagenase/Hyaluronidase digestion medium (1:10 in 5% serum DMEM, StemCell Technologies, Cat. No:7919). Following red blood cell lysis in ACK buffer, cells were pelleted, resuspended in 32.3 μM DNase I (Sigma, Cat. No:10104159001) and passed through a 40 μm strainer to obtain a single-cell suspension.

Cells were sequentially incubated with Zombie NIR viability dye (BioLegend, Cat. No:423106; 1:500) and TruStain FcX (anti-mouse CD16/32) Fc Block (BioLegend, Cat. No:101320; 1:200), each for 20 minutes with washes in 1% BSA/PBS between steps. Surface staining was then performed using the following antibodies: biotinylated Ter-119 (BioLegend, Cat. No:116203; 1:200), CD31 (BioLegend, Cat. No:102503; 1:200), CD45 (BioLegend, Cat. No:103103; 1:200), and Ly-51 (BioLegend, Cat. No:108303; 1:200); Brilliant Violet 421-conjugated CD49f (BioLegend, Cat. No:313623; 1:400); PE-Dazzle 594-conjugated CD61 (BioLegend, Cat. No:104321; 1:200); PerCP/Cyanine5.5-conjugated CD24 (BioLegend, Cat. No:101823; 1:200); and Brilliant Violet 711 streptavidin (BioLegend, Cat. No:405241; 1:400) for secondary detection of biotinylated antibodies. Flow cytometry acquisition was performed on a Cytek Aurora spectral cytometer.

For cell line staining, the following antibodies were used: Brilliant Violet 421-conjugated CD49f (BioLegend, Cat. No:313623; 1:400), Brilliant Violet 421-conjugated CD66a (BioLegend, Cat. No:134531; 1:200), and Alexa Fluor 647-conjugated CD326 (BioLegend, Cat. No:118212; 1:400). Antibody surface flow cytometry acquisition was performed on a Cytek Aurora spectral cytometer.

For RFP sorting following CRISPR/Cas9 inactivation of Sox10, cell suspensions were stained with FC block (BioLegend, Cat. No:101320; 1:200) for 20 min and sorted for RFP^+ populations. FACS sorting was completed using a Sony MA900.

2.6 Bioinformatics

2.6.1 RNA-sequencing processing and quantification

Triplicate RNA samples were subjected to RNA-seq at the Genome Quebec Facility using the Illumina NovaSeq 6000. Mouse RNA-seq reads were quality filtered using the rfastp R package and filtered paired-end reads were aligned to the mm10 reference genome using subjunc (Rsubread v2.14.2) (296,297). Differentially expressed genes were identified with DESeq2 (v1.40.2) (298). A DESeqDataSet was created from the raw count matrix with group information (NTC, sgRNA2.1, sgRNA2.2) and genes with adjusted $p < 0.05$ (Benjamini-Hochberg) and $|log2FC| > 1$ were considered significant. Rlog-transformed counts were used to compute a Pearson-correlation matrix; sample distances were defined as 1 minus the correlation value. The distance matrix was displayed as a heatmap using the pheatmap package (v1.0.12) with Euclidean distance used for hierarchical clustering (299). Pathway activity scores were computed with PROGENy (v1.18.2) using the top 100 downstream target genes per pathway to calculate scores (300). Z-score-normalized samples were visualized using a heatmap with unsupervised hierarchical clustering.

Shared DEGs (adjusted $p < 0.05$, $|log2FC| > 1$) from both Sox10 knockout clones were analysed using the enrichPathway() function from the ReactomePA package (v1.42.0) (301). The ten most significant (adjusted $p < 0.05$) pathways were selected for visualization. GSEA was performed using the clusterProfiler package (v4.6.2) with mouse gene sets from the MSigDB C2: Chemical and Genetic Perturbations (CGP) collection obtained through msigdbr (v7.5.1) (302–305). The top 10 positively and negatively enriched gene sets were visualized (gseaplot2) and ordered by normalized enrichment score (NES). Rlog-transformed gene expression values were used to generate a heatmap for a curated list of lineage-related genes. Expression values were row-scaled (z-score) and hierarchical clustering was performed using Euclidean distance.

2.6.2 scRNA-seq processing and gene set scoring

Raw UMI count data from previously published breast cancer scRNA-seq data was downloaded from the source publications (306–309). The data was then integrated using scVI and scANVI with default parameters, using sample identifiers as the batch variable. The scANVI embedding was then used to generate subsequent clustering and UMAP embeddings. Gene set scoring was performed using the AddModuleScore function implemented in Seurat.

2.7 Reproducibility and statistical analyses

For analyses comparing two independent variables, unpaired t-tests were used. For analyses comparing two or more independent factors with repeated measurements of the same experimental unit, repeated measures two-way ANOVA were performed. For Kaplan-Meier survival studies, log-rank (Mantel-Cox) was used. Power calculations were performed to estimate cohort sizes required to detect phenotypic differences among genotypes in tumor-free survival using a two-sided log-rank test ($\alpha = 0.05$, power = 0.8). Based on these estimates and prior

experience with tumor latency studies in this model, cohorts of approximately 8 mice per genotype were considered sufficient to detect biologically meaningful differences in disease-free survival. For all analyses, a significance cut-off of $p < 0.05$ was used. In all figures, ns represents not significant ($p > 0.05$), * represents $p \leq 0.05$, ** represents $p \leq 0.01$, *** represents $p \leq 0.001$, **** represents $p \leq 0.0001$. All data is represented as the mean with error bars representing the standard error of the mean (SEM). All statistical analyses were completed using GraphPad Prism 10.2.3.

For *in vitro* experiments, 3 independent biological replicates were performed. Quantification of immunohistochemistry or immunofluorescent images was conducted by taking ≥ 5 biological samples per genotype for *in vivo* experiments, or 3 biological replicates per cell line for *in vitro* experiments. For all images, ≥ 10 random regions of interest per section were taken and quantified. For tumor cell injections, ≥ 4 mice were injected per cell line used.

Table 2.1 List of Primers

qPCR Primers	Supplier	Cat. No:
Krt8 Forward: TCCATCAGGGTGACTCAGAAA	This manuscript	N/A
Krt8 Reverse: CCAGCTTCAAGGGGCTCAA	This manuscript	N/A
Krt18 Forward: TCAAGATCATCGAAGACCTGAGG	This manuscript	N/A
Krt18 Reverse: GCGCATGGCTAGTTCTGTC	This manuscript	N/A
Elf5 Forward: ATGTTGGACTCCGTAACCCAT	This manuscript	N/A
Elf5 Reverse: GCAGGGTAGTAGTCTTCATTGCT	This manuscript	N/A
Foxa1 Forward: ATGAGAGCAACGACTGGAACA	This manuscript	N/A
Foxa1 Reverse: TCATGGAGTTCATAGAGCCCA	This manuscript	N/A
Etv1 Forward: GCAAGTGCCTTACGTGGTCA	This manuscript	N/A
Etv1 Reverse: GCTTCAGCAAGCCATGTTTCTT	This manuscript	N/A
Krt5 Forward: TCTGCCATCACCCCATCTGT	This manuscript	N/A
Krt5 Reverse: CCTCCGCCAGAACTGTAGGA	This manuscript	N/A
Krt14 Forward: AGCGGCAAGAGTGAGATTTCT	This manuscript	N/A
Krt14 Reverse: CCTCCAGGTTATTCTCCAGGG	This manuscript	N/A

Acta2 Forward: GTCCCAGACATCAGGGAGTAA	This manuscript	N/A
Acta2 Reverse: TCGGATACTTCAGCGTCAGGA	This manuscript	N/A
Trp63 Forward: TACTGCCCCGACCCTTACAT	This manuscript	N/A
Trp63 Reverse: GCTGAGGAACTCGCTTGTCTG	This manuscript	N/A
Sox10 Forward: AGGTTGCTGAACGAAAGTGAC	This manuscript	N/A
Sox10 Reverse: CCGAGGTTGGTACTTGTAGTCC	This manuscript	N/A
18S Forward: AGTCCCTGCCCTTTGTACACA	This manuscript	N/A
18S Reverse: GATCCGAGGCCTCACTAAAC	This manuscript	N/A
Genotyping Primers		
Sox10 Forward: CAGGTGGGCGGGGCTCTT	This manuscript	N/A
Sox10 Reverse 1: GTGAGCCTGGATAGCAGCAG	This manuscript	N/A
Sox10 Reverse 2: TCCCAGGCTAGCCCTAGTG	This manuscript	N/A
Cre Forward: TATTCGGATCATCAGCTACACCAGAG	This manuscript	N/A
Cre Reverse: GGGATTGCTTATAACACCCTGTTACG	This manuscript	N/A
Neu Forward: GTTTCCTGCAGCAGCCTACGC	This manuscript	N/A
Neu Reverse: TTCCGGAACCCACATCAGGCC	This manuscript	N/A

R26RForward: AATCCATCTTGTTCAATGGCCGATC	This manuscript	N/A
R26R Reverse: CCGGATTGATGGTAGTGGTC	This manuscript	N/A
rtTA Forward: CTG GTC ATC ATC CTG CCT TT	This manuscript	N/A
rtTA Reverse: GGC GAG TTT ACG GGT TGT TA	This manuscript	N/A
CRISPR sgRNA Guides		
sgNTC: CACCGATCGGTATGTTTAGGGTT	This manuscript	N/A
sgNTC: AAACAACCCTAAACATAACCGATC	This manuscript	N/A
sgSox10-1: CACCGGTTGGTACTTGTAGTCCGGA	This manuscript	N/A
sgSox10-1: AAACTCCGGACTACAAGTACCAACC	This manuscript	N/A
sgSox10-2: CACCGGTTCCCCGTGTGCATCCGCG	This manuscript	N/A
sgSox10-2: AAACCGCGGATGCACACGGGGAACC	This manuscript	N/A

Table 2.2 List of Antibodies

Antibody	**Supplier**	**Identifier**
Sox10	Abcam	Cat. No:ab180862
		IHC - 1:400
		WB - 1:1000
Cleaved Caspase 3	CST	Cat. No: 9661
		IHC - 1:400
Ki67	Santa Cruz	Cat. No: sc-23900
		IHC - 1:150
Cre	CST	Cat. No: D7L7L
		IHC - 1:50
Keratin 8	Abcam	Cat. No: 15036S
		WB - 1:1000
		IHC - 1:800
Keratin 14	Abcam	Cat. No: ab7800
		IHC - 1:100
Neu	Sigma	Cat. No: OP15
		WB - 1:2000
		IHC - 1:100
Actin	Sigma	Cat. No: A5316
		WB - 1:20000
alpha-Smooth Muscle Actin	CST	Cat. No: 19245
		IF - 1:500

Cas9	CST	Cat. No: 14697S
		IHC - 1:100
Sox9	CST	Cat. No: 82630S
		WB - 1:20000
		IHC - 1:200
phospho-AKT	CST	Cat. No: 9271
		WB - 1:1000
AKT	CST	Cat. No: 9272
		WB - 1:1000
phospho-ERK	Santa Cruz	Cat. No: sc-7383
		WB - 1:1000
ERK	Santa Cruz	Cat. No: sc-154
		WB - 1:1000
Vinculin	CST	Cat. No: 13901
		WB - 1:1000
Goat anti-mouse IgG HRP conjugate	BioRad	Cat. No: 1706516
		WB – 1:5000
Goat anti-rabbit IgG HRP conjugate	BioRad	Cat. No: 1706515
		WB – 1:5000
Goat anti-rabbit IgG (H+L) Alexa Fluor™ 488	Invitrogen	Cat. No: A-11008
		IF: 1:1000
Goat anti-mouse IgG (H+L) Alexa Fluor™ 594	Invitrogen	Cat. No: A-11005
		IF: 1:1000

Brilliant Violet 711™ Streptavidin	BioLegend	Cat. No: 405241
		Flow – 1:400
Biotin anti-mouse Ly-51	BioLegend	Cat. No: 108303
		Flow – 1:200
Biotin anti-mouse CD31	BioLegend	Cat. No: 102503
		Flow – 1:200
Biotin anti-mouse CD45	BioLegend	Cat. No: 103103
		Flow – 1:200
Biotin anti-mouse TER-119/Erythroid Cells	BioLegend	Cat. No: 116203
		Flow – 1:200
Brilliant Violet 421 anti-human/mouse CD49f	BioLegend	Cat. No: 313623
		Flow – 1:400
PEDazzle 594 anti-mouserat CD61	BioLegend	Cat. No: 104321
		Flow – 1:200
PerCP/Cyanine5.5 anti-mouse CD24	BioLegend	Cat. No: 101823
		Flow – 1:200
Brilliant Violet 421™ anti-mouse CD66a	BioLegend	Cat. No: 134531
		Flow – 1:200
Alexa Fluor® 647 anti-mouse CD326	BioLegend	Cat. No: 118212
		Flow – 1:400
Brilliant Violet 421™ anti-mouse CD66a	BioLegend	Cat. No:134531
		Flow – 1:400
TruStain FcX™ anti-mouse CD16/32	BioLegend	Cat. No: 101320

		Flow – 1:200
NIR Zombie Live Dead	BioLegend	Cat. No: 423106
		Flow – 1:500

Chapter 3: Sox10 regulates mammary ductal morphogenesis through regulation of the luminal progenitor population.

3.1 Introduction and Rationale

As mentioned previously, Sox10 has recently been identified as a key mediator of the mammary stem/progenitor cell population and lineage plasticity, and is required for normal mammary gland morphogenesis (267,278,279,289). However, prior studies employed the use of the transgenic MMTV-Cre A strain, which has been shown to exhibit non-specific Cre expression within the myoepithelial compartment as well as intrinsic developmental abnormalities due to transgene positional effects (116,117,119).

To better understand the role of Sox10 specifically in the luminal mammary epithelium, we utilized MMTV-Cre lines that drive expression predominantly within the luminal compartment (126,310–312). We therefore first assessed the requirement for Sox10 in mammary gland development with this genetic background to avoid confounding strain-specific developmental effects. Based on Sox10's previously defined roles in mammary development and stem cell regulation, specifically of the MaSC, BP and LP compartments, we hypothesised that luminal-restricted excision of Sox10 would result in less severe developmental defects than those observed in models with broader epithelial recombination.

3.2 Generation of MMTV-Cre: Sox10$^{fl/fl}$ mice

To achieve luminal epithelium-specific deletion of Sox10, mice harboring conditional *Sox10*^{fl} alleles were crossed with MMTV-Cre transgenic animals, in which Cre recombinase is expressed under control of the MMTV promoter (Fig. 3.1A). In this system, Cre-mediated recombination excises a loxP-flanked *Sox10* open reading frame, resulting in functional gene inactivation specifically within the luminal mammary epithelium (313). Offspring were genotyped by PCR to assess recombination of the *Sox10* allele and the presence of the MMTV-Cre transgene (Fig. 3.1 B, C).

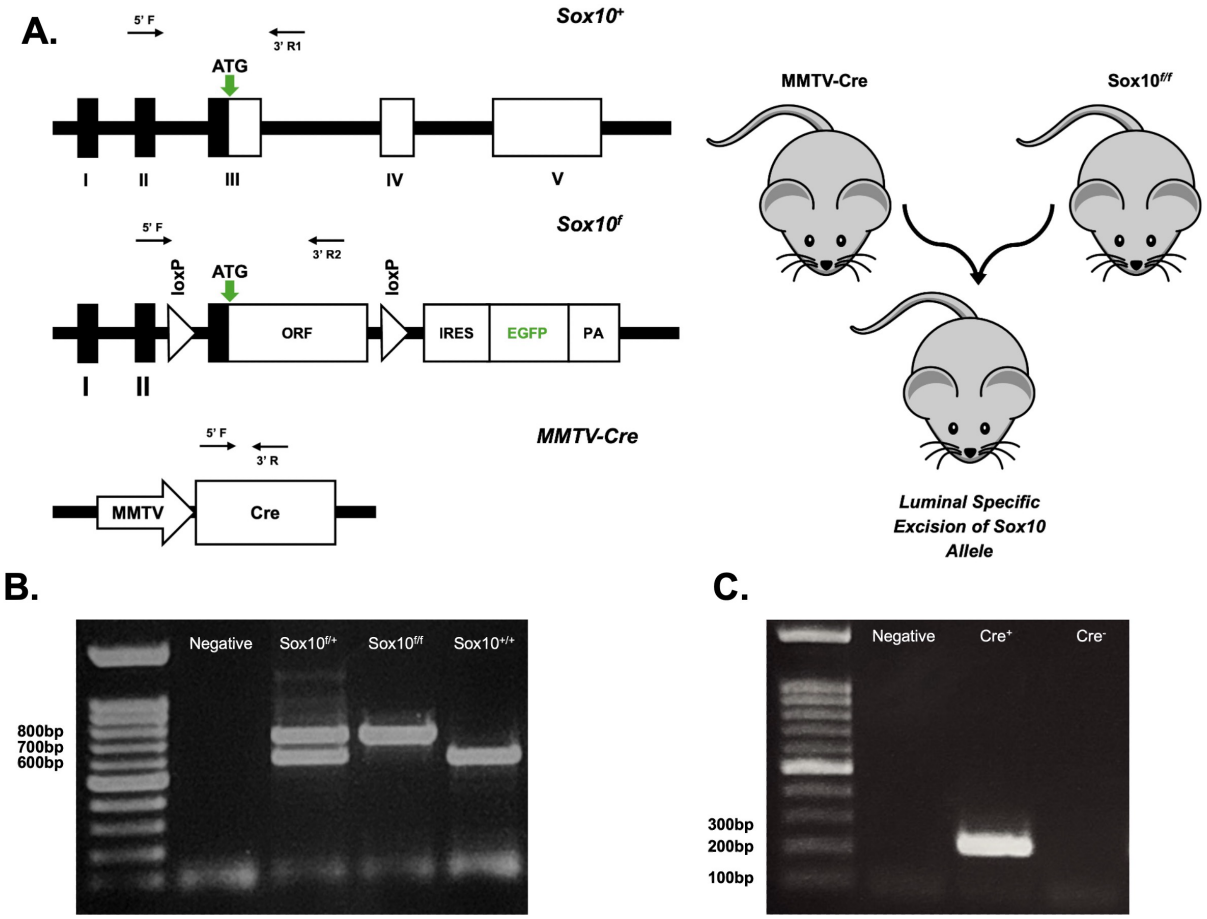

Figure 3.1. Schematic Representation of the MMTV-Cre: Sox10$^{fl/fl}$ animal model. (A) MMTV-Cre mice were crossed with Sox10$^{fl/fl}$-EGFP for luminal-specific expression of Cre recombinase for *Sox10* excision. **(B)** Representative PCR genotyping products of Sox10$^{fl/+}$, Sox10$^{fl/fl}$, and Sox10$^{+/+}$ mice. **(C)** Representative PCR genotyping products of Cre^{+}, and Cre^{-} mice.

3.3 MMTV-Cre: Sox10$^{fl/fl}$ mice show delayed but normal mammary gland development

To assess the requirement of luminal Sox10 in mammary gland development, whole mounts of the 4th inguinal mammary glands from pubescent and adult virgin female MMTV-Cre: Sox10$^{+/+, fl/+, fl/fl}$ mice were prepared (Fig. 3.2 A). Enumeration of epithelial end buds, ductal branch points, and fat pad invasion showed delayed ductal morphogenesis in pubescent 4-week-old MMTV-Cre: Sox10$^{fl/fl}$ females (Fig. 3.2 B-D) Interestingly, age matched hemizygous MMTV-Cre: Sox10$^{fl/+}$ mice did not exhibit any obvious developmental defects. As MMTV-Cre: Sox10$^{fl/fl}$ mice progressed through puberty, however, these developmental defects were abrogated. No significant defects in mammary gland structure and morphology were observed in adult virgin females at 11-weeks of age, which displayed complete ductal penetration and branching complexity comparable to wild-type controls (Fig. 3.2 B-D).

Together, these data suggest that while luminal-specific Sox10 loss impairs pubertal ductal morphogenic events, normal adult ductal morphology is achieved as mice progress through pubertal developmental stages.

3.4 Luminal-specific Sox10 excision does not affect epithelial organization

Hormone-dependent mass morphogenic events leading to murine mammary rudiment bifurcation and ductal elongation occur around 21-days of age (159). However, previous reports have demonstrated latent mammary epithelium-specific expression of Cre in MMTV-Cre D strains (116). Therefore, to coincide the observed pubertal delay with Cre expression during early mammary gland development, MMTV-Cre mice were crossed with ROSA26R-LacZ reporter animals. In these mice, Cre-mediated recombination excises a *loxP*-flanked transcriptional STOP cassette to permit LacZ expression (Fig. 3.3 A). Whole-mount β-galactosidase staining of

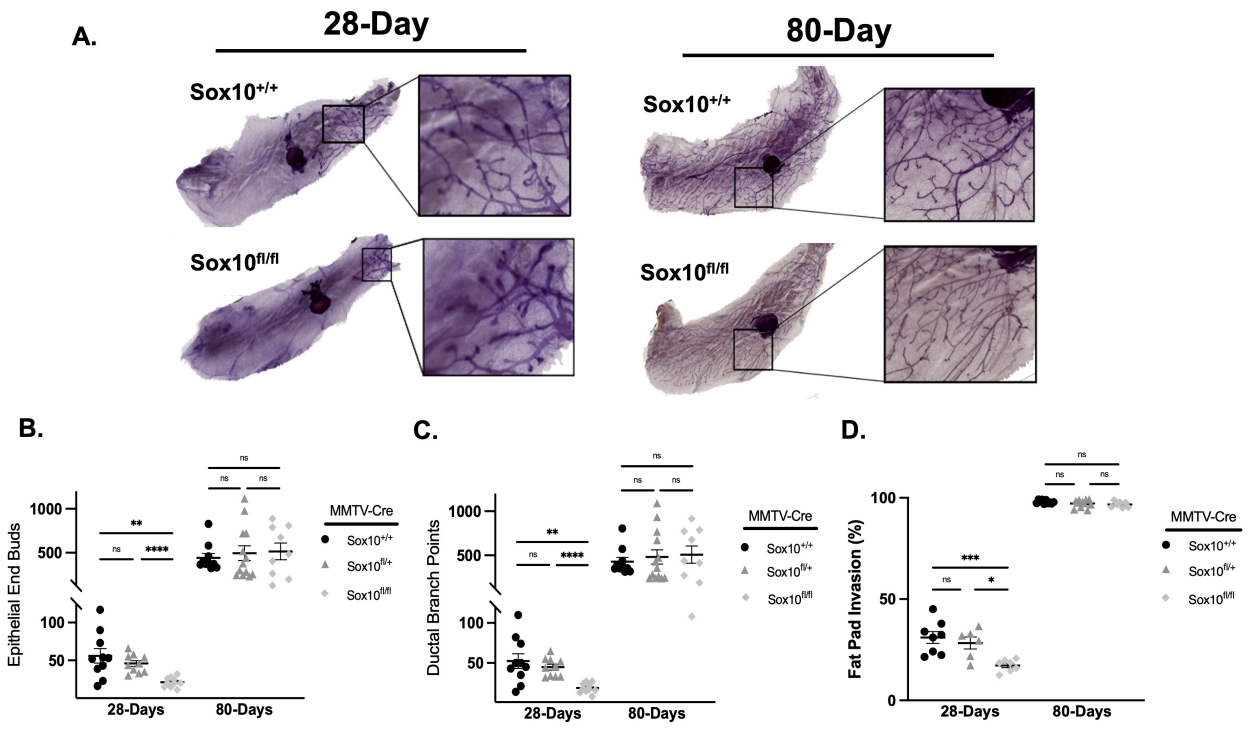

Figure 3.2. Luminal Sox10-deletion delays mammary gland development. (A) Representative images of hematoxylin stained MMTV-Cre: Sox10$^{+/+}$ and $^{fl/fl}$ pubescent and adult mammary gland whole-mounts at 28-, and 80-days of age, respectively. **(B-D)** Quantification of epithelial end buds (B), ductal branch points (C), and fat pad invasion (D) in hematoxylin stained MMTV-Cre: Sox10$^{+/+}$, $^{fl/+}$ and $^{fl/fl}$ mice. *, **, ***, **** represents $p < 0.05$, 0.01, 0.001 and 0.0001, respectively. Data shown as mean ± SEM. n ≥ 6 mice/group.

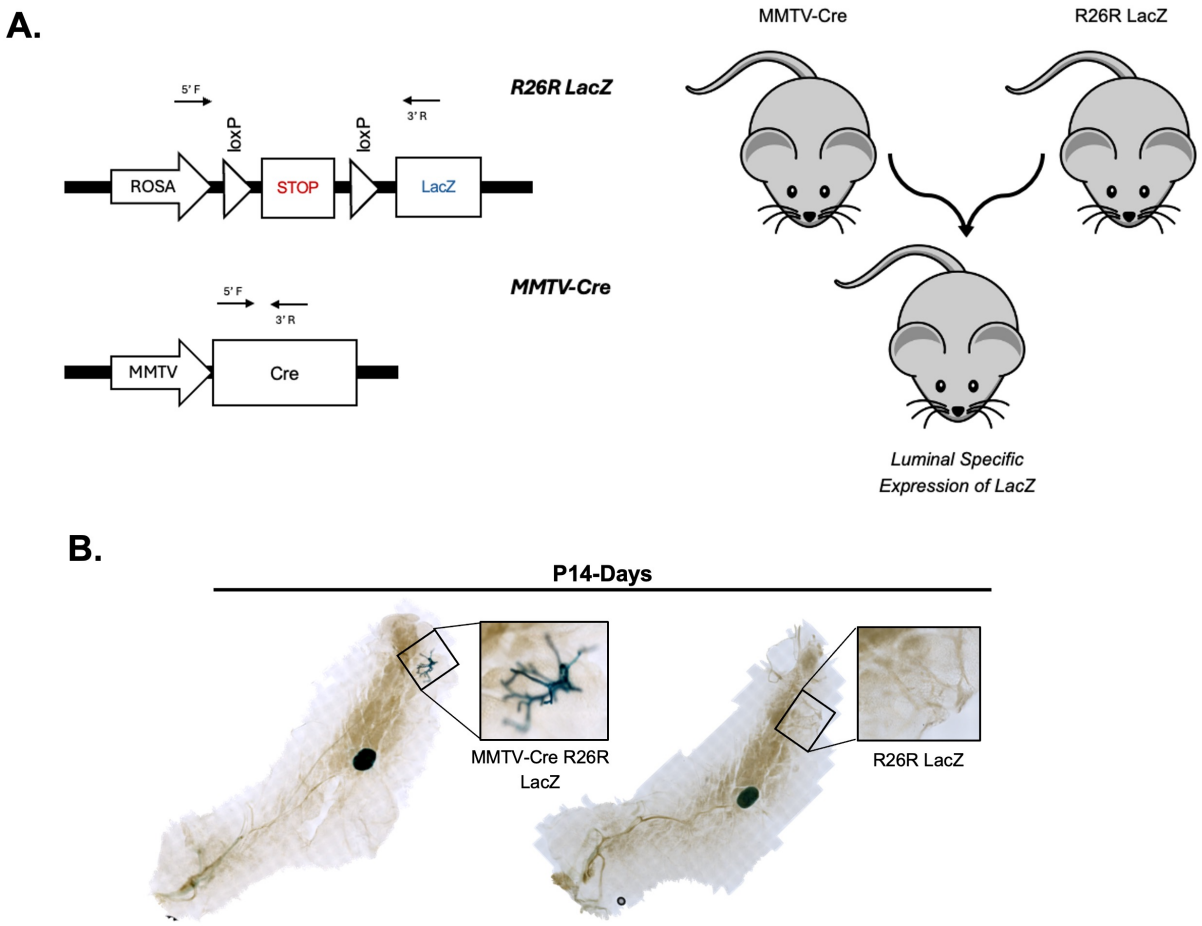

Figure 3.3. Ductal-specific Cre expression is present in P14 MMTV-Cre mice. (A) Schematic representation of the MMTV-Cre: R26R LacZ animal model where R26R LacZ mice were crossed with MMTV-Cre to monitor LacZ expression following Cre excision of *loxP* flanked stop codon. **(B)** Whole mounted P14 mammary glands from R26R LacZ and MMTV-Cre: R26R LacZ mice stained for β-galactosidase activity.

mammary glands from postnatal day 14 (P14) female pups confirmed Cre activity specifically within the ductal epithelium of MMTV-Cre: ROSA26R LacZ mice, demonstrating active Cre expression prior to the onset of pubertal ductal outgrowth (Fig. 3.3 B).

Next, to confirm efficient inactivation of Sox10 within the luminal epithelium, co-immunofluorescence for the luminal marker CK8, and Sox10 was performed on formalin-fixed paraffin embedded (FFPE) mammary gland sections from adult MMTV-Cre: $Sox10^{+/+}$ and $^{fl/fl}$ mice. As expected, basal cells retained Sox10 expression, however, immunofluorescence showed a significant reduction of luminal-specific $CK8^{+}$ $Sox10^{+}$ nuclei by approximately 75% in MMTV-Cre: $Sox10^{fl/fl}$ females when compared to wild-type (Fig. 3.4 A, B). A similar and progressive deletion of this *Sox10* allele throughout the lifespan of the animals has also been previously observed (313).

Although total end buds, ductal branch points, and fat pad invasion remained unchanged in Sox10-deficient adult females, we wanted to assess whether Sox10 inactivation resulted in more subtle defects in mammary epithelial organization. Immunofluorescence for CK8 and αSMA revealed normal bilayered ductal organization in MMTV-Cre: $Sox10^{fl/fl}$ glands (Fig. 3.4 C). Further quantification of luminal and myoepithelial cell proportions showed no significant differences between genotypes (Fig. 3.4 D, E).

Together, these data indicate that MMTV-Cre-mediated Sox10 excision is initiated prior to puberty and transiently delays pubertal ductal development with no lasting defects to overall epithelial organization or lineage composition in the adult mammary gland.

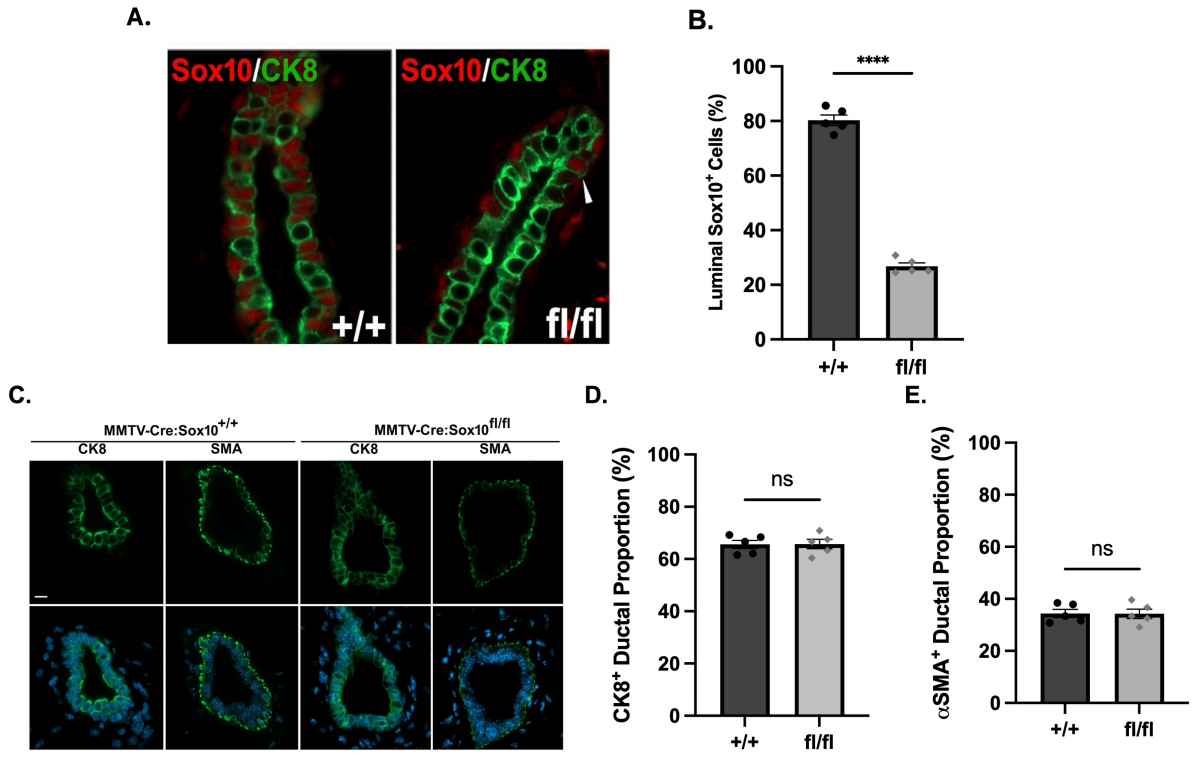

Figure 3.4. Luminal excision of Sox10 in MMTV-Cre mice does not affect epithelial organization. (A) Representative images of adult MMTV-Cre: $Sox10^{+/+}$ and $^{fl/fl}$ glands dual stained for Sox10 and CK8 show efficient Sox10 deletion in the luminal epithelium. **(B)** Quantification of $Sox10^{+}$ $CK8^{+}$ cells in (A). **(C)** Representative images of adult MMTV-Cre: $Sox10^{+/+}$ and $^{fl/fl}$ glands stained for CK8 and αSMA show normal epithelial organization. **(D, E)** Quantification of $CK8^{+}$ (D) and αSMA^{+} ductal cell proportions in (C). **** represents $p < 0.0001$. Data shown as mean ± SEM. n ≥ 5 mice/group. Scale bar 20μm.

3.5 Loss of Sox10 does not impair ductal cell survival or proliferation in adult MMTV-Cre females

Although adult MMTV-Cre: Sox10$^{fl/fl}$ females show no apparent morphological developmental defects in the mammary epithelium, we tested whether this was due to potential compensatory mechanisms from Sox10 inactivation resulting in altered cell proliferation or cell death. Adult virgin females were stained with Ki67 or cleaved caspase-3 (CC3) to assess proliferation, and apoptosis, respectively. Occasional CC3-positive cells were detected in both genotypes (Fig. 3.5 A), however, the proportion of ducts containing at least one CC3-positive cell did not differ between Sox10$^{+/+}$ and Sox10$^{fl/fl}$ animals (Fig. 3.5 B). Similarly, Ki67 immunostaining revealed comparable proportions of proliferating ductal epithelial cells in both groups (Fig. 3.5 C, D).

These data indicate that luminal-specific deletion of Sox10 does not measurably affect epithelial cell survival or proliferation in the adult mammary gland, consistent with the absence of apparent developmental abnormalities in adult mice.

3.6 Sox10 is required for maintenance of the luminal progenitor pool

The term “luminal adaptive secretory precursor” has been proposed to describe the most disparate group of mammary luminal cells encompassing all luminal/alveolar progenitors/precursors, luminal secretory, and hormone receptor-negative populations (314). We will hereafter use LPs to refer to luminal cells with potential stem/progenitor activity. Due to the previous reports identifying critical roles of Sox10 in murine mammary stem/progenitor cell function, we assessed the pan-luminal and LP-specific compartments of MMTV-Cre: Sox10$^{+/+}$ and $^{fl/fl}$ adult females using flow cytometry (267,279). Lineage-negative epithelial cells were segregated into luminal and basal compartments based on CD24 and CD49f expression (181,182,186,187).

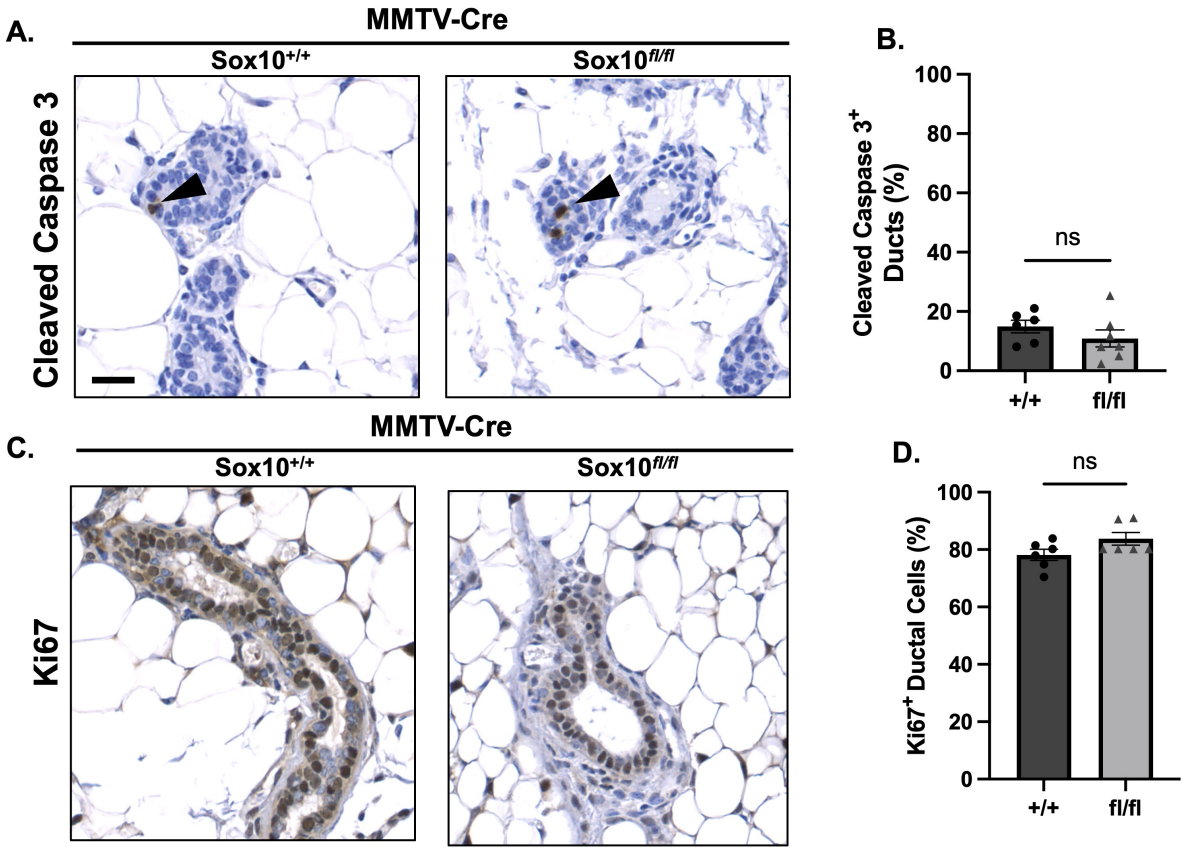

Figure 3.5. Loss of Sox10 does not impair ductal cell survival or proliferation in adult MMTV-Cre females. (A) Representative images of adult MMTV-Cre: $Sox10^{+/+}$ and $^{fl/fl}$ glands stained with cleaved-caspase 3 (CC3). Arrowheads indicate $CC3^{+}$ cells. **(B)** Quantification of the proportion of ducts with ≥ 1 $CC3^{+}$ cell from (A). **(C)** Representative images of adult MMTV-Cre: $Sox10^{+/+}$ and $^{fl/fl}$ glands stained with Ki67. **(D)** Quantification of $Ki67^{+}$ ductal cells from (C). Data shown as mean ± SEM. n ≥ 6 mice/group. Scale bar 50µm.

Luminal Lin^{-} CD24^{hi} CD49f^{+} cell populations in adult MMTV-Cre virgin females showed no difference in total luminal populations between wild-type and Sox10$^{fl/fl}$ mice (Fig. 3.6 A). These observations are consistent with the preserved ductal architecture in Sox10$^{fl/fl}$ glands observed. Interestingly, further sorting of the pan-luminal compartment into the LP-enriched Lin^{-} CD24^{hi}CD49f^{+}CD61^{+} population enriched for LP activity (181,182), showed a 2-fold reduction in the LP population in MMTV-Cre: Sox10$^{fl/fl}$ females (Fig. 3.6 B, C).

In this model, the *Sox10^{fl}* allele is linked to an EGFP construct which, when unrecombined, acts as a reporter for Sox10 expression. However, EGFP expression is lost upon Cre excision (313). This retention of EGFP expression permits the usage of this system to identify cells that escaped Cre excision. To assess the efficiency of Cre-mediated recombination in MMTV-Cre: Sox10$^{fl/fl}$ mice, we quantified residual EGFP expression in the Lin^{-}CD49f^{+}CD24^{hi} luminal epithelial compartment.

A detectable EGFP^{+} population was observed in MMTV-Cre: Sox10$^{fl/fl}$ mice and absent in wild-type controls (Fig. 3.7 A). Quantification revealed that fewer than 5% of luminal cells retained EGFP expression in MMTV-Cre: Sox10$^{fl/fl}$ animals (Fig. 3.7 B), indicating relatively efficient Cre excision in this population. Robust EGFP fluorescence can be seen in whole-mount mammary glands from Sox10$^{fl/fl}$ mice (Fig. 3.7 C).

Together, these findings indicate that while Sox10 is not required for maintenance of the total luminal epithelial population, it is specifically important for sustaining the LP compartment in the adult mammary gland.

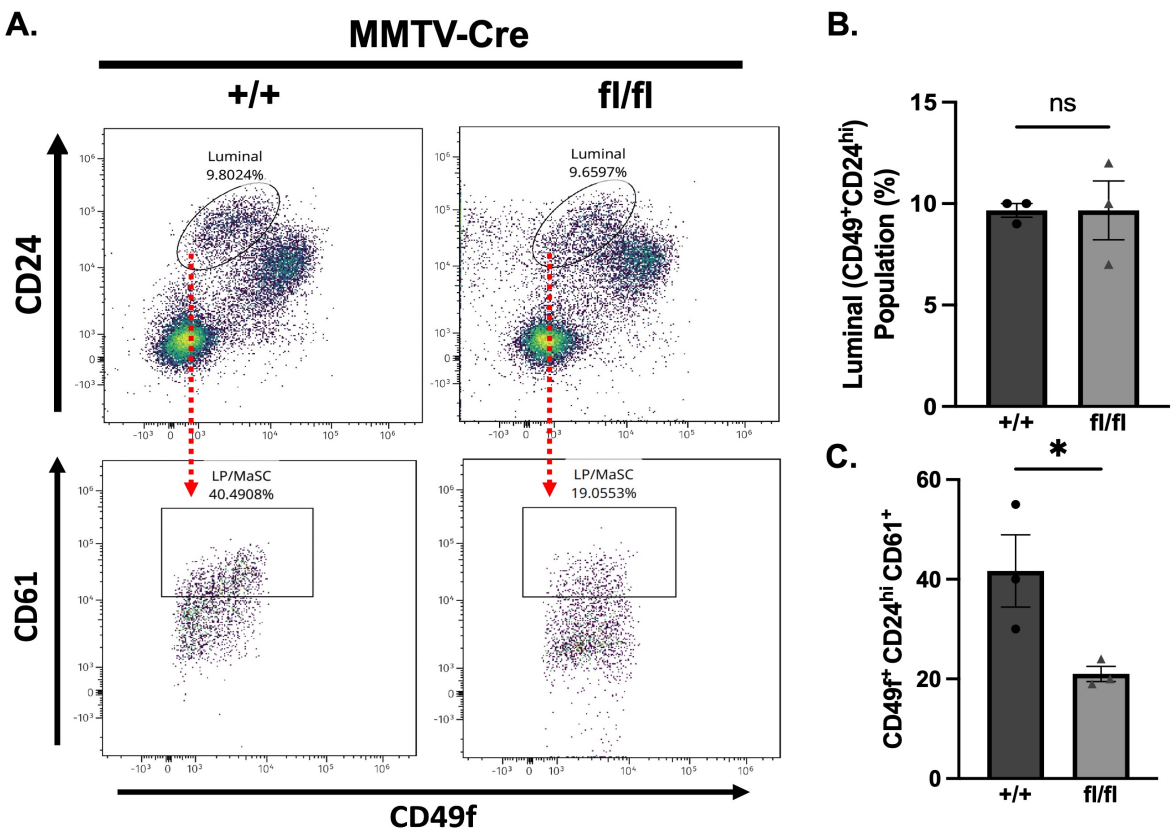

Figure 3.6. Sox10 is not required for adult ductal morphogenesis but required for maintenance of the LP pool. (A) Representative flow cytometry plots of 8-week-old adult MMTV-Cre: $Sox10^{+/+}$ and MMTV-Cre: $Sox10^{fl/fl}$ glands. Luminal cells were identified by the $Lin^-CD49f^+CD24^{hi}$ population further enriched for $CD61^+$ to identify the LP compartment ($Lin^-CD49f^+CD24^{hi}CD61^+$). **(B)** Quantification of total luminal cells ($Lin^-CD49f^+CD24^{hi}$) in (A). **(C)** Quantification of the LP compartment ($Lin^-CD49f^+CD24^{hi}CD61^+$). * represents $p < 0.05$. Data shown as mean ± SEM. n ≥ 3 mice/group.

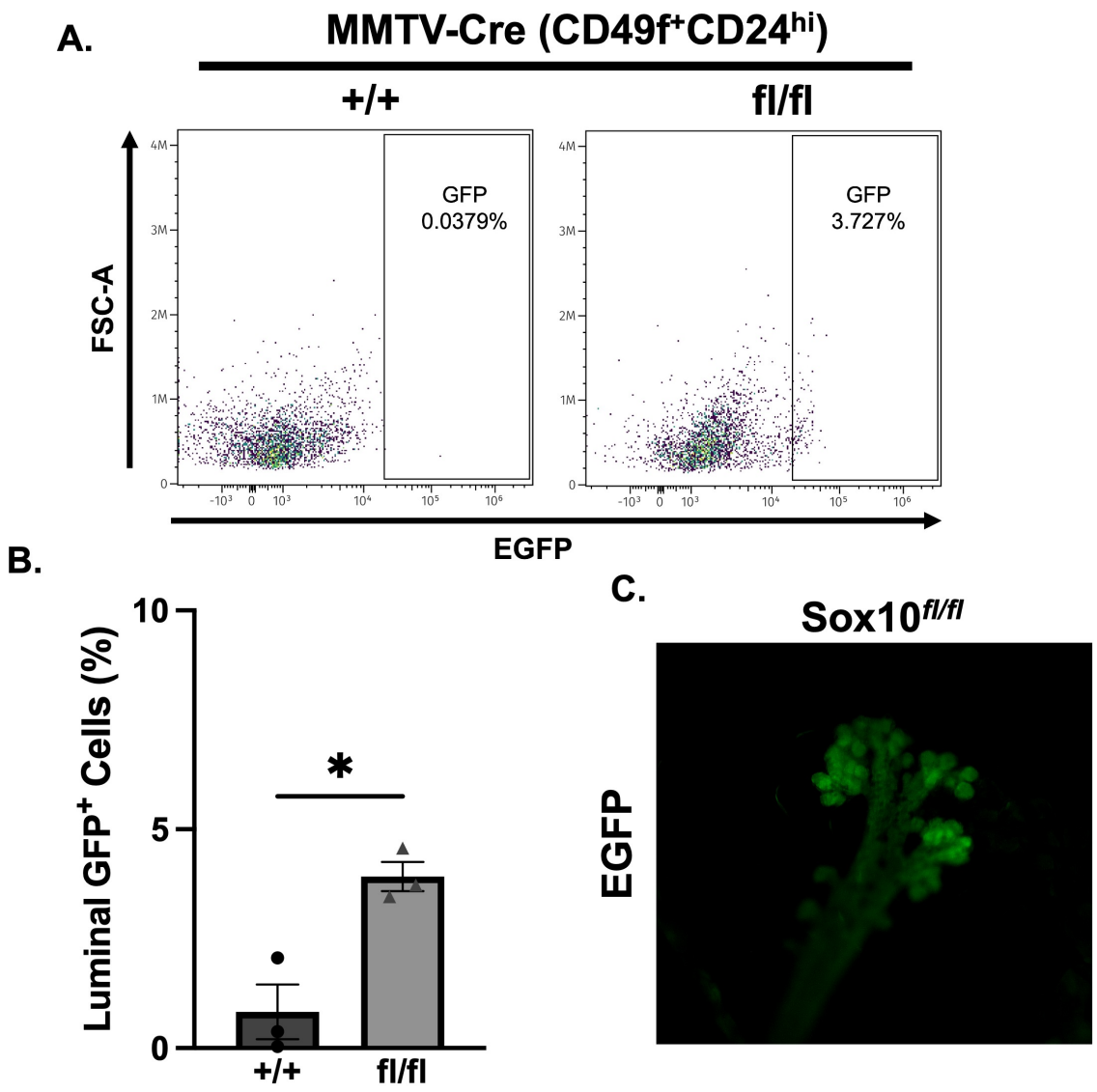

Figure 3.7. Minimal Cre escape indicates efficient *Sox10* recombination in luminal epithelium. (A). Representative flow cytometry plots showing residual EGFP expression under the Sox10$^{fl/fl}$-EGFP reporter in the luminal (CD49f^{+}CD24^{hi}) population in MMTV-Cre: Sox10$^{fl/fl}$. EGFP expression marks the cells retaining an unrecombined Sox10$^{fl/fl}$-EGFP allele. **(B)** Quantification of EGFP expressing luminal cells (CD49f^{+}CD24^{hi}) in (A). **(C)** Representative image of EGFP expression in an 8-week-old pre-fixed Sox10$^{fl/fl}$ whole mounted mammary gland. * represents $p < 0.05$. Data shown as mean ± SEM. n ≥ 3 mice/group.

3.7 Summary

Previously, it has been shown that Sox10 acts as a key regulator of the mammary stem cell population and lineage plasticity, and is required for normal mammary gland morphogenesis (267,278,279,289). Specifically, it was found that early *Sox10* excision in both luminal and basal epithelial compartments prevents expansion of mammary rudiments during puberty-dependent morphogenic events (278).

Here, we have shown that luminal-specific Sox10 deletion leads to a delay in pubertal mammary gland developmental that is fully resolved by adulthood with no apparent effect on overall mammary gland epithelial organization. It appears that although loss of Sox10 does not result in depletion of the adult total luminal population, there is a selective deficit in the LP compartment, suggesting that Sox10 may be dispensable for maintenance of the differentiated luminal epithelium but is necessary to sustain the LP pool.

Chapter 4: Loss of Sox10 abrogates HER2/Neu-induced mammary tumorigenesis through depletion of tumor-initiating cell population.

4.1 Introduction and Rationale

The role of Sox10 in cancer progression remains elusive and controversial with contrasting observations reported across cancer types (268,280). In the context of breast cancer, we and others have shown that Sox10 is a marker for select basal-like carcinomas such as triple-negative breast cancers (216,282–288). Although its precise biological function in cancer remains unclear, it appears that Sox10 actively maintains mammary stem/progenitor populations and contributes to the malignancy of TNBC cells *in vitro* by modulating lineage plasticity (267,279,286,289).

Using murine models of luminal-, and basal-like mammary tumorigenesis, Sox10-expressing tumors exhibit a de-differentiated state and acquire a more basal-like phenotype (279). Mechanistically, Sox10 was found to directly bind promoter regions of genes regulating EMT, stem/progenitor cell activity, and NC identity (279). Functional studies using C3-TAg mice, a model of basal-like breast cancer, have revealed that Sox10 haploinsufficiency significantly prolongs survival, directly implicating it in disease progression (279).

While Sox10 appears to be functionally implicated in basal-like breast cancers, the current body of evidence for its role in HER2/Neu-induced tumorigenesis is limited. Our recent analysis of TCGA datasets shows that approximately 15% of HER2-positive breast cancers are $Sox10^{hi}$ (294). Consistent with this, others have demonstrated substantial variability in proportions of the $Sox10^{+}$ populations (2%-79%) among HER2-positive tumor samples (291–293,295). Interestingly, $Sox10^{hi}$ cohorts were associated with a worse grade and a stem-like phenotype, suggesting that $Sox10^{+}$/HER2-positive tumors represent a more aggressive de-differentiated subtype (291,293,294). Supporting this, using a murine model of HER2-positive breast cancer, we have recently shown that endpoint tumors and cell lines harboring elevated $Sox10^{+}$ expression levels exhibit increased stemness and enhanced tumorigenic capacity (294).

Despite these observations, it remains unclear whether the $Sox10^{+}$ luminal population is functionally required for HER2-driven tumorigenesis, or whether Sox10 expression instead reflects a transient state of cellular plasticity that accompanies tumor progression. To directly address this question, we investigated the functional and genetic consequences of conditional Sox10 deletion in murine models of breast cancer, including the MMTV-NIC and MMTV-rtTA/MIC systems. As previous associations between Sox10 expression and aggressive breast cancers have been reported, we hypothesized that luminal-specific deletion of Sox10 in murine models of such breast cancers would result in reduced overall tumorigenicity.

4.2 Generation of MMTV-NIC: $Sox10^{fl/fl}$ mice

To achieve luminal epithelium-specific HER2/Neu expression coupled with Sox10 inactivation, mice harboring *Sox10*^{fl} alleles were crossed with MMTV-NIC transgenic animals (126). In the NIC model, expression of a constitutively active Neu oncogene is linked to Cre recombinase via an IRES, resulting in bicistronic expression of Neu and Cre under control of the MMTV promoter. This configuration ensures that oncogene activation and Cre-mediated recombination occur within the same luminal epithelial cells. MMTV-NIC mice develop spontaneous mammary adenocarcinomas that histologically resemble human HER2-positive breast cancer (122). When crossed with mice carrying a *loxP*-flanked target allele, this model enables simultaneous oncogene expression and conditional gene deletion specifically in the luminal mammary epithelium (Fig. 4.1).

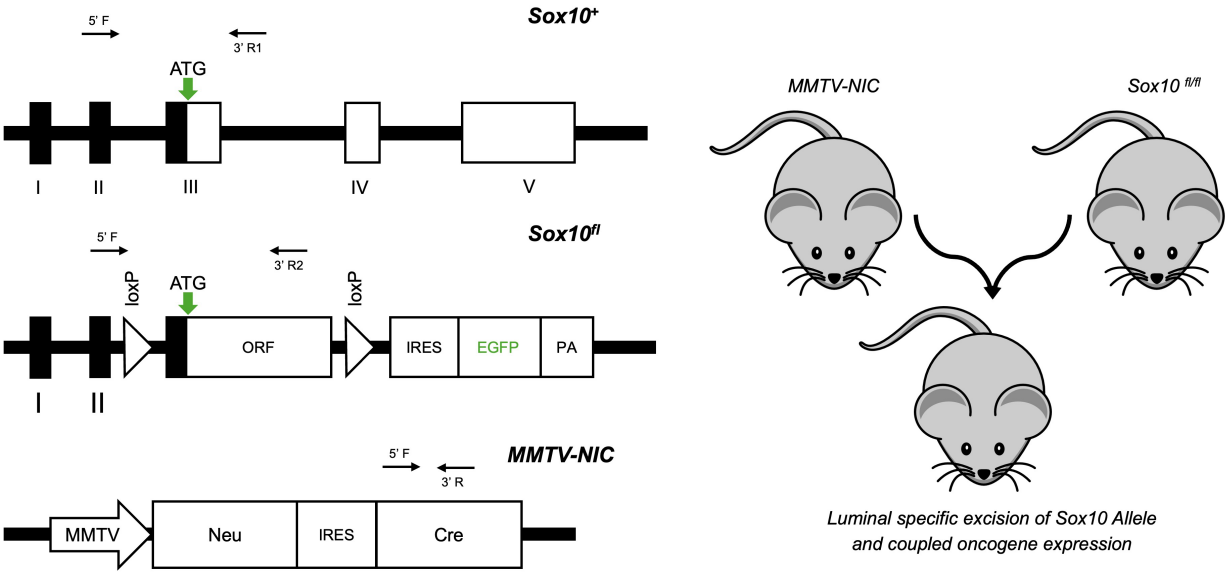

Figure 4.1. Schematic representation of the MMTV-NIC: Sox10$^{fl/fl}$ animal model. Schematic representation of wild-type, and Sox10^{fl} alleles, as well as the MMTV-NIC transgene. MMTV-MIC mice were crossed with Sox10$^{fl/fl}$-EGFP for luminal-specific bicistronic expression of the NeuNDL oncogene coupled to Cre recombinase for *Sox10* excision.

4.3 Loss of Sox10 in MMTV-NIC mice confers a dose-dependent survival advantage

To determine whether Sox10 is functionally required for HER2/Neu-driven mammary tumorigenesis**,** disease-free survival was assessed for all MMTV-NIC: Sox10 genotypes. Kaplan-Meier analysis revealed a significant, dose-dependent increase in disease-free survival following Sox10 inactivation (Fig. 4.2 A). Hemizygous MMTV-NIC: Sox10$^{fl/+}$ mice exhibited a marked delay in tumor onset relative to wild-type controls as palpable tumors were readily detectable by about 80 days later in MMTV-NIC: Sox10$^{fl/+}$ mice when compared to wild-type (Fig. 4.2 B). Strikingly, MMTV-NIC: Sox10$^{fl/fl}$ mice remained disease free for the duration of the study, indicating a complete failure of tumor initiation. Despite the pronounced delay in tumor onset, once tumors became palpable, the time from tumor onset to endpoint did not differ between hemizygous MMTV-NIC: Sox10$^{fl/+}$and wild-type mice (Fig. 4.2 C).

To validate that reduced tumorigenicity in hemizygous MMTV-NIC: Sox10$^{fl/+}$ mice is not due to developmental defects arising from potential differences in MMTV-LTR kinetics between Cre and NIC models, total epithelial end buds and total fat pad invasion in adult MMTV-NIC: Sox10$^{fl/+}$ were assessed. Corroborating our previous findings, no overt mammary gland defects were observed in MMTV-NIC Sox10$^{fl/+}$ adult virgin mammary glands when compared to age matched wild-type controls (Fig. 4.3 A, B).

To determine whether this convergence in growth kinetics reflected differences in Sox10 expression, total mRNA and protein, as well as FFPE sections from endpoint tumors were examined. Western blot analysis revealed comparable levels of Sox10, CK8, and Neu across genotypes (Fig. 4.4 A, B). Immunohistochemical analysis similarly demonstrated equivalent

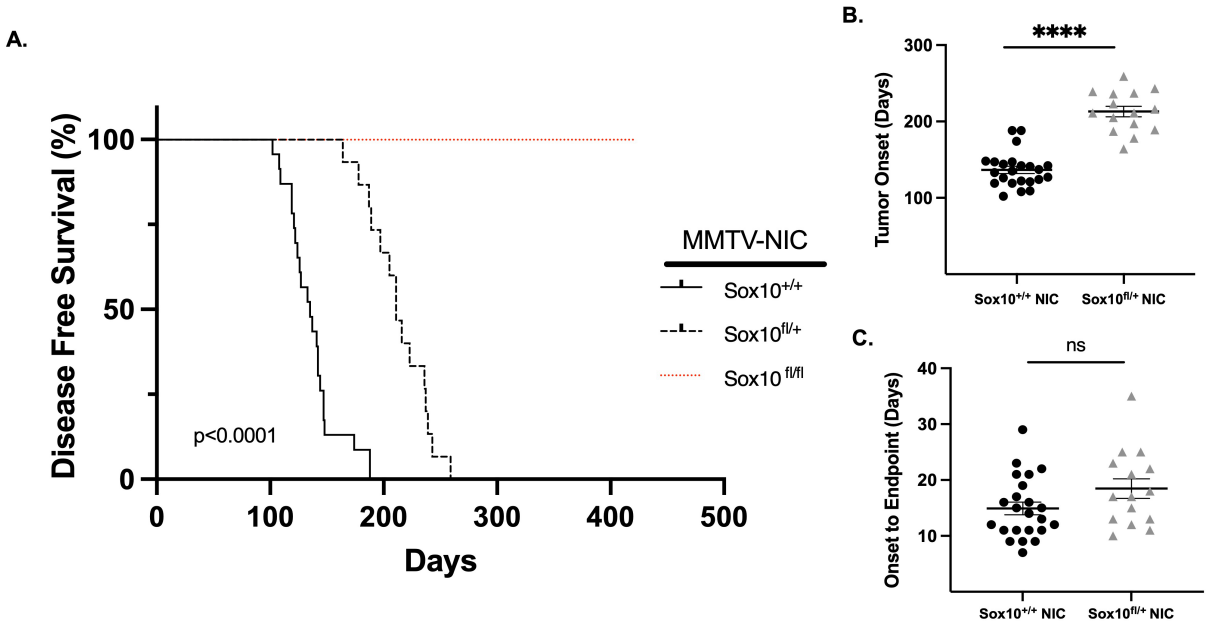

Figure 4.2. Luminal Sox10-deletion impairs Neu-induced tumor initiation. (A) Kaplan-Meier disease-free survival curves in MMTV-NIC: $Sox10^{+/+,}$ $^{fl/,}$ and $^{fl/fl}$ mice. Significance assessed by log-rank test ($n \geq 8$ mice/group). **(B, C)** Tumor onset (B) ($0.5cm^3$) and progression to endpoint (C) ($1.7\ cm^3$) were measured for all tumor bearing MMTV-NIC genotypes. $n \geq 15$ mice/group. **** represents $p < 0.0001$. Data shown as mean $\pm$ SEM.

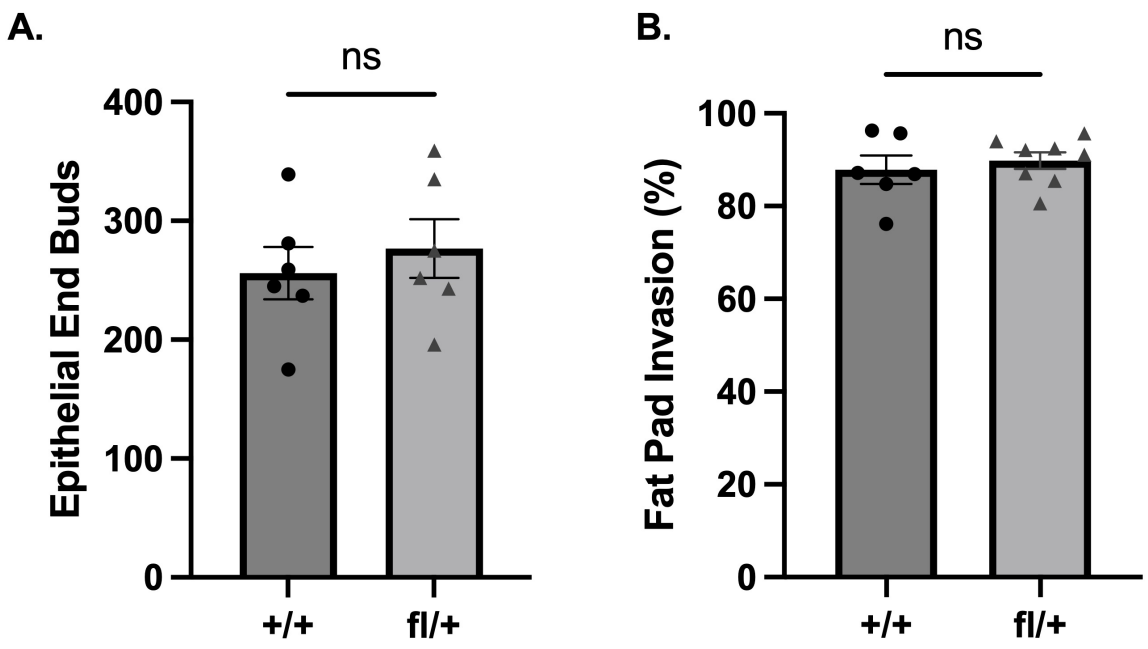

Figure 4.3. Loss of Sox10 in MMTV-NIC mammary glands does not result in overt morphological defects. (A, B) Quantification of epithelial end buds (A), and fat pad invasion (B) in hematoxylin stained adult MMTV-NIC: $Sox10^{+/+}$ and $Sox10^{fl/+}$ females. Data shown as mean ± SEM. n ≥ 6 mice/group.

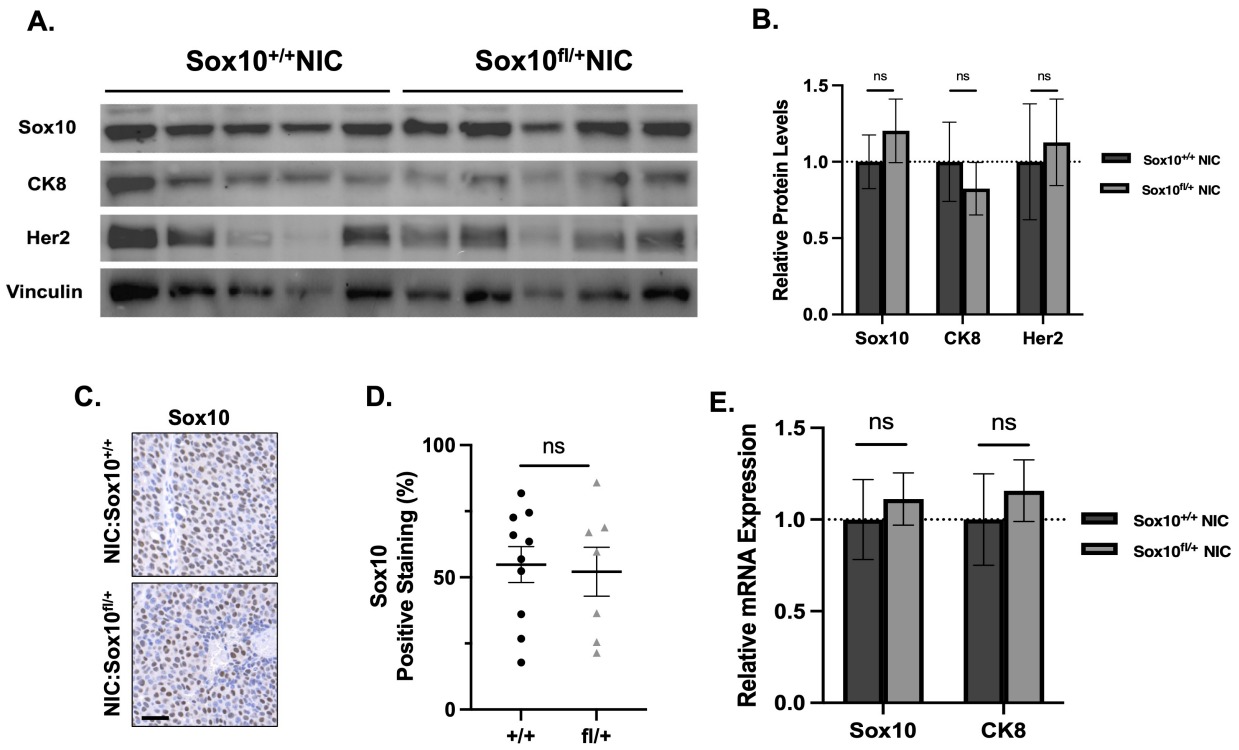

Figure 4.4. Endpoint hemizygous Sox10 NIC tumors exhibit endogenous Sox10 expression levels equivalent to that of wildtype. (A) Endpoint tumor lysates were assessed for the expression of Sox10, CK8, and Neu using Western blot analysis. **(B)** Densitometric quantitation of Western blots shown in (A). Three independent runs were used for quantification. **(C)** Representative images of FFPE endpoint tumor sections from MMTV-NIC: $Sox10^{+/+}$ and $^{fl/+}$ stained for Sox10. **(D)** Quantification of $Sox10^{+}$ stained cells from (C). **(E)** Relative expression of Sox10 and CK8 using RT-qPCR in endpoint tumors from from MMTV-NIC: $Sox10^{+/+}$ and $^{fl/+}$ mice. Data shown as mean ± SEM. n ≥ 5 mice/group. Scale bar represents 50µm.

proportions of Sox10-positive cells in endpoint tumors (Fig. 4.4 C, D), and RT-qPCR confirmed no significant differences in Sox10 transcript abundance (Fig. 4.4 E).

Together, these data support a model by which Sox10 functions in a dose-dependent manner during HER2/Neu-induced tumor initiation, wherein hemizygous MMTV-NIC: $Sox10^{fl/+}$ exhibit significantly increased survival, while Sox10-deficient MMTV-NIC: $Sox10^{fl/fl}$ mice completely abrogate tumorigenesis for up to a year. Interestingly, tumors that eventually arise in MMTV-NIC: $Sox10^{fl/+}$mice exhibit Sox10 expression levels similar to wild-type tumors. Thus, the comparable tumor progression kinetics observed in wild-type and heterozygote Sox10 mice likely reflects restored Sox10 dosage within those tumors.

4.4 Sox10 loss does not affect endpoint tumor growth or survival

Given the marked delay in tumor onset observed in Sox10-deficient MMTV-NIC mice, we next assessed whether this phenotype reflected modifications to tumor cell proliferative or survival programs in established tumors. Endpoint tumor sections and lysates from MMTV-NIC: $Sox10^{+/+}$ and MMTV-NIC: $Sox10^{fl/+}$ mice were analyzed for markers of proliferation, apoptosis, and downstream oncogenic signalling.

Immunohistochemical staining for Ki67 revealed comparable proportions of proliferating tumor cells between genotypes (Fig. 4.5 A, B). Consistent with this, no significant differences in CC3 staining were observed (Fig. 4.5 C, D). Similarly, western blot analysis of endpoint tumor lysates showed no significant differences in the expression of proliferative markers PCNA and Cyclin D1, and apoptotic markers PARP, and CC3

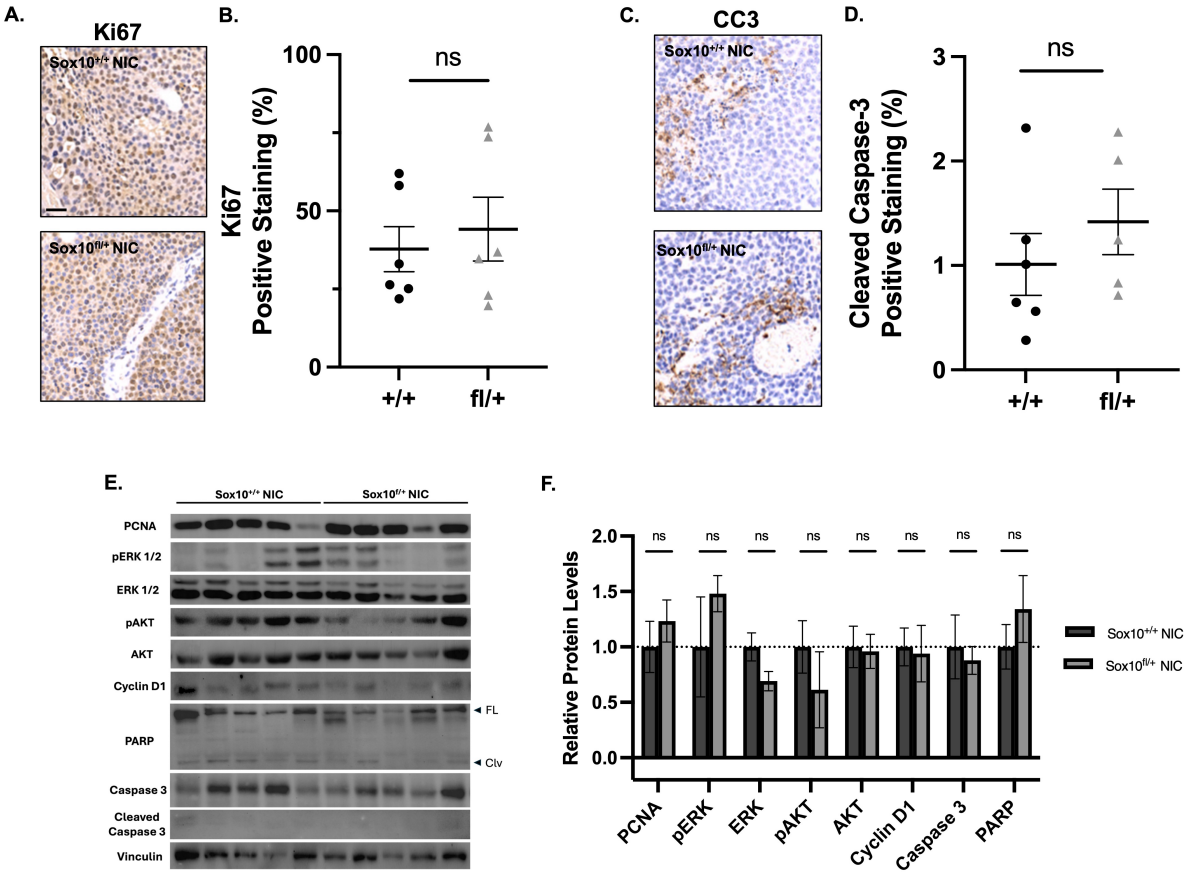

Figure 4.5. Hemizygous Sox10 MMTV-NIC endpoint tumors do not show altered tumor proliferative or survival programs. (A) Representative images of Ki67 stained FFPE endpoint sections from MMTV-NIC: $Sox10^{+/+}$ and $^{fl/+}$ tumor bearing mice. **(B)** Quantification of $Ki67^{+}$ stained cells from (A). **(C)** Representative images of CC3 stained FFPE endpoint sections from MMTV-NIC: $Sox10^{+/+}$ and $^{fl/+}$ tumor bearing mice. **(D)** Quantification of $CC3^{+}$ stained cells from (C). **(E)** Endpoint tumor lysates were assessed for the expression of various proliferative and apoptotic markers using Western blot analysis. Three independent runs were used for quantification. **(F)** Densitometric quantitation of Western blots shown in (E). $n \geq 5$ mice/group. Data shown as mean $\pm$ SEM. Scale bar represents 50µm.

(Fig. 4.5 E, F) Importantly, no obvious dysregulation of canonical HER2/Neu downstream pathways, as assessed by levels of phosphorylated ERK1/2 and AKT, were detected; indicating that MAPK and PI3K signalling remained largely intact in hemizygous Sox10 tumors (Fig. 4.5 E, F).

Together, these findings indicate that endpoint tumors arising in hemizygous MMTV-NIC: $Sox10^{fl/+}$ mice maintain equal Sox10 expression, tumor cell growth and survival, and intact downstream oncogenic signalling pathways that are indistinguishable from wild-type tumors. To this end, the delayed tumor onset observed in Sox10-deficient mice is therefore unlikely due to impaired growth or survival programs in established tumors, further supporting a role for Sox10 during early tumor initiation.

4.5 Hyperplastic lesion formation is delayed in Sox10-deficient MMTV-NIC mice

Although Sox10 expression is comparable in MMTV-NIC: $Sox10^{+/+}$ and $^{fl/+}$ endpoint tumors, we hypothesized that reduced Sox10 dosage in hemizygous non-transformed luminal cells at the hyperplastic stage prior to onset might be sufficient to delay tumor initiation. To test this, mammary glands were collected at 16-weeks of age, prior to the emergence of palpable tumors and assessed for lesion formation.

Hematoxylin staining of 16-week-old mammary glands revealed numerous hyperplastic lesions in wild-type MMTV-NIC: $Sox10^{+/+}$ mice (Fig. 4.6 A-C). Strikingly, lesions were not observed in age matched MMTV-NIC: $Sox10^{fl/+}$ mice (Fig. 4.6 A-C). On average, an additional 8 weeks were required for hemizygous mice to display detectable hyperplastic lesions (Fig. 4.6 A-C). Sox10 staining in 16-week-old Sox10-deficient MMTV-NIC: $Sox10^{fl/fl}$ revealed a marked luminal-specific reduction in $Sox10^{+}CK8^{+}$ luminal cells, while Sox10 expression was retained in the basal

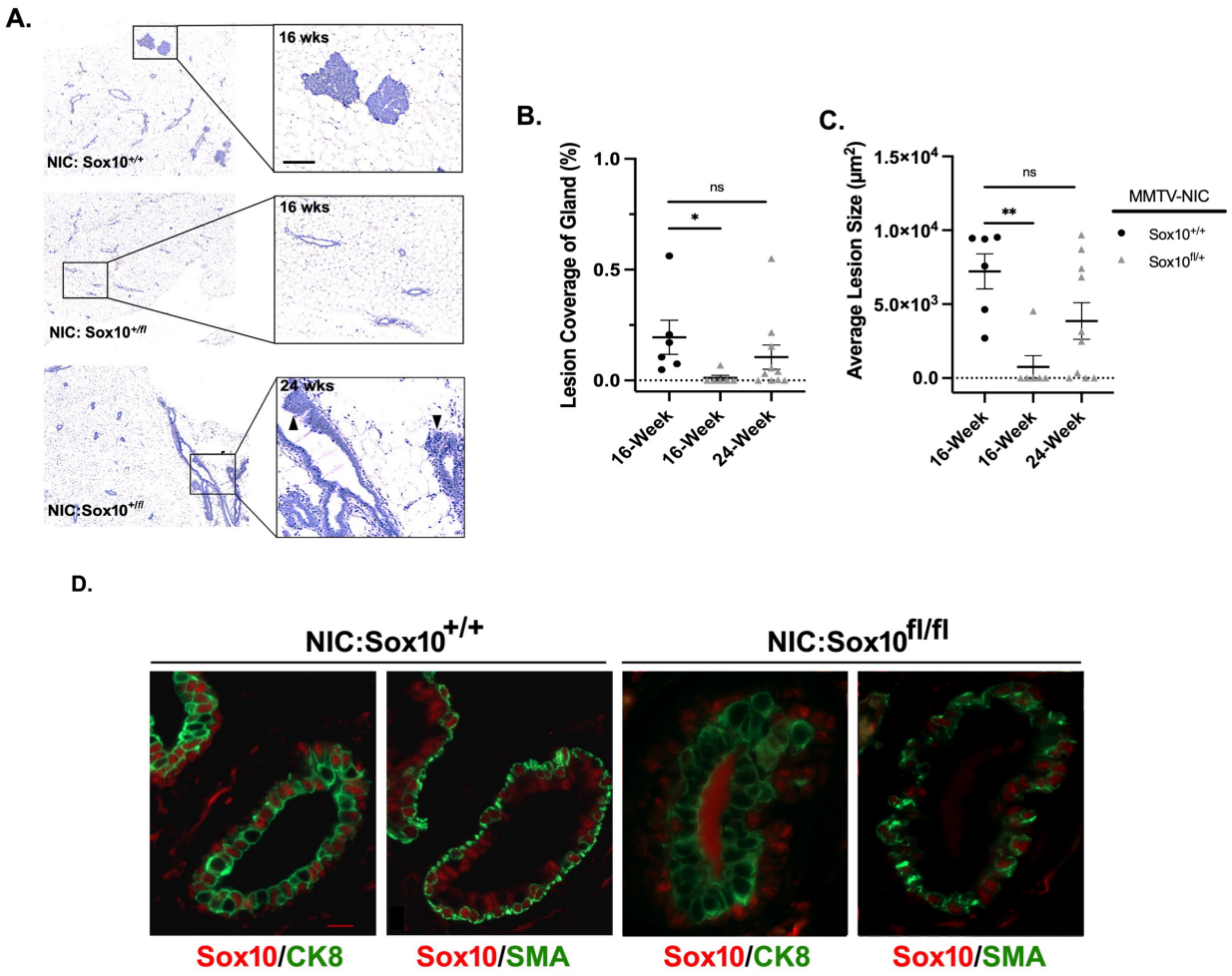

Figure 4.6. Hyperplastic lesion formation is delayed in Sox10-deficient MMTV-NIC mice. **(A)** Representative images of hematoxylin stained FFPE mammary gland sections from 16-, and 24-week-old MMTV-NIC mice. Arrows indicating areas of transformed lumen in 24-week-old mice. **(B, C)** Quantification of total mammary gland coverage (B) and average size of hyperplastic lesions (C) in section from (A). **(D)** Representative images of 16-week-old MMTV-NIC: $Sox10^{+/+}$ and $^{fl/fl}$ glands stained for Sox10, CK8, and αSMA. Scale bar represents 200µm and 20µm, respectively. n≥ 6 mice/group. Data shown as mean ± SEM. *, ** represent $p < 0.05$, and 0.01, respectively.

αSMA^{+} layer, suggesting efficient luminal Sox10 excision prior to the age of tumor onset (Fig. 4.6 D).

Since Sox10 hemizygosity in MMTV-NIC: Sox10$^{fl/+}$ mice is expected to reduce total Sox10 expression without altering the proportion of Sox10^{+} luminal cells, we next quantified the relative Sox10 protein levels using relative fluorescence intensity. Indeed, total Sox10^{+} CK8^{+} cells remained unchanged between groups, while immunostaining revealed a marked reduction of Sox10 expression in 16-week-old hemizygous MMTV-NIC: Sox10$^{fl/+}$ females (Fig. 4.7 A, B). Notably, hyperplasia-bearing 24-week-old MMTV-NIC: Sox10$^{fl/+}$ females exhibited higher relative Sox10 expression than at 16-weeks of age, coinciding with the emergence of detectable hyperplastic lesions (Fig. 4.7 C).

Together, these findings support that reduced Sox10 expression in the luminal epithelium delays the onset of hyperplastic lesion formation in MMTV-NIC mice. Furthermore, increased Sox10 expression accompanies the transition from normal epithelium to early hyperplasia, suggesting a critical role for Sox10 during the earliest stages of HER2/Neu-induced tumorigenesis.

4.6 Sox10-deficient MMTV-NIC females remain disease free up to 1 year of age

Given the complete absence of palpable tumors in Sox10-deficient MMTV-NIC Sox10$^{fl/fl}$ mice, we next asked whether early hyperplastic lesions formed but failed to progress into adenocarcinomas. To address this, mammary glands were harvested from one-year-old MMTV-NIC: Sox10$^{fl/fl}$ females and examined histologically. Sox10-deficient mice displayed normal ductal architecture and were indistinguishable from age-matched wild-type controls, with no evidence of hyperplastic lesions or tumor formation (Fig. 4.8 A). When assessed for expression of Sox10, immunofluorescent staining of year old MMTV-NIC Sox10$^{fl/fl}$ mice showed that

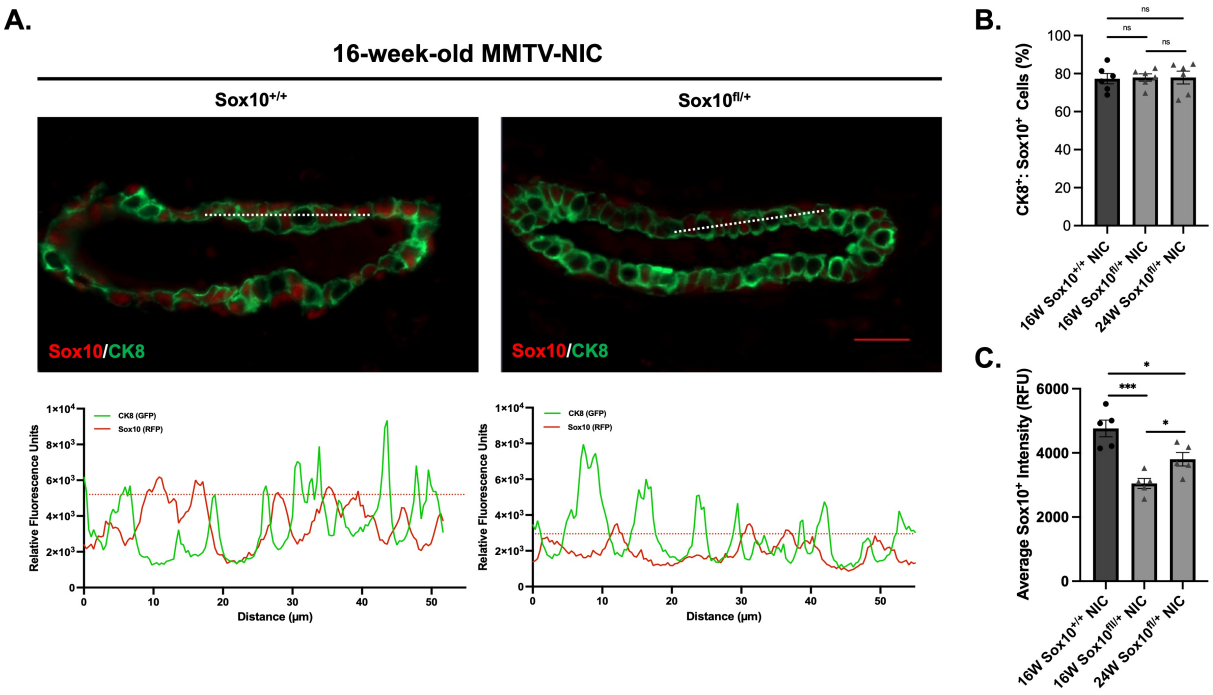

Figure 4.7. Sox10 hemizygosity in MMTV-NIC: Sox10$^{fl/+}$ mice reduces relative Sox10 expression in luminal cells. (A) Representative images of 16-week-old MMTV-NIC: Sox10$^{+/+,}$ and $^{fl/+}$ mammary gland sections stained with Sox10 and CK8. White dotted lines on ductal structures represent relative fluorescent profiles of approximately ten CK8^{+} cells and their associated Sox10 expression levels. Red dotted lines on accompanying RFU plots represent average fluorescent intensity of cellular Sox10 detected in each profile. **(B, C)** Quantification of total Sox10 expressing CK8^{+} luminal cells (B) and average intensity of detected Sox10 signal (C) in (A). Scale bar represents 20 µm. Data shown as average quantification for 10 ductal structures per animal. n≥ 5 mice/group. Data shown as mean ± SEM. *, *** represent $p < 0.05$, and 0.001, respectively.

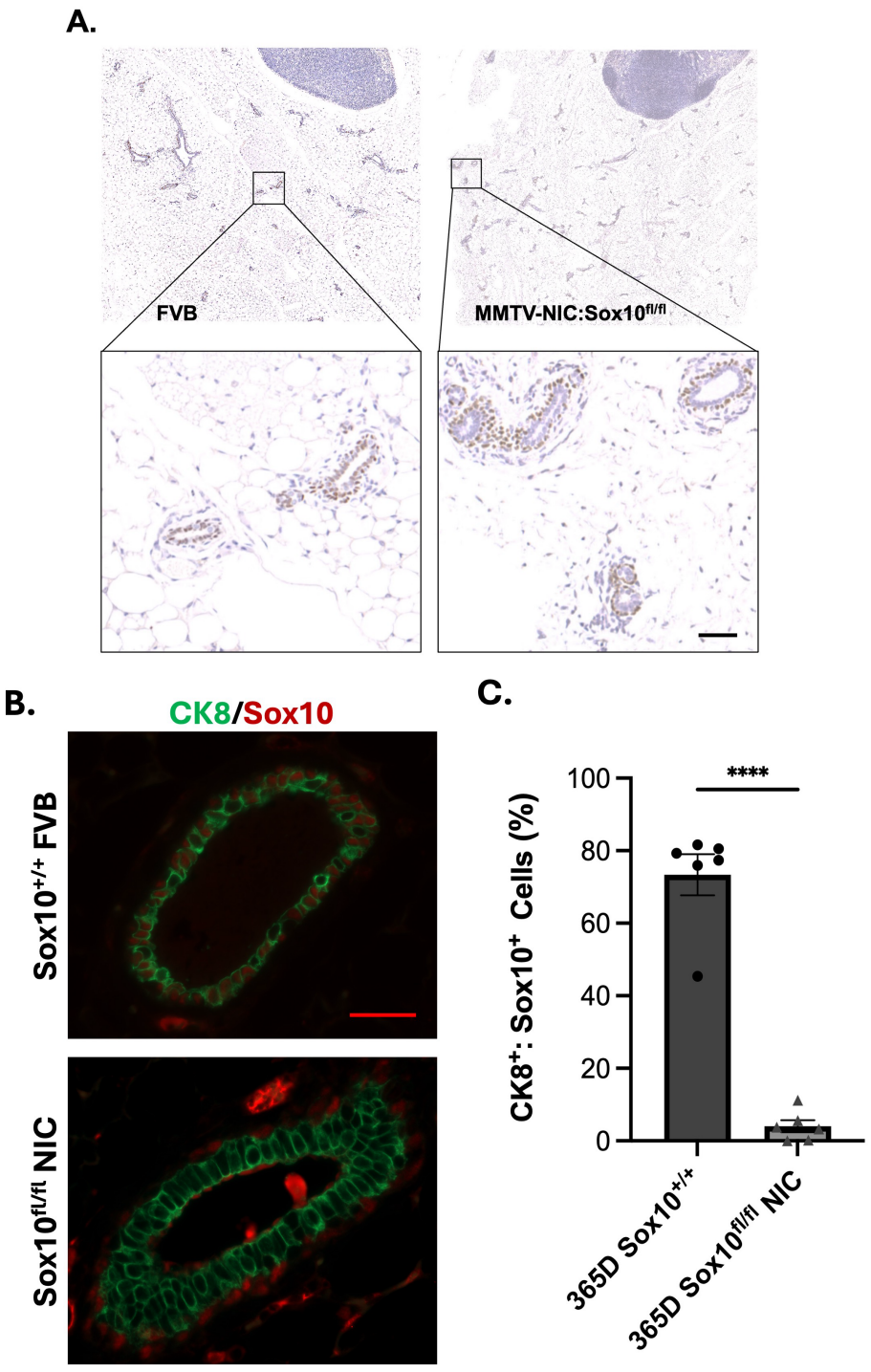

Figure 4.8. Sox10-deficient MMTV-NIC remain tumor free for up to one year. (A) Representative images of Sox10-stained mammary glands from 365D old FVB and MMTV-NIC: Sox10$^{fl/fl}$ mice. **(B)** Representative images of 365D old Sox10$^{+/+}$ FVB and MMTV-NIC: Sox10$^{fl/fl}$ glands stained for Sox10 and CK8. **(C)** Quantification of Sox10^{+}CK8^{+} luminal cells from mammary gland sections in (B). n≥ 5 mice/group. Scale bar represents 50µm. Data shown as mean ± SEM. **** represent $p < 0.0001$.

Sox10 was absent in the majority of luminal $CK8^+$ ducts with low expression observed in some (Fig. 4.8 B, C).

Together, these data suggest that *Sox10* is efficiently recombined prior to the onset of palpable tumor formation in hemizygous MMTV-NIC: $Sox10^{fl/+}$ females and that the altered temporal Sox10 expression profile in these mice parallels the observed delay in tumorigenesis. Importantly, efficient luminal-specific *Sox10* excision throughout the lifetime of Sox10-deficient MMTV-NIC: $Sox10^{fl/fl}$ females completely abrogates any evidence of malignant transformation while preserving normal ductal architecture.

4.7 Loss of Sox10 reduces tumor-initiating cell compartment and stemness

Previous lineage tracing studies have shown that basal-like breast tumors etiologically arise from LPs rather than from basal stem cells, supporting a model of luminal-to-basal reprogramming during tumorigenesis (185,219,220). To this end, past reports using MMTV-Neu and MMTV-PyMT models have demonstrated that mammary tumors likely originate from LP populations (215–218). Specifically in the case of MMTV-Neu spontaneous mammary tumors, the cellular fraction harboring the highest degree of TIC potential has been found to be enriched in the CD61-expressing LP compartment (190,215,217). Thus, to evaluate the tumor-initiating cell population in Sox10-deficient NIC females, mammary glands from pre-cancerous 16-week-old MMTV-NIC: $Sox10^{+/+,}$ $^{fl/+,}$ and $^{fl/fl}$ mice were stained for the $Lin^-CD49f^+CD61^+$ TIC population. Strikingly, a dose-dependent reduction in this TIC population was observed in the Sox10-deficient groups of MMTV-NIC mice, supporting a depletion of tumor-initiating activity upon *Sox10* inactivation (Fig. 4.9 A, B). Cells from this TIC compartment were further isolated and seeded in mammosphere formation assays to evaluate their capacity for functional stemness.

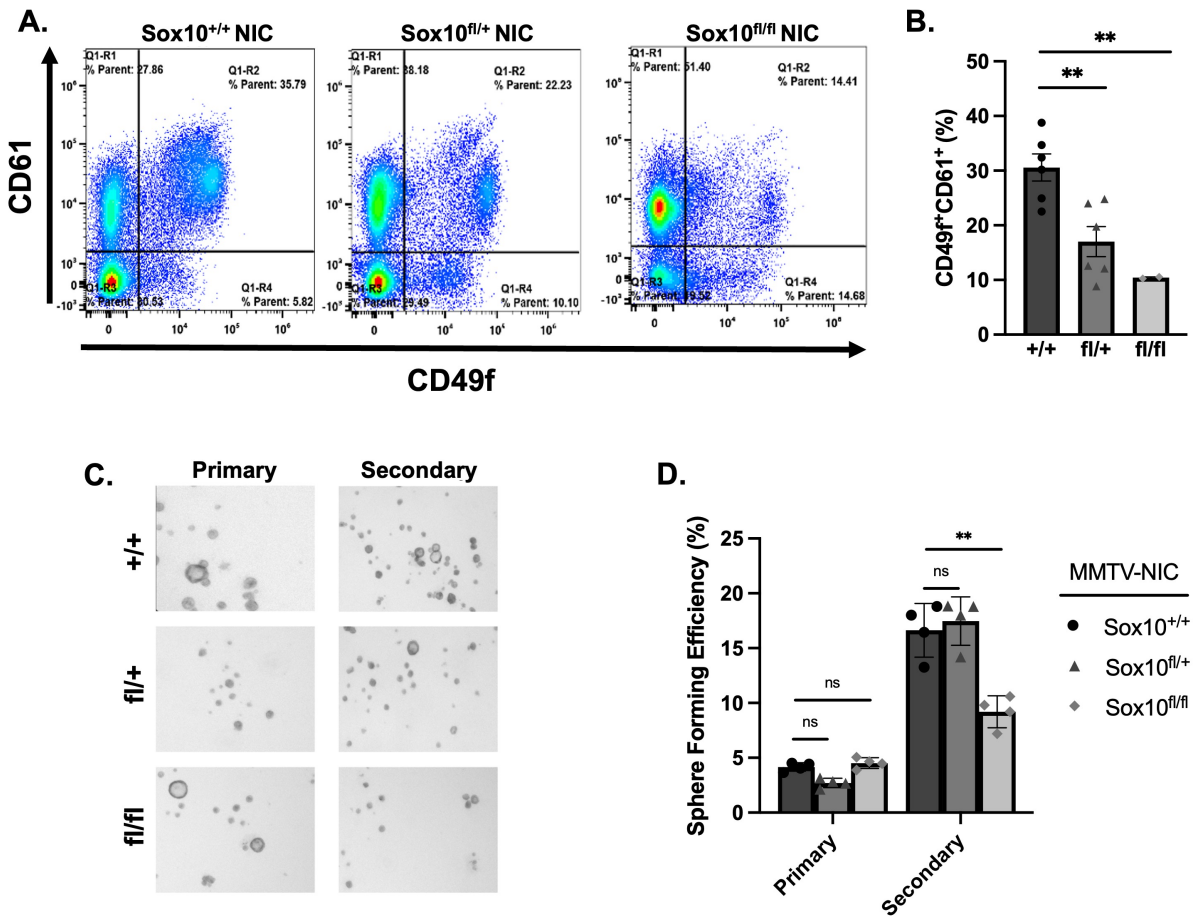

Figure 4.9. Sox10 defines the tumor-initiating cell compartment in hyperplastic MMTV-NIC mice. (A) Representative flow plots of 16-week-old MMTV-NIC: $Sox10^{+/+}$, $^{fl/+}$, and $^{fl/fl}$ mammary glands sorted for the TIC-enriched $Lin^{-}CD49f^{+}CD61^{+}$ compartment. **(B)** Quantification of the TIC compartment from (A). **(C)** Representative images of primary and secondary mammospheres from cells isolated from the luminal ($Lin^{-}CD49f^{+}CD24^{hi}$) compartment in (A). **(D)** Quantification of mammosphere forming efficiency from (C). n $\geq$ 2 mice/group. Data shown as mean $\pm$ SEM. ** represent $p < 0.01$.

MMTV-NIC: Sox10$^{fl/fl}$ mice showed a significantly reduced capacity for secondary sphere formation, suggesting a reduction in self-renewal abilities (Fig. 4.9 C, D). Interestingly, Sox10 hemizygous MMTV-NIC Sox10$^{fl/+}$ females did not show any indication of reduced stemness when compared to wild-type mice.

4.8 Generation of MMTV-rtTA: tetO-MIC: Sox10$^{fl/fl}$ mice

While we have established a key role for Sox10 in primary HER2/Neu-induced mammary tumor formation, we next wanted to assess whether Sox10 maintains a similar function in metastatic dissemination. However, due to the relatively low propensity for overt metastases in the MMTV-NIC model, we used an additional transgenic model that enables robust assessment of spontaneous metastases (126,127). To specifically assess the requirement for Sox10 in the development of invasive lesions, we used the doxycycline-inducible rtTA/MIC model, which drives expression of PyMT specifically within the luminal mammary epithelium.

Following treatment with doxycycline, these mice develop aggressive, multifocal mammary adenocarcinomas with high incidence of metastatic lesions (146). Importantly, this model permits temporal control of oncogene expression, thereby uncoupling mammary gland development from oncogene-dependent transformation. This key feature allows full mammary gland development prior to oncogene activation, alleviating potential developmental defects arising from target gene excision and oncogene expression. Although this tumor model is not driven by HER2/Neu, PyMT-induced mammary tumors have been shown to recapitulate key receptor tyrosine kinase-dependent signalling pathways, including activation of PI3K and MAPK cascades that are central to HER2-mediated tumorigenesis pathways, and frequently acquire transcriptional profiles that are similar to HER2-positive breast cancer (135,143,151).

To achieve concomitant doxycycline-dependent luminal-specific excision of *Sox10* and oncogene expression, MMTV-rtTA mice were first crossed with tetO-MIC mice. Resulting bigenic rtTA/MIC mice were then crossed with $Sox10^{fl}$ mice (Fig. 4. 10 A, B). In this model, luminal-epithelium-specific expression of rtTA is driven by the MMTV-promoter. When paired with doxycycline, rtTA drives bicistronic expression of PyMT and Cre recombinase specifically through the tetO, resulting in luminal-specific oncogene expression and excision of the floxed *Sox10* allele. Offspring were genotyped by PCR to confirm the presence of MMTV-rtTA and tetO-MIC transgenes, as well as *Sox10* allele status (Fig. 4.10 C).

4.9 Loss of Sox10 in rtTA/MIC mice confers a dose-dependent survival advantage

To determine whether Sox10 is required for primary tumor development in a PyMT-driven context, survival studies using rtTA/MIC: $Sox10^{+/+, fl/+}$ and $^{fl/fl}$ mice treated with doxycycline were conducted. Consistent with the MMTV-NIC data, Kaplan-Meier analysis revealed a significant, dose-dependent increase in disease-free survival following Sox10 inactivation (Fig. 4.11 A). Hemizygous rtTA/MIC: $Sox10^{fl/+}$ mice exhibited a moderate delay in palpable tumor onset relative to wild-type controls, with an average extension of approximately 11 days. In contrast, Sox10-deficient rtTA/MIC: $Sox10^{fl/fl}$ mice remained disease free for the duration of the study, indicating a complete failure to form palpable tumors (Fig. 4.11 A).

Since PyMT-induced mammary tumorigenesis is characterized by multifocal and synchronous transformation of ductal structures, with the majority exhibiting complete transformation with continued doxycycline treatment, efficient and reliable measurement of individual tumor progression through conventional palpation methods is not possible (146). Therefore, to effectively assess tumor burden in rtTA/MIC: $Sox10^{+/+, fl/+}$ and $^{fl/fl}$ mice, total mammary gland weights were quantified relative to body weight at endpoint. Consistent with

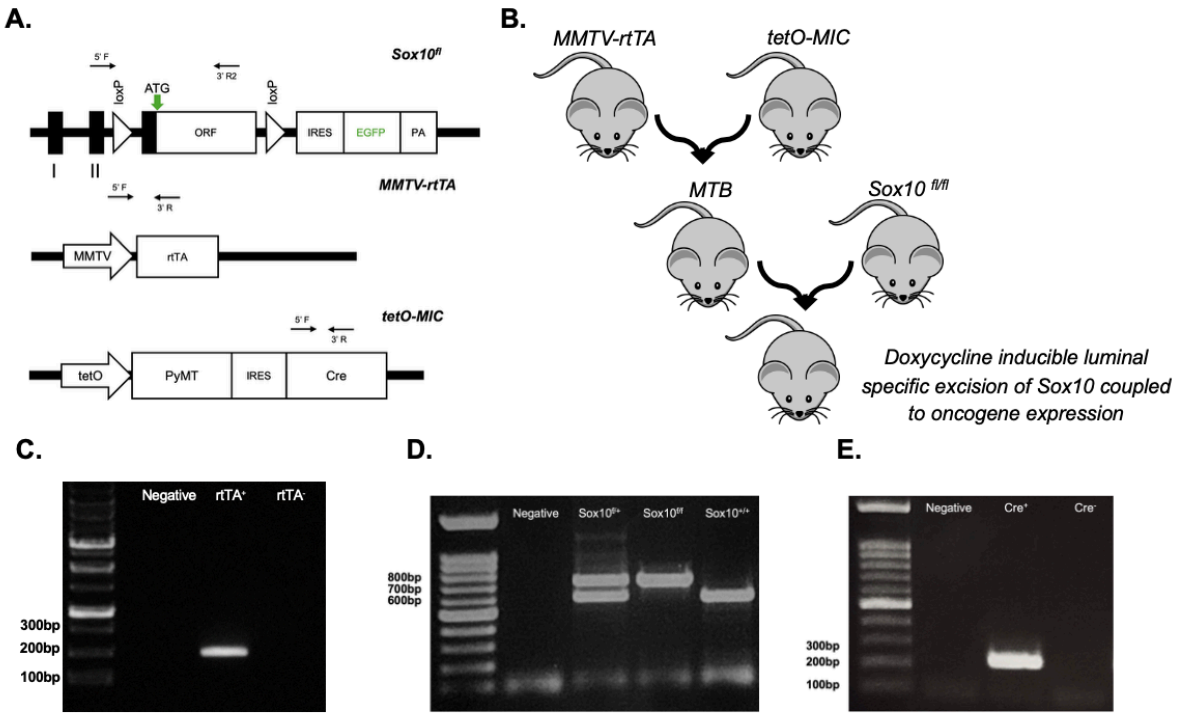

Figure 4.10. Schematic Representation of the MMTV-rtTA: tetO-MIC: Sox10$^{fl/fl}$ animal model. (A, B) MMTV-rtTA mice were first crossed with tetO-MIC mice then subsequently crossed with Sox10$^{fl/fl}$-EGFP for doxycycline inducible luminal-specific bicistronic expression of the PyMT oncogene coupled to Cre recombinase for *Sox10* excision. **(C)** Representative PCR genotyping products of rtTA^{+}, and rtTA^{-} mice. **(D)** Representative PCR genotyping products of Sox10$^{+/+}$, Sox10$^{fl/+}$, Sox10$^{fl/fl}$, and Sox10$^{+/+}$ mice. **(E)** Representative PCR genotyping products of Cre^{+}, and Cre^{-} mice.

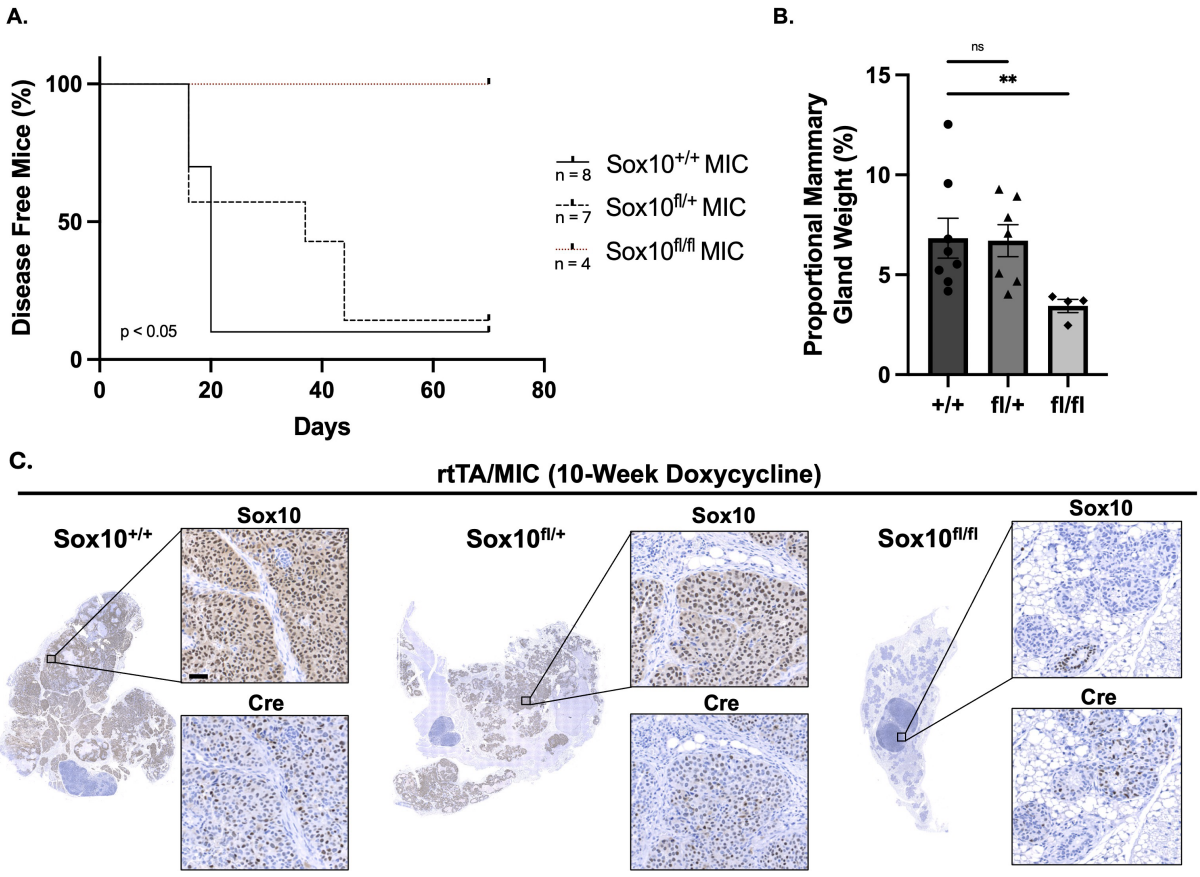

Figure 4.11. Loss of Sox10 provides a dose-dependent survival advantage in rtTA/MIC mice. **(A)** Kaplan-Meier disease-free survival curves in rtTA/MIC: $Sox10^{+/+, fl/+, fl/fl}$ mice. Significance assessed by log-rank test. **(B)** Proportional total mammary gland weight of mice in (A) at endpoint. **(C)** Representative IHC images of mammary gland FFPE sections from rtTA/MIC: $Sox10^{+/+, fl/+, fl/fl}$ mice treated with doxycycline for 10-weeks and stained with Sox10 and Cre. n $\geq$ 4 mice/group. Scale bar represents 50µm. n $\geq$ 4 mice/group. Data shown as mean $\pm$ SEM. ** represents $p < 0.01$.

delayed tumor initiation, Sox10-deficient rtTA/MIC: Sox10$^{fl/fl}$ mice displayed a significant decrease in total mammary gland tumor burden (Fig. 4.11 B). When interrogated for ductal lesion formation, histological sections from in rtTA/MIC: Sox10$^{+/+,}$ and $^{fl/+}$mice revealed extensive development of multifocal lesions that strongly stained for Sox10 (Fig. 4.11 C). Interestingly, rtTA/MIC: Sox10$^{fl/fl}$ mice similarly showed the presence of multifocal lesions, however, these were markedly smaller and lacked detectable Sox10, consistent with efficient Sox10 ablation. Importantly, Cre staining was evident across all genotypes, confirming that oncogene activation was maintained following *Sox10* deletion (Fig. 4.11 C).

Together, these findings demonstrate that Sox10 is required for efficient PyMT-driven mammary tumorigenesis, and that its loss confers a dose-dependent survival advantage.

4.10 Sox10 ablation completely abrogates lung metastasis in rtTA/MIC mice

To determine whether Sox10 is required for metastatic dissemination in PyMT-driven mammary tumorigenesis, lungs from doxycycline-treated rtTA/MIC: *Sox10*$^{+/+,\ fl/+}$ and $^{fl/fl}$ mice were examined for the presence of metastatic lesions. Gross inspection of lung tissue from rtTA/MIC: *Sox10*$^{+/+}$ and $^{fl/+}$ mice revealed numerous visible macro-metastatic nodules, whereas lungs from rtTA/MIC: *Sox10*$^{fl/fl}$ mice lacked any visible lesions (Fig. 4.12 A). Further histological examination of lung sections confirmed the presence of micro-metastatic niches in rtTA/MIC: *Sox10*$^{+/+}$ and $^{fl/+}$ mice, with metastatic foci staining strongly positive for Sox10 and Cre (Fig. 4.12 B-E). In contrast, lungs from rtTA/MIC: *Sox10*$^{fl/fl}$ mice exhibited a complete absence of Sox10 or Cre staining, suggesting an absence of metastatic niches. (Fig. 4.12 B-E).

Together, these data suggest that Sox10 is essential for the seeding of metastatic niches in the lungs during PyMT-driven mammary tumorigenesis.

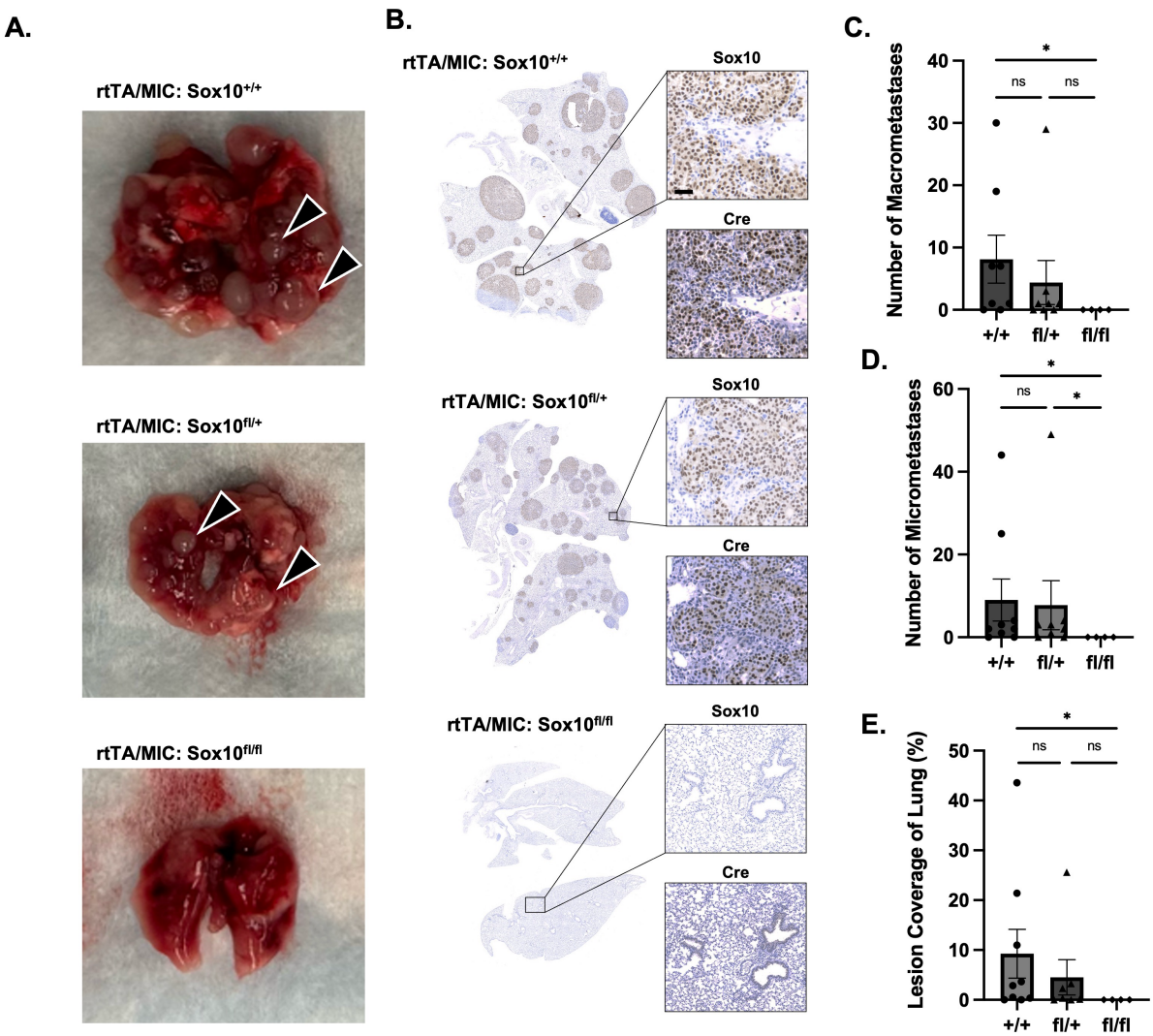

Figure 4.12. Sox10 is required for establishment of metastatic niches in the lungs of rtTA/MIC mice. (A) Representative whole lungs from rtTA/MIC: Sox10$^{+/+, fl/+, fl/fl}$ mice treated with doxycycline for 10-weeks. Macrometastases are indicated with black arrow. **(B)** Representative IHC images of lung FFPE sections from (A) stained with Sox10 and Cre. **(C-E)** Quantification of total number (C), lung coverage (D) and average lesion size (E) of lung metastases in (B). n $\geq$ 4 mice/group. Scale bar represents 50µm. Data shown as mean $\pm$ SEM. * represents $p < 0.05$.

4.11 Sox10-deficient lesions do not progress with continued doxycycline treatment

To better assess the kinetics of PyMT-induced transformation early on in tumorigenesis, a short-term doxycycline induction study was performed. As no significant differences were observed between rtTA/MIC: *Sox10*$^{+/+}$ and $^{fl/+}$ mice, subsequent analyses focused solely on rtTA/MIC: *Sox10*$^{+/+}$ and $^{fl/fl}$ mice. Mammary glands were assessed following 2 weeks of doxycycline treatment, corresponding to an early stage of oncogene induction where approximately half of ductal lumen show evidence of transformation (146). Lesion sizes were then compared to that observed after the 10-week doxycycline course. Histological examination revealed that PyMT induction for 2 weeks resulted in significantly larger lesions in rtTA/MIC: *Sox10*$^{+/+}$ mice when compared to that of rtTA/MIC: *Sox10*$^{fl/fl}$ (Fig. 4.13 A). Furthermore, lesions in rtTA/MIC: *Sox10*$^{+/+}$ mice, appeared to progress with continued doxycycline treatment, giving rise to enlarged lesions by 10 weeks in some mice. In contrast, lesions arising in rtTA/MIC: *Sox10*$^{fl/fl}$ mice failed to increase in size with extended doxycycline exposure and remained comparable in size to those observed at the 2-week time point (Fig. 4.13 B). Immunohistochemical staining demonstrated efficient Sox10 ablation in rtTA/MIC: *Sox10*$^{fl/fl}$ lesions as well as Cre expression, once again supporting that oncogene activation is maintained despite the absence of tumor progression (Fig. 4.13 B).

4.12 rtTA/MIC mice exhibit latent *Sox10* allele excision

In contrast to MMTV-NIC mice, the development of hyperplastic lesions in Sox10-deficient rtTA/MIC: *Sox10*$^{fl/fl}$ glands suggests potentially different roles of Sox10 in HER/Neu-, and PyMT-induced tumorigenesis. However, an alternative hypothesis is that PyMT activation merely occurs prior to efficient *Sox10* deletion in this model. Thus, to determine the potential

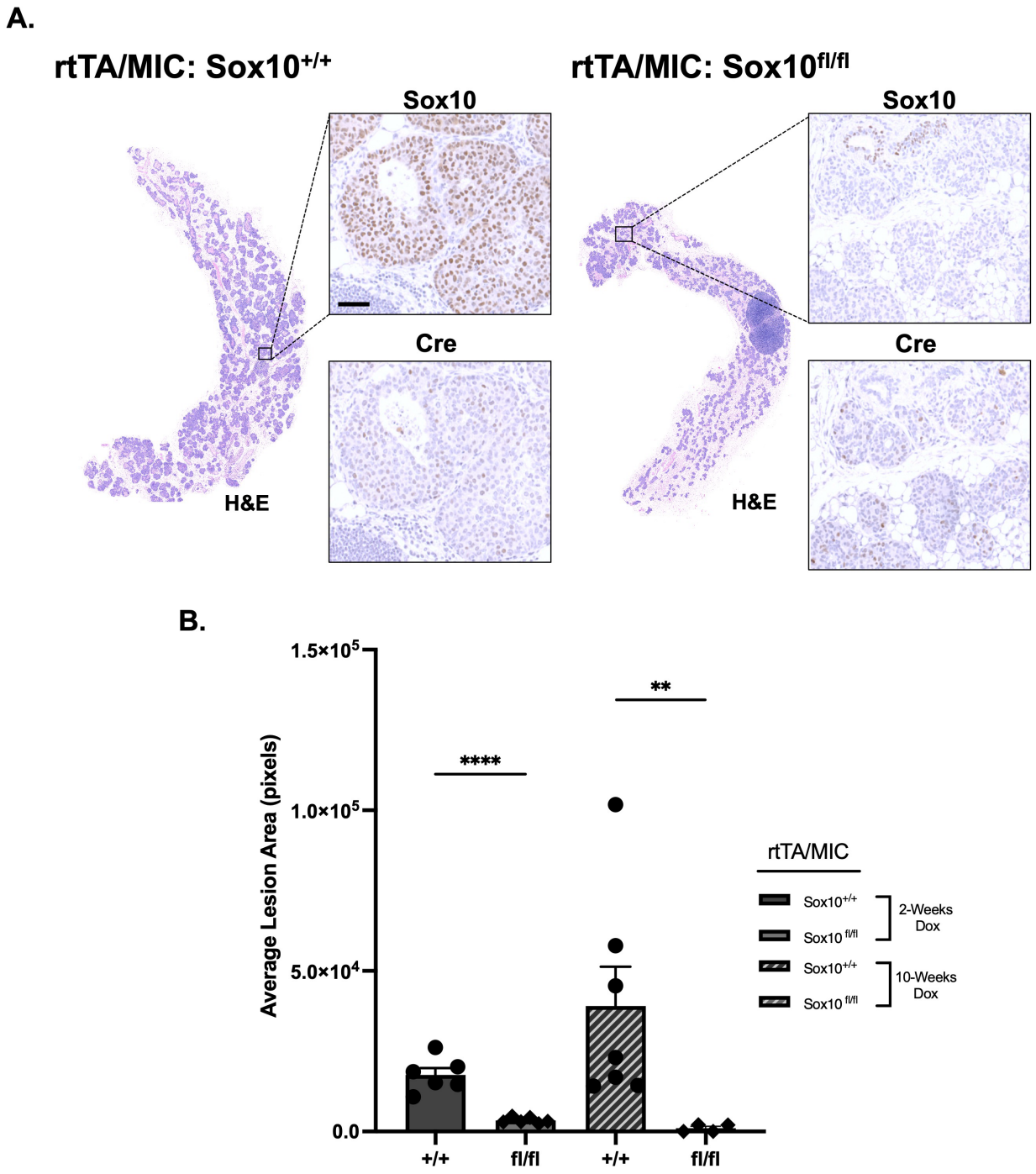

Figure 4.13. Sox10-deficient lesions do not progress after 2-weeks post induction in rtTA/MIC mice. (A) Representative IHC images of mammary gland FFPE sections from rtTA/MIC: Sox10$^{+/+,\ fl/+,\ fl/fl}$ mice treated with doxycycline for 2-weeks and stained with hematoxylin and eosin, Sox10 and Cre. **(B)** Quantification of average area of lesions in (A)**.** n ≥ 4 mice/group. Scale bar represents 100µm. Data shown as mean ± SEM. **, and **** represents $p < 0.01$, and 0.0001, respectively.

latency of *Sox10* excision following doxycycline induction of the MIC transgene, a short time-course analysis was performed in rtTA/MIC: $Sox10^{+/+}$ and $^{fl/fl}$ mice following 5, 8, and 14 days of doxycycline treatment. Cre immunostaining was readily detectable within early ductal lesions of both groups of mice at all time points, confirming spatial and temporal activation of the tetO-MIC locus (Fig. 4.14). In contrast, Sox10 staining in rtTA/MIC: $Sox10^{fl/fl}$ lesions demonstrated delayed loss relative to Cre induction. Sox10 expression remained detectable at early time points despite Cre positivity and was progressively lost over time, with substantially diminished Sox10 signal in later time points (Fig. 4.14). These findings indicate that *Sox10* excision is not immediate following activation of the tetO-MIC, indeed supporting a temporal lag in target allele recombination following oncogene expression. Together, these data support a mechanism by which Sox10 retention during early oncogene induction gives rise to a temporal window that permits Sox10-dependent lesion establishment, while prolonged doxycycline exposure leads to eventual Sox10 ablation and subsequent failure of tumor progression.

4.13 Sox9 cannot compensate for Sox10 loss in NIC and rtTA/MIC models

The SoxE family member Sox9 has been established as a mediator of luminal lineage commitment via LP regulation as well as tumor progression in basal-like breast cancer models (200,251,315,316). Given its role in LP maintenance and luminal-basal plasticity, as well as its high sequence homology and functional overlap with Sox10, we next wanted to evaluate whether Sox9 expression was modulated following Sox10 ablation (238). Since we saw depletion of TIC compartment in Sox10-deficient mice at 16 weeks of age, Sox9 levels were therefore similarly examined in 16-week-old MMTV-NIC mammary glands (Fig. 4.15 A). Robust Sox9 expression in both luminal and basal compartments was observed across all Sox10 genotypes, suggesting that the loss of Sox10 does not affect Sox9 expression and, importantly, that Sox10's function in

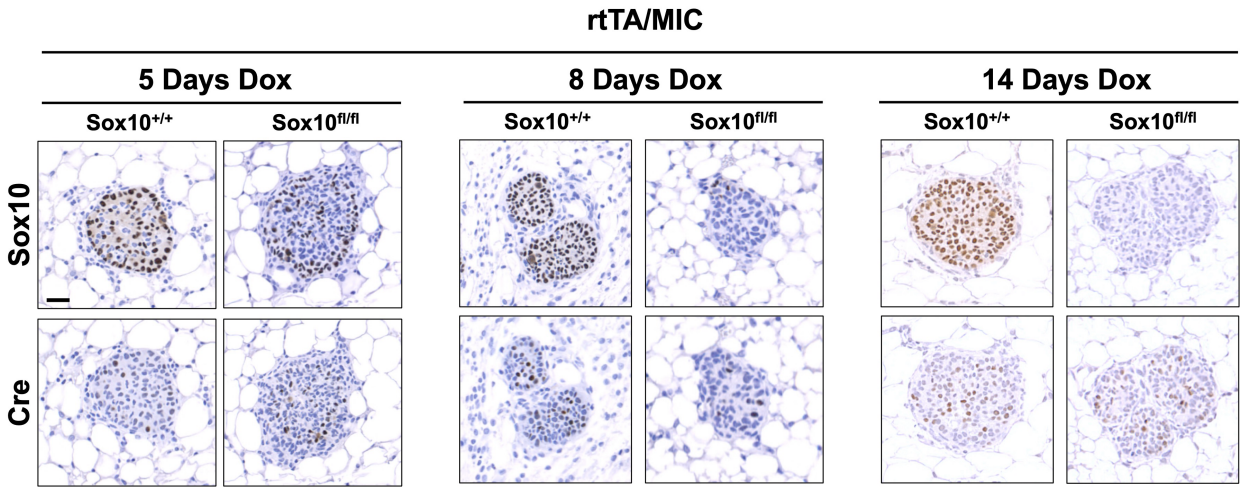

Figure 4.14. rtTA/MIC: Sox10$^{fl/fl}$ mice exhibit latent *Sox10* excision following doxycycline induction of the PyMT locus. Representative images of lung FFPE sections from of 5-, 8-, and 14-day doxycycline treated rtTA/MIC: Sox10$^{+/+,}$ and $^{fl/fl}$ mice stained with Sox10 and Cre. Scale bar represents 50µm.

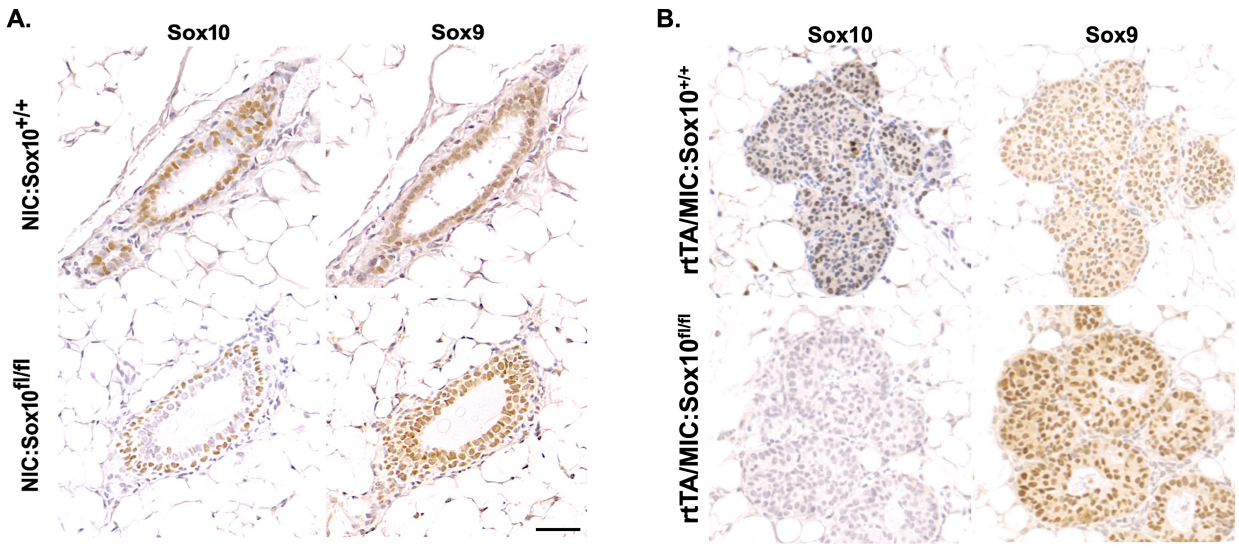

Figure 4.15. Sox10 inactivation does not affect expression of Sox9 in the ductal epithelium. **(A)** Representative images of mammary gland sections from 16-week-old MMTV-NIC: $Sox10^{+/+}$ and $^{fl/fl}$ stained with Sox10 and Sox9. **(B)** Representative images of mammary gland sections from 14-day doxycycline treated rtTA/MIC: $Sox10^{+/+}$ and $^{fl/fl}$ stained with Sox10 and Sox9. Scale bar represents 50 µm.

HER2/Neu-induced malignant transformation appears to be independent to that of Sox9. Supporting this, Sox9 similarly remained unchanged in wild-type and Sox10-deficient rtTA/MIC mice (Fig. 4.15 B). Together, these data suggest a critical role for Sox10 in the maintenance of TICs in RTK-dependent mammary tumorigenesis that is independent of other SoxE family members.

4.14 Summary

Previously, it has been shown that Sox10 is a key regulator of cellular plasticity, stem/progenitor identity, and malignant progression in mammary tumorigenesis, particularly in basal-like and triple-negative breast cancer models. In HER2/Neu-driven contexts, Sox10 expression has been associated with aggressive tumor phenotypes and poor clinical outcome. However, whether Sox10 plays a functional role in tumor initiation and progression, or instead reflects a transient state of cellular plasticity, has not been addressed.

Here, we have shown that Sox10 is a dose-dependent regulator of mammary tumorigenesis in luminal HER2/Neu-, and PyMT-driven mouse models. Using the MMTV-NIC model, we show that luminal-specific Sox10 deletion markedly delays tumor initiation, with hemizygous loss prolonging disease-free survival and complete Sox10 ablation fully preventing tumor formation for up to one year. Consistent with this interpretation, Sox10 depletion significantly delays the formation of hyperplastic lesions. It appears that Sox10 acts as a key regulator of the $Lin^{-}CD49f^{+}CD61^{+}$ tumor-initiating cell compartment in the mammary epithelium and upon its inactivation, tumor formation is markedly affected. We further demonstrate that Sox10 is required not only for efficient primary tumor initiation but also for tumor progression and metastatic dissemination using the dox-inducible rtTA/MIC model.

Chapter 5: Sox10-deficient HER2/Neu-transformed epithelial cells exhibit reduced stemness and erosion of luminal progenitor identity.

5.1 Introduction and Rationale

We have demonstrated that Sox10 is functionally required for HER2/Neu-induced mammary tumor initiation and progression potentially through regulation of the luminal TIC compartment. While these *in vivo* studies establish a central role for Sox10 during mammary tumorigenesis, precisely how Sox10 confers the tumorigenic capacity to this TIC compartment remains unclear. Immunohistochemical analyses of endpoint tumors from wild-type and hemizygous MMTV-NIC: *Sox10*$^{fl/+}$ mice in the previous chapter have shown very high incidence of Sox10^{+} cells in tumor sections and tissues. While we have yet to see HER2/Neu-, or PyMT-transformed tissues that lack considerable Sox10^{+} cell contribution, the range of total Sox10-positivity is quite broad, and the full extent of this Sox10 expression has not been comprehensively studied. Consistent with this murine heterogeneity, the proportion of Sox10^{+} nuclei varies markedly between human HER2^{+} breast cancer tumors, ranging from approximately 15% to 80% (130,291–293,295). This variability likely reflects differences in tumor cell state, cellular plasticity, and tumor-initiating or stem-like cell content across tumors.

Such heterogeneity at endpoint ultimately limits the ability to directly interrogate Sox10 function *in vivo*. Thus, to further define the role of Sox10 in HER2/Neu-driven mammary tumorigenesis, we employed an *in vitro* based approach. Here, Neu-transformed luminal epithelial cell lines isolated from tumor-bearing MMTV-NDL mice were established, subjected to CRISPR-Cas9-mediated Sox10 inactivation, and assessed for functional behavior and transcriptional response.

5.2 Generation of CRISPR-Cas9 Sox10-inactivated Neu-derived cell lines

To further investigate the role of Sox10 in HER2/Neu-induced mammary tumorigenesis *in vitro*, low-passage Sox10-expressing mammary tumor cell lines were derived from endpoint tumors arising in MMTV-NeuNDL mice (Fig. 5.1). Two independent $Sox10^{+}$ tumor cell lines (BG1 and BG2) were successfully established. To achieve targeted Sox10 inactivation, cells were stably transduced with Cas9, and RFP-tagged single-guide RNAs (sgRNAs) directed against the Sox10 coding sequence, specifically in the D (sgRNA-1) and HMG (sgRNA-2) domains in exons 3 and 4, respectively. A non-targeting RFP-tagged single-guide RNA (NTC) was used as a negative control. Following transduction, RFP^{+} cells were isolated by flow cytometry and expanded for downstream applications.

Both guides demonstrated efficient inactivation of Sox10 in the BG2 cells as indicated by a significant loss of Sox10 immunofluorescent nuclear staining, with less than 5% of cells retaining detectable Sox10 expression (Fig. 5.2 A, B). Sox10 depletion was further verified through RT-qPCR, which revealed a marked reduction in *Sox10* transcript levels relative to NTC controls (Fig. 5.2 C). Finally, western blot analysis confirmed that Sox10 knockout had no effect on Neu expression and the luminal marker CK8 (Fig. 5.2 D). sgRNA-2 transduced cell lines were randomly selected for subsequent functional analyses with the BG2 cell line.

5.3 Sox10 is dispensable for tumor cell growth *in vitro* but is required for 3D-ECM invasion

First, we wanted to assess whether the reduced tumorigenesis observed *in vivo* was in part attributed to altered tumor cell growth following Sox10 inactivation. To assess this, $BG2^{sgNTC}$ and

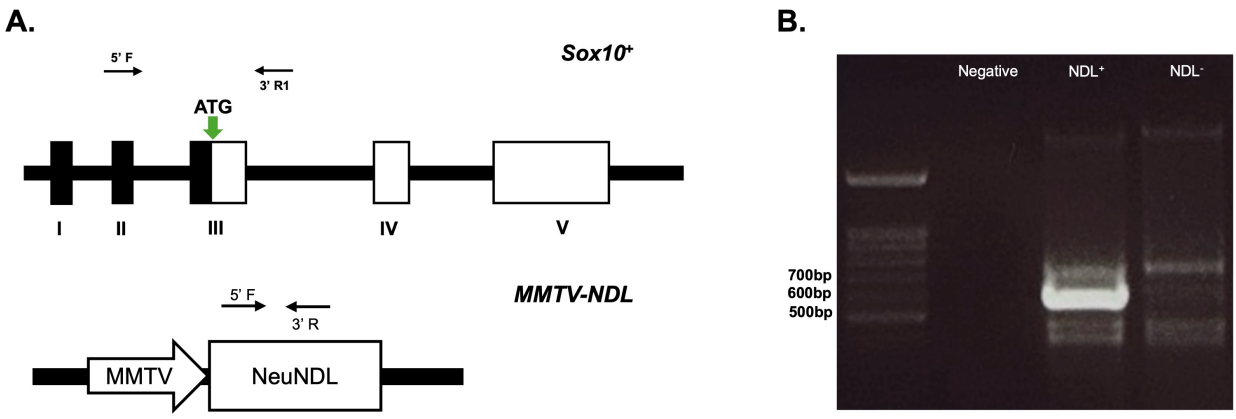

Figure 5.1. Schematic Representation of the MMTV-NeuNDL: Sox10$^{fl/fl}$ animal model. MMTV-NeuNDL female mice exhibit luminal-specific expression of the Neu oncogene. **(B)** Representative PCR genotyping products of NDL^{+}, and NDL^{-} mice.

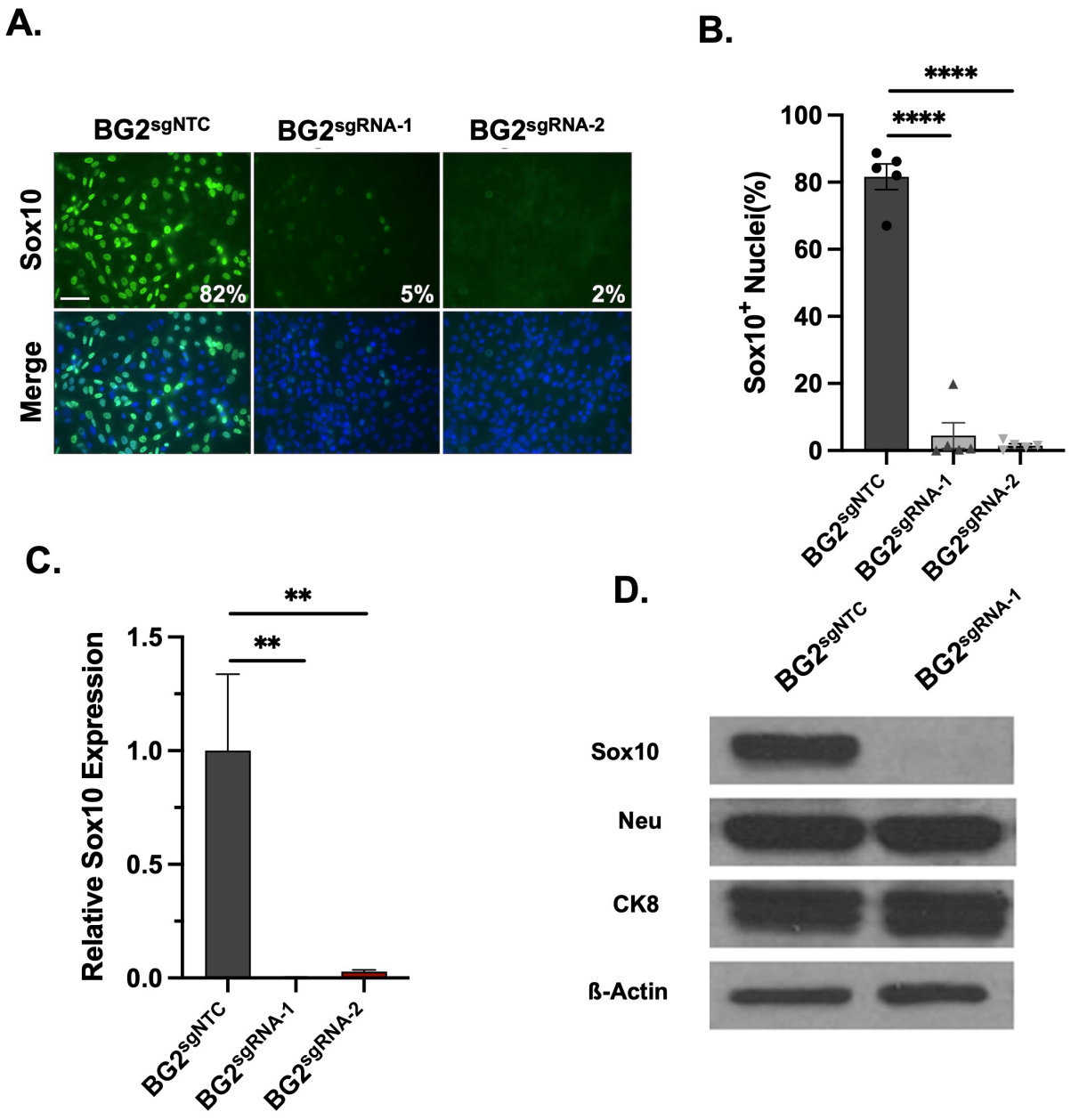

Figure 5.2. Efficient CRISPR-Cas9 mediated Sox10-inactivation in MMTV-NDL mammary tumor isolated cell lines. (A) Representative immunofluorescence images of BG2^{sgNTC} control, and Sox10-deficient BG2$^{sgRNA-1}$ and BG2$^{sgRNA-2}$ cells stained for Sox10 and DAPI. **(B)** Quantification of Sox10^{+} nuclei from (A). **(C)** RT-qPCR analysis of Sox10 mRNA expression in BG2$^{sgNTC,\ sgRNA-1,}$ and $^{sgRNA-2}$ lines. **(D)** Immunoblot analysis of Sox10, Neu, and CK8 expression in BG2^{sgNTC} and BG2$^{sgRNA-1}$ cell lines. Data shown as mean ± SEM. *), and **** represents $p <$ 0.01, and 0.0001, respectively.

BG2$^{sgRNA-1}$ cell lines were seeded in proliferation assays. Absolute cell counts over a four-day period revealed no significant differences between control and Sox10-deficient cells, indicating that Sox10 loss does not impair HER2/Neu tumor cell proliferation under standard *in vitro* growth conditions (Fig. 5.3 A).

Given the established role of Sox10 in regulating stem/progenitor activity and EMT-associated programs, we next assessed whether Sox10 inactivation altered ECM-dependent migration. Haptotactic Boyden chamber assays using collagen-coated membranes revealed no significant difference in the proportion of migrating cells between BG2^{sgNTC} and BG2$^{sgRNA-1}$ lines, suggesting that Sox10 is not required for haptotaxis in a two-dimensional context (Fig. 5.3 B, C). In contrast, when cells were assessed in a three-dimensional invasion assay, Sox10-deficient cells exhibited reduced in invasive outgrowth. Tumorspheres embedded within a Matrigel: Collagen matrix showed a modest, but significant reduction in serum-free radial invasion over a six-day period following Sox10 loss when compared to NTC controls (Fig. 5.3 D, E). This reduction in invasion was evident despite comparable serum-dependent proliferation rates (Fig. 5.3 A), indicating that Sox10 selectively regulates invasive behavior in a three-dimensional extracellular matrix environment, without affecting general cell growth or motility.

Consistent with its proposed role in regulating stem-like and EMT-associated tumor cell behaviors, these data demonstrate that Sox10 is dispensable for tumor cell proliferation and 2D migration but may be required for efficient invasive growth in complex extracellular matrices.

5.4 Sox10 loss is associated with reduced stemness in vitro and tumor growth *in vivo*

As Sox10 has been shown regulate mammary stem/progenitor activity *in vivo* (267,279,289) (Fig. 4.9), we next assessed the functional stemness of the established cell lines *in vitro.* Consistent with prior observations in mammary organoid systems (267), Sox10-

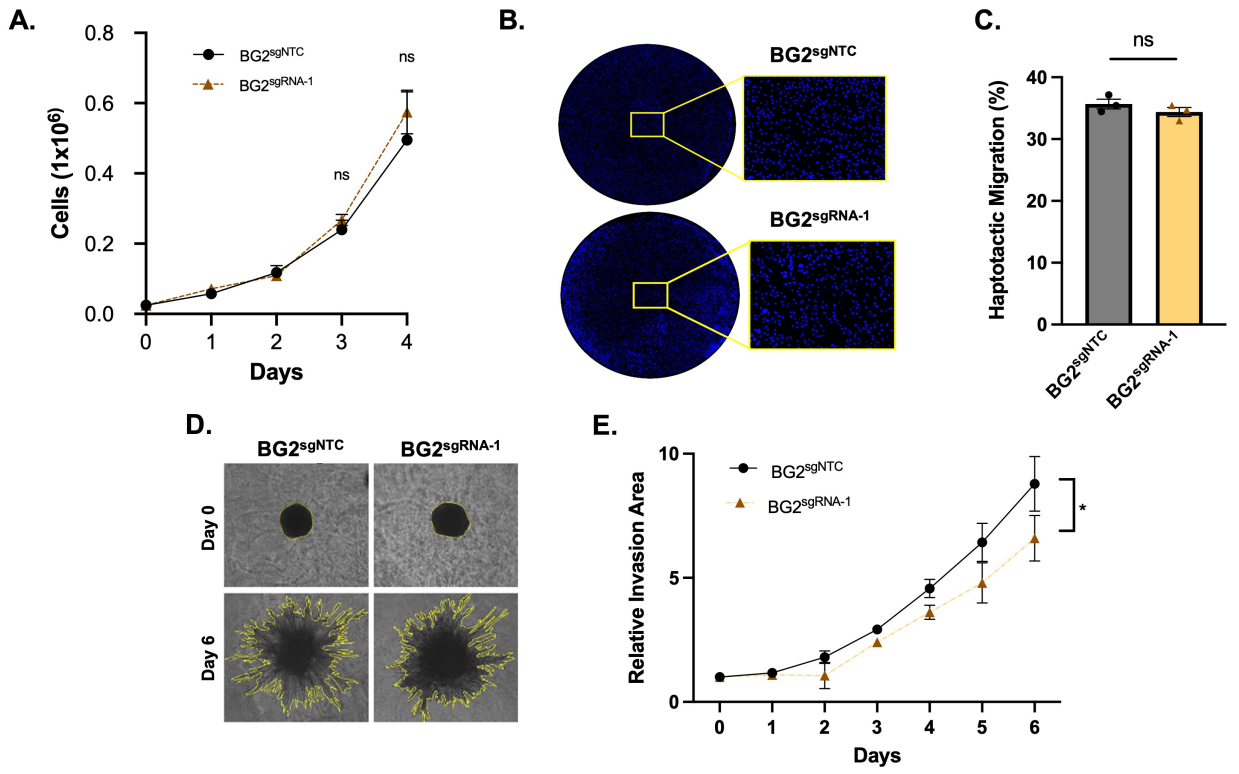

Figure 5.3. Loss of Sox10 does not affect cell growth and motility but decreases invasiveness in MMTV-NDL cell lines. (A) Cell growth of BG2^{sgNTC} and BG2$^{sgRNA-1}$ cell lines was measured over 4 days using absolute cell counts. **(B)** Representative images of DAPI stained BG2^{sgNTC} and BG2$^{sgRNA-1}$ cells following 4-hours of haptotactic Boyden chamber migration. **(C)** Quantification of successfully migrated cells in (B). **(D)** Representative bright-field images of 3D tumor spheroid invasion of BG2^{sgNTC} and BG2$^{sgRNA-1}$ cell lines through a Matrigel: Collagen matrix over the course of 6 days. Yellow outlines indicate spheroid boundary. **(E)** Quantification of invasion relative to day 0 from (D). n = 3 biological replicates/cell line. Data shown as mean ± SEM. * represents $p < 0.05$.

deficient HER2/Neu-transformed cell lines exhibited a significant reduction in functional stem/progenitor activity. Specifically, Sox10-deficient BG2 cells formed fewer secondary mammospheres compared to control cells, indicating impaired self-renewal capacity (Fig. 5.4 A, B). Despite this reduced functional stemness, Sox10 loss did not affect proliferation *in vitro*, suggesting that Sox10 is dispensable for bulk tumor cell growth under standard '*in plastico'* conditions. To evaluate if this phenotype is preserved in 3D *in vivo growth*, $BG2^{sgNTC}$ and $BG2^{sgRNA\text{-}1}$ cell lines were orthotopically injected into the mammary fat pad of immunodeficient mice. We observed that Sox10-deficient cells display a marked delay in tumor growth relative to control cells in NCG mice (Fig. 5.4 C, D). Surprisingly, when the tumors from the Sox10-deficient cells were further analyzed, Sox10 immunohistochemistry revealed that the proportion of $Sox10^{+}$ cells was similar to that seen in the control lines (Fig. 5.4 E). Seeing as the pool of $BG2^{sgRNA\text{-}1}$ cells did not show a complete loss of Sox10 (Fig. 5.2 A, B), these data support a mechanism by which tumors arising from injection of Sox10-deficient cells may be due to the residual population of Sox10-positive cells that undergo selective expansion *in vivo*. Regardless, as Sox10 deletion does not affect cell growth *in vitro*, these data suggest that Sox10 loss impairs tumorigenic growth *in vivo*.

5.5 Clonally selected $Sox10^{-}$ cells exhibit severe impairment of tumor-initiating potential

To assess the requirement for Sox10 in tumor growth and to exclude contributions from residual Sox10-expressing subpopulations, we next sought to generate clonally selected $Sox10^{-}$ HER2/Neu-transformed cell lines. However, during extended passaging of independently derived NIC-, and MMTV-NDL tumor cell lines, we observed substantial variability in Sox10 protein

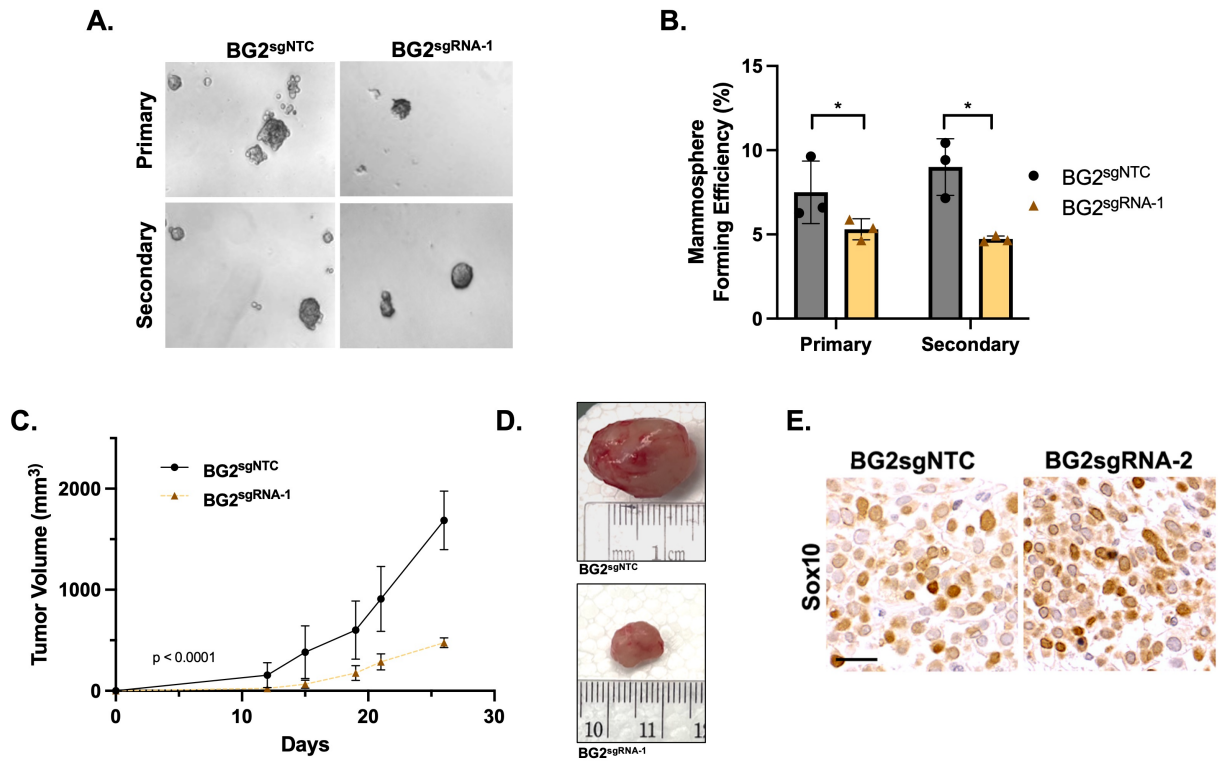

Figure 5.4. Sox10 is required to maintain functional stemness *in vitro* and tumor growth *in vivo*. **(A)** Representative images of primary and secondary mammospheres formed following 7-days growth of BG2^{sgNTC} and BG2$^{sgRNA-1}$ cell lines in ultra-low attachment plates. **(B)** Quantification of spheres ≥ 50 µm in diameter formed in (A). **(C)** Tumor growth curves of BG2^{sgNTC} and BG2$^{sgRNA-1}$ cell lines following orthotopic injection into the mammary fat pad of NCG mice. n ≥ 4 mice/group. **(D)** Representative images of tumors 28-days post injection from (C). **(E)** IHC staining for Sox10 in FFPE sections from endpoint tumors formed following orthotopic transplantation. n = 3 biological replicates/cell line. Data shown as mean ± SEM. * represents $p < 0.05$.

expression, with several lines exhibiting progressive or complete loss of Sox10 with continued passage (Fig. 5.5 A). These findings indicate that programs sustaining Sox10 expression may be unstable in long-term 2D culture. Strikingly, HER2/Neu-transformed cell lines that lose Neu and Sox10 expression with continued passage are able to eventually form tumors that re-induce Neu and Sox10 following orthotopic transplantation (Fig. 5.5 B-D). This suggests that Sox10-dependent signalling programs have a certain degree of plasticity in 2D growth conditions but are essential for 3D tumor growth. Consistent with the observations that Sox10 is lost in 2D conditions, BG2 cells used in the preceding functional assays displayed gradual loss of Sox10 expression, raising concerns that clonal selection from this background could be problematic. In contrast, the independently derived HER2/Neu-transformed line, BG1, maintained stable Sox10 expression across multiple passages. Owing to this stability, BG1 cells were selected as a more suitable platform for clonal selection and expansion of $Sox10^{-}$ populations.

To validate that the phenotypes observed using the $BG2^{sgRNA\text{-}1}$ cell line were not guide dependent from specifically targeting amino acids 168-175 (sgRNA-1), a second, independent sgRNA was used to target amino acids 67-74 (sgRNA-2). Cas9-expressing BG1 cells transduced with either guide showed efficient Sox10 inactivation as confirmed via RT-qPCR (Fig. 5.6 A). $BG1^{sgRNA\text{-}2}$ cells were selected for subsequent analyses. As for BG2 cells, $BG1^{sgRNA\text{-}2}$ cells exhibited no change in proliferation but showed a significant reduction in secondary mammosphere formation, confirming the previously reported impaired self-renewal capacity (Fig. 5.6 B, C).

Individual $BG1^{sgRNA\text{-}2}$ cells were clonally expanded, and two randomly selected populations ($BG1^{sgRNA\text{-}2.1}$ and $BG1^{sgRNA\text{-}2.2}$) were chosen for subsequent downstream analyses.

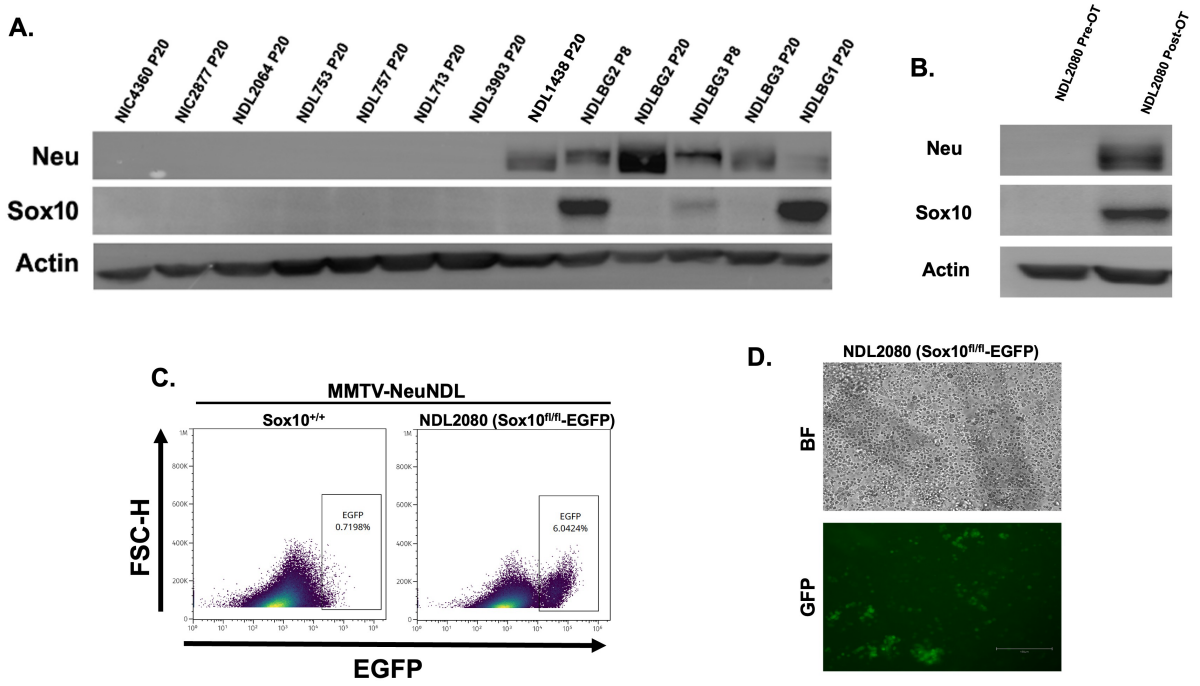

Figure 5.5. Neu-transformed cells frequently lose stable Sox10 expression in 2D growth but can be reinduced following orthotopic transplantation. (A) Immunoblot analysis of Neu and Sox10 expression across independently derived NIC-, and MMTV-NDL derived tumor cell lines at the indicated passages. **(B)** Immunoblot of Neu and Sox10 expression in pre- and post-injected Neu-transformed cell lines**. (C)** Flow cytometry of EGFP induction in tumors formed from injection of MMTV-NDL Sox10$^{fl/fl}$ cells. **(D)** Representative brightfield and EGFP images of tumors formed from injection of MMTV-NDL Sox10$^{fl/fl}$ cells.

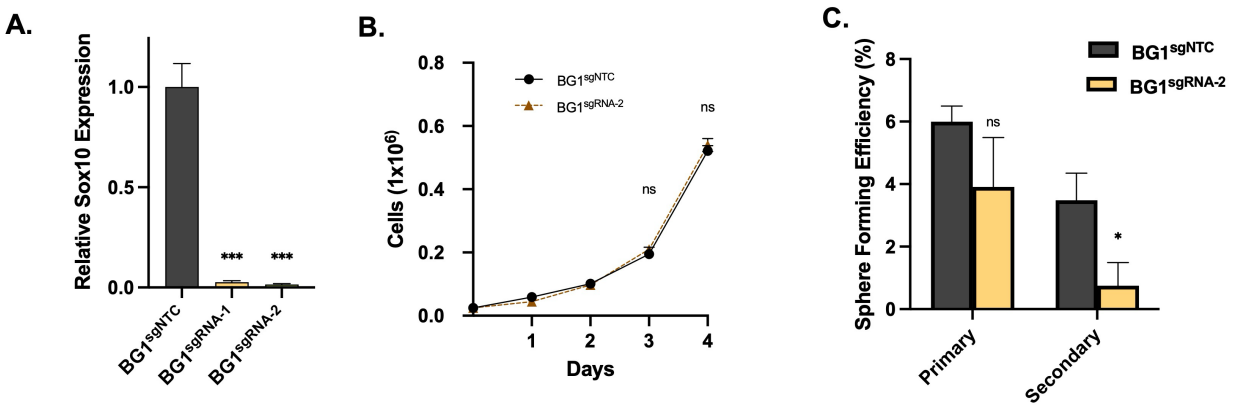

Figure 5.6. Sox10-retaining BG1 cells recapitulate growth and stemness phenotypes following Sox10 ablation. (A) Quantitative RT-qPCR analysis of Sox10 mRNA levels in BG2^{sgNTC}, $^{sgRNA\text{-}1}$ and $^{sgRNA\text{-}2}$ cell lines. **(B)** Cell proliferation curves of BG1^{sgNTC} and BG1$^{sgRNA\text{-}2}$ cells over four days. **(C)** Mammosphere formation efficiency of primary and secondary spheres formed by BG1^{sgNTC} and BG1$^{sgRNA\text{-}2}$ cell lines under non-adherent conditions. Only spheres ≥ 50 µm in diameter were enumerated. Data are presented as mean ± SEM. * and *** represent $p <$ 0.05 and 0.001, respectively.

The Sox10^{-} clones of BG1$^{sgRNA\text{-}2.1}$ and BG1$^{sgRNA\text{-}2.2}$ cells were stained for Sox10 using immunofluorescence and neither clone showed any detectable Sox10-positive nuclei (Fig. 5.7 A). To confirm whether clonal selection of Sox10^{-} BG1$^{sgRNA\text{-}2}$ cells altered Neu expression or downstream RTK-dependent oncogenic signalling, western blot analysis was performed. While bulk Sox10-deficient BG2$^{sgRNA\text{-}2}$ lines showed no significant differences in phosphorylated ERK1/2 or AKT levels compared to NTC controls, Sox10^{-} clones exhibited increased pAKT levels (Fig. 5.7 B, C). Furthermore, Sox10^{-} clones also exhibited increased Sox9 expression (Fig. 5.7 D). For both clones, targeted sequencing confirmed frameshift deletions resulting in premature stop codons within exon 4 of the *Sox10* locus (Fig. 5.7 E).

5.6 Sox10^{-} HER2/Neu-transformed clonal cell lines have reduced tumorigenic potential *in vivo*

To directly assess the tumorigenic capacity and TIC activity of clonally derived Sox10^{-} cells, BG1$^{sgRNA\text{-}2.1}$ and BG1$^{sgRNA\text{-}2.2}$ clones were subjected to an orthotopic limiting dilution assay. Ten-fold dilutions of NTC control and Sox10^{-} clones were orthotopically injected in the mammary fat pad of NCG mice.

Across all injected cell dilutions (10^6, 10^5, and 10^4 cells), BG1^{sgNTC} control cells formed rapidly expanding tumors (Fig. 5.8 A). In contrast, while a subset of mice injected with Sox10^{-} clones developed masses at early time points, these lesions failed to undergo any sustained growth over time and plateaued immediately after palpation (Fig. 5.8 A). Consistent with this observation, endpoint tumor weights were markedly reduced in all animals injected with Sox10^{-} clones relative to controls, irrespective of initial cell numbers (Fig. 5.8 B, C). Extreme limiting dilution analysis revealed a profound reduction in TIC frequency in Sox10^{-} clones, with estimated frequencies of

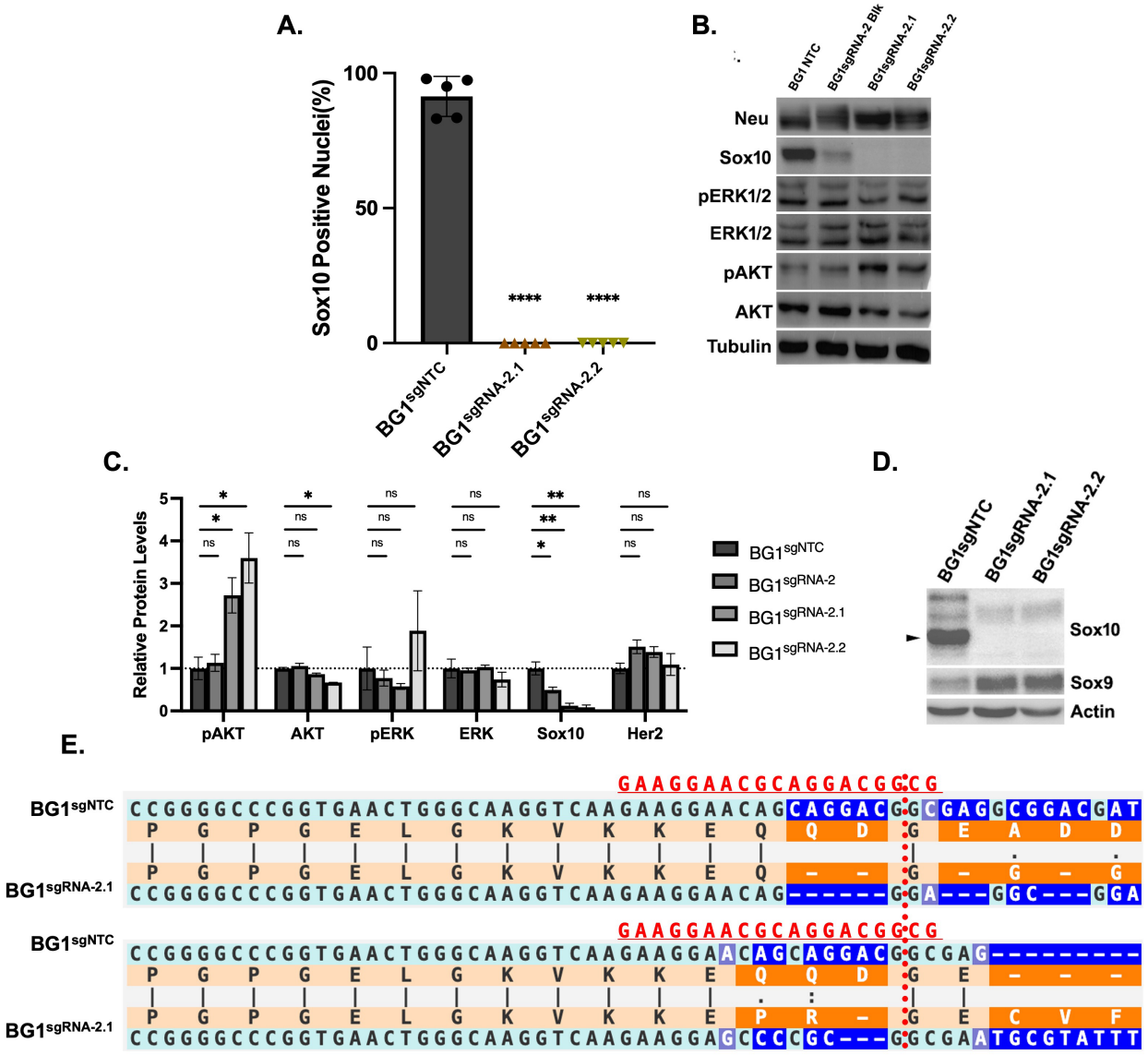

Figure 5.7. BG1 clones are devoid of Sox10 expression but exhibit upregulated AKT activity. **(A)** Quantification of Sox10-positive nuclei by immunofluorescence in BG1^{sgNTC} and BG1$^{sgRNA-2.1}$ and $^{sgRNA-2.2}$ clones. **(B)** Immunoblot analysis of Neu expression and downstream MAPK and PI3K signalling pathways (pERK1/2, ERK1/2, pAKT, AKT) in BG1^{sgNTC}, BG1$^{sgRNA-2}$ bulk knockout, and BG1$^{sgRNA-2.1}$ and $^{sgRNA-2.2}$ clones. **(C)** Densitometric quantitation of Western blots shown in (B). Three independent runs were used for quantification. **(D)** Immunoblot analysis of Sox9 expression in BG1^{sgNTC}, and BG1$^{sgRNA-2.1}$ and $^{sgRNA-2.2}$ clones. **(E)** Sanger sequencing alignment comparing control sgNTC cells to two independent Sox10^{-} clones (sgRNA-2.1 and sgRNA-2.2). Both edited clones contain frameshift-inducing indels at the sgRNA target sites leading to predicted premature truncation of Sox10. Data are presented as mean ± SEM. *, **, and **** denote $p < 0.05$, 0.01, and 0.0001, respectively.

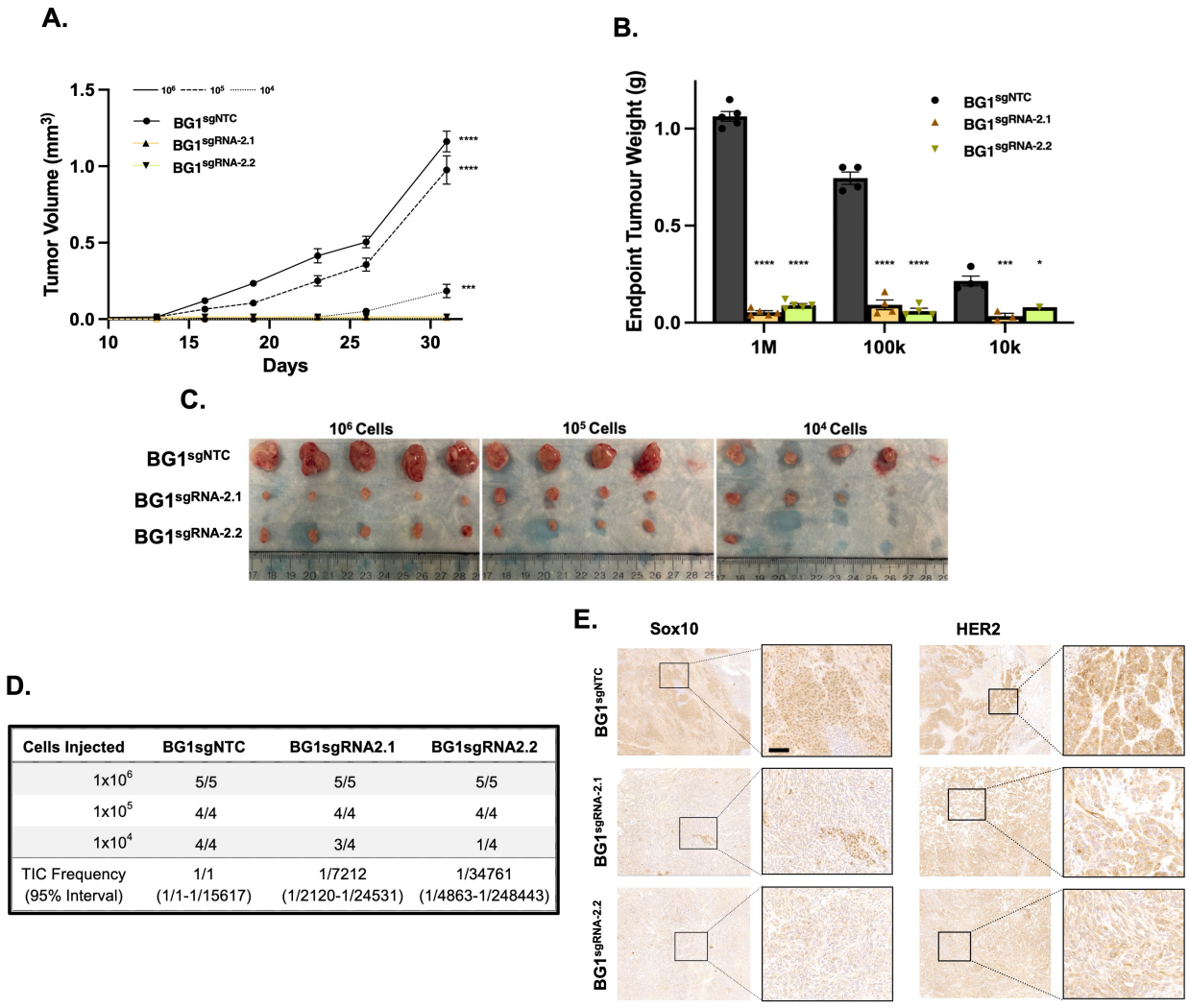

D.

Cells Injected	BG1sgNTC	BG1sgRNA2.1	BG1sgRNA2.2
$1x10^6$	5/5	5/5	5/5
$1x10^5$	4/4	4/4	4/4
$1x10^4$	4/4	3/4	1/4
TIC Frequency (95% Interval)	1/1 (1/1-1/15617)	1/7212 (1/2120-1/24531)	1/34761 (1/4863-1/248443)

Figure 5.8. Clonally selected Sox10$^-$ cell lines completely arrest tumor growth in limiting dilution assay. (A) Tumor growth curves of BG1^{sgNTC}, BG1$^{sgRNA-2.1}$ and BG1$^{sgRNA-2.2}$ NDL clones injected orthotopically at 10^6, 10^5, or 10^4 cells into mammary fat pads of NCG mice. **(B)** Tumor weights of endpoint tumors from (A). **(C)** Representative images of tumors formed following injection of 10^6, 10^5, or 10^4 cells. **(D)** Tumor take rate and TIC frequencies of BG1^{sgNTC}, BG1$^{sgRNA-2.1}$ and BG1$^{sgRNA-2.2}$ clones. **(E)** IHC staining for Sox10 and HER2 in FFPE endpoint tumor sections formed following orthotopic transplantation. n ≥ 4 mice/group. Data shown as mean ± SEM. Scale bar represents 100µm. *, ***, and **** represent $p < 0.05$, 0.001 and 0.0001, respectively.

1/7,212 and 1/34,761 for BG1$^{sgRNA\text{-}2.1}$ and BG1$^{sgRNA\text{-}2.2}$ cells, respectively (Fig. 5.8 D). Other than rare small pockets of Sox10^{+} cells, immunohistochemical analysis of residual tissue confirmed the absence of Sox10 expression (Fig. 5.8 E). Importantly, HER2/Neu expression was maintained across all genotypes, indicating that impaired tumor growth was not due to loss of oncogene expression. Together, these data demonstrate that Sox10 inactivation profoundly compromises tumor-initiating capacity and abrogates sustained tumor growth *in vivo*, supporting a critical role for Sox10 in maintaining functional TIC activity in HER2/Neu-driven mammary tumors.

5.7 Sox10^{-} HER2/Neu-transformed cell lines fail to establish metastatic niches

Next, we wanted to determine whether Sox10 is required for metastatic colonization. While lung colonization assays do not fully recapitulate the entire metastatic cascade, they can provide a measure of ability to survive in circulation, extravasate into host tissue, and establish metastatic niches; all functions of stem/progenitor like cells (317–319). Indeed, previous studies have demonstrated that propensity to form lung metastases following bloodstream injections of breast cancer cell lines is predominantly mediated by TIC/CSC rich populations (320–322). To test this, BG1 NTC control cells and Sox10^{-} clones were injected intravenously into immunodeficient NCG mice. Lung tissues were harvested 28 days post-injection and assessed for metastatic burden. Supporting the limiting dilution assay results, mice injected with Sox10^{+} control cells developed extensive lung colonization, characterized by increased lung mass and numerous macroscopic lesions (Fig. 5.9 A, B). In contrast, mice injected with Sox10^{-} clones exhibited lung weights comparable to uninjected controls and showed no evidence of detectable metastatic lesions (Fig. 5.9 A, B), indicating a profound impairment in metastatic outgrowth .

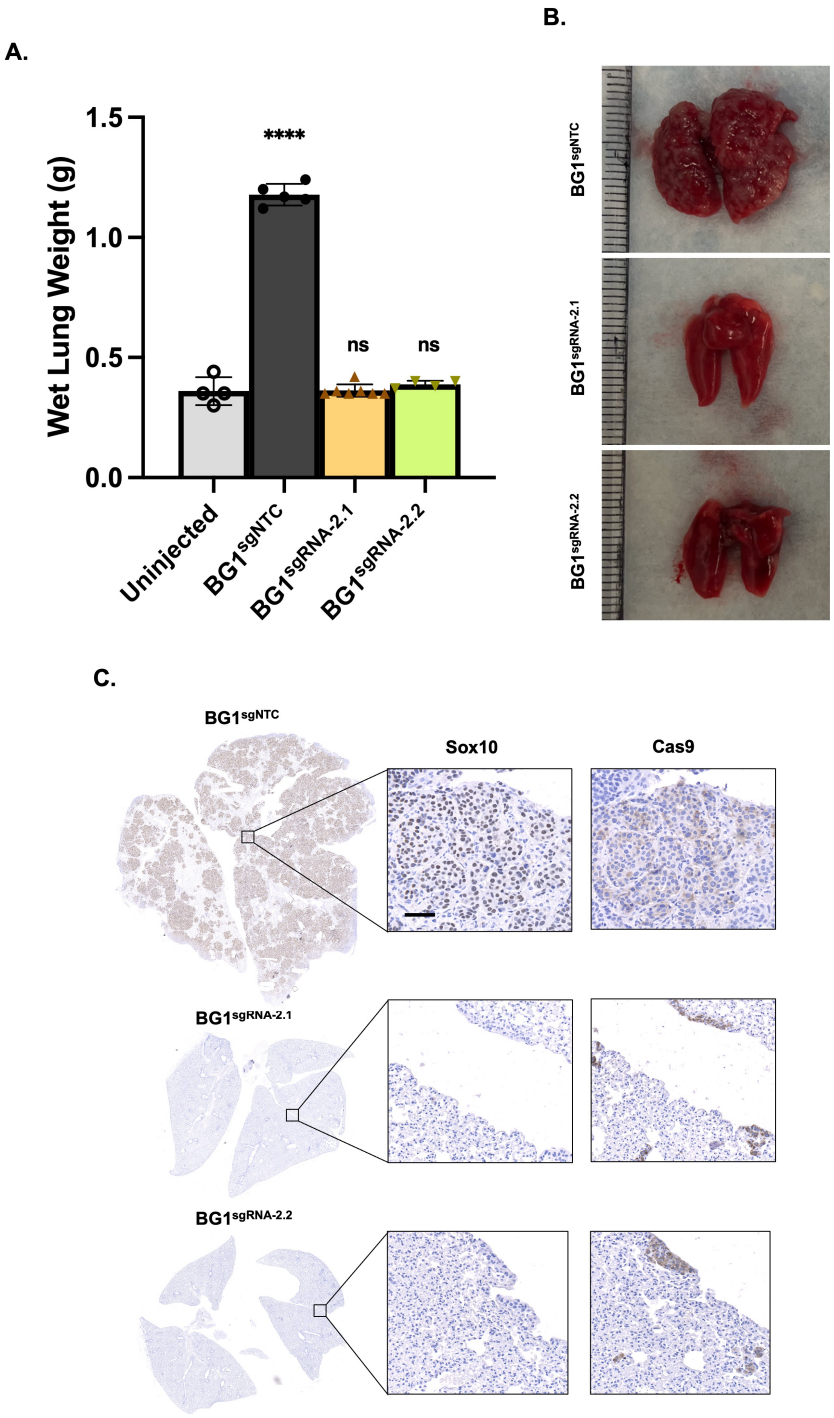

Figure 5.9. HER2/Neu-transformed Sox10^{-} clones fail to establish metastatic niches in the lungs in colonization assay. (A) Wet lung weight of NCG mice 28-days post intravenous injection of with10^{6} BG1^{sgNTC}, BG1$^{sgRNA\text{-}2.1}$ and BG1$^{sgRNA\text{-}2.2}$ NDL cells. **(B)** Representative images of lungs from (A). **(C)** IHC staining for Sox10 and Cas9 in FFPE lung sections following intravenous injections. n ≥ 4 mice/group. Data shown as mean ± SEM. Scale bar represent 100µm. **** represents $p < 0.0001$.

Immunohistochemical analysis of adjacent lung sections revealed rare Cas9-positive niches in mice injected with Sox10$^-$ clones, confirming the presence of injected tumor cells within the lung tissue (Fig. 5.9 C). Notably, Cas9-positive populations lacked detectable Sox10 expression, indicating that Sox10$^-$ tumor cells can intravasate into the lung environment. However, the absence of discernible metastatic lesions suggests that these cells fail to undergo efficient expansion or niche establishment.

Together, these data demonstrate that while Sox10$^-$ tumor cells may reach secondary sites, Sox10 is required for the establishment and expansion of metastatic niches in the lungs, further supporting its essential role in TIC maintenance in HER2/Neu-driven mammary cancer.

5.8 Sox10 depletion in HER2/Neu-transformed cells induces loss of luminal identity

To gain further insights into Sox10-dependent genetic programs in our HER2/Neu-transformed mammary tumor cell lines, RNA sequencing was performed on Sox10$^-$ BG1$^{sgRNA\text{-}2.1}$ and BG1$^{sgRNA\text{-}2.2}$ clones and compared to the bulk BG1^{sgNTC} cells. Unsupervised clustering based on Euclidean distances of rlog-transformed gene expression values revealed tight clustering of the two Sox10$^-$ clones, which segregated distinctly from NTC samples (Fig. 5.10 A). Differential expression analysis identified large and highly overlapping sets of downregulated and upregulated genes that were significantly altered in both Sox10$^-$ clones relative to NTC controls (adjusted $p < 0.05$, $|\log_2 FC| > 1$) with over 1500 common genes in each set (Fig. 5.10 B).

Unbiased transcriptomic analysis of Sox10-deficient HER2/Neu-transformed cells revealed a profound loss of luminal identity accompanied by acquisition of basal and stem-like transcriptional features. Across both Sox10$^-$ clones, multiple canonical luminal lineage and luminal progenitor markers were significantly downregulated (EpCAM, CK8, CK18, Foxa1, Ngfr, Etv1, and Elf5)

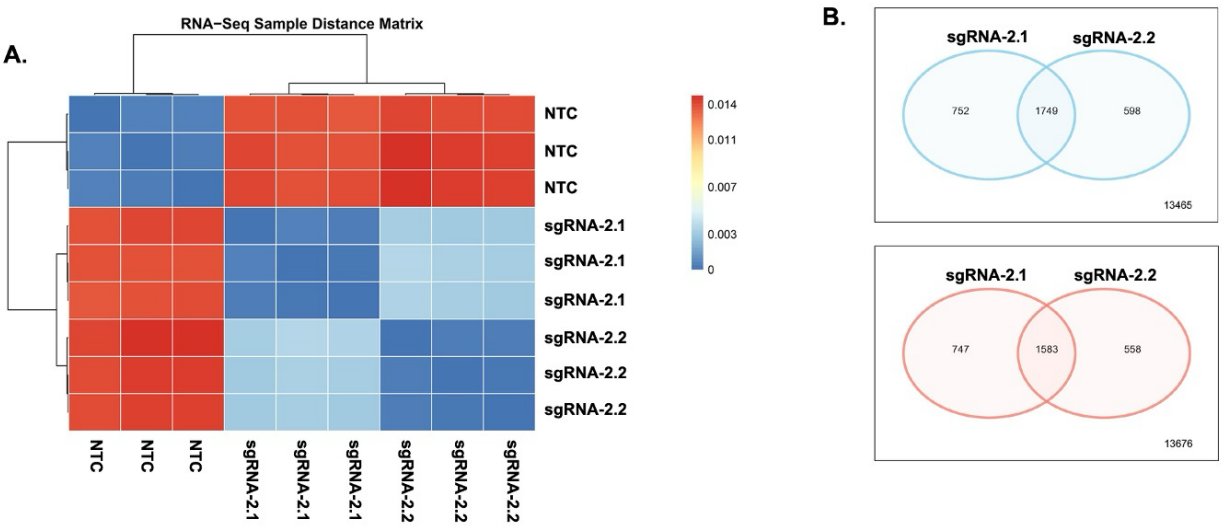

Figure 5.10. Sox10 deletion induces a defined transcriptional program in Neu-transformed mammary tumor cells. (A) Euclidean distance matrix of rlog-transformed RNA-seq data showing sample clustering based on 1 minus Pearson correlation, comparing Sox10^{-} clones and NTC controls. **(B)** Venn diagrams illustrating overlap of significantly downregulated (blue) and upregulated (red) genes (adjusted $p < 0.05$, $|\log_2 FC| > 1$) identified in independent Sox10 knockout clones relative to NTC.

(Fig. 5. 11 A, B). However, some differences in expression (e.g. Esr1) were observed between the two clones, suggesting that they might represent different cell states. Nevertheless, both clones showed a marked luminal-to-basal shift based of their gene expression profile. Consistent with loss of luminal identity upon the loss of Sox10, markers associated with a MaSC phenotype (Lgr6, Id4, Snai2, Foxc1, and Wnt6) and classical basal identity (keratins 5 and 14, Acta2, and Trp63) were upregulated (Fig. 5.11 A, B). However, only a subset of genes associated with the MaSC phenotype was upregulated in Sox10$^-$ lines, indicating that Sox10$^-$ cells do not fully recapitulate a canonical mammary stem cell transcriptional program. Loss of luminal identity markers and acquisition of basal markers was validated via RT-qPCR (Fig. 5.11 C, D).

Gene set enrichment analysis (GSEA) on the common DEGs using the MSigDB C2:CGP (Curated - Chemical and Genetic Perturbations) gene set collection identified multiple gene signatures associated with reduced luminal and increased mesenchymal/MaSC identity (Fig. 5.12 A). Comparison to previous genetic profiling of murine and human breast cancers revealed that our Sox10$^-$ HER2/Neu-transformed cells displayed specific enrichment patterns consistent with genes associated with MaSCs and luminal breast cancers (323–325) Specifically, we observed a positive enrichment (NES = 1.84) for genes up-regulated in MaSCs (Fig. 5.12 B) but strong negative enrichment (NES = -2.16) for down-regulated genes (Fig. 5.12 C). Supporting this, Sox10 knockout enriched (NES = 1.91) for genes down-regulated in luminal-like breast cancer cell lines (Fig. 5.12 D) and negatively enriched (NES = -1.95) for those up regulated (Fig. 5.12 E).

Using the Reactome database and overrepresentation analysis on the list of common DEGs, we found that cytoskeletal remodelling, integrin interactions and ECM production were all likely affected by Sox10 ablation (Fig. 5.13 A). Notably, these pathways are commonly linked to processes that are central to invasive and progenitor-associated cellular states.

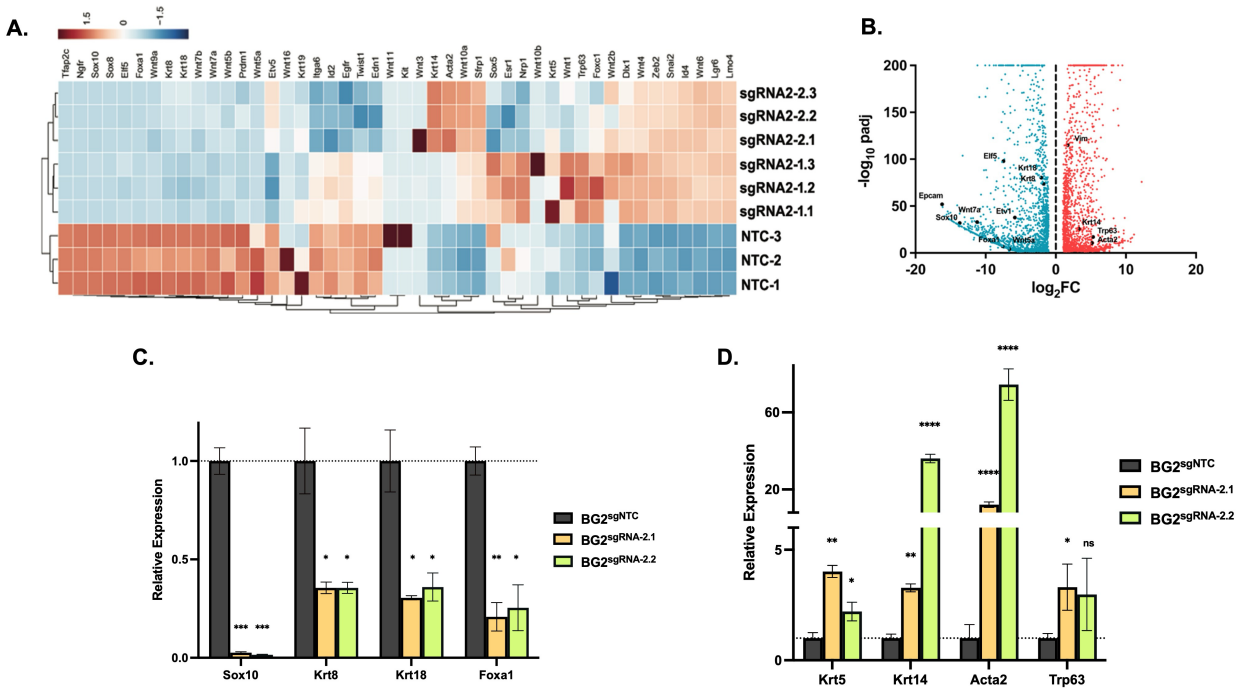

Figure 5.11. Sox10 ablation in HER2/Neu-transformed tumor cells promotes a luminal to basal/stem-like reprogramming. (A) Triplicate rlog-transformed gene expression values were used to generate a heatmap for a curated list of luminal and basal markers in BG1$^{sgRNA\text{-}2.1}$ and $^{sgRNA\text{-}2.2}$ cells after analysis of all differentially expressed genes. **(B)** Volcano plot of differentially expressed genes common to both Sox10^{-} clones. **(C, D)** RT-qPCR analysis of luminal lineage markers Krt8, Krt18, and Foxa1 (C) and basal/stem-associated markers Krt5, Krt14, Acta2, and Trp63 (D) in Sox10^{+} BG2^{sgNTC} and Sox10^{-} BG2$^{sgRNA\text{-}2.1}$ and $^{sgRNA\text{-}2.2}$ clones. Data shown as mean ± SEM. *, **, ***, and **** represents $p < 0.05$, 0.01, 0.001, and 0.0001, respectively.

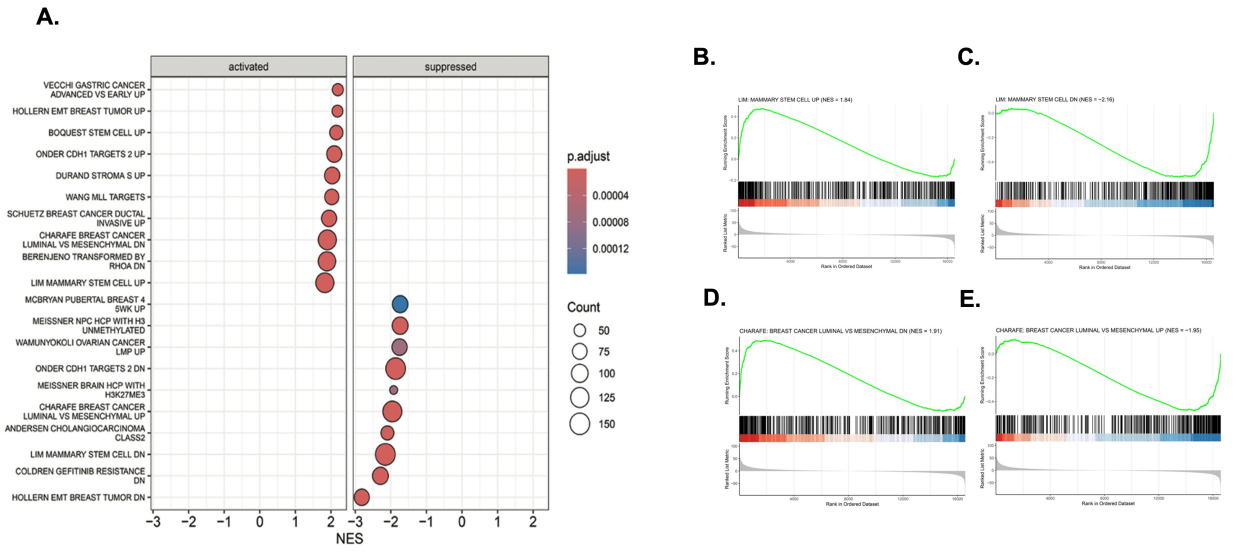

Figure 5.12. Clonal Sox10^{-} tumor cells exhibit genetic shift towards mesenchymal/stem-like state. (A) Gene Set Enrichment Analysis (GSEA) of genes ranked by the average Wald statistic of both Sox10^{-} clones. Gene sets were derived from the MSigDB C2: Curated Gene Sets – Chemical and Genetic Perturbations (CGP) collection for *Mus musculus*. The dot plot displays the top positively (activated in Sox10^{-}) and negatively (supressed in Sox10^{-}) enriched gene sets by NES with adjusted $p < 0.05$. Dot size reflects the number of contributing genes, and color indicates adjusted *p*-value. **(B, C)** Enrichment plots for the LIM_MAMMARY_STEM_CELL gene sets identified in (A). The UP gene set (B) (genes elevated in mammary stem cells) is positively enriched (NES = 1.84) in Sox10^{-} clones while the down gene set (C) (genes downregulated in mammary stem cells) is negatively enriched (NES = -2.16). **(D, E)** Enrichment plots for the CHARAFE_BREAST_CANCER_LUMINAL_VS_ MESENCHYMAL gene sets identified in (A). The DN gene set (genes elevated in mesenchymal compared to luminal breast cancer) is positively enriched (NES = 1.91) in Sox10^{-} clones (D) while the UP gene set (genes elevated in luminal compared to mesenchymal breast cancer) is negatively enriched (NES = -1.95) (E).

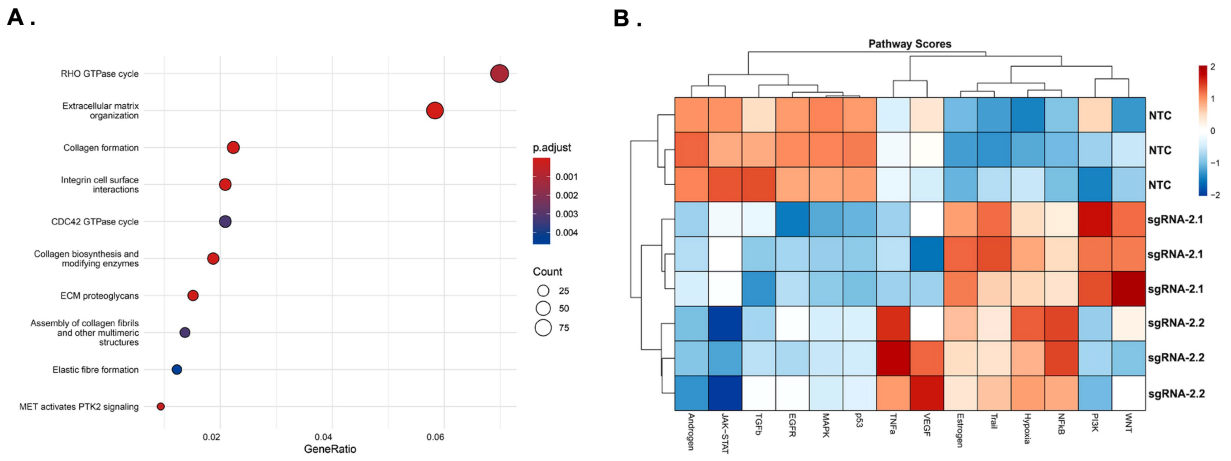

Figure 5.13. Sox10 loss alters cytoskeletal, ECM, and oncogenic signalling pathways associated with luminal identity. (A) Overrepresentation analysis of shared differentially expressed genes (adjusted $p < 0.05$, $|\log_2 FC| > 1$) using the Reactome database. The top 10 enriched pathways were selected based on adjusted p-value and are displayed ordered by gene ratio. Dot size represents the number of enriched genes per pathway, and dot color indicates adjusted p-value. **(B)** PROGENy pathway activity scores inferred from rlog-transformed gene expression of pathway target genes, calculated per replicate. Scores were z-score normalized across samples (row-wise), and hierarchical clustering was applied to both pathways and samples.

To further assess the directionality of these overrepresented programs, pathway activity was inferred using PROGENy. In line with our GSEA data, NFkB and hypoxia signalling pathways are significantly increased, both of which have been associated with mammary stem/progenitor-like cellular states (Fig. 5.13 B) (326,327). Conversely, MAPK, JAK-STAT, and TGFb signalling programs were reduced following Sox10 deletion, pathways previously implicated in the maintenance of progenitor identity, Neu-driven tumorigenic signalling, and ECM-associated invasive programs (328–331). The repression of these signalling programs supports the disruption of ECM-associated pathways identified by Reactome analysis, suggesting impaired ECM interaction. Thus, despite the apparent mesenchymal/stem-like transcriptional shift reported in the GSEA analysis, Sox10$^-$ cells exhibited functionally impaired invasion, stemness, and tumor-initiating capacity. Together, these data suggest that Sox10 is required for the maintenance of a functionally competent tumorigenic state and that its loss may induce a transcriptional reprogramming event that does not faithfully recapitulate a true mesenchymal /stem-like state.

Although CRISPR/Cas9-mediated Sox10 inactivation in bulk BG1 populations resulted in incomplete loss of Sox10 expression, transcriptomic profiling of these bulk Sox10-deficient cells revealed highly concordant genetic responses to those observed in clonally derived Sox10$^-$ lines. Many of the differentially expressed genes and enriched pathways identified in the bulk Sox10 knockout population overlapped with those observed in independently derived Sox10$^-$ clones, indicating that the transcriptional reprogramming associated with Sox10 loss is not solely attributable to clonal selection or long-term culture adaptation (Fig. 5.14 A, B). GSEA of bulk Sox10-deficient cells identified significant enrichment of gene signatures associated with reduced luminal identity and increased mesenchymal or progenitor-like programs (Fig. 5.14 C). In parallel,

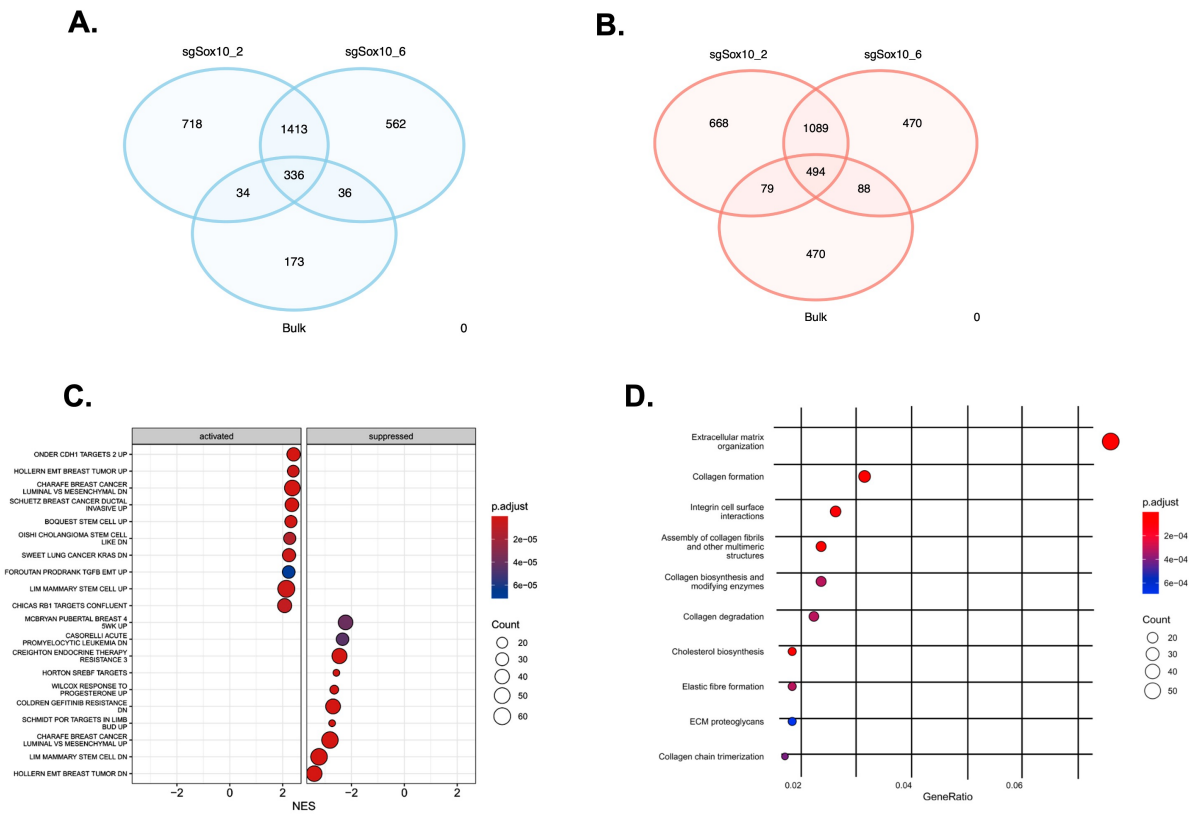

Figure 5.14. Bulk BG1 Sox10-deficient cells adapt genetic signatures similar to Sox10$^-$ clones. **(A, B)** Venn diagrams illustrating overlap of significantly downregulated (A) and upregulated (B) genes (adjusted $p < 0.05$, $|\log_2 FC| > 1$) identified in independent Sox10 knockout clones relative to knockout pool. **(C)** GSEA of genes ranked by the average Wald statistic for the Sox10-deficient pool. The dot plot displays the top positively (activated in Sox10$^-$) and negatively (supressed in Sox10$^-$) enriched gene sets by NES with adjusted $p < 0.05$. **(D)** Overrepresentation analysis of shared differentially expressed genes (adjusted $p < 0.05$, $|\log_2 FC| > 1$) using the Reactome database for the Sox10-deficient pool. The top 10 enriched pathways were selected based on adjusted p-value and are displayed ordered by gene ratio. Dot size represents the number of enriched genes per pathway, and dot color indicates adjusted *p*-value.

overrepresentation analysis using the Reactome database similarly revealed enrichment of pathways involved in integrin-mediated cell-matrix interactions, extracellular matrix organization, and collagen biosynthesis and remodeling (Fig. 5.14 D).

Together, these analyses indicate that Sox10 loss induces coordinated alterations in lineage-specific transcriptional programs that collectively collapse LP-maintaining programs and lead to partial acquisition of a basal/mesenchymal-like identity.

5.9 Sox10-associated transcriptional programs are conserved in human breast cancer

To assess whether the transcriptional programs associated with Sox10 expression in murine Neu-driven tumor cells are conserved in human breast cancer, we analyzed a large single-cell RNA-sequencing dataset comprising approximately 278,000 cells derived from 91 primary human breast tumors spanning multiple molecular subtypes (332–335). Dimensionality reduction and cell-type annotation revealed heterogeneous epithelial, immune, and stromal populations, within which SOX10 expression was enriched in a discrete subset of epithelial cells (Fig. 5.15 A, B).

To directly compare murine and human Sox10-associated transcriptional states, we performed gene set scoring using the top 50 genes downregulated upon Sox10 deletion in murine BG1 cells. This Sox10-dependent murine gene signature exhibited elevated activity in the $SOX10^{hi}$ epithelial population in human tumors, as well as in a subset of hybrid epithelial/mesenchymal cells (Fig. 5.15 C). A similar pattern was observed when applying the luminal/basal signature derived from $Sox10^{-}$ murine cells in Fig. 5.11 A, further supporting conservation of Sox10-associated lineage programs across species (Fig. 5.15 D). Consistent with murine findings, basal-associated markers such as TP63 were enriched in hybrid epithelial/mesenchymal populations, whereas luminal progenitor-associated genes such as KIT (c-Kit), which are downregulated

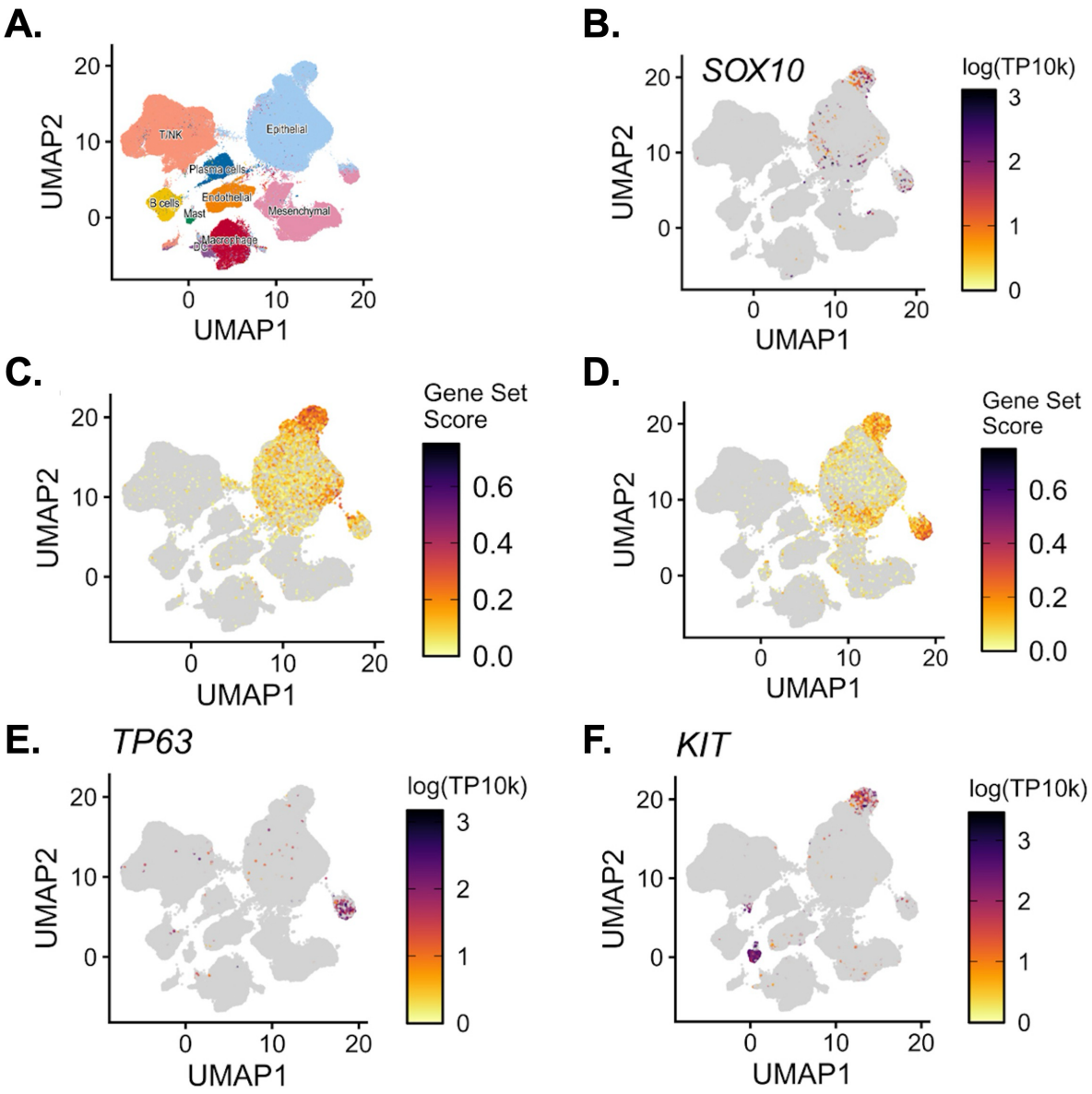

Figure 5.15. Human Sox10^{hi} and murine Sox10^{+} breast cancer cells share significant genetic overlap. (A) UMAP plot of scRNA-Seq data processed from 91 human breast cancers showing the various cell types in the tumor samples. **(B)** UMAP of Sox10 transcripts showing a Sox10^{hi} cluster in the epithelial population of all breast cancer subtypes. **(C)** Gene set scoring of the top 50 common downregulated genes in the Sox10^{-} clones. **(D)** Gene set scoring for the luminal/basal markers in Fig. 5.11. High scoring was observed in the Sox10^{hi} cluster and in a hybrid mesenchymal/epithelial population. **(E, F)** Examples of a basal marker TP63 (E) and c-Kit (F), up- and down-regulated in Sox10-deficient cells, respectively. High TP63 counts were enriched in the mesenchymal/epithelial cluster whereas c-Kit was highly represented in the Sox10^{hi} group.

following Sox10 loss in murine tumor cells, were preferentially expressed in $SOX10^{hi}$ epithelial cells (Fig. 5.15 E, F). Together, these analyses demonstrate that human $SOX10^{hi}$ breast cancer cells share a conserved transcriptional program with murine $Sox10^{+}$ Neu-driven tumor cells, directly supporting the relevance of Sox10-regulated lineage states identified in this model to human disease.

5.10 Prospective strategies for identification of $Sox10^{+}$ tumor cell populations

Given the central role of Sox10 in regulating tumor-initiating capacity and metastatic competency, we next sought to determine whether Sox10-expressing tumor cell populations could be prospectively identified using cell surface markers. Flow cytometric analysis of HER2/Neu-transformed BG1 cells revealed highly polarized epithelial marker expression, including distinct $EpCAM^{+}/EpCAM^{-}$ and $Ceacam1^{+}/Ceacam1^{-}$ populations (Fig. 5.16 A, B). When further interrogated with $Sox10^{-}$ cells, $BG1^{sgRNA\text{-}2.1}$ clones exhibited a complete loss of the $EpCAM^{+}$ fraction, while $BG1^{sgRNA\text{-}2}$ bulk knockout cell lines showed significant, albeit incomplete, silencing of the $Ceacam1^{+}$ population (Fig. 5.16 A, B). It is possible that the residual $Ceacam1^{+}$ population present in the $BG1^{sgRNA\text{-}2}$ bulk knockout cells is due to incomplete Sox10 ablation in this population. When the respective $Ceacam1^{+}/Ceacam1^{-}$ populations identified in the control $BG1^{sgNTC}$ cells were FACS sorted and subsequently stained for Sox10, it was revealed that $Ceacam1^{+}$ cells were almost exclusively $Sox10^{+}$, while the $Ceacam1^{-}$ population was largely devoid of Sox10 (Fig. 5.16 C).

Together, these approaches establish both surface marker based and transcriptional strategies to identify and isolate Sox10-expressing tumor cell populations, providing a foundation for future functional interrogation and targeted perturbation of Sox10-dependent tumor states.

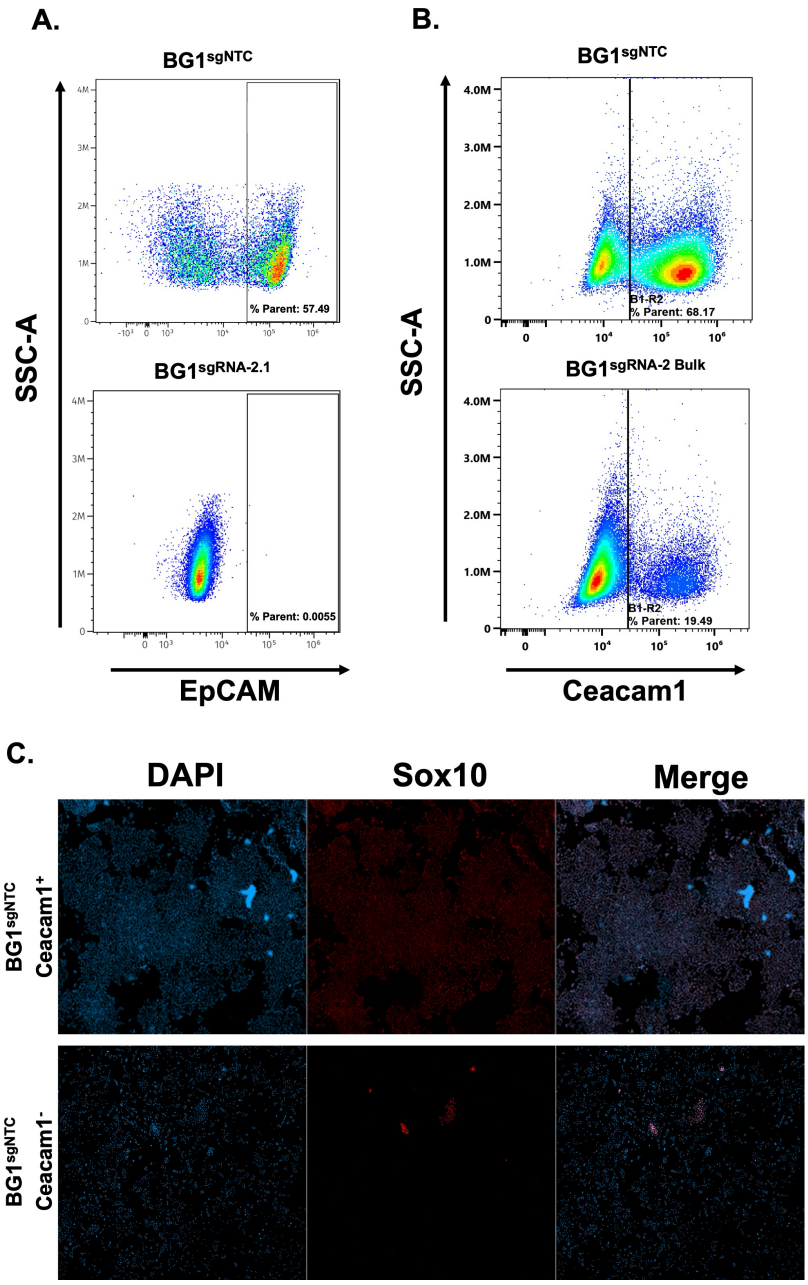

Figure 5.16. EpCAM and Ceacam1 identify Sox10^{+} populations in HER2/Neu-transformed cell lines. (A) Representative flow cytometry plots of Sox10^{+} BG1^{sgNTC} and Sox10^{-} BG1$^{sgRNA-2.1}$ clones stained for EpCAM. **(B)** Representative flow cytometry plots of BG1^{sgNTC} and bulk BG1$^{sgRNA-2}$ cell lines stained for Ceacam1. **(C)** Immunofluorescence staining of Sox10 and DAPI in Ceacam1^{+} and Ceacam1^{-} populations sorted from BG1^{sgNTC} cell lines in (B).

5.11 Summary

Previously, we established Sox10 as a critical determinant of HER2/Neu-driven mammary tumorigenesis *in vivo*. Using conditional genetic models, we demonstrated that Sox10 is required for efficient tumor initiation, progression, and metastatic dissemination. However, interpretation of Sox10 function in established tumors was complicated by inter-tumoral heterogeneity and re-establishment of Sox10 expression at endpoint. Such observations warranted an alternative approach to more directly interrogate Sox10 function in HER2/Neu-transformed mammary epithelial cells.

Here, we employed HER2/Neu-driven mammary tumor derived cell lines to define the functional and genetic consequences of Sox10 loss *in vitro* and *in vivo* following CRISPR-Cas9 mediated inactivation. Using both bulk and clonally selected Sox10-null lines, we demonstrate that Sox10 is essential for functional stemness *in vitro,* and tumor initiation and progression in various xenotransplantation assays *in vivo*. These functional impairments occurred despite conserved Neu expression, suggesting that Sox10 may regulate tumorigenic competency through pathways independent from canonical oncogenic signalling.

Transcriptomic profiling of Sox10-deficient cells revealed that loss of Sox10 induces transcriptional reprogramming characterized by loss of luminal lineage and progenitor markers and gain of basal/stem-associated identity programs. Gene set enrichment and pathway analyses also demonstrated that cytoskeletal remodeling, integrin signalling, and extracellular matrix organization programs were dysregulated upon Sox10 inactivation, consistent with the observed defects in invasion and metastatic colonization. Notably, Sox10-deficient cells adopted a partial basal/stem-like transcriptional state that was functionally distinct from bona fide mammary stem

cells. Cross-species comparison with human breast cancer scRNA-seq data further demonstrated that murine Sox10-dependent gene signatures are selectively enriched in Sox10^{hi} epithelial populations in human tumors, highlighting the translational relevance of Sox10-dependent lineage programs in murine HER2/Neu-induced mammary tumorigenesis to that of human disease. Finally, this chapter establishes foundational strategies for the prospective identification and experimental targeting of Sox10-expressing tumor cell populations.

Chapter 6: General Discussion

6.1 Summary

The association of Sox10 with biological processes mediating mammary progenitor maintenance and basal-like/TNBCs has been well documented (267,276,278,279,289). Recently, we and others have shown that HER2-positive breast cancers exhibit substantial heterogeneity in their proportions of $Sox10^{+}$ populations ranging from 2% to 79% of malignant tissues (130,291–293,295). Despite these observations, the specific role of Sox10 in the maintenance of luminal epithelial populations and malignant transformation has not been fully elucidated.

With this work, we aimed to address whether Sox10 is functionally required for HER2/Neu-, and RTK-dependent tumorigenesis, or whether it merely demarcates a transient state of cellular plasticity associated with tumor progression. To directly address this question, we investigated the consequences of luminal-specific *Sox10* deletion in murine models of breast cancer, including the MMTV-NIC and rtTA/MIC systems. Collectively, the data presented in this thesis suggest that Sox10 is a critical determinant of mammary gland biology and, importantly, as a functional mediator of HER2/Neu-induced mammary tumorigenesis potentially through lineage stabilization of the LP-derived TIC compartment.

6.2 Elucidating the role for Sox10 in mammary gland development

6.2.1 Sox10 in ductal outgrowth

We have demonstrated that luminal-specific *Sox10* deletion results in a transient delay in pubertal ductal development, with adult glands ultimately exhibiting normal architecture and epithelial organization (Fig. 3.2). Despite an overall preserved ductal integrity in adult females, Sox10 loss led to a selective depletion of LP populations, suggesting that Sox10 may play a role in LP function, but not in the maintenance of the differentiated epithelium (Fig. 3.4, 3.6).

Beginning at approximately three weeks of age, ductal outgrowth from the mammary rudiment during puberty is a hormone-dependent morphogenic event characterized by active progenitor expansion driving terminal end bud proliferation and ductal elongation (159). We show that Sox10 regulates LPs, which are disproportionately responsible for supporting these processes (Fig. 3.6). In agreement with this, Sox10 deletion in the luminal compartment reduces the LP pool, resulting in delayed ductal invasion of the mammary fat pad. However, once puberty is complete and developmental pressures subside, the requirement for maximal progenitor function relaxes. This may permit slower, and potentially Sox10-independent, processes to complete ductal morphogenesis. Notably, hemizygous Sox10 MMTV-Cre females do not exhibit detectable delays in pubertal mammary gland development, suggesting that developmental programs are buffered against reduced Sox10 dosage (Fig. 3.2). These findings point to the possibility of a 'goldilocks' zone of $Sox10^{+}$ LPs required for development. This is in contrast to the observed Sox10 dosage requirements in Neu-driven malignant transformation. Indeed, Sox10 hemizygous NIC females display significantly impaired tumor initiation, suggesting that Sox10-dependent programs are more dispensable during normal tissue morphogenesis than during malignant transformation (Fig. 4.2).

The delayed, but eventual development of mammary epithelium reported here contrasts with the previously reported complete developmental arrest observed in Sox10-deficient mammary glands (278). This disparity in reported absolute versus partial requirements for Sox10 in development is likely attributable to the various MMTV-Cre strains and genetic backgrounds used in each respective study. In the present study, the luminal-restricted MMTV-Cre D strain was used in a pure FVB/n background. This strain has been shown to exhibit delayed and mosaic Cre expression, with complete penetrance only observed in older mice (116–118). In contrast, the

adjacent study employed the use of the MMTV-Cre A strain in a mixed background. While this strain exhibits higher penetrance and early temporal expression, it exhibits substantial epithelial promiscuity showing both luminal and basal expression (116,118,329). In this model, it is therefore likely that all $Sox10^{+}$ BP and LP populations were subject to recombination, completely abrogating ductal outgrowth.

Nevertheless, there remains the possibility that, as a whole, luminal-specific Sox10 may be required for ductal development. Thus, in a system with absolute luminal Sox10 ablation prior to pubertal development, ductal morphogenesis may not proceed past the development of the mammary rudiment. In the luminal-restricted model used here, the eventual development of the adult mammary gland may therefore have occurred through potential compensatory mechanisms.

The most likely mechanism lending to eventual development is that our MMTV-Cre D mediated recombination is not instantaneous and has been shown to occur in a mosaic and progressive manner (117,313). By four weeks of age, most LPs may have efficiently recombined the Sox10 locus, resulting in delayed outgrowth. However, a small number of residual $Sox10^{+}$ LPs may be sufficient to expand and complete ductal filling prior to complete Sox10 recombination. Thus, a model where Cre recombinase exhibits full penetrance in the luminal compartment prior to puberty may prevent this potential rescue phenotype.

Second, the model implemented here was used by design to inactivate Sox10 only in luminal cells, leaving only basal/myoepithelial $Sox10^{+}$ cells intact. While lineage plasticity is typically restricted during normal homeostasis, it is possible that the depletion of early lineage restricted luminal populations Sox10 inactivation may have eroded lineage-maintaining paracrine signalling events. This could ultimately result in a reprogramming of $Sox10^{+}$ BPs to give rise to a luminal lineage (182,191). Such dysregulation in normal tissue homeostasis may have permitted

basal-to-luminal plasticity, whereby Sox10^{+} BPs contribute to luminal lineages in an inefficient manner, supporting the observed delay during puberty.

Finally, it is possible that the role of Sox10 is not limited to intrinsic regulation of LPs but may also influence ductal morphogenesis by modulating responsiveness to stromal signalling cues. Indeed, Sox10 activation has been reported to be downstream of stromal signalling, specifically FGF, which coordinates epithelial restructuring programs during morphogenesis (263,267,268). While previous studies have demonstrated that Sox10^{+} luminal cells are exclusively PR^{-}, and thus are unlikely to be direct hormone-sensing cells, others have shown that FGF signalling enhances fibroblast-induced branching of mammary epithelium by modulating paracrine signalling (267,336). Thus, if Sox10 is required for maintenance of the LP state, its loss could reduce this compartment's ability to respond to stromal factors that drive epithelial restructuring programs during pubertal outgrowth. In our model, these stromal-dependent paracrine signals may select for residual Sox10^{+} cells, allowing delayed completion of morphogenesis. As an aside, the reciprocal relationship between Sox10 and PR expression may underscore the observed mosaicism of luminal Sox10 expression in the adult mammary gland. It is possible that mature Sox10^{+} cells may represent the HR^{-} alveolar/secretory lineage, where Sox10^{-} mature luminal likely demarcate the HR^{+} lineage.

Importantly, these compensation mechanisms are likely not mutually exclusive and could have an additive effect permitting eventual development. Given the role of Sox10 in neural stem cell function, the delay in ductal outgrowth seen here is likely to be a result of reduced LP fitness following Sox10 loss.

6.2.2 Sox10 in maintaining established epithelial populations

Morphologically, no overt defects were observed following luminal-specific Sox10 ablation in adult virgin mammary glands (Fig. 3.2, 3.4, 3.5). Consistent with this, Sox10 loss does not alter mature luminal epithelial proportions nor disrupt the basal/luminal organization (Fig. 3.4 C, 3.6 B). However, the cellular composition within the luminal compartment is skewed, as evidenced by a marked reduction in LP populations (Fig. 3.6 C). These findings suggest that Sox10 is dispensable for the maintenance of the epithelial architecture but is required to sustain progenitor identity within the luminal lineage.

The present study examined the dynamics of mammary gland pubertal development exclusively in adult virgin females. Consequently, it remains unclear how luminal Sox10 loss affects subsequent mammary remodeling processes that require extensive morphogenic events such as pregnancy, lactation, and involution. Similarly, although adult virgin glands appear morphologically normal, we cannot exclude more subtle defects associated with estrous cycling dependent remodeling. These considerations raise the possibility that Sox10 may contribute to epithelial plasticity during latent physiological events not addressed in the current study. To this end, transcriptomic analyses using Reactome and PROGENy pathways revealed downregulation of cytoskeletal and extracellular matrix-associated programs following Sox10 deletion in Neu-transformed epithelial cell lines, pathways known to be critical for mammary epithelial restructuring (Fig. 5.13). While these analyses were completed in Neu-transformed epithelium rather than normal tissue, they point to developmentally important programs that Sox10 may contribute to. Future studies will be required to determine whether luminal-specific Sox10 is required for such morphogenic cycles through successive pregnancies.

The data presented in Ch. 4 and 5 support a prerequisite for Sox10 expression in luminal epithelial cells to establish a transformation competent state. Given that mammary tumor initiation in HER2/Neu-driven models has been demonstrated to arise from LPs, the reduced tumor-initiating cells observed in Sox10-deficient mammary glands may represent the most overt consequence of the Sox10-dependent LP depletion (215–218). Thus, $Sox10^{+}$ LPs required for normal mammary development likely represent, or at least give rise to, the cellular compartment required for transformation later in life. Progressive Cre-mediated deletion of Sox10 throughout the lifespan of MMTV-NIC: $Sox10^{fl/fl}$ mice likely erodes this competent population prior to the onset of oncogenic transformation, thereby wholly preventing HER2/Neu-driven tumor initiation in Sox10-deficient mice.

Finally, the data presented here build on previous observations from our lab and help further contextualize our findings. Using the MMTV-NIC model, it was found that conditional deletion of the Ste-20-like Kinase (SLK) resulted in faster tumor formation. It was subsequently found that SLK deletion results in an increase in $Sox10^{+}$ cells in vivo, accelerating tumor initiation (130). Supporting this, expression of Sox10 was sufficient to increase tumorigenicity in NIC derived cell lines (130). Interestingly, no overt defects were observed in adult virgin mammary gland development and similar proportions of total $Sox10^{+}$ epithelial cells were observed between wild-type and SLK- mice (130). This led to the conclusion that, in a non-oncogenic background, SLK deletion does not cause the expansion of progenitor populations, suggesting that oncogenic transformation in combination with SLK deletion alters the luminal stem cell pool. However, the data presented here support a more nuanced interpretation of these findings. While we similarly show no overt developmental defects in adult mammary glands, it is apparent that depletion of LP populations can result in more subtle developmental defects that are not obvious when

interrogating fully developed glands (Fig. 3.2, 3.4, 3.6). Importantly, Sox10 expression within the mammary epithelium is heterogeneous, and bulk Sox10 immunostaining does not resolve functionally distinct progenitor subsets (Fig. 3.4 A, B). Thus, our current findings offer an additional layer of interpretation of the increased tumorigenicity observed in SLK-deficient NIC females, wherein enhanced Sox10 activity within the developing mammary epithelium may expand transformation-competent LP populations that were not resolved by prior bulk analyses.

6.3 Sox10 in mammary tumorigenesis

6.3.1 Sox10 is required for RTK-driven tumor initiation

Previous studies have reported conserved expression of Sox10 in murine and human mammary progenitors (267,278,279,289). Supporting a role for Sox10 in mammary stem/progenitor cell function, its conditional deletion in the basal and luminal compartments impairs mammary gland development (278). Variable proportions of $Sox10^{+}$ cells have been reported for both TNBC and HER2-positive breast cancers, suggesting that it is expressed in subpopulations of cancer cells (130,291–293,295). Using a conditional *Sox10* allele, we tested the effect of Sox10 luminal deletion on overall tumorigenesis in a HER2/Neu-positive mouse model. Our data show that Sox10-deficient luminal cells abrogate Neu-induced tumor initiation in a dose-dependent manner (Fig. 4.2 A). Consistent with previous data showing that hemizygous expression of Sox10 delays tumor progression in a basal-like model, the investigations here show a similar dose-dependent phenotype for Sox10 in a HER2/Neu-positive mouse model (279). Notably, once tumors arise in Sox10 hemizygous mice, they progress at rates similar to those observed in wild-type mice (Fig. 4.2 B, C). Indeed, orthotopic injections of bulk Sox10-deficient cell lines demonstrated slow, but eventual growth of tumors (Fig. 5.4 C, D). Subsequent analyses revealed

similar levels of $Sox10^+$ nuclei in the "deficient" tumor lines compared to wild-type controls, suggesting that residual $Sox10^+$ cells were able to obviate selective pressures and eventually sustain tumorigenic growth (Fig. 5.4 E). Together, these observations across distinct models suggest that Sox10 dosage plays a rate-limiting role in mammary tumorigenesis.

To determine whether related SoxE family members could compensate for Sox10 loss, we examined Sox9 expression in Sox10-deficient contexts. In a large T antigen mouse model, Sox9 upregulation can drive luminal-to-basal plasticity and its deletion prevents the progression of hyperplasia to breast carcinomas (200). Interestingly, Sox9 protein levels were upregulated in Sox10-deficient HER2/Neu-transformed tumor cells, potentially contributing to the upregulation of basal genes (Fig. 5.7 D). However, we found that Sox9 expression was readily detectable in luminal cells following Sox10 deletion *in vivo* and that endogenous Sox9 was unable to rescue tumor growth in orthotopic transplants of Sox10-deficient cells, suggesting that Sox9 cannot compensate for Sox10 in driving tumor initiation (Fig. 4.15).

6.3.2 Sox10's function in tumor initiation versus progression

Based on our data showing that Sox10 hemizygous mice eventually form tumors that progress at the same rate of wild-types, it may seem that Sox10 is selectively required for tumor initiation, but not in tumor progression. However, this interpretation is confounded by the fact that the tumors in NIC Sox10 hemizygous mice eventually acquire Sox10 expression levels similar to wild-type endpoint tumors (Fig. 4.4). Due to this upregulation of Sox10 in these tumors, it is not clear whether the effect of Sox10 on tumorigenesis is restricted to initiation, or if progression is also affected. Surprisingly, dox-treated rtTA/MIC $Sox10^{fl/fl}$ mice appear to develop transformed lumens prior to complete Sox10 excision (Fig. 4.15, 4.16). However, with sustained oncogene activation through chronic doxycycline treatment, these Sox10-deficient lesions do not progress

in size as observed in wild-type mice, supporting a Sox10-dependent role in tumor progression (Fig. 4.15 B). This is further supported in the LDA assay findings. While a drastic reduction in tumor-initiating potential was observed in $Sox10^-$ cells, the cell injections that formed small <0.5 cm^3 masses did so at rates comparable to controls (Fig. 5.8 A). Upon reaching this 'onset' stage, however, the $Sox10^-$ clones completely arrested tumor progression while the control cells were able to rapidly expand until endpoint (Fig. 5.8 C, D). Importantly, these small masses were devoid of Sox10 but retained Neu expression, while control tumors were composed of strikingly high proportions of $Sox10^+$ cells (Fig. 5.8 E). Thus, if Sox10 were only required for tumor initiation, then Sox10-deficient tumors that successfully seeded would be expected to progress past this onset stage.

Although we did not report any overt defects in growth and survival programs in tumor sections and lysates at endpoint, it is important to acknowledge that these represent a snapshot of tumor cell biology at the time of collection (Fig. 4.5). Such limitations may not capture more dynamic alterations to these signalling pathways. Indeed, Reactome and pathway analysis of the BG1 cell lines indicated overrepresentation of genes in ECM-associated programs with profound downregulation of MAPK, JAK-STAT, EGFR, and TGFb pathways upon Sox10 deletion (Fig. 5.13). Notably, while we did observe a significant loss of 3D-invasion, downregulation of cytoskeletal/ECM-associated programs, and reduced functional stemness, there were no obvious changes to these cells proliferative capacity in 2D culture conditions (Fig. 5.3, 5.4).

This presents a model where upstream oncogenic HER2/Neu and PyMT-mediated RTK signalling may be biochemically intact following Sox10 loss, but complex morphogenic programs downstream of these signalling cascades are dysregulated. Such mechanisms would support the apparent Sox10-independent survival and engraftment, but eventual plateau observed in the LDA

and tail-vein injection assays (Fig. 5.8, 5.9). Perhaps Sox10-deficient cells maintain the ability to survive injection and acutely respond to intact HER2/Neu expression, allowing them to give rise to rapidly developing lesions at either primary orthotopic sites or distant tissues during 'metastatic' spread. However, these local masses may ultimately fail to interact with the ECM and maintain progenitor-driven and stromal-dependent invasive growth. The HER2-HER3 heterodimer pair produces highly potent downstream activation of PI3K and MAPK and are one of the most abundant signalling pairs $HER2^{+}$ breast cancers (337). As previously mentioned, Sox10 has been shown to drive expression of HER3 during NC developmental programs (274,275). Indeed, we found that Sox10 ablation resulted in significant depletion of HER3 transcripts. Thus, it is possible that loss of Sox10 erodes HER3-dependent migratory and invasive signalling programs necessary for ECM-interaction ultimately uncoupling malignant growth from late stage tumorigenicity, wherein established lesions still require Sox10 for disease progression.

Regardless of the precise mechanisms, the observed dose-dependent phenotype highlights attractive translational implications. Seeing that partial suppression of Sox10 is sufficient to significantly increase survival in mice, the prospective for targeting Sox10-dependent signalling programs present a promising mechanism for therapeutic intervention in the treatment of such breast cancers.

6.3.3 Luminal-to-basal shift and reduced stemness paradox

Transcriptomic analyses of Sox10-deficient HER2/Neu-transformed tumor cells revealed reprogramming events leading to loss of luminal identity and the acquisition of basal/mesenchymal-specific markers (Fig. 5.11, 5.12, 5.14). However, it appears that these reprogramming events did not fully recapitulate canonical basal/mesenchymal-like programs commonly associated with increased aggressiveness and worse prognosis. Indeed, acquisition of

such transcriptional programs did not equate to functional stemness, as indicated by reduced functional tumorigenicity in Sox10-deficient cells (Fig. 5.8, 5.9). Supporting this, flow sorting analyses revealed a significant reduction in the number of LPs (MMTV-Cre:Sox10$^{fl/fl}$) and mammary cells with tumor-initiating activity (MMTV-NIC:Sox10$^{fl/fl}$) upon Sox10 deletion (Fig. 3.6, 4.9). Our data also shows that Sox10 loss disrupts expression of canonical and non-canonical Wnt signalling pathways, as well as downregulation of several luminal-defining and stemness factors such as Foxa1, Notch3, Etv1, Elf5, and Msx1 (Fig. 5.11 A, B). Interestingly, Sox10 inactivation also upregulates *Sfrp1*, a Wnt suppressor upregulated upon deletion of Ezh2 (338). Conversely, loss of Sox10 downregulates *Etv1*, shown to be required for the maintenance of the TIC phenotype (339).

This dissociation between acquired basal signatures and tumorigenic potential presents a paradox wherein basal-like reprogramming events do not necessarily confer stem-like behaviors. Previous studies examining the role of p38α, an established LP mediator, observed a similar disparity when luminal-specific p38α inactivation was associated with reduced tumorigenicity, erosion of luminal identity markers and induction of basal-like programs (223). The possibility that inactivation of such LP regulators could downregulate luminal-defining programs that supress basal lineages should therefore be considered. Indeed, previous studies have demonstrated that luminal populations actively repress basal programs through epigenetic modifications (340). Other luminal identity factors, including FOXA1, have been shown to sustain luminal integrity by directly binding and repressing genes associated with basal-like programs (341). The extent of such lineage repression is further evidenced in previous reports of intercellular-dependent preservation of basal identity by paracrine luminal cell signalling (191,194). Thus, loss of luminal identity following Sox10 deletion may upend these lineage-defining epigenetic programs,

derepressing basal gene signatures without conferring the commonly associated increased functional stemness. This would ultimately result in a poorly defined luminal-basal hybrid state.

Finally, previous studies in MMTV-Neu and MMTV-PyMT mice supported the notion that mammary tumors originate from LP cells (342,343). Similarly, lineage tracing studies showed that basal-like breast tumors etiologically arise from LPs rather than from BPs, suggesting luminal-to-basal reprogramming (185,219,220). To this end, the seeding of distant metastases in PyMT-based models has been associated with tumor cells of luminal origin (216). Thus, the erosion of luminal identity in Sox10-deficient rtTA/MIC may be a rate-limiting step that precedes luminal-dependent tumor cell dissemination, resulting in the observed impaired lung colonization (Fig. 4.14). This hypothesis would be supported by the phenotype observed in HER2/Neu-transformed cell lines exhibiting reduced lung colonization and failure to expand metastatic niches (Fig. 5.9). While these models are representative of distinct stages of metastatic dissemination (full metastatic cascade vs survival in circulation and intravasation), together they suggest that Sox10 is required both for tumor-initiating competence as well as driving downstream luminal-dependent programs that support metastatic colonization and niche establishment. Importantly, the overall reduction of tumorigenic phenotypes across the respective models does not appear to be a product of MMTV promoter inactivation upon the loss of luminal identity as evidenced by retained Cre expression in rtTA/MIC *in vivo* and sustained HER2/Neu expression of Sox10-deficient MMTV-NDL cell lines *in vitro* and *in vivo* (Fig. 4.13, Fig. 4.14, 5.5 A, 5.8 E).

6.4 Discrepancy of Sox10$^+$ populations in human and mouse HER2/Neu-transformed tumors

A notable incongruency reported between human HER2-positive samples and Neu-based murine models is that the Sox10$^+$ proportions seem to differ quite dramatically. As previously

reported by us and others, there is a considerable range in Sox10-positivity found in human HER2-positive samples (130,291–293,295). Conversely, to date we have not observed NIC, NeuNDL, or even RTK-dependent rtTA/MIC tumor sections that show considerably low levels of $Sox10^+$ cells. While the minimum amount of $Sox10^+$ cells required for a tumor to be considered "$Sox10^+$" has not been defined, it is uncommon to see hyperplastic or endpoint tumor sections that lack considerable $Sox10^+$ cell contribution in murine tumors. This raises the question of whether the observed variability in Sox10 staining across species represents a species-specific role for Sox10 in mice that is not as profound in humans.

A few possible hypotheses for such disparity should be entertained. First, tumor samples derived from murine models of HER2-positive cancer are exclusively treatment naïve and are therefore not subject to therapeutic or immune pressures. As a result, the seemingly more tumorigenic $Sox10^+$ populations are therefore not disproportionally targeted, consequently lending to elevated $Sox10^+$ endpoint tumor cell proportions. This posits that highly heterogenous human HER2-positive samples may be a product of therapy-induced Sox10 selection pressures rather than a lack of requirement for Sox10 in tumorigenesis. While this mechanism may hold true, limited Sox10 association studies have specifically interrogated treatment naïve human samples, the few of which report significant variability in $Sox10^+$ proportions in TNBC (15% vs 67%) (344,345).

Another possible mechanism may be a disproportionate requirement for Sox10 in the respective stages of disease progression. Such phenomenon would be exacerbated by the vastly different kinetics observed between murine and human cancers. For instance, Sox10 appears to be absolutely required for the seeding of malignant niches as well as invasion and dissemination in murine models, but may be less important in their subsequent progression once established. This would suggest that Sox10 expression levels at endpoint may not be as pertinent as in early

malignant programs. Accordingly, while murine tumors are often analyzed near endpoint, they are still relatively early in evolutionary time compared to human disease. The high murine levels of Sox10 at endpoint may therefore be the result of compounding effects from the early Sox10 requirement and rapid disease progression. Conversely, by the time human tumors are sampled, $Sox10^+$ cells may have already successfully seeded disease, facilitated progression and then differentiated or been outcompeted by rapidly proliferating populations resulting in Sox10 expression that may be silenced, or spatially restricted to select subpopulations. Thus, human breast cancer samples may represent a snapshot of advanced cellular heterogeneity that murine models cannot recapitulate.

Finally, transgenic models do not represent a neutral sampling of mammary epithelium as they are driven by potent oncogenes often not physiologically equivalent to those observed in the human malignancies they aim to model. For instance, murine models of HER2-positive tumorigenesis employ the use of constitutively active oncogenes that preferentially drive rapid expansion of transformation-competent progenitor populations. Thus, if Sox10 programs disproportionally contributes to LP populations, and if oncogene expression is biased to such populations due to tissue-specific promoters, then these $Sox10^+$ populations will certainly be most permissive to malignant transformation ultimately resulting in an amplified founder effect. In human disease, however, it is more likely that malignant transformation will occur over a longer time scale through loss of tumor suppressors or other mutational events across luminal states with higher degrees of heterogeneity. The consequences of such incongruencies can be observed when comparing tumor latency in murine models to natural human disease progression. Onset of spontaneous tumors in murine models, specifically in those employing HER/Neu and PyMT oncogenes, do not often exceed 6 months of age, with some arising prior to completion of puberty

(125,126,141,146). On a developmental scale, even the most latent models would be equivalent to early mid-life age in humans; approximately early to mid 20's (346). While TNBCs are more frequently diagnosed in women under 40 years of age compared to other subtypes, the average age for diagnosis is 54 years of age (347,348). Interestingly, while TNBC is typically more aggressive and poorly differentiated in younger patients, there is limited evidence of age association in $Sox10^+$-TNBC studies (287,348,349). Thus, while these models effectively capture qualitative stages and subtype biology, their compressed timescale cannot fully represent the natural temporal progression of human breast cancer.

Rather than varying species-specific requirements for Sox10 in disease progression, it is plausible that the observed discrepancy between Sox10 contribution in murine and human breast cancers may be a consequence of fundamental limitations of murine models that do not earnestly recapitulate the physiological nuances of human breast cancer.

6.5 Selective pressures sustaining Sox10 expression *in vitro*

As previously discussed, elevated Sox10 expression is a prominent feature in all transformed tissues that arise from the murine models employed here. Sox10 expression appears so fundamental for *in vivo* tumor growth that even in derived tumors cell lines that silence Sox10 expression *in vitro*, Sox10 expression is either reactivated, or imperceptibly small $Sox10^+$ populations propagate the ensuing $Sox10^+$ tumors following orthotopic transplantation (Fig. 5.5). In contrast, loss of Sox10 expression with continued passage *in vitro* appear to be a frequent occurrence during the establishment of Neu-transformed cell lines. Sox10 expression has been reported to be absent in the PY230 cell line as well as several human HER2-positive and TNBC lines (279). Consistent with this, while 100% of NDL/NIC primary tumors show Sox10 expression at endpoint, only 10-20% of derived tumor lines retain Sox10 beyond early passaging (Fig. 5.5 A).

In our hands, early passage BG1 and BG2 lines display ~ 60-90% Sox10$^+$ cells, but only BG1 cells retain their Sox10$^+$ subpopulation with long-term passage (Fig. 5.5 A). This then raises the question of physiological or epigenetic requirements that are needed for Sox10 expression *in vitro* and how this may affect downstream studies employing these cell lines.

A possible explanation is that 2D culture conditions impose selective pressures acting against Sox10$^+$ progenitor populations, while more physiologically relevant orthotopic growth actively selects for this population. Given the role of Sox10 in stem-like LPs, Sox10$^+$ populations would likely be more quiescent. As slow cycling cells prioritize plasticity over rapid growth, Sox10$^+$ cells could be selected against in the pro-proliferative environment that serially passaged 2D culture fosters. Apart from proliferative selection pressures, Sox10 expression likely also depends on ECM engagement and stromal-derived paracrine signalling. Specifically, the absence of fibroblast-secreted FGF in 2D culture, which has been demonstrated to be a determinant for Sox10 expression, may lead to the collapse of programs required for maintaining Sox10 levels (263,267). This absence of paracrine cues may lead to progressive collapse of progenitor-associated transcriptional programs and corresponding chromatin accessibility at Sox10-dependent regulatory elements. Such epigenetic plasticity would be in agreement with the reacquisition of Sox10 expression following orthotopic transplantation (Fig. 5.5 B-D).

The stable retention of Sox10 expression in BG1 cells further suggests that, in rare cases, Sox10-dependent programs may become intrinsically stabilized possibly through epigenetic maintenance of Sox10 regulatory elements. Such intrinsic features likely reflect the differentiation state of the respective tumor from which this line was derived. If Sox10 retention in BG1/2 reflects epigenetic stabilization of progenitor-associated programs, this would confer a cellular state that would be more permissive for stem-like behavior *in vivo*. Supporting this, isolated cell lines that

have retained Sox10 expression, namely BG1/2, exhibit strikingly more rapid *in vivo* tumor growth when compared to other Neu-transformed cell lines that lose Sox10 *in vitro* (our unpublished data). This may be in part due to lack of requirement for epigenetic reprogramming, or selection to regain Sox10-dependent tumor-initiating competence following transplantation. Thus, it is likely that the tumors of origin where $Sox10^{+}$ lines can be derived represent less differentiated cellular state that presumably retained their respective LP-like characteristics following *in vitro* propagation.

Finally, these observations establish a framework that provides more contextualized insight to the luminal-basal/mesenchymal transcriptional reprogramming reported upon Sox10 loss. Rather than reflecting erosion of pan-luminal identity, perhaps Sox10 loss preferentially disrupts LP-associated programs within the luminal lineage such that 'luminal marker' downregulation largely reflects collapse of an LP-biased luminal state. Although GSEA signatures indicate numerous gene sets with increased stemness following Sox10 loss, these findings might be framed as derepression of stem cell programs, rather than activation (Fig. 5.12). Given that LP identity is an actively constrained state and not merely a halfway point between MaSCs and mature luminal cells, active repression of basal/MaSC programs are essential for LP identity preservation (340). Thus, acquisition of such GSEA signatures following Sox10 loss may indirectly reflect the destabilization of LP-mediated repressive programs. Furthermore, enrichment of stem-related gene sets in the GSEA analysis may largely be driven by the observed loss of luminal differentiation markers combined with increased expression of basal/mesenchymal-associated genes. As stem-like populations are not expected to retain features of a defined luminal state, coordinated loss of luminal markers in $Sox10^{-}$ cells would bias enrichment toward stemness-associated signatures. Indeed, if Sox10 loss resulted in bona fide acquisition of stem cell identity, one would expect enrichment of core functional stemness pathways such as canonical WNT/β-

catenin, Notch, Hedgehog, or quiescence-associated programs. Instead, Sox10-deficient cells primarily exhibit enrichment of comparative basal gene signatures. Combined with the observed reduced functional tumor-initiating capacity, this framework argues against acquisition of true stemness programs but rather supports a model of maladaptive reprogramming from lineage destabilization. Importantly, parallel analyses of human breast cancer scRNA-seq datasets reveal that *SOX*10 expression similarly marks discrete epithelial subpopulations that share conserved Sox10-dependent transcriptional features with murine tumors, including enrichment of LP-associated genes and exclusion of basal-associated programs (Fig. 5.15). Together, these cross-species observations indicate that Sox10 maintains a conserved, stemness-permissive lineage competence state that is selectively reinforced *in vivo*, while its loss compromises tumor initiation and progression by destabilizing epithelial identity.

6.6 Conclusions and future perspectives

Previous studies have associated Sox10 expression with aggressive behavior in basal-like and TNBCs, as well as with stem/progenitor populations. In line with our initial hypothesis, our findings corroborate these observations by demonstrating that Sox10 functions as a regulator of lineage maintenance by mediating a progenitor state capable of tumor initiation and expansion. In the absence of Sox10, cells appear to undergo transcriptional lineage drift without retaining functional stemness. The transcriptional mechanisms by which Sox10 supports progenitor competence, including potential epigenetic regulation or interaction with other lineage-plasticity factors, remain unclear. Addressing these limitations will be important for fully elucidating how Sox10 integrates developmental and oncogenic programs in mammary epithelial biology.

Whether acting to enforce lineage identity or sustaining self-renewal programs, Sox10 appears to be a regulator of tumor competency and progression across distinct breast cancer

subtypes. In luminal tumors, Sox10 may be required to sustain a progenitor-like state permissive to transformation. In basal-like contexts, it may support lineage reprogramming from luminal origins. This dual role suggests that therapeutic targeting of Sox10 or its downstream effectors could impact not only tumor initiation, but also the maintenance of TICs and the evolutionary trajectory of tumors as they acquire more aggressive phenotypes. Currently, our lab is investigating potential candidates in Sox10-dependent HER2/Neu-induced tumorigenic programs through the use of various screens and reporters. These platforms may identify therapeutic strategies to disrupt Sox10-dependent transcriptional programs and therefore limit disease progression by impairing the maintenance of tumor-initiating cell populations that underlie aggressiveness and treatment resistance.

References

1. cancer CCS/ S canadienne du. Canadian Cancer Society [Internet]. [cited 2026 Jan 15]. Canadian Cancer Statistics. Available from: https://cancer.ca/en/research/cancer-statistics/canadian-cancer-statistics

2. Carvalho E, Canberk S, Schmitt F, Vale N. Molecular Subtypes and Mechanisms of Breast Cancer: Precision Medicine Approaches for Targeted Therapies. Cancers. 2025 Mar 25;17(7):1102. doi:10.3390/cancers17071102 PubMed PMID: 40227634; PubMed Central PMCID: PMC11987866.

3. Mohammed AA. The clinical behavior of different molecular subtypes of breast cancer. Cancer Treat Res Commun. 2021 Jan 1;29:100469. doi:10.1016/j.ctarc.2021.100469

4. Łukasiewicz S, Czeczelewski M, Forma A, Baj J, Sitarz R, Stanisławek A. Breast Cancer—Epidemiology, Risk Factors, Classification, Prognostic Markers, and Current Treatment Strategies—An Updated Review. Cancers. 2021 Jan;13(17):4287. doi:10.3390/cancers13174287

5. Johnson KS, Conant EF, Soo MS. Molecular Subtypes of Breast Cancer: A Review for Breast Radiologists. J Breast Imaging. 2021 Jan 26;3(1):12–24. doi:10.1093/jbi/wbaa110

6. Russnes HG, Lingjærde OC, Børresen-Dale AL, Caldas C. Breast Cancer Molecular Stratification. Am J Pathol. 2017 Oct;187(10):2152–62. doi:10.1016/j.ajpath.2017.04.022

7. Ades F, Zardavas D, Bozovic-Spasojevic I, Pugliano L, Fumagalli D, de Azambuja E, et al. Luminal B Breast Cancer: Molecular Characterization, Clinical Management, and Future Perspectives. J Clin Oncol. 2014 Sep;32(25):2794–803. doi:10.1200/JCO.2013.54.1870

8. Cheang MCU, Chia SK, Voduc D, Gao D, Leung S, Snider J, et al. Ki67 Index, HER2 Status, and Prognosis of Patients With Luminal B Breast Cancer. JNCI J Natl Cancer Inst. 2009 May 20;101(10):736–50. doi:10.1093/jnci/djp082

9. Inic Z, Zegarac M, Inic M, Markovic I, Kozomara Z, Djurisic I, et al. Difference between Luminal A and Luminal B Subtypes According to Ki-67, Tumor Size, and Progesterone Receptor Negativity Providing Prognostic Information. Clin Med Insights Oncol. 2014 Jan 1;8:CMO.S18006. doi:10.4137/CMO.S18006

10. Maisonneuve P, Disalvatore D, Rotmensz N, Curigliano G, Colleoni M, Dellapasqua S, et al. Proposed new clinicopathological surrogate definitions of luminal A and luminal B (HER2-negative) intrinsic breast cancer subtypes. Breast Cancer Res. 2014 Jun 20;16(3):R65. doi:10.1186/bcr3679

11. Luo HB, Du MY, Liu YY, Wang M, Qing HM, Wen Z peng, et al. Differentiation between Luminal A and B Molecular Subtypes of Breast Cancer Using Pharmacokinetic Quantitative Parameters with Histogram and Texture Features on Preoperative Dynamic Contrast-

Enhanced Magnetic Resonance Imaging. Acad Radiol. 2020 Mar 1;27(3):e35–44. doi:10.1016/j.acra.2019.05.002 PubMed PMID: 31151899.

12. Prat A, Pineda E, Adamo B, Galván P, Fernández A, Gaba L, et al. Clinical implications of the intrinsic molecular subtypes of breast cancer. The Breast. 2015 Nov 1;24:S26–35. doi:10.1016/j.breast.2015.07.008

13. Rios-Hoyo A, Shan NL, Karn PL, Pusztai L. Clinical Implications of Breast Cancer Intrinsic Subtypes. In: Sørlie T, Clarke RB, editors. A Guide to Breast Cancer Research: From Cellular Heterogeneity and Molecular Mechanisms to Therapy [Internet]. Cham: Springer Nature Switzerland; 2025 [cited 2026 Jan 15]. p. 435–48. Available from: https://doi.org/10.1007/978-3-031-70875-6_21 doi:10.1007/978-3-031-70875-6_21

14. Miah S, Bagu E, Goel R, Ogunbolude Y, Dai C, Ward A, et al. Estrogen receptor signaling regulates the expression of the breast tumor kinase in breast cancer cells. BMC Cancer. 2019 Jan 16;19:78. doi:10.1186/s12885-018-5186-8 PubMed PMID: 30651078; PubMed Central PMCID: PMC6335685.

15. Orrantia-Borunda E, Anchondo-Nuñez P, Acuña-Aguilar LE, Gómez-Valles FO, Ramírez-Valdespino CA. Subtypes of Breast Cancer. In: Mayrovitz HN, editor. Breast Cancer [Internet]. Brisbane (AU): Exon Publications; 2022 [cited 2026 Jan 15]. Available from: http://www.ncbi.nlm.nih.gov/books/NBK583808/ PubMed PMID: 36122153.

16. ZHANG MH, MAN HT, ZHAO XD, DONG N, MA SL. Estrogen receptor-positive breast cancer molecular signatures and therapeutic potentials (Review). Biomed Rep. 2014 Jan;2(1):41–52. doi:10.3892/br.2013.187 PubMed PMID: 24649067; PubMed Central PMCID: PMC3916982.

17. Asgari-Karchekani S, Aryannejad A, Mousavi SA, Shahsavarhaghighi S, Tavangar SM. The role of HER2 alterations in clinicopathological and molecular characteristics of breast cancer and HER2-targeted therapies: a comprehensive review. Med Oncol. 2022 Sep 29;39(12):210. doi:10.1007/s12032-022-01817-6

18. Atallah NM, Alsaleem M, Toss MS, Mongan NP, Rakha E. Differential response of HER2-positive breast cancer to anti-HER2 therapy based on HER2 protein expression level. Br J Cancer. 2023 Nov;129(10):1692–705. doi:10.1038/s41416-023-02426-4

19. Schettini F, Prat A. Dissecting the biological heterogeneity of HER2-positive breast cancer. The Breast. 2021 Oct 1;59:339–50. doi:10.1016/j.breast.2021.07.019 PubMed PMID: 34392185.

20. Ahuja S, Khan AA, Zaheer S. Understanding the spectrum of HER2 status in breast cancer: From HER2-positive to ultra-low HER2. Pathol - Res Pract. 2024 Oct 1;262:155550. doi:10.1016/j.prp.2024.155550

21. Horimoto Y, Ishizuka Y, Ueki Y, Higuchi T, Arakawa A, Saito M. Comparison of tumors with HER2 overexpression versus HER2 amplification in HER2-positive breast cancer patients. BMC Cancer. 2022 Mar 5;22(1):242. doi:10.1186/s12885-022-09351-4

22. Venetis K, Crimini E, Sajjadi E, Corti C, Guerini-Rocco E, Viale G, et al. HER2 Low, Ultra-low, and Novel Complementary Biomarkers: Expanding the Spectrum of HER2 Positivity in Breast Cancer. Front Mol Biosci. 2022 Mar 15;9. doi:10.3389/fmolb.2022.834651

23. Yin L, Duan JJ, Bian XW, Yu S cang. Triple-negative breast cancer molecular subtyping and treatment progress. Breast Cancer Res. 2020 Jun 9;22(1):61. doi:10.1186/s13058-020-01296-5

24. Pareja F, Geyer FC, Marchiò C, Burke KA, Weigelt B, Reis-Filho JS. Triple-negative breast cancer: the importance of molecular and histologic subtyping, and recognition of low-grade variants. Npj Breast Cancer. 2016 Nov 16;2(1):16036. doi:10.1038/npjbcancer.2016.36

25. Hubalek M, Czech T, Müller H. Biological Subtypes of Triple-Negative Breast Cancer. Breast Care. 2017 Feb 20;12(1):8–14. doi:10.1159/000455820

26. Lee KL, Kuo YC, Ho YS, Huang YH. Triple-Negative Breast Cancer: Current Understanding and Future Therapeutic Breakthrough Targeting Cancer Stemness. Cancers. 2019 Sep;11(9):1334. doi:10.3390/cancers11091334

27. Zagami P, Carey LA. Triple negative breast cancer: Pitfalls and progress. Npj Breast Cancer. 2022 Aug 20;8(1):95. doi:10.1038/s41523-022-00468-0

28. Borri F, Granaglia A. Pathology of triple negative breast cancer. Semin Cancer Biol. 2021 Jul 1;Precision Medicine in Breast Cancer72:136–45. doi:10.1016/j.semcancer.2020.06.005

29. Foulkes WD, Smith IE, Reis-Filho JS. Triple-Negative Breast Cancer. N Engl J Med. 2010 Nov 11;363(20):1938–48. doi:10.1056/NEJMra1001389

30. Maqbool M, Bekele F, Fekadu G. Treatment Strategies Against Triple-Negative Breast Cancer: An Updated Review . Breast Cancer Targets Ther. 2022 Jan 11;14:15–24. doi:10.2147/BCTT.S348060

31. Rubin E, Shan KS, Dalal S, Vu DUD, Milillo-Naraine AM, Guaqueta D, et al. Molecular Targeting of the Human Epidermal Growth Factor Receptor-2 (HER2) Genes across Various Cancers. Int J Mol Sci. 2024 Jan;25(2):1064. doi:10.3390/ijms25021064

32. Rubin I, Yarden Y. The basic biology of HER2. Ann Oncol. 2001;12:S3–8. doi:10.1093/annonc/12.suppl_1.S3

33. Cheng X. A Comprehensive Review of HER2 in Cancer Biology and Therapeutics. Genes. 2024 Jul;15(7):903. doi:10.3390/genes15070903

34. Iqbal N, Iqbal N. Human Epidermal Growth Factor Receptor 2 (HER2) in Cancers: Overexpression and Therapeutic Implications. Mol Biol Int. 2014;2014(1):852748. doi:10.1155/2014/852748

35. Raghav KPS, Moasser MM. Molecular Pathways and Mechanisms of HER2 in Cancer Therapy. Clin Cancer Res. 2023 Jul 5;29(13):2351–61. doi:10.1158/1078-0432.CCR-22-0283

36. Yarden Y, Sliwkowski MX. Untangling the ErbB signalling network. Nat Rev Mol Cell Biol. 2001 Feb;2(2):127–37. doi:10.1038/35052073 PubMed PMID: 11252954.

37. Moasser MM. The oncogene HER2; Its signaling and transforming functions and its role in human cancer pathogenesis. Oncogene. 2007 Oct 4;26(45):6469–87. doi:10.1038/sj.onc.1210477 PubMed PMID: 17471238; PubMed Central PMCID: PMC3021475.

38. Leahy DJ. Structure and function of the epidermal growth factor (EGF/ErbB) family of receptors. Adv Protein Chem. 2004;68:1–27. doi:10.1016/S0065-3233(04)68001-6 PubMed PMID: 15500857.

39. Roskoski R. The ErbB/HER family of protein-tyrosine kinases and cancer. Pharmacol Res. 2014 Jan 1;79:34–74. doi:10.1016/j.phrs.2013.11.002

40. Singh B, Carpenter G, Coffey RJ. EGF receptor ligands: recent advances [Internet]. F1000Research; 2016 [cited 2026 Jan 16]. Available from: https://f1000research.com/articles/5-2270 doi:10.12688/f1000research.9025.1

41. Crovello CS, Lai C, Cantley LC, Carraway KL. Differential Signaling by the Epidermal Growth Factor-like Growth Factors Neuregulin-1 and Neuregulin-2 *. J Biol Chem. 1998 Oct 9;273(41):26954–61. doi:10.1074/jbc.273.41.26954 PubMed PMID: 9756944.

42. Deguchi E, Lin S, Hirayama D, Matsuda K, Tanave A, Sumiyama K, et al. Low-affinity ligands of the epidermal growth factor receptor are long-range signal transmitters in collective cell migration of epithelial cells. Cell Rep. 2024 Nov 26;43(11). doi:10.1016/j.celrep.2024.114986 PubMed PMID: 39546398.

43. Riese DJ, Bermingham Y, van Raaij TM, Buckley S, Plowman GD, Stern DF. Betacellulin activates the epidermal growth factor receptor and erbB-4, and induces cellular response patterns distinct from those stimulated by epidermal growth factor or neuregulin-beta. Oncogene. 1996 Jan 18;12(2):345–53. PubMed PMID: 8570211.

44. Beerli RR, Hynes NE. Epidermal Growth Factor-related Peptides Activate Distinct Subsets of ErbB Receptors and Differ in Their Biological Activities (∗). J Biol Chem. 1996 Mar 15;271(11):6071–6. doi:10.1074/jbc.271.11.6071

45. Maennling AE, Tur MK, Niebert M, Klockenbring T, Zeppernick F, Gattenlöhner S, et al. Molecular Targeting Therapy against EGFR Family in Breast Cancer: Progress and Future Potentials. Cancers. 2019 Dec;11(12):1826. doi:10.3390/cancers11121826

46. Cho HS, Mason K, Ramyar KX, Stanley AM, Gabelli SB, Denney DW, et al. Structure of the extracellular region of HER2 alone and in complex with the Herceptin Fab. Nature. 2003 Feb;421(6924):756–60. doi:10.1038/nature01392

47. Kovacs E, Zorn JA, Huang Y, Barros T, Kuriyan J. A Structural Perspective on the Regulation of the EGF Receptor. Annu Rev Biochem. 2015 Jun 2;84:739–64. doi:10.1146/annurev-biochem-060614-034402 PubMed PMID: 25621509; PubMed Central PMCID: PMC4452390.

48. Graus-Porta D, Beerli RR, Daly JM, Hynes NE. ErbB-2, the preferred heterodimerization partner of all ErbB receptors, is a mediator of lateral signaling. EMBO J. 1997 Apr 1;16(7):1647–55. doi:10.1093/emboj/16.7.1647 PubMed PMID: 9130710; PubMed Central PMCID: PMC1169769.

49. Daemen A, Manning G. HER2 is not a cancer subtype but rather a pan-cancer event and is highly enriched in AR-driven breast tumors. Breast Cancer Res. 2018 Jan 30;20(1):8. doi:10.1186/s13058-018-0933-y

50. Natrajan R, Weigelt B, Mackay A, Geyer FC, Grigoriadis A, Tan DSP, et al. An integrative genomic and transcriptomic analysis reveals molecular pathways and networks regulated by copy number aberrations in basal-like, HER2 and luminal cancers. Breast Cancer Res Treat. 2010 Jun 1;121(3):575–89. doi:10.1007/s10549-009-0501-3

51. Staaf J, Jönsson G, Ringnér M, Vallon-Christersson J, Grabau D, Arason A, et al. High-resolution genomic and expression analyses of copy number alterations in HER2-amplified breast cancer. Breast Cancer Res. 2010 May 6;12(3):R25. doi:10.1186/bcr2568

52. Marotta M, Onodera T, Johnson J, Budd GT, Watanabe T, Cui X, et al. Palindromic amplification of the ERBB2 oncogene in primary HER2-positive breast tumors. Sci Rep. 2017 Feb 17;7(1):41921. doi:10.1038/srep41921

53. Orsetti B, Nugoli M, Cervera N, Lasorsa L, Chuchana P, Ursule L, et al. Genomic and Expression Profiling of Chromosome 17 in Breast Cancer Reveals Complex Patterns of Alterations and Novel Candidate Genes. Cancer Res. 2004 Sep 16;64(18):6453–60. doi:10.1158/0008-5472.CAN-04-0756

54. Monni O, Bärlund M, Mousses S, Kononen J, Sauter G, Heiskanen M, et al. Comprehensive copy number and gene expression profiling of the 17q23 amplicon in human breast cancer. Proc Natl Acad Sci U S A. 2001 May 8;98(10):5711–6. doi:10.1073/pnas.091582298 PubMed PMID: 11331760; PubMed Central PMCID: PMC33278.

55. Kauraniemi P, Bärlund M, Monni O, Kallioniemi A. New amplified and highly expressed genes discovered in the ERBB2 amplicon in breast cancer by cDNA microarrays. Cancer Res. 2001 Nov 15;61(22):8235–40. PubMed PMID: 11719455.

56. Miller S, Suen T, Sexton T, Hung M. MECHANISMS OF DEREGULATED HER2/NEU EXPRESSION IN BREAST-CANCER CELL-LINES. Int J Oncol. 1994 Mar 1;4(3):599–608. doi:10.3892/ijo.4.3.599

57. Benz CC, O'Hagan RC, Richter B, Scott GK, Et. A. HER2/Neu and the Ets transcription activator PEA3 are coordinately upregulated in human breast cancer. Oncogene. 1997. doi:10.1038/sj.onc.1201331

58. Cocco E, Lopez S, Santin AD, Scaltriti M. Prevalence and role of HER2 mutations in cancer. Pharmacol Ther. 2019. doi:10.1016/j.pharmthera.2019.03.010

59. Bon G, Di Lisa FS, Filomeno L, Arcuri T, Krasniqi E, Pizzuti L, et al. HER2 mutation as an emerging target in advanced breast cancer. Cancer Sci. 2024;115(7):2147–58. doi:10.1111/cas.16148

60. Ishiyama N, O'Connor M, Salomatov A, Romashko D, Thakur S, Mentes A, et al. Computational and Functional Analyses of HER2 Mutations Reveal Allosteric Activation Mechanisms and Altered Pharmacologic Effects. Cancer Res. 2023 May 2;83(9):1531–42. doi:10.1158/0008-5472.CAN-21-0940

61. Cooke T, Reeves J, Lanigan A, Stanton P. HER2 as a prognostic and predictive marker for breast cancer. Ann Oncol. 2001;12:S23–8. doi:10.1093/annonc/12.suppl_1.S23

62. Ruiz-Saenz A, Dreyer C, Campbell MR, Steri V, Gulizia N, Moasser MM. HER2 Amplification in Tumors Activates PI3K/Akt Signaling Independent of HER3. Cancer Res. 2018 Jul 1;78(13):3645–58. doi:10.1158/0008-5472.CAN-18-0430

63. Fry EA, Taneja P, Inoue K. Oncogenic and tumor-suppressive mouse models for breast cancer engaging HER2/neu. Int J Cancer. 2017;140(3):495–503. doi:10.1002/ijc.30399

64. Moasser MM. The oncogene HER2: its signaling and transforming functions and its role in human cancer pathogenesis. Oncogene. 2007 Oct;26(45):6469–87. doi:10.1038/sj.onc.1210477

65. Dankort D, Maslikowski B, Warner N, Kanno N, Kim H, Wang Z, et al. Grb2 and Shc adapter proteins play distinct roles in Neu (ErbB-2)-induced mammary tumorigenesis: implications for human breast cancer. Mol Cell Biol. 2001 Mar;21(5):1540–51. doi:10.1128/MCB.21.5.1540-1551.2001 PubMed PMID: 11238891; PubMed Central PMCID: PMC86700.

66. Dankort DL, Wang Z, Blackmore V, Moran MF, Muller WJ. Distinct tyrosine autophosphorylation sites negatively and positively modulate neu-mediated transformation. Mol Cell Biol. 1997 Sep;17(9):5410–25. doi:10.1128/mcb.17.9.5410 PubMed PMID: 9271418; PubMed Central PMCID: PMC232391.

67. Hodgson JG, Malek T, Bornstein S, Hariono S, Ginzinger DG, Muller WJ, et al. Copy Number Aberrations in Mouse Breast Tumors Reveal Loci and Genes Important in Tumorigenic Receptor Tyrosine Kinase Signaling. Cancer Res. 2005 Nov 1;65(21):9695–704. doi:10.1158/0008-5472.CAN-05-0755

68. Weiner DB, Liu J, Cohen JA, Williams WV, Greene MI. A point mutation in the neu oncogene mimics ligand induction of receptor aggregation. Nature. 1989 May 18;339(6221):230–1. doi:10.1038/339230a0 PubMed PMID: 2654648.

69. Bargmann CI, Hung MC, Weinberg RA. Multiple independent activations of the neu oncogene by a point mutation altering the transmembrane domain of p185. Cell. 1986 Jun 6;45(5):649–57. doi:10.1016/0092-8674(86)90779-8 PubMed PMID: 2871941.

70. Shih C, Padhy LC, Murray M, Weinberg RA. Transforming genes of carcinomas and neuroblastomas introduced into mouse fibroblasts. Nature. 1981 Mar 19;290(5803):261–4. doi:10.1038/290261a0 PubMed PMID: 7207618.

71. Schechter AL, Stern DF, Vaidyanathan L, Decker SJ, Drebin JA, Greene MI, et al. The neu oncogene: an erb-B-related gene encoding a 185,000-Mr tumour antigen. Nature. 1984 Dec;312(5994):513–6. doi:10.1038/312513a0

72. Guy CT, Webster MA, Schaller M, Parsons TJ, Cardiff RD, Muller WJ. Expression of the neu protooncogene in the mammary epithelium of transgenic mice induces metastatic disease. Proc Natl Acad Sci U S A. 1992 Nov 15;89(22):10578–82. doi:10.1073/pnas.89.22.10578 PubMed PMID: 1359541; PubMed Central PMCID: PMC50384.

73. Siegel PM, Dankort DL, Hardy WR, Muller WJ. Novel activating mutations in the neu proto-oncogene involved in induction of mammary tumors. Mol Cell Biol. 1994 Nov;14(11):7068–77. doi:10.1128/mcb.14.11.7068-7077.1994 PubMed PMID: 7935422; PubMed Central PMCID: PMC359240.

74. Siegel PM, Muller WJ. Mutations affecting conserved cysteine residues within the extracellular domain of Neu promote receptor dimerization and activation. Proc Natl Acad Sci. 1996 Aug 20;93(17):8878–83. doi:10.1073/pnas.93.17.8878

75. Woods Ignatoski KM, Grewal NK, Markwart S, Livant DL, Ethier SP. p38MAPK induces cell surface alpha4 integrin downregulation to facilitate erbB-2-mediated invasion. Neoplasia N Y N. 2003;5(2):128–34. doi:10.1016/s1476-5586(03)80004-0 PubMed PMID: 12659685; PubMed Central PMCID: PMC1550346.

76. Muthuswamy SK, Li D, Lelievre S, Bissell MJ, Brugge JS. ErbB2, but not ErbB1, reinitiates proliferation and induces luminal repopulation in epithelial acini. Nat Cell Biol. 2001 Sep;3(9):785–92. doi:10.1038/ncb0901-785 PubMed PMID: 11533657; PubMed Central PMCID: PMC2952547.

77. Benz CC, Scott GK, Sarup JC, Johnson RM, Tripathy D, Coronado E, et al. Estrogen-dependent, tamoxifen-resistant tumorigenic growth of MCF-7 cells transfected with HER2/neu. Breast Cancer Res Treat. 1992;24(2):85–95. doi:10.1007/BF01961241 PubMed PMID: 8095168.

78. Chazin VR, Kaleko M, Miller AD, Slamon DJ. Transformation mediated by the human HER-2 gene independent of the epidermal growth factor receptor. Oncogene. 1992 Sep;7(9):1859–66. PubMed PMID: 1354348.

79. Hudziak RM, Schlessinger J, Ullrich A. Increased expression of the putative growth factor receptor p185HER2 causes transformation and tumorigenesis of NIH 3T3 cells. Proc Natl

Acad Sci U S A. 1987 Oct;84(20):7159–63. doi:10.1073/pnas.84.20.7159 PubMed PMID: 2890160; PubMed Central PMCID: PMC299249.

80. Di Fiore PP, Pierce JH, Kraus MH, Segatto O, King CR, Aaronson SA. erbB-2 is a potent oncogene when overexpressed in NIH/3T3 cells. Science. 1987 Jul 10;237(4811):178–82. doi:10.1126/science.2885917 PubMed PMID: 2885917.

81. Segatto O, King CR, Pierce JH, Di Fiore PP, Aaronson SA. Different structural alterations upregulate in vitro tyrosine kinase activity and transforming potency of the erbB-2 gene. Mol Cell Biol. 1988 Dec;8(12):5570–4. doi:10.1128/mcb.8.12.5570-5574.1988 PubMed PMID: 2907606; PubMed Central PMCID: PMC365664.

82. Wang J, Xu B. Targeted therapeutic options and future perspectives for HER2-positive breast cancer. Signal Transduct Target Ther. 2019 Sep 13;4(1):34. doi:10.1038/s41392-019-0069-2

83. Pinto AC, Ades F, de Azambuja E, Piccart-Gebhart M. Trastuzumab for patients with HER2 positive breast cancer: delivery, duration and combination therapies. Breast Edinb Scotl. 2013 Aug;22 Suppl 2:S152-155. doi:10.1016/j.breast.2013.07.029 PubMed PMID: 24074778.

84. Molina MA, Codony-Servat J, Albanell J, Rojo F, Arribas J, Baselga J. Trastuzumab (herceptin), a humanized anti-Her2 receptor monoclonal antibody, inhibits basal and activated Her2 ectodomain cleavage in breast cancer cells. Cancer Res. 2001 Jun 15;61(12):4744–9. PubMed PMID: 11406546.

85. Shak S. Overview of the trastuzumab (Herceptin) anti-HER2 monoclonal antibody clinical program in HER2-overexpressing metastatic breast cancer. Herceptin Multinational Investigator Study Group. Semin Oncol. 1999 Aug;26(4 Suppl 12):71–7. PubMed PMID: 10482196.

86. Hurvitz SA, Martin M, Symmans WF, Jung KH, Huang CS, Thompson AM, et al. Neoadjuvant trastuzumab, pertuzumab, and chemotherapy versus trastuzumab emtansine plus pertuzumab in patients with HER2-positive breast cancer (KRISTINE): a randomised, open-label, multicentre, phase 3 trial. Lancet Oncol. 2018 Jan 1;19(1):115–26. doi:10.1016/S1470-2045(17)30716-7 PubMed PMID: 29175149.

87. Scheuer W, Friess T, Burtscher H, Bossenmaier B, Endl J, Hasmann M. Strongly Enhanced Antitumor Activity of Trastuzumab and Pertuzumab Combination Treatment on HER2-Positive Human Xenograft Tumor Models. Cancer Res. 2009 Dec 14;69(24):9330–6. doi:10.1158/0008-5472.CAN-08-4597

88. Patel A, Unni N, Peng Y. The Changing Paradigm for the Treatment of HER2-Positive Breast Cancer. Cancers. 2020 Aug;12(8):2081. doi:10.3390/cancers12082081

89. Gajria D, Chandarlapaty S. HER2-amplified breast cancer: mechanisms of trastuzumab resistance and novel targeted therapies. Expert Rev Anticancer Ther. 2011 Feb;11(2):263–

75. doi:10.1586/era.10.226 PubMed PMID: 21342044; PubMed Central PMCID: PMC3092522.

90. Mercogliano MF, De Martino M, Venturutti L, Rivas MA, Proietti CJ, Inurrigarro G, et al. TNFα-Induced Mucin 4 Expression Elicits Trastuzumab Resistance in HER2-Positive Breast Cancer. Clin Cancer Res. 2017 Jan 31;23(3):636–48. doi:10.1158/1078-0432.CCR-16-0970

91. Berns K, Horlings HM, Hennessy BT, Madiredjo M, Hijmans EM, Beelen K, et al. A functional genetic approach identifies the PI3K pathway as a major determinant of trastuzumab resistance in breast cancer. Cancer Cell. 2007 Oct;12(4):395–402. doi:10.1016/j.ccr.2007.08.030 PubMed PMID: 17936563.

92. Saal LH, Holm K, Maurer M, Memeo L, Su T, Wang X, et al. PIK3CA mutations correlate with hormone receptors, node metastasis, and ERBB2, and are mutually exclusive with PTEN loss in human breast carcinoma. Cancer Res. 2005 Apr 1;65(7):2554–9. doi:10.1158/0008-5472-CAN-04-3913 PubMed PMID: 15805248.

93. Sáez R, Molina MA, Ramsey EE, Rojo F, Keenan EJ, Albanell J, et al. p95HER-2 predicts worse outcome in patients with HER-2-positive breast cancer. Clin Cancer Res Off J Am Assoc Cancer Res. 2006 Jan 15;12(2):424–31. doi:10.1158/1078-0432.CCR-05-1807 PubMed PMID: 16428482.

94. Scaltriti M, Rojo F, Ocaña A, Anido J, Guzman M, Cortes J, et al. Expression of p95HER2, a truncated form of the HER2 receptor, and response to anti-HER2 therapies in breast cancer. J Natl Cancer Inst. 2007 Apr 18;99(8):628–38. doi:10.1093/jnci/djk134 PubMed PMID: 17440164.

95. Sergina NV, Rausch M, Wang D, Blair J, Hann B, Shokat KM, et al. Escape from HER-family tyrosine kinase inhibitor therapy by the kinase-inactive HER3. Nature. 2007 Jan 25;445(7126):437–41. doi:10.1038/nature05474 PubMed PMID: 17206155; PubMed Central PMCID: PMC3025857.

96. Nagy P, Friedländer E, Tanner M, Kapanen AI, Carraway KL, Isola J, et al. Decreased Accessibility and Lack of Activation of ErbB2 in JIMT-1, a Herceptin-Resistant, MUC4-Expressing Breast Cancer Cell Line. Cancer Res. 2005 Feb 3;65(2):473–82. doi:10.1158/0008-5472.473.65.2

97. Nagata Y, Lan KH, Zhou X, Tan M, Esteva FJ, Sahin AA, et al. PTEN activation contributes to tumor inhibition by trastuzumab, and loss of PTEN predicts trastuzumab resistance in patients. Cancer Cell. 2004 Aug;6(2):117–27. doi:10.1016/j.ccr.2004.06.022 PubMed PMID: 15324695.

98. Veeraraghavan J, De Angelis C, Gutierrez C, Liao FT, Sabotta C, Rimawi MF, et al. HER2-Positive Breast Cancer Treatment and Resistance. Adv Exp Med Biol. 2025;1464:495–525. doi:10.1007/978-3-031-70875-6_24 PubMed PMID: 39821040.

99. Czopek J, Pawlęga J, Fijorek K, Püsküllüoğlu M, Różanowski P, Okoń K. HER-3 expression in HER-2-amplified breast carcinoma. Contemp Oncol. 2013;17(5):446–9.

doi:10.5114/wo.2013.38564 PubMed PMID: 24596534; PubMed Central PMCID: PMC3934027.

100. Bittner JJ. SOME POSSIBLE EFFECTS OF NURSING ON THE MAMMARY GLAND TUMOR INCIDENCE IN MICE. Science. 1936 Aug 14;84(2172):162. doi:10.1126/science.84.2172.162 PubMed PMID: 17793252.

101. Callahan R, Smith GH. The Mouse as a Model for Mammary Tumorigenesis: History and Current Aspects. J Mammary Gland Biol Neoplasia. 2008. doi:10.1007/s10911-008-9094-4

102. Ross SR. Mouse Mammary Tumor Virus Molecular Biology and Oncogenesis. Viruses. 2010 Sep;2(9):2000–12. doi:10.3390/v2092000

103. Ross SR, Schofield JJ, Farr CJ, Bucan M. Mouse transferrin receptor 1 is the cell entry receptor for mouse mammary tumor virus. Proc Natl Acad Sci. 2002 Sep 17;99(19):12386–90. doi:10.1073/pnas.192360099

104. Ross SR. MMTV Infectious Cycle and the Contribution of Virus-encoded Proteins to Transformation of Mammary Tissue. J Mammary Gland Biol Neoplasia. 2008 Sep 1;13(3):299–307. doi:10.1007/s10911-008-9090-8

105. Beutner U, Kraus E, Kitamura D, Rajewsky K, Huber BT. B cells are essential for murine mammary tumor virus transmission, but not for presentation of endogenous superantigens. J Exp Med. 1994 May 1;179(5):1457–66. doi:10.1084/jem.179.5.1457

106. Held W, Shakhov AN, Izui S, Waanders GA, Scarpellino L, MacDonald HR, et al. Superantigen-reactive CD4+ T cells are required to stimulate B cells after infection with mouse mammary tumor virus. J Exp Med. 1993 Feb 1;177(2):359–66. doi:10.1084/jem.177.2.359

107. Mink S, Ponta H, Cato ACB. The long terminal repeat region of the mouse mammary tumour virus contains multiple regulatory elements. Nucleic Acids Res. 1990 Apr 25;18(8):2017–23. doi:10.1093/nar/18.8.2017

108. Lefebvre P, Berard DS, Cordingley MG, Hager GL. Two Regions of the Mouse Mammary Tumor Virus Long Terminal Repeat Regulate the Activity of Its Promoter in Mammary Cell Lines. Mol Cell Biol. 1991 May 1;11(5):2529–37. doi:10.1128/mcb.11.5.2529-2537.1991 PubMed PMID: 1708094.

109. Haraguchi S, Good RA, Engelman RW, Greene S, Day NK. Prolactin, epidermal growth factor or transforming growth factor-α activate a mammary cell-specific enhancer in mouse mammary tumor virus-long terminal repeat. Mol Cell Endocrinol. 1997 May 16;129(2):145–55. doi:10.1016/S0303-7207(97)04053-7

110. Otten AD, Sanders MM, McKnight GS. The MMTV LTR Promoter is Induced by Progesterone and Dihydrotestosterone but not by Estrogen. Mol Endocrinol. 1988. doi:10.1210/mend-2-2-143

111. Gouilleux F, Sola B, Couette B, Richard-Foy H. Cooperation between structural elements in hormonoregulated transcription from the mouse mammary tumor virus promoter. Nucleic Acids Res. 1991 Apr 11;19(7):1563–9. doi:10.1093/nar/19.7.1563

112. Henrard D, Ross SR. Endogenous mouse mammary tumor virus is expressed in several organs in addition to the lactating mammary gland. J Virol. 1988 Aug;62(8):3046–9. doi:10.1128/jvi.62.8.3046-3049.1988 PubMed PMID: 2839721; PubMed Central PMCID: PMC253747.

113. Stewart TA, Hollingshead PG, Pitts SL. Multiple regulatory domains in the mouse mammary tumor virus long terminal repeat revealed by analysis of fusion genes in transgenic mice. Mol Cell Biol. 1988. doi:10.1128/mcb.8.1.473

114. Zhang J, Zhao J, Jiang W jie, Shan X wei, Yang X mei, Gao J gang. Conditional gene manipulation: Cre-ating a new biological era. J Zhejiang Univ Sci B. 2012 Jul;13(7):511–24. doi:10.1631/jzus.B1200042 PubMed PMID: 22761243; PubMed Central PMCID: PMC3390709.

115. Wagner KU, Wall RJ, St-Onge L, Gruss P, Wynshaw-Boris A, Garrett L, et al. Cre-mediated gene deletion in the mammary gland. Nucleic Acids Res. 1997 Nov 1;25(21):4323–30. doi:10.1093/nar/25.21.4323

116. Wagner KU, Ward T, Davis B, Wiseman R, Hennighausen L. Spatial and temporal expression of the Cre gene under the control of the MMTV-LTR in different lines of transgenic mice. Transgenic Res. 2001 Dec 1;10(6):545–53. doi:10.1023/A:1013063514007

117. Robinson GW, Hennighausen L. MMTV-Cre transgenes can adversely affect lactation: Considerations for conditional gene deletion in mammary tissue. Anal Biochem. 2011. doi:10.1016/j.ab.2011.01.020

118. Buono KD, Robinson GW, Martin C, Shi S, Stanley P, Tanigaki K, et al. The canonical Notch/RBP-J signaling pathway controls the balance of cell lineages in mammary epithelium during pregnancy. Dev Biol. 2006 May 15;293(2):565–80. doi:10.1016/j.ydbio.2006.02.043 PubMed PMID: 16581056.

119. Yuan T, Wang Y, Pao L, Anderson SM, Gu H. Lactation Defect in a Widely Used MMTV-Cre Transgenic Line of Mice. PLOS ONE. 2011 Apr 29;6(4):e19233. doi:10.1371/journal.pone.0019233

120. Cui Y, Riedlinger G, Miyoshi K, Tang W, Li C, Deng CX, et al. Inactivation of Stat5 in Mouse Mammary Epithelium during Pregnancy Reveals Distinct Functions in Cell Proliferation, Survival, and Differentiation. Mol Cell Biol. 2004 Sep;24(18):8037–47. doi:10.1128/MCB.24.18.8037-8047.2004 PubMed PMID: 15340066; PubMed Central PMCID: PMC515028.

121. Ci B, Mc H, Ra W. Multiple independent activations of the neu oncogene by a point mutation altering the transmembrane domain of p185. Cell. 1986 Jun 6;45(5). doi:10.1016/0092-8674(86)90779-8 PubMed PMID: 2871941.

122. Muller WJ, Sinn E, Pattengale PK, Wallace R, Et. A. Single-step induction of mammary adenocarcinoma in transgenic mice bearing the activated c-neu oncogene. Cell. 1988. doi:10.1016/0092-8674(88)90184-5

123. Pm S, Wj M. Mutations affecting conserved cysteine residues within the extracellular domain of Neu promote receptor dimerization and activation. Proc Natl Acad Sci U S A. 1996 Aug 20;93(17). doi:10.1073/pnas.93.17.8878 PubMed PMID: 8799121.

124. Pm S, Dl D, Wr H, Wj M. Novel activating mutations in the neu proto-oncogene involved in induction of mammary tumors. Mol Cell Biol. 1994 Nov;14(11). doi:10.1128/mcb.14.11.7068-7077.1994 PubMed PMID: 7935422.

125. Siegel PM, Ryan ED, Cardiff RD, Muller WJ. Elevated expression of activated forms of Neu/ErbB-2 and ErbB-3 are involved in the induction of mammary tumors in transgenic mice: implications for human breast cancer. EMBO J. 1999 Apr 15;18(8):2149–64. doi:10.1093/emboj/18.8.2149 PubMed PMID: 10205169; PubMed Central PMCID: PMC1171299.

126. Ursini-Siegel J, Hardy WR, Zuo D, Lam SHL, Sanguin-Gendreau V, Cardiff RD, et al. ShcA signalling is essential for tumour progression in mouse models of human breast cancer. EMBO J. 2008 Mar 1;27(6):910–20. doi:10.1038/emboj.2008.22

127. Schade B, Rao T, Dourdin N, Lesurf R, Hallett M, Cardiff RD, et al. PTEN Deficiency in a Luminal ErbB-2 Mouse Model Results in Dramatic Acceleration of Mammary Tumorigenesis and Metastasis. J Biol Chem. 2009 Jul 10;284(28):19018–26. doi:10.1074/jbc.M109.018937 PubMed PMID: 19435886; PubMed Central PMCID: PMC2707232.

128. Creedon H, Balderstone LA, Muir M, Balla J, Gomez-Cuadrado L, Tracey N, et al. Use of a genetically engineered mouse model as a preclinical tool for HER2 breast cancer. Dis Model Mech. 2016 Feb 1;9(2):131–40. doi:10.1242/dmm.023143 PubMed PMID: 26721874; PubMed Central PMCID: PMC4770148.

129. Kuang X, Salinger A, Benavides F, Muller WJ, Dent SYR, Koutelou E. USP22 overexpression fails to augment tumor formation in MMTV-ERBB2 mice but loss of function impacts MMTV promoter activity. PLOS ONE. 2024 Jan 18;19(1):e0290837. doi:10.1371/journal.pone.0290837 PubMed PMID: 38236941; PubMed Central PMCID: PMC10796002.

130. Al-Zahrani KN, Abou-Hamad J, Cook DP, Pryce BR, Hodgins JJ, Labrèche C, et al. Loss of the Ste20-like kinase induces a basal/stem-like phenotype in HER2-positive breast cancers. Oncogene. 2020 Jun;39(23):4592–602. doi:10.1038/s41388-020-1315-3 PubMed PMID: 32393835.

131. Labrèche C, Cook DP, Abou-Hamad J, Pascoal J, Pryce BR, Al-Zahrani KN, et al. Periostin gene expression in neu-positive breast cancer cells is regulated by a FGFR signaling cross talk with TGFβ/PI3K/AKT pathways. Breast Cancer Res. 2021 Nov 22;23(1):107. doi:10.1186/s13058-021-01487-8

132. Gross L. A Filterable Agent, Recovered from Ak Leukemic Extracts, Causing Salivary Gland Carcinomas in C3H Mice. Exp Biol Med. 1953. doi:10.3181/00379727-83-20376

133. Treisman R, Novak U, Favaloro J, Kamen R. Transformation of rat cells by an altered polyoma virus genome expressing only the middle-T protein. Nature. 1981. doi:10.1038/292595a0

134. Regua AT, Arrigo A, Doheny D, Wong GL, Lo HW. Transgenic Mouse Models of Breast Cancer. Cancer Lett. 2021 Sep 28;516:73–83. doi:10.1016/j.canlet.2021.05.027 PubMed PMID: 34090924; PubMed Central PMCID: PMC8260455.

135. Fluck MM, Schaffhausen BS. Lessons in Signaling and Tumorigenesis from Polyomavirus Middle T Antigen. Microbiol Mol Biol Rev. 2009. doi:10.1128/mmbr.00009-09

136. Hunter T, Hutchinson MA, Eckhart W. Polyoma middle-sized T antigen can be phosphorylated on tyrosine at multiple sites in vitro. EMBO J. 1984 Jan;3(1):73–9. doi:10.1002/j.1460-2075.1984.tb01763.x PubMed PMID: 6200324; PubMed Central PMCID: PMC557299.

137. Campbell KS, Ogris E, Burke B, Su W, Auger KR, Druker BJ, et al. Polyoma middle tumor antigen interacts with SHC protein via the NPTY (Asn-Pro-Thr-Tyr) motif in middle tumor antigen. Proc Natl Acad Sci U S A. 1994 Jul 5;91(14):6344–8. doi:10.1073/pnas.91.14.6344 PubMed PMID: 8022784; PubMed Central PMCID: PMC44198.

138. Dunant NM, Senften M, Ballmer-Hofer K. Polyomavirus middle-T antigen associates with the kinase domain of Src-related tyrosine kinases. J Virol. 1996 Mar;70(3):1323–30. doi:10.1128/JVI.70.3.1323-1330.1996 PubMed PMID: 8627648; PubMed Central PMCID: PMC189951.

139. Su W, Liu W, Schaffhausen BS, Roberts TM. Association of Polyomavirus Middle Tumor Antigen with Phospholipase C-γ1 (∗). J Biol Chem. 1995 May 26;270(21):12331–4. doi:10.1074/jbc.270.21.12331 PubMed PMID: 7759472.

140. Whitman M, Kaplan DR, Schaffhausen B, Cantley L, Roberts TM. Association of phosphatidylinositol kinase activity with polyoma middle-T competent for transformation. Nature. 1985 May;315(6016):239–42. doi:10.1038/315239a0

141. Attalla S, Taifour T, Bui T, Muller W. Insights from transgenic mouse models of PyMT-induced breast cancer: recapitulating human breast cancer progression in vivo. Oncogene. 2021 Jan;40(3):475–91. doi:10.1038/s41388-020-01560-0

142. Webster MA, Hutchinson JN, Rauh MJ, Muthuswamy SK, Anton M, Tortorice CG, et al. Requirement for both Shc and phosphatidylinositol 3’ kinase signaling pathways in polyomavirus middle T-mediated mammary tumorigenesis. Mol Cell Biol. 1998 Apr;18(4):2344–59. doi:10.1128/MCB.18.4.2344 PubMed PMID: 9528804; PubMed Central PMCID: PMC121489.

143. Dilworth SM. Polyoma virus middle T antigen: meddler or mimic? Trends Microbiol. 1995. doi:10.1016/s0966-842x(00)88866-6

144. Guy CT, Cardiff RD, Muller WJ. Induction of mammary tumors by expression of polyomavirus middle T oncogene: a transgenic mouse model for metastatic disease. Mol Cell Biol. 1992 Mar;12(3):954–61. doi:10.1128/mcb.12.3.954-961.1992 PubMed PMID: 1312220; PubMed Central PMCID: PMC369527.

145. Gunther EJ, Belka GK, Wertheim GBW, Wang J, Et. A. A novel doxycycline-inducible system for the transgenic analysis of mammary gland biology. FASEB J. 2002. doi:10.1096/fj.01-0551com

146. Rao T, Ranger JJ, Smith HW, Lam SH, Chodosh L, Muller WJ. Inducible and coupled expression of the polyomavirus middle T antigen and Cre recombinase in transgenic mice: an in vivo model for synthetic viability in mammary tumour progression. Breast Cancer Res BCR. 2014 Jan 23;16(1):R11. doi:10.1186/bcr3603 PubMed PMID: 24457046; PubMed Central PMCID: PMC3978996.

147. Lin EY, Jones JG, Li P, Zhu L, Whitney KD, Muller WJ, et al. Progression to malignancy in the polyoma middle T oncoprotein mouse breast cancer model provides a reliable model for human diseases. Am J Pathol. 2003 Nov;163(5):2113–26. doi:10.1016/S0002-9440(10)63568-7 PubMed PMID: 14578209; PubMed Central PMCID: PMC1892434.

148. Hirukawa A, Smith HW, Zuo D, Dufour CR, Savage P, Bertos N, et al. Targeting EZH2 reactivates a breast cancer subtype-specific anti-metastatic transcriptional program. Nat Commun. 2018 Jun 29;9(1):2547. doi:10.1038/s41467-018-04864-8 PubMed PMID: 29959321; PubMed Central PMCID: PMC6026192.

149. Lifsted T, Le Voyer T, Williams M, Muller W, Klein-Szanto A, Buetow KH, et al. Identification of inbred mouse strains harboring genetic modifiers of mammary tumor age of onset and metastatic progression. Int J Cancer. 1998 Aug 12;77(4):640–4. doi:10.1002/(sici)1097-0215(19980812)77:4<640::aid-ijc26>3.0.co;2-8 PubMed PMID: 9679770.

150. Davie SA, Maglione JE, Manner CK, Young D, Cardiff RD, MacLeod CL, et al. Effects of FVB/NJ and C57Bl/6J strain backgrounds on mammary tumor phenotype in inducible nitric oxide synthase deficient mice. Transgenic Res. 2007 Apr;16(2):193–201. doi:10.1007/s11248-006-9056-9 PubMed PMID: 17206489; PubMed Central PMCID: PMC1829418.

151. Rennhack JP, To B, Swiatnicki M, Dulak C, Ogrodzinski MP, Zhang Y, et al. Integrated analyses of murine breast cancer models reveal critical parallels with human disease. Nat Commun. 2019 Jul 22;10:3261. doi:10.1038/s41467-019-11236-3 PubMed PMID: 31332182; PubMed Central PMCID: PMC6646342.

152. Ben-David U, Ha G, Khadka P, Jin X, Wong B, Franke L, et al. The landscape of chromosomal aberrations in breast cancer mouse models reveals driver-specific routes to

tumorigenesis. Nat Commun. 2016 Jul 4;7:12160. doi:10.1038/ncomms12160 PubMed PMID: 27374210; PubMed Central PMCID: PMC4932194.

153. Rennhack J, To B, Wermuth H, Andrechek ER. Mouse Models of Breast Cancer Share Amplification and Deletion Events with Human Breast Cancer. J Mammary Gland Biol Neoplasia. 2017 Mar;22(1):71–84. doi:10.1007/s10911-017-9374-y PubMed PMID: 28124185; PubMed Central PMCID: PMC5313323.

154. Montagna C, Lyu MS, Hunter K, Lukes L, Lowther W, Reppert T, et al. The Septin 9 (MSF) gene is amplified and overexpressed in mouse mammary gland adenocarcinomas and human breast cancer cell lines. Cancer Res. 2003 May 1;63(9):2179–87. PubMed PMID: 12727837.

155. McNally S, Stein T. Overview of Mammary Gland Development: A Comparison of Mouse and Human. Methods Mol Biol. 2017;1501:1–17. doi:10.1007/978-1-4939-6475-8_1 PubMed PMID: 27796946.

156. Parmar H, Cunha GR. Epithelial-stromal interactions in the mouse and human mammary gland in vivo. Endocr Relat Cancer. 2004 Sep;11(3):437–58. doi:10.1677/erc.1.00659 PubMed PMID: 15369447.

157. Sakakura T, Kusano I, Kusakabe M, Inaguma Y, Nishizuka Y. Biology of mammary fat pad in fetal mouse: capacity to support development of various fetal epithelia in vivo. Development. 1987 Jul;100(3):421–30. doi:10.1242/dev.100.3.421 PubMed PMID: 3308404.

158. Veltmaat JM, Mailleux AA, Thiery JP, Bellusci S. Mouse embryonic mammogenesis as a model for the molecular regulation of pattern formation. Differ Res Biol Divers. 2003 Jan;71(1):1–17. doi:10.1046/j.1432-0436.2003.700601.x PubMed PMID: 12558599.

159. Sinha YN, Tucker HA. Mammary gland growth of rats between 10 and 100 days of age. Am J Physiol. 1966 Mar;210(3):601–5. doi:10.1152/ajplegacy.1966.210.3.601 PubMed PMID: 5933214.

160. Neville MC, Daniel CW. The Mammary gland: development, regulation, and function. New York: Plenum Press; 1987. xxi+625.

161. Radice GL, Ferreira-Cornwell MC, Robinson SD, Rayburn H, Chodosh LA, Takeichi M, et al. Precocious Mammary Gland Development in P-Cadherin–deficient Mice. J Cell Biol. 1997 Nov 17;139(4):1025–32. doi:10.1083/jcb.139.4.1025 PubMed PMID: 9362520; PubMed Central PMCID: PMC2139972.

162. Asch HL, Asch BB. Expression of keratins and other cytoskeletal proteins in mouse mammary epithelium during the normal developmental cycle and primary culture. Dev Biol. 1985 Feb;107(2):470–82. doi:10.1016/0012-1606(85)90328-8 PubMed PMID: 2578999.

163. Sakakura T, Sakagami Y, Nishizuka Y. Persistence of responsiveness of adult mouse mammary gland to induction by embryonic mesenchyme. Dev Biol. 1979 Oct 1;72(2):201–10. doi:10.1016/0012-1606(79)90111-8

164. Sakakura T, Nishizuka Y, Dawe CJ. Mesenchyme-dependent morphogenesis and epithelium-specific cytodifferentiation in mouse mammary gland. Science. 1976 Dec 24;194(4272):1439–41. doi:10.1126/science.827022 PubMed PMID: 827022.

165. Ingthorsson S, Traustadottir GA, Gudjonsson T. Breast Morphogenesis: From Normal Development to Cancer. Adv Exp Med Biol. 2025;1464:29–44. doi:10.1007/978-3-031-70875-6_3 PubMed PMID: 39821019.

166. Williams JM, Daniel CW. Mammary ductal elongation: differentiation of myoepithelium and basal lamina during branching morphogenesis. Dev Biol. 1983 Jun;97(2):274–90. doi:10.1016/0012-1606(83)90086-6 PubMed PMID: 6852366.

167. Silberstein GB, Daniel CW. Elvax 40P implants: Sustained, local release of bioactive molecules influencing mammary ductal development. Dev Biol. 1982 Sep 1;93(1):272–8. doi:10.1016/0012-1606(82)90259-7

168. Ingman WV, Robertson SA. Mammary gland development in transforming growth factor beta1 null mutant mice: systemic and epithelial effects. Biol Reprod. 2008 Oct;79(4):711–7. doi:10.1095/biolreprod.107.067272 PubMed PMID: 18614704.

169. Topper YJ, Freeman CS. Multiple hormone interactions in the developmental biology of the mammary gland. Physiol Rev. 1980 Oct;60(4):1049–106. doi:10.1152/physrev.1980.60.4.1049 PubMed PMID: 7001510.

170. Daniel CW, DeOme KB. Growth of Mouse Mammary Glands in vivo after Monolayer Culture. Science. 1965 Aug 6;149(3684):634–6. doi:10.1126/science.149.3684.634

171. Richards J, Guzman R, Konrad M, Yang J, Nandi S. Growth of mouse mammary gland end buds cultured in a collagen gel matrix. Exp Cell Res. 1982 Oct 1;141(2):433–43. doi:10.1016/0014-4827(82)90231-2

172. Yang J, Richards J, Guzman R, Imagawa W, Nandi S. Sustained growth in primary culture of normal mammary epithelial cells embedded in collagen gels. Proc Natl Acad Sci U S A. 1980 Apr;77(4):2088–92. doi:10.1073/pnas.77.4.2088 PubMed PMID: 6929540; PubMed Central PMCID: PMC348657.

173. Yuan L, Xie S, Bai H, Liu X, Cai P, Lu J, et al. Reconstruction of dynamic mammary mini gland in vitro for normal physiology and oncogenesis. Nat Methods. 2023 Dec;20(12):2021–33. doi:10.1038/s41592-023-02039-y

174. Silberstein GB, Strickland P, Coleman S, Daniel CW. Epithelium-dependent extracellular matrix synthesis in transforming growth factor-beta 1-growth-inhibited mouse mammary gland. J Cell Biol. 1990 Jun;110(6):2209–19. doi:10.1083/jcb.110.6.2209 PubMed PMID: 2351697; PubMed Central PMCID: PMC2116118.

175. Sternlicht MD, Kouros-Mehr H, Lu P, Werb Z. Hormonal and local control of mammary branching morphogenesis. Differ Res Biol Divers. 2006 Sep;74(7):365–81. doi:10.1111/j.1432-0436.2006.00105.x PubMed PMID: 16916375; PubMed Central PMCID: PMC2580831.

176. Faulkin LJ, Deome KB. Regulation of growth and spacing of gland elements in the mammary fat pad of the C3H mouse. J Natl Cancer Inst. 1960 Apr;24:953–69. PubMed PMID: 13821714.

177. Biswas SK, Banerjee S, Baker GW, Kuo CY, Chowdhury I. The Mammary Gland: Basic Structure and Molecular Signaling during Development. Int J Mol Sci. 2022 Mar 31;23(7):3883. doi:10.3390/ijms23073883 PubMed PMID: 35409243; PubMed Central PMCID: PMC8998991.

178. Deome KB, Faulkin LJ, Bern HA, Blair PB. Development of mammary tumors from hyperplastic alveolar nodules transplanted into gland-free mammary fat pads of female C3H mice. Cancer Res. 1959 Jun;19(5):515–20. PubMed PMID: 13663040.

179. Shackleton M, Vaillant F, Simpson KJ, Stingl J, Smyth GK, Asselin-Labat ML, et al. Generation of a functional mammary gland from a single stem cell. Nature. 2006 Jan 5;439(7072):84–8. doi:10.1038/nature04372 PubMed PMID: 16397499.

180. Visvader JE. Keeping abreast of the mammary epithelial hierarchy and breast tumorigenesis. Genes Dev. 2009 Nov 15;23(22):2563–77. doi:10.1101/gad.1849509 PubMed PMID: 19933147; PubMed Central PMCID: PMC2779757.

181. Visvader JE, Stingl J. Mammary stem cells and the differentiation hierarchy: current status and perspectives. Genes Dev. 2014 Jun 1;28(11):1143–58. doi:10.1101/gad.242511.114 PubMed PMID: 24888586; PubMed Central PMCID: PMC4052761.

182. Fu NY, Nolan E, Lindeman GJ, Visvader JE. Stem Cells and the Differentiation Hierarchy in Mammary Gland Development. Physiol Rev. 2020 Apr 1;100(2):489–523. doi:10.1152/physrev.00040.2018 PubMed PMID: 31539305.

183. Smith GH. Label-retaining epithelial cells in mouse mammary gland divide asymmetrically and retain their template DNA strands. Development. 2005 Feb 15;132(4):681–7. doi:10.1242/dev.01609

184. Iggo R, MacGrogan G. Classification of Breast Cancer Through the Perspective of Cell Identity Models. Adv Exp Med Biol. 2025;1464:185–207. doi:10.1007/978-3-031-70875-6_11 PubMed PMID: 39821027.

185. Lim E, Vaillant F, Wu D, Forrest NC, Pal B, Hart AH, et al. Aberrant luminal progenitors as the candidate target population for basal tumor development in BRCA1 mutation carriers. Nat Med. 2009 Aug;15(8):907–13. doi:10.1038/nm.2000 PubMed PMID: 19648928.

186. Shehata M, Teschendorff A, Sharp G, Novcic N, Russell IA, Avril S, et al. Phenotypic and functional characterisation of the luminal cell hierarchy of the mammary gland. Breast Cancer Res BCR. 2012 Oct 22;14(5):R134. doi:10.1186/bcr3334 PubMed PMID: 23088371; PubMed Central PMCID: PMC4053112.

187. Stingl J, Eirew P, Ricketson I, Shackleton M, Vaillant F, Choi D, et al. Purification and unique properties of mammary epithelial stem cells. Nature. 2006 Feb;439(7079):993–7. doi:10.1038/nature04496

188. Bai L, Rohrschneider LR. s-SHIP promoter expression marks activated stem cells in developing mouse mammary tissue. Genes Dev. 2010 Sep 1;24(17):1882–92. doi:10.1101/gad.1932810 PubMed PMID: 20810647; PubMed Central PMCID: PMC2932970.

189. Asselin-Labat ML, Sutherland KD, Vaillant F, Gyorki DE, Wu D, Holroyd S, et al. Gata-3 negatively regulates the tumor-initiating capacity of mammary luminal progenitor cells and targets the putative tumor suppressor caspase-14. Mol Cell Biol. 2011 Nov;31(22):4609–22. doi:10.1128/MCB.05766-11 PubMed PMID: 21930782; PubMed Central PMCID: PMC3209243.

190. Vaillant F, Asselin-Labat ML, Shackleton M, Forrest NC, Lindeman GJ, Visvader JE. The mammary progenitor marker CD61/beta3 integrin identifies cancer stem cells in mouse models of mammary tumorigenesis. Cancer Res. 2008 Oct 1;68(19):7711–7. doi:10.1158/0008-5472.CAN-08-1949 PubMed PMID: 18829523.

191. Van Keymeulen A, Rocha AS, Ousset M, Beck B, Bouvencourt G, Rock J, et al. Distinct stem cells contribute to mammary gland development and maintenance. Nature. 2011 Oct 1;479(7372):189–93. doi:10.1038/nature10573 PubMed PMID: 21983963.

192. Davis FM, Lloyd-Lewis B, Harris OB, Kozar S, Winton DJ, Muresan L, et al. Single-cell lineage tracing in the mammary gland reveals stochastic clonal dispersion of stem/progenitor cell progeny. Nat Commun. 2016 Oct 25;7(1):13053. doi:10.1038/ncomms13053

193. Joyce R, Visvader JE. Cells-of-Origin of Breast Cancer and Intertumoral Heterogeneity. Adv Exp Med Biol. 2025;1464:151–65. doi:10.1007/978-3-031-70875-6_9 PubMed PMID: 39821025.

194. Centonze A, Lin S, Tika E, Sifrim A, Fioramonti M, Malfait M, et al. Heterotypic cell–cell communication regulates glandular stem cell multipotency. Nature. 2020 Aug;584(7822):608–13. doi:10.1038/s41586-020-2632-y

195. Van Keymeulen A. Mechanisms of Regulation of Cell Fate in Breast Development and Cancer. Adv Exp Med Biol. 2025;1464:167–84. doi:10.1007/978-3-031-70875-6_10 PubMed PMID: 39821026.

196. Koren S, Reavie L, Couto JP, De Silva D, Stadler MB, Roloff T, et al. PIK3CA(H1047R) induces multipotency and multi-lineage mammary tumours. Nature. 2015 Sep 3;525(7567):114–8. doi:10.1038/nature14669 PubMed PMID: 26266975.

197. Van Keymeulen A, Lee MY, Ousset M, Brohée S, Rorive S, Giraddi RR, et al. Reactivation of multipotency by oncogenic PIK3CA induces breast tumour heterogeneity. Nature. 2015 Sep;525(7567):119–23. doi:10.1038/nature14665

198. Hein SM, Haricharan S, Johnston AN, Toneff MJ, Reddy JP, Dong J, et al. Luminal epithelial cells within the mammary gland can produce basal cells upon oncogenic stress. Oncogene. 2016 Mar 17;35(11):1461–7. doi:10.1038/onc.2015.206 PubMed PMID: 26096929; PubMed Central PMCID: PMC4688047.

199. Rios AC, Capaldo BD, Vaillant F, Pal B, van Ineveld R, Dawson CA, et al. Intraclonal Plasticity in Mammary Tumors Revealed through Large-Scale Single-Cell Resolution 3D Imaging. Cancer Cell. 2019 Apr 15;35(4):618-632.e6. doi:10.1016/j.ccell.2019.02.010 PubMed PMID: 30930118.

200. Christin JR, Wang C, Chung CY, Liu Y, Dravis C, Tang W, et al. Stem Cell Determinant SOX9 Promotes Lineage Plasticity and Progression in Basal-like Breast Cancer. Cell Rep. 2020 Jun 9;31(10):107742. doi:10.1016/j.celrep.2020.107742 PubMed PMID: 32521267; PubMed Central PMCID: PMC7658810.

201. Lupien M, Eeckhoute J, Meyer CA, Wang Q, Zhang Y, Li W, et al. FoxA1 translates epigenetic signatures into enhancer-driven lineage-specific transcription. Cell. 2008 Mar 21;132(6):958–70. doi:10.1016/j.cell.2008.01.018 PubMed PMID: 18358809; PubMed Central PMCID: PMC2323438.

202. Oakes SR, Naylor MJ, Asselin-Labat ML, Blazek KD, Gardiner-Garden M, Hilton HN, et al. The Ets transcription factor Elf5 specifies mammary alveolar cell fate. Genes Dev. 2008 Jan 3;22(5):581–6. doi:10.1101/gad.1614608 PubMed PMID: 18316476.

203. Prat A, Parker JS, Karginova O, Fan C, Livasy C, Herschkowitz JI, et al. Phenotypic and molecular characterization of the claudin-low intrinsic subtype of breast cancer. Breast Cancer Res BCR. 2010;12(5):R68. doi:10.1186/bcr2635 PubMed PMID: 20813035; PubMed Central PMCID: PMC3096954.

204. Fu NY, Rios AC, Pal B, Law CW, Jamieson P, Liu R, et al. Identification of quiescent and spatially restricted mammary stem cells that are hormone responsive. Nat Cell Biol. 2017 Mar;19(3):164–76. doi:10.1038/ncb3471 PubMed PMID: 28192422.

205. Wellings SR. A hypothesis of the origin of human breast cancer from the terminal ductal lobular unit. Pathol Res Pract. 1980;166(4):515–35. doi:10.1016/S0344-0338(80)80248-2 PubMed PMID: 6253967.

206. Russo J, Tay LK, Russo IH. Differentiation of the mammary gland and susceptibility to carcinogenesis. Breast Cancer Res Treat. 1982;2(1):5–73. doi:10.1007/BF01805718 PubMed PMID: 6216933.

207. Visvader JE. Cells of origin in cancer. Nature. 2011 Jan;469(7330):314–22. doi:10.1038/nature09781

208. Armitage P, Doll R. The age distribution of cancer and a multi-stage theory of carcinogenesis. Br J Cancer. 1954 Mar;8(1):1–12. doi:10.1038/bjc.1954.1 PubMed PMID: 13172380; PubMed Central PMCID: PMC2007940.

209. Tomasetti C, Li L, Vogelstein B. Stem cell divisions, somatic mutations, cancer etiology, and cancer prevention. Science. 2017 Mar 24;355(6331):1330–4. doi:10.1126/science.aaf9011 PubMed PMID: 28336671; PubMed Central PMCID: PMC5852673.

210. Van Keymeulen A, Fioramonti M, Centonze A, Bouvencourt G, Achouri Y, Blanpain C. Lineage-Restricted Mammary Stem Cells Sustain the Development, Homeostasis, and Regeneration of the Estrogen Receptor Positive Lineage. Cell Rep. 2017 Aug 15;20(7):1525–32. doi:10.1016/j.celrep.2017.07.066 PubMed PMID: 28813665; PubMed Central PMCID: PMC5575359.

211. Wang C, Christin JR, Oktay MH, Guo W. Lineage-Biased Stem Cells Maintain Estrogen-Receptor-Positive and -Negative Mouse Mammary Luminal Lineages. Cell Rep. 2017 Mar 21;18(12):2825–35. doi:10.1016/j.celrep.2017.02.071 PubMed PMID: 28329676; PubMed Central PMCID: PMC5408864.

212. Tao L, van Bragt MPA, Li Z. A Long-Lived Luminal Subpopulation Enriched with Alveolar Progenitors Serves as Cellular Origin of Heterogeneous Mammary Tumors. Stem Cell Rep. 2015 Jul 14;5(1):60–74. doi:10.1016/j.stemcr.2015.05.014

213. Miyano M, LaBarge MA. ELF5: A Molecular Clock for Breast Aging and Cancer Susceptibility. Cancers. 2024 Jan 19;16(2):431. doi:10.3390/cancers16020431 PubMed PMID: 38275872.

214. Rios AC, Fu NY, Lindeman GJ, Visvader JE. In situ identification of bipotent stem cells in the mammary gland. Nature. 2014 Feb;506(7488):322–7. doi:10.1038/nature12948

215. Lo PK, Kanojia D, Liu X, Singh UP, Berger FG, Wang Q, et al. CD49f and CD61 identify Her2/neu-induced mammary tumor-initiating cells that are potentially derived from luminal progenitors and maintained by the integrin–TGFβ signaling. Oncogene. 2012 May;31(21):2614–26. doi:10.1038/onc.2011.439

216. Mohamed GA, Mahmood S, Ognjenovic NB, Lee MK, Wilkins OM, Christensen BC, et al. Lineage plasticity enables low-ER luminal tumors to evolve and gain basal-like traits. Breast Cancer Res. 2023 Mar 1;25(1):23. doi:10.1186/s13058-023-01621-8

217. Lo PK, Chen H. Cancer stem cells and cells of origin in MMTV-Her2/neu-induced mammary tumorigenesis. Oncogene. 2013 Mar;32(10):1339–40. doi:10.1038/onc.2012.456

218. Valdés-Mora F, Salomon R, Gloss BS, Law AMK, Venhuizen J, Castillo L, et al. Single-cell transcriptomics reveals involution mimicry during the specification of the basal breast cancer subtype. Cell Rep. 2021 Apr 13;35(2). doi:10.1016/j.celrep.2021.108945 PubMed PMID: 33852842.

219. Rädler PD, Wehde BL, Triplett AA, Shrestha H, Shepherd JH, Pfefferle AD, et al. Highly metastatic claudin-low mammary cancers can originate from luminal epithelial cells. Nat Commun. 2021 Jun 18;12(1):3742. doi:10.1038/s41467-021-23957-5 PubMed PMID: 34145248; PubMed Central PMCID: PMC8213728.

220. Molyneux G, Geyer FC, Magnay FA, McCarthy A, Kendrick H, Natrajan R, et al. BRCA1 basal-like breast cancers originate from luminal epithelial progenitors and not from basal stem cells. Cell Stem Cell. 2010 Sep 3;7(3):403–17. doi:10.1016/j.stem.2010.07.010 PubMed PMID: 20804975.

221. Santagata S, Thakkar A, Ergonul A, Wang B, Woo T, Hu R, et al. Taxonomy of breast cancer based on normal cell phenotype predicts outcome. J Clin Invest. 2014 Feb;124(2):859–70. doi:10.1172/JCI70941 PubMed PMID: 24463450; PubMed Central PMCID: PMC3904619.

222. Gusterson B. Do "basal-like" breast cancers really exist? Nat Rev Cancer. 2009 Feb;9(2):128–34. doi:10.1038/nrc2571

223. del Barco Barrantes I, Stephan-Otto Attolini C, Slobodnyuk K, Igea A, Gregorio S, Gawrzak S, et al. Regulation of Mammary Luminal Cell Fate and Tumorigenesis by p38α. Stem Cell Rep. 2017 Dec 28;10(1):257–71. doi:10.1016/j.stemcr.2017.11.021 PubMed PMID: 29290625; PubMed Central PMCID: PMC5768988.

224. Sinclair AH, Berta P, Palmer MS, Hawkins JR, Griffiths BL, Smith MJ, et al. A gene from the human sex-determining region encodes a protein with homology to a conserved DNA-binding motif. Nature. 1990 Jul 19;346(6281):240–4. doi:10.1038/346240a0 PubMed PMID: 1695712.

225. Gubbay J, Collignon J, Koopman P, Capel B, Economou A, Münsterberg A, et al. A gene mapping to the sex-determining region of the mouse Y chromosome is a member of a novel family of embryonically expressed genes. Nature. 1990 Jul 19;346(6281):245–50. doi:10.1038/346245a0 PubMed PMID: 2374589.

226. Guth SIE, Wegner M. Having it both ways: Sox protein function between conservation and innovation. Cell Mol Life Sci CMLS. 2008 Oct;65(19):3000–18. doi:10.1007/s00018-008-8138-7 PubMed PMID: 18516494; PubMed Central PMCID: PMC11131603.

227. Sarkar A, Hochedlinger K. The Sox Family of Transcription Factors: Versatile Regulators of Stem and Progenitor Cell Fate. Cell Stem Cell. 2013 Jan 3;12(1):15–30. doi:10.1016/j.stem.2012.12.007 PubMed PMID: 23290134; PubMed Central PMCID: PMC3608206.

228. Schepers GE, Teasdale RD, Koopman P. Twenty pairs of sox: extent, homology, and nomenclature of the mouse and human sox transcription factor gene families. Dev Cell. 2002 Aug;3(2):167–70. doi:10.1016/s1534-5807(02)00223-x PubMed PMID: 12194848.

229. Wegner M. From head to toes: the multiple facets of Sox proteins. Nucleic Acids Res. 1999 Mar 15;27(6):1409–20. doi:10.1093/nar/27.6.1409 PubMed PMID: 10037800; PubMed Central PMCID: PMC148332.

230. Werner MH, Burley SK. Architectural Transcription Factors: Proteins That-Remodel DNA. Cell. 1997 Mar 21;88(6):733–6. doi:10.1016/S0092-8674(00)81917-0 PubMed PMID: 9118214.

231. Südbeck P, Scherer G. Two independent nuclear localization signals are present in the DNA-binding high-mobility group domains of SRY and SOX9. J Biol Chem. 1997 Oct 31;272(44):27848–52. doi:10.1074/jbc.272.44.27848 PubMed PMID: 9346931.

232. Pingault V, Zerad L, Bertani-Torres W, Bondurand N. SOX10: 20 years of phenotypic plurality and current understanding of its developmental function. J Med Genet. 2022 Feb 1;59(2):105–14. doi:10.1136/jmedgenet-2021-108105 PubMed PMID: 34667088.

233. King N, Westbrook MJ, Young SL, Kuo A, Abedin M, Chapman J, et al. The genome of the choanoflagellate Monosiga brevicollis and the origin of metazoans. Nature. 2008 Feb 14;451(7180):783–8. doi:10.1038/nature06617 PubMed PMID: 18273011; PubMed Central PMCID: PMC2562698.

234. Weider M, Wegner M. SoxE factors: Transcriptional regulators of neural differentiation and nervous system development. Semin Cell Dev Biol. 2017 Mar;63:35–42. doi:10.1016/j.semcdb.2016.08.013 PubMed PMID: 27552919.

235. She ZY, Yang WX. Sry and SoxE genes: How they participate in mammalian sex determination and gonadal development? Semin Cell Dev Biol. 2017 Mar;63:13–22. doi:10.1016/j.semcdb.2016.07.032 PubMed PMID: 27481580.

236. Huang YH, Jankowski A, Cheah KSE, Prabhakar S, Jauch R. SOXE transcription factors form selective dimers on non-compact DNA motifs through multifaceted interactions between dimerization and high-mobility group domains. Sci Rep. 2015 May 27;5(1):10398. doi:10.1038/srep10398

237. Harris ML, Baxter LL, Loftus SK, Pavan WJ. Sox proteins in melanocyte development and melanoma. Pigment Cell Melanoma Res. 2010 Aug;23(4):496–513. doi:10.1111/j.1755-148X.2010.00711.x PubMed PMID: 20444197; PubMed Central PMCID: PMC2906668.

238. Haseeb A, Lefebvre V. The SOXE transcription factors—SOX8, SOX9 and SOX10—share a bi-partite transactivation mechanism. Nucleic Acids Res. 2019 Jul 26;47(13):6917–31. doi:10.1093/nar/gkz523 PubMed PMID: 31194875; PubMed Central PMCID: PMC6649842.

239. Peirano RI, Wegner M. The glial transcription factor Sox10 binds to DNA both as monomer and dimer with different functional consequences. Nucleic Acids Res. 2000 Aug 15;28(16):3047–55. doi:10.1093/nar/28.16.3047 PubMed PMID: 10931919; PubMed Central PMCID: PMC108444.

240. González Alvarado MN, Aprato J. Sox8: a multifaceted transcription factor in development and disease. Biol Open. 2025 Feb 12;14(2):bio061840. doi:10.1242/bio.061840

241. Molin AN, Contentin R, Angelozzi M, Karvande A, Kc R, Haseeb A, et al. Skeletal growth is enhanced by a shared role for SOX8 and SOX9 in promoting reserve chondrocyte commitment to columnar proliferation. Proc Natl Acad Sci. 2024 Feb 20;121(8):e2316969121. doi:10.1073/pnas.2316969121

242. Sock E, Schmidt K, Hermanns-Borgmeyer I, Bösl MR, Wegner M. Idiopathic Weight Reduction in Mice Deficient in the High-Mobility-Group Transcription Factor Sox8. Mol Cell Biol. 2001 Oct;21(20):6951–9. doi:10.1128/MCB.21.20.6951-6959.2001 PubMed PMID: 11564878; PubMed Central PMCID: PMC99871.

243. O'Bryan MK, Takada S, Kennedy CL, Scott G, Harada S ichi, Ray MK, et al. Sox8 is a critical regulator of adult Sertoli cell function and male fertility. Dev Biol. 2008 Apr 15;316(2):359–70. doi:10.1016/j.ydbio.2008.01.042 PubMed PMID: 18342849; PubMed Central PMCID: PMC2375044.

244. Gonen N, Futtner CR, Wood S, Garcia-Moreno SA, Salamone IM, Samson SC, et al. Sex reversal following deletion of a single distal enhancer of Sox9. Science. 2018 Jun 29;360(6396):1469–73. doi:10.1126/science.aas9408 PubMed PMID: 29903884; PubMed Central PMCID: PMC6034650.

245. Barrionuevo F, Scherer G. *SOX E* genes: *SOX9* and *SOX8* in mammalian testis development. Int J Biochem Cell Biol. 2010 Mar 1;SOX Transcription Factors42(3):433–6. doi:10.1016/j.biocel.2009.07.015

246. Vidal VP, Chaboissier MC, de Rooij DG, Schedl A. Sox9 induces testis development in XX transgenic mice. Nat Genet. 2001 Jul;28(3):216–7. doi:10.1038/90046 PubMed PMID: 11431689.

247. Akiyama H, Chaboissier MC, Martin JF, Schedl A, de Crombrugghe B. The transcription factor Sox9 has essential roles in successive steps of the chondrocyte differentiation pathway and is required for expression of Sox5 and Sox6. Genes Dev. 2002 Nov 1;16(21):2813–28. doi:10.1101/gad.1017802 PubMed PMID: 12414734; PubMed Central PMCID: PMC187468.

248. Jo A, Denduluri S, Zhang B, Wang Z, Yin L, Yan Z, et al. The versatile functions of Sox9 in development, stem cells, and human diseases. Genes Dis. 2014 Dec 1;1(2):149–61. doi:10.1016/j.gendis.2014.09.004

249. Martini S, Bernoth K, Main H, Ortega GDC, Lendahl U, Just U, et al. A Critical Role for Sox9 in Notch-Induced Astrogliogenesis and Stem Cell Maintenance. Stem Cells. 2013 Apr 1;31(4):741–51. doi:10.1002/stem.1320

250. Scott CE, Wynn SL, Sesay A, Cruz C, Cheung M, Gaviro MVG, et al. SOX9 induces and maintains neural stem cells. Nat Neurosci. 2010 Oct;13(10):1181–9. doi:10.1038/nn.2646

251. Guo W, Keckesova Z, Donaher JL, Shibue T, Tischler V, Reinhardt F, et al. Slug and Sox9 cooperatively determine the mammary stem cell state. Cell. 2012 Mar 2;148(5):1015–28. doi:10.1016/j.cell.2012.02.008 PubMed PMID: 22385965; PubMed Central PMCID: PMC3305806.

252. Jeselsohn R, Cornwell M, Pun M, Buchwalter G, Nguyen M, Bango C, et al. Embryonic transcription factor SOX9 drives breast cancer endocrine resistance. Proc Natl Acad Sci. 2017 May 30;114(22):E4482–91. doi:10.1073/pnas.1620993114

253. Wright EM, Snopek B, Koopman P. Seven new members of the Sox gene family expressed during mouse development. Nucleic Acids Res. 1993 Feb 11;21(3):744. doi:10.1093/nar/21.3.744 PubMed PMID: 8441686; PubMed Central PMCID: PMC309180.

254. Weider M, Wegner M. SoxE factors: Transcriptional regulators of neural differentiation and nervous system development. Semin Cell Dev Biol. 2017. doi:10.1016/j.semcdb.2016.08.013

255. Qi J, Ma L, Guo W. Recent advances in the regulation mechanism of SOX10. J Otol. 2022 Oct;17(4):247–52. doi:10.1016/j.joto.2022.08.003 PubMed PMID: 36249926; PubMed Central PMCID: PMC9547104.

256. Aoki Y, Saint-Germain N, Gyda M, Magner-Fink E, Lee YH, Credidio C, et al. Sox10 regulates the development of neural crest-derived melanocytes in Xenopus. Dev Biol. 2003 Jul 1;259(1):19–33. doi:10.1016/s0012-1606(03)00161-1 PubMed PMID: 12812785.

257. Herbarth B, Pingault V, Bondurand N, Kuhlbrodt K, Hermans-Borgmeyer I, Puliti A, et al. Mutation of the Sry-related Sox10 gene in Dominant megacolon, a mouse model for human Hirschsprung disease. Proc Natl Acad Sci U S A. 1998 Apr 28;95(9):5161–5. doi:10.1073/pnas.95.9.5161 PubMed PMID: 9560246; PubMed Central PMCID: PMC20231.

258. Britsch S, Goerich DE, Riethmacher D, Peirano RI, Rossner M, Nave KA, et al. The transcription factor Sox10 is a key regulator of peripheral glial development. Genes Dev. 2001 Jan 1;15(1):66–78. doi:10.1101/gad.186601 PubMed PMID: 11156606.

259. Herbarth B, Pingault V, Bondurand N, Kuhlbrodt K, Hermans-Borgmeyer I, Puliti A, et al. Mutation of the Sry-related Sox10 gene in Dominant megacolon, a mouse model for human Hirschsprung disease. Proc Natl Acad Sci U S A. 1998 Apr 28;95(9):5161–5. doi:10.1073/pnas.95.9.5161 PubMed PMID: 9560246; PubMed Central PMCID: PMC20231.

260. Pingault V, Bondurand N, Kuhlbrodt K, Goerich DE, Préhu MO, Puliti A, et al. SOX10 mutations in patients with Waardenburg-Hirschsprung disease. Nat Genet. 1998 Feb;18(2):171–3. doi:10.1038/ng0298-171 PubMed PMID: 9462749.

261. Southard-Smith EM, Kos L, Pavan WJ. Sox10 mutation disrupts neural crest development in Dom Hirschsprung mouse model. Nat Genet. 1998 Jan;18(1):60–4. doi:10.1038/ng0198-60 PubMed PMID: 9425902.

262. Antonellis A, Huynh JL, Lee-Lin SQ, Vinton RM, Renaud G, Loftus SK, et al. Identification of neural crest and glial enhancers at the mouse Sox10 locus through transgenesis in zebrafish. PLoS Genet. 2008 Sep 5;4(9):e1000174. doi:10.1371/journal.pgen.1000174 PubMed PMID: 18773071; PubMed Central PMCID: PMC2518861.

263. Chen Z, Huang J, Liu Y, Dattilo LK, Huh SH, Ornitz D, et al. FGF signaling activates a Sox9-Sox10 pathway for the formation and branching morphogenesis of mouse ocular glands. Development. 2014 Jul;141(13):2691–701. doi:10.1242/dev.108944 PubMed PMID: 24924191; PubMed Central PMCID: PMC4067963.

264. Cheung M, Briscoe J. Neural crest development is regulated by the transcription factor Sox9. Development. 2003 Dec;130(23):5681–93. doi:10.1242/dev.00808 PubMed PMID: 14522876.

265. Shakhova O, Cheng P, Mishra PJ, Zingg D, Schaefer SM, Debbache J, et al. Antagonistic cross-regulation between Sox9 and Sox10 controls an anti-tumorigenic program in melanoma. PLoS Genet. 2015 Jan;11(1):e1004877. doi:10.1371/journal.pgen.1004877 PubMed PMID: 25629959; PubMed Central PMCID: PMC4309598.

266. Al-Zahrani KN, Abou-Hamad J, Pascoal J, Labrèche C, Garland B, Sabourin LA. AKT-mediated phosphorylation of Sox9 induces Sox10 transcription in a murine model of HER2-positive breast cancer. Breast Cancer Res BCR. 2021 May 13;23(1):55. doi:10.1186/s13058-021-01435-6 PubMed PMID: 33985544; PubMed Central PMCID: PMC8120776.

267. Dravis C, Spike BT, Harrell JC, Johns C, Trejo CL, Southard-Smith EM, et al. Sox10 Regulates Stem/Progenitor and Mesenchymal Cell States in Mammary Epithelial Cells. Cell Rep. 2015 Sep 29;12(12):2035–48. doi:10.1016/j.celrep.2015.08.040 PubMed PMID: 26365194; PubMed Central PMCID: PMC4591253.

268. Yu L, Peng F, Dong X, Chen Y, Sun D, Jiang S, et al. Sex-Determining Region Y Chromosome-Related High-Mobility-Group Box 10 in Cancer: A Potential Therapeutic Target. Front Cell Dev Biol. 2020 Dec 3;8:564740. doi:10.3389/fcell.2020.564740 PubMed PMID: 33344444; PubMed Central PMCID: PMC7744619.

269. Saldana-Caboverde A, Perera EM, Watkins-Chow DE, Hansen NF, Vemulapalli M, Mullikin JC, et al. The transcription factors Ets1 and Sox10 interact during murine melanocyte development. Dev Biol. 2015 Nov 15;407(2):300–12. doi:10.1016/j.ydbio.2015.04.012 PubMed PMID: 25912689; PubMed Central PMCID: PMC4618791.

270. Kim GC, Kwon HK, Lee CG, Verma R, Rudra D, Kim T, et al. Upregulation of Ets1 expression by NFATc2 and NFKB1/RELA promotes breast cancer cell invasiveness. Oncogenesis. 2018 Nov 23;7(11):91. doi:10.1038/s41389-018-0101-3 PubMed PMID: 30467308; PubMed Central PMCID: PMC6250664.

271. Tudrej KB, Czepielewska E, Kozłowska-Wojciechowska M. SOX10-MITF pathway activity in melanoma cells. Arch Med Sci AMS. 2017 Oct;13(6):1493–503.

doi:10.5114/aoms.2016.60655 PubMed PMID: 29181082; PubMed Central PMCID: PMC5701683.

272. Küspert M, Weider M, Müller J, Hermans-Borgmeyer I, Meijer D, Wegner M. Desert hedgehog links transcription factor Sox10 to perineurial development. J Neurosci Off J Soc Neurosci. 2012 Apr 18;32(16):5472–80. doi:10.1523/JNEUROSCI.5759-11.2012 PubMed PMID: 22514309; PubMed Central PMCID: PMC6703490.

273. Fujiwara S, Hoshikawa S, Ueno T, Hirata M, Saito T, Ikeda T, et al. SOX10 Transactivates S100B to Suppress Schwann Cell Proliferation and to Promote Myelination. PLoS ONE. 2014 Dec 23;9(12):e115400. doi:10.1371/journal.pone.0115400 PubMed PMID: 25536222; PubMed Central PMCID: PMC4275212.

274. Britsch S, Goerich DE, Riethmacher D, Peirano RI, Rossner M, Nave KA, et al. The transcription factor Sox10 is a key regulator of peripheral glial development. Genes Dev. 2001 Jan 1;15(1):66–78. doi:10.1101/gad.186601 PubMed PMID: 11156606; PubMed Central PMCID: PMC312607.

275. Kim J, Lo L, Dormand E, Anderson DJ. SOX10 Maintains Multipotency and Inhibits Neuronal Differentiation of Neural Crest Stem Cells. Neuron. 2003 Apr 10;38(1):17–31. doi:10.1016/S0896-6273(03)00163-6 PubMed PMID: 12691661.

276. Satta JP, Lan Q, Taketo MM, Mikkola ML. Stabilization of Epithelial β-Catenin Compromises Mammary Cell Fate Acquisition and Branching Morphogenesis. J Invest Dermatol. 2024 Jun 1;144(6):1223-1237.e10. doi:10.1016/j.jid.2023.11.018

277. Myllymäki SM, Lan Q, Mikkola ML. Embryonic Mammary Gland Morphogenesis. Adv Exp Med Biol. 2025;1464:9–27. doi:10.1007/978-3-031-70875-6_2 PubMed PMID: 39821018.

278. Mertelmeyer S, Weider M, Baroti T, Reiprich S, Fröb F, Stolt CC, et al. The transcription factor Sox10 is an essential determinant of branching morphogenesis and involution in the mouse mammary gland. Sci Rep. 2020 Oct 20;10(1):17807. doi:10.1038/s41598-020-74664-y

279. Dravis C, Chung CY, Lytle NK, Herrera-Valdez J, Luna G, Trejo CL, et al. Epigenetic and Transcriptomic Profiling of Mammary Gland Development and Tumor Models Disclose Regulators of Cell State Plasticity. Cancer Cell. 2018 Sep 10;34(3):466-482.e6. doi:10.1016/j.ccell.2018.08.001 PubMed PMID: 30174241; PubMed Central PMCID: PMC6152943.

280. Xu YR, Yang WX. SOX-mediated molecular crosstalk during the progression of tumorigenesis. Semin Cell Dev Biol. 2017 Mar 1;Regulation of development by SOX proteins63:23–34. doi:10.1016/j.semcdb.2016.07.028

281. Nonaka D, Chiriboga L, Rubin BP. Sox10: a pan-schwannian and melanocytic marker. Am J Surg Pathol. 2008 Sep;32(9):1291–8. doi:10.1097/PAS.0b013e3181658c14 PubMed PMID: 18636017.

282. Cimino-Mathews A, Subhawong AP, Elwood H, Warzecha HN, Sharma R, Park BH, et al. Neural crest transcription factor Sox10 is preferentially expressed in triple-negative and metaplastic breast carcinomas. Hum Pathol. 2013 Jun;44(6):959–65. doi:10.1016/j.humpath.2012.09.005 PubMed PMID: 23260325; PubMed Central PMCID: PMC3978178.

283. Al-Zahrani KN, Cook DP, Vanderhyden BC, Sabourin LA. Assessing the efficacy of androgen receptor and Sox10 as independent markers of the triple-negative breast cancer subtype by transcriptome profiling. Oncotarget. 2018 Sep 7;9(70):33348–59. doi:10.18632/oncotarget.26072 PubMed PMID: 30279965; PubMed Central PMCID: PMC6161783.

284. Peevey J, Sumpter I, Paintal A, Laskin W, Sullivan M. SOX10 Is a Useful Marker for Triple Negative Breast Cancer. Am J Clin Pathol. 2015 Oct 1;144(suppl_2):A299. doi:10.1093/ajcp/144.suppl2.299

285. Ivanov SV, Panaccione A, Nonaka D, Prasad ML, Boyd KL, Brown B, et al. Diagnostic SOX10 gene signatures in salivary adenoid cystic and breast basal-like carcinomas. Br J Cancer. 2013 Jul 23;109(2):444–51. doi:10.1038/bjc.2013.326 PubMed PMID: 23799842; PubMed Central PMCID: PMC3721393.

286. Yang K, Yun F, Shi L, Liu X, Jia YF. SOX10 promotes the malignant biological behavior of basal-like breast cancer cells by regulating EMT process. Heliyon. 2023 Dec 1;9(12). doi:10.1016/j.heliyon.2023.e23162

287. Kriegsmann K, Flechtenmacher C, Heil J, Kriegsmann J, Mechtersheimer G, Aulmann S, et al. Immunohistological Expression of SOX-10 in Triple-Negative Breast Cancer: A Descriptive Analysis of 113 Samples. Int J Mol Sci. 2020 Jan;21(17):6407. doi:10.3390/ijms21176407

288. Jamidi SK, Hu J, Aphivatanasiri C, Tsang JY, Poon IK, Li JJ, et al. Sry-related high-mobility-group/HMG box 10 (SOX10) as a sensitive marker for triple-negative breast cancer. Histopathology. 2020 Dec;77(6):936–48. doi:10.1111/his.14118 PubMed PMID: 32304249.

289. Saunus JM, De Luca XM, Northwood K, Raghavendra A, Hasson A, McCart Reed AE, et al. Epigenome erosion and SOX10 drive neural crest phenotypic mimicry in triple-negative breast cancer. Npj Breast Cancer. 2022 May 2;8(1):57. doi:10.1038/s41523-022-00425-x

290. Kim YJ, Lim H, Li Z, Oh Y, Et. A. Generation of Multipotent Induced Neural Crest by Direct Reprogramming of Human Postnatal Fibroblasts with a Single Transcription Factor. Cell Stem Cell. 2014. doi:10.1016/j.stem.2014.07.013

291. Pomp V, Leo C, Mauracher A, Korol D, Guo W, Varga Z. Differential expression of epithelial–mesenchymal transition and stem cell markers in intrinsic subtypes of breast cancer. Breast Cancer Res Treat. 2015 Nov;154(1):45–55. doi:10.1007/s10549-015-3598-6 PubMed PMID: 26467042.

292. Qazi MS, McGregor SM. Combined use of SOX10 and GATA3 in mammary carcinoma. Pathol - Res Pract. 2020 Feb 1;216(2):152801. doi:10.1016/j.prp.2019.152801

293. Weisman P, Yu Q, Xu J. Clinicopathological characteristics of the SOX10+ subset of HER2+ breast cancer. Ann Diagn Pathol. 2023 Apr 1;63:152087. doi:10.1016/j.anndiagpath.2022.152087

294. Al-Zahrani KN, Abou-Hamad J, Cook DP, Pryce BR, Hodgins JJ, Labrèche C, et al. Loss of the Ste20-like kinase induces a basal/stem-like phenotype in HER2-positive breast cancers. Oncogene. 2020 Jun;39(23):4592–602. doi:10.1038/s41388-020-1315-3 PubMed PMID: 32393835.

295. Aphivatanasiri C, Li J, Chan R, Jamidi SK, Tsang JY, Poon IK, et al. Combined SOX10 GATA3 is most sensitive in detecting primary and metastatic breast cancers: a comparative study of breast markers in multiple tumors. Breast Cancer Res Treat. 2020 Nov;184(1):11–21. doi:10.1007/s10549-020-05818-9 PubMed PMID: 32737715.

296. Liao Y, Smyth GK, Shi W. The Subread aligner: fast, accurate and scalable read mapping by seed-and-vote. Nucleic Acids Res. 2013 May;41(10):e108. doi:10.1093/nar/gkt214 PubMed PMID: 23558742; PubMed Central PMCID: PMC3664803.

297. Liao Y, Smyth GK, Shi W. featureCounts: an efficient general purpose program for assigning sequence reads to genomic features. Bioinformatics. 2014 Apr 1;30(7):923–30. doi:10.1093/bioinformatics/btt656

298. Love MI, Huber W, Anders S. Moderated estimation of fold change and dispersion for RNA-seq data with DESeq2. Genome Biol. 2014;15(12):550. doi:10.1186/s13059-014-0550-8 PubMed PMID: 25516281; PubMed Central PMCID: PMC4302049.

299. Kolde R. pheatmap: Pretty Heatmaps [Internet]. 2010 [cited 2026 Apr 13]. p. 1.0.13. Available from: https://CRAN.R-project.org/package=pheatmap doi:10.32614/CRAN.package.pheatmap

300. Schubert M, Klinger B, Klünemann M, Sieber A, Uhlitz F, Sauer S, et al. Perturbation-response genes reveal signaling footprints in cancer gene expression. Nat Commun. 2018 Jan 2;9(1):20. doi:10.1038/s41467-017-02391-6 PubMed PMID: 29295995; PubMed Central PMCID: PMC5750219.

301. Yu G, He QY. ReactomePA: an R/Bioconductor package for reactome pathway analysis and visualization. Mol Biosyst. 2016 Feb;12(2):477–9. doi:10.1039/c5mb00663e PubMed PMID: 26661513.

302. Yu G, Wang LG, Han Y, He QY. clusterProfiler: an R package for comparing biological themes among gene clusters. Omics J Integr Biol. 2012 May;16(5):284–7. doi:10.1089/omi.2011.0118 PubMed PMID: 22455463; PubMed Central PMCID: PMC3339379.

303. Dolgalev I. msigdbr: MSigDB Gene Sets for Multiple Organisms in a Tidy Data Format [Internet]. 2018 [cited 2026 Apr 13]. p. 26.1.0. Available from: https://CRAN.R-project.org/package=msigdbr doi:10.32614/CRAN.package.msigdbr

304. Liberzon A, Birger C, Thorvaldsdóttir H, Ghandi M, Mesirov JP, Tamayo P. The Molecular Signatures Database (MSigDB) hallmark gene set collection. Cell Syst. 2015 Dec 23;1(6):417–25. doi:10.1016/j.cels.2015.12.004 PubMed PMID: 26771021; PubMed Central PMCID: PMC4707969.

305. Liberzon A, Subramanian A, Pinchback R, Thorvaldsdóttir H, Tamayo P, Mesirov JP. Molecular signatures database (MSigDB) 3.0. Bioinformatics. 2011 Jun 15;27(12):1739–40. doi:10.1093/bioinformatics/btr260 PubMed PMID: 21546393; PubMed Central PMCID: PMC3106198.

306. Wu SZ, Al-Eryani G, Roden DL, Junankar S, Harvey K, Andersson A, et al. A single-cell and spatially resolved atlas of human breast cancers. Nat Genet. 2021 Sep;53(9):1334–47. doi:10.1038/s41588-021-00911-1

307. Qian J, Olbrecht S, Boeckx B, Vos H, Laoui D, Etlioglu E, et al. A pan-cancer blueprint of the heterogeneous tumor microenvironment revealed by single-cell profiling. Cell Res. 2020 Sep;30(9):745–62. doi:10.1038/s41422-020-0355-0

308. Pal B, Chen Y, Vaillant F, Capaldo BD, Joyce R, Song X, et al. A single-cell RNA expression atlas of normal, preneoplastic and tumorigenic states in the human breast. EMBO J. 2021 Jun 1;40(11):e107333. doi:10.15252/embj.2020107333 PubMed PMID: 33950524; PubMed Central PMCID: PMC8167363.

309. Bassez A, Vos H, Van Dyck L, Floris G, Arijs I, Desmedt C, et al. A single-cell map of intratumoral changes during anti-PD1 treatment of patients with breast cancer. Nat Med. 2021 May;27(5):820–32. doi:10.1038/s41591-021-01323-8

310. Andrechek ER, Hardy WR, Siegel PM, Rudnicki MA, Cardiff RD, Muller WJ. Amplification of the neu/erbB-2 oncogene in a mouse model of mammary tumorigenesis. Proc Natl Acad Sci. 2000 Mar 28;97(7):3444–9. doi:10.1073/pnas.97.7.3444

311. Andrechek ER, White D, Muller WJ. Targeted disruption of ErbB2/Neu in the mammary epithelium results in impaired ductal outgrowth. Oncogene. 2005 Jan 27;24(5):932–7. doi:10.1038/sj.onc.1208230 PubMed PMID: 15580295.

312. White DE, Kurpios NA, Zuo D, Hassell JA, Blaess S, Mueller U, et al. Targeted disruption of beta1-integrin in a transgenic mouse model of human breast cancer reveals an essential role in mammary tumor induction. Cancer Cell. 2004 Aug;6(2):159–70. doi:10.1016/j.ccr.2004.06.025 PubMed PMID: 15324699.

313. Finzsch M, Schreiner S, Kichko T, Reeh P, Tamm ER, Bösl MR, et al. Sox10 is required for Schwann cell identity and progression beyond the immature Schwann cell stage. J Cell Biol. 2010 May 17;189(4):701–12. doi:10.1083/jcb.200912142 PubMed PMID: 20457761; PubMed Central PMCID: PMC2872908.

314. Gray GK, Carlson EG, Lev T, Marshall B, Reed AD, Sánchez-Covarrubias AP, et al. Defining breast epithelial cell types in the single-cell era. Dev Cell. 2025 Sep 8;60(17):2218–36. doi:10.1016/j.devcel.2025.06.032 PubMed PMID: 40925326.

315. Malhotra GK, Zhao X, Edwards E, Kopp JL, Naramura M, Sander M, et al. The role of Sox9 in mouse mammary gland development and maintenance of mammary stem and luminal progenitor cells. BMC Dev Biol. 2014 Dec 20;14:47. doi:10.1186/s12861-014-0047-4 PubMed PMID: 25527186; PubMed Central PMCID: PMC4297388.

316. Kogata N, Bland P, Tsang M, Oliemuller E, Lowe A, Howard BA. Sox9 regulates cell state and activity of embryonic mouse mammary progenitor cells. Commun Biol. 2018 Dec 13;1(1):228. doi:10.1038/s42003-018-0215-3

317. Shiozawa Y, Nie B, Pienta KJ, Morgan TM, Taichman RS. Cancer Stem Cells and their Role in Metastasis. Pharmacol Ther. 2013 May;138(2):285–93. doi:10.1016/j.pharmthera.2013.01.014 PubMed PMID: 23384596; PubMed Central PMCID: PMC3602306.

318. Fantozzi A, Christofori G. Mouse models of breast cancer metastasis. Breast Cancer Res. 2006 Jul 26;8(4):212. doi:10.1186/bcr1530

319. Rashid OM, Nagahashi M, Ramachandran S, Dumur CI, Schaum JC, Yamada A, et al. Is tail vein injection a relevant breast cancer lung metastasis model? J Thorac Dis. 2013 Aug;5(4):385–92. doi:10.3978/j.issn.2072-1439.2013.06.17 PubMed PMID: 23991292; PubMed Central PMCID: PMC3755653.

320. Velasco-Velázquez MA, Popov VM, Lisanti MP, Pestell RG. The Role of Breast Cancer Stem Cells in Metastasis and Therapeutic Implications. Am J Pathol. 2011 Jul;179(1):2–11. doi:10.1016/j.ajpath.2011.03.005 PubMed PMID: 21640330; PubMed Central PMCID: PMC3123864.

321. Charafe-Jauffret E, Ginestier C, Iovino F, Wicinski J, Cervera N, Finetti P, et al. Breast cancer cell lines contain functional cancer stem cells with metastatic capacity and a distinct molecular signature. Cancer Res. 2009 Feb 15;69(4):1302–13. doi:10.1158/0008-5472.CAN-08-2741 PubMed PMID: 19190339; PubMed Central PMCID: PMC2819227.

322. Charafe-Jauffret E, Ginestier C, Iovino F, Tarpin C, Diebel M, Esterni B, et al. Aldehyde dehydrogenase 1-positive cancer stem cells mediate metastasis and poor clinical outcome in inflammatory breast cancer. Clin Cancer Res Off J Am Assoc Cancer Res. 2010 Jan 1;16(1):45–55. doi:10.1158/1078-0432.CCR-09-1630 PubMed PMID: 20028757; PubMed Central PMCID: PMC2874875.

323. Charafe-Jauffret E, Ginestier C, Monville F, Finetti P, Adélaïde J, Cervera N, et al. Gene expression profiling of breast cell lines identifies potential new basal markers. Oncogene. 2006 Apr 6;25(15):2273–84. doi:10.1038/sj.onc.1209254 PubMed PMID: 16288205.

324. Lim E, Wu D, Pal B, Bouras T, Asselin-Labat ML, Vaillant F, et al. Transcriptome analyses of mouse and human mammary cell subpopulations reveal multiple conserved

genes and pathways. Breast Cancer Res BCR. 2010;12(2):R21. doi:10.1186/bcr2560 PubMed PMID: 20346151; PubMed Central PMCID: PMC2879567.

325. Pal B, Chen Y, Milevskiy MJG, Vaillant F, Prokopuk L, Dawson CA, et al. Single cell transcriptome atlas of mouse mammary epithelial cells across development. Breast Cancer Res BCR. 2021 Jun 29;23(1):69. doi:10.1186/s13058-021-01445-4 PubMed PMID: 34187545; PubMed Central PMCID: PMC8243869.

326. Wu T, Wang Y, Jiang R, Lu X, Tian J. A pathways-based prediction model for classifying breast cancer subtypes. Oncotarget. 2017 Jun 17;8(35):58809–22. doi:10.18632/oncotarget.18544 PubMed PMID: 28938599; PubMed Central PMCID: PMC5601695.

327. Gao T, Li JZ, Lu Y, Zhang CY, Li Q, Mao J, et al. The mechanism between epithelial mesenchymal transition in breast cancer and hypoxia microenvironment. Biomed Pharmacother Biomedecine Pharmacother. 2016 May;80:393–405. doi:10.1016/j.biopha.2016.02.044 PubMed PMID: 27133080.

328. Vafaizadeh V, Klemmt P, Brendel C, Weber K, Doebele C, Britt K, et al. Mammary epithelial reconstitution with gene-modified stem cells assigns roles to Stat5 in luminal alveolar cell fate decisions, differentiation, involution, and mammary tumor formation. Stem Cells. 2010 May;28(5):928–38. doi:10.1002/stem.407 PubMed PMID: 20235097.

329. Yamaji D, Na R, Feuermann Y, Pechhold S, Chen W, Robinson GW, et al. Development of mammary luminal progenitor cells is controlled by the transcription factor STAT5A. Genes Dev. 2009 Oct 15;23(20):2382–7. doi:10.1101/gad.1840109 PubMed PMID: 19833766; PubMed Central PMCID: PMC2764497.

330. Balko JM, Miller TW, Morrison MM, Hutchinson K, Young C, Rinehart C, et al. The receptor tyrosine kinase ErbB3 maintains the balance between luminal and basal breast epithelium. Proc Natl Acad Sci U S A. 2012 Jan 3;109(1):221–6. doi:10.1073/pnas.1115802109 PubMed PMID: 22178756; PubMed Central PMCID: PMC3252958.

331. Ikushima H, Todo T, Ino Y, Takahashi M, Miyazawa K, Miyazono K. Autocrine TGF-β Signaling Maintains Tumorigenicity of Glioma-Initiating Cells through Sry-Related HMG-Box Factors. Cell Stem Cell. 2009 Nov 6;5(5):504–14. doi:10.1016/j.stem.2009.08.018 PubMed PMID: 19896441.

332. Wu SZ, Al-Eryani G, Roden DL, Junankar S, Harvey K, Andersson A, et al. A single-cell and spatially resolved atlas of human breast cancers. Nat Genet. 2021 Sep;53(9):1334–47. doi:10.1038/s41588-021-00911-1

333. Bassez A, Vos H, Van Dyck L, Floris G, Arijs I, Desmedt C, et al. A single-cell map of intratumoral changes during anti-PD1 treatment of patients with breast cancer. Nat Med. 2021 May;27(5):820–32. doi:10.1038/s41591-021-01323-8 PubMed PMID: 33958794.

334. Qian J, Olbrecht S, Boeckx B, Vos H, Laoui D, Etlioglu E, et al. A pan-cancer blueprint of the heterogeneous tumor microenvironment revealed by single-cell profiling. Cell Res. 2020 Sep;30(9):745–62. doi:10.1038/s41422-020-0355-0

335. Pal B, Chen Y, Vaillant F, Capaldo BD, Joyce R, Song X, et al. A single-cell RNA expression atlas of normal, preneoplastic and tumorigenic states in the human breast. EMBO J. 2021 Jun 1;40(11):e107333. doi:10.15252/embj.2020107333 PubMed PMID: 33950524; PubMed Central PMCID: PMC8167363.

336. Sumbal J, Koledova Z. FGF signaling in mammary gland fibroblasts regulates multiple fibroblast functions and mammary epithelial morphogenesis. Development. 2019 Dec 2;146(23):dev185306. doi:10.1242/dev.185306 PubMed PMID: 31699800.

337. Lee-Hoeflich ST, Crocker L, Yao E, Pham T, Munroe X, Hoeflich KP, et al. A central role for HER3 in HER2-amplified breast cancer: implications for targeted therapy. Cancer Res. 2008 Jul 15;68(14):5878–87. doi:10.1158/0008-5472.CAN-08-0380 PubMed PMID: 18632642.

338. Liu L, Xiao B, Hirukawa A, Smith HW, Zuo D, Sanguin-Gendreau V, et al. Ezh2 promotes mammary tumor initiation through epigenetic regulation of the Wnt and mTORC1 signaling pathways. Proc Natl Acad Sci U S A. 2023 Aug 15;120(33):e2303010120. doi:10.1073/pnas.2303010120 PubMed PMID: 37549258; PubMed Central PMCID: PMC10438390.

339. Li Z, Koch KE, Thompson DT, Van der Heide DM, Chang J, Franke CM, et al. Sumoylated Etv1 establishes mouse mammary cancer stem cells that support tumorigenesis by non-stem cancer cells. Dev Cell. 2025 Sep 8;60(17):2264-2278.e7. doi:10.1016/j.devcel.2025.04.005 PubMed PMID: 40315856; PubMed Central PMCID: PMC12353075.

340. Milevskiy MJG, Coughlan HD, Kane SR, Johanson TM, Kordafshari S, Chan WF, et al. Three-dimensional genome architecture coordinates key regulators of lineage specification in mammary epithelial cells. Cell Genomics. 2023 Nov 8;3(11). doi:10.1016/j.xgen.2023.100424 PubMed PMID: 38020976.

341. Bernardo GM, Bebek G, Ginther CL, Sizemore ST, Lozada KL, Miedler JD, et al. FOXA1 represses the molecular phenotype of basal breast cancer cells. Oncogene. 2013 Jan 31;32(5):554–63. doi:10.1038/onc.2012.62 PubMed PMID: 22391567; PubMed Central PMCID: PMC3371315.

342. Ahmed F, Wyckoff J, Lin EY, Wang W, Wang Y, Hennighausen L, et al. GFP expression in the mammary gland for imaging of mammary tumor cells in transgenic mice. Cancer Res. 2002 Dec 15;62(24):7166–9. PubMed PMID: 12499251.

343. Henry MD, Triplett AA, Oh KB, Smith GH, Wagner KU. Parity-induced mammary epithelial cells facilitate tumorigenesis in MMTV-neu transgenic mice. Oncogene. 2004 Sep 9;23(41):6980–5. doi:10.1038/sj.onc.1207827 PubMed PMID: 15286714.

344. Umair M, Khan AA, Jamal N, Bajwa AA, Khan MU, Hassan T. Immunohistochemical expression of SOX10 and GATA3 in triple negative breast carcinoma and metastatic breast carcinoma. Prof Med J. 2025 Mar 10;32(03):290–6. doi:10.29309/TPMJ/2025.32.03.8797

345. Jin L, Qin C, Qi X, Hong T, Yang X, Zhu X. Clinicopathological significance of Sox10 expression in triple-negative breast carcinoma. Transl Cancer Res. 2020 Sep;9(9):5603–13. doi:10.21037/tcr-20-2634 PubMed PMID: 35117924; PubMed Central PMCID: PMC8797416.

346. Dutta S, Sengupta P. Men and mice: Relating their ages. Life Sci. 2016 May 1;152:244–8. doi:10.1016/j.lfs.2015.10.025 PubMed PMID: 26596563.

347. National Breast Cancer Foundation [Internet]. [cited 2026 Feb 10]. Triple Negative Breast Cancer. Available from: https://www.nationalbreastcancer.org/triple-negative-breast-cancer/

348. Tzikas AK, Nemes S, Linderholm BK. A comparison between young and old patients with triple-negative breast cancer: biology, survival and metastatic patterns. Breast Cancer Res Treat. 2020;182(3):643–54. doi:10.1007/s10549-020-05727-x PubMed PMID: 32524352; PubMed Central PMCID: PMC7320950.

349. Tariq MU, Siddiqui MA, Ud Din N, Kayani N. Role of SOX10 Immunohistochemical Expression in Diagnosing Triple Negative Breast Cancer and Its Correlation With Clinicopathological Features. Cureus. 2024 Apr;16(4):e59276. doi:10.7759/cureus.59276 PubMed PMID: 38813332; PubMed Central PMCID: PMC11135236.